Development of high capacity transmission systems for future optical access networks

Paul D. Sheridan
B.Sc. Physics

A thesis submitted in fulfilment of the
requirements for the award of
Master of Engineering (M.Eng.)

to

DCU
Ollscoil Chathair
Bhaile Átha Cliath
Dublin City University

School of Electronic Engineering
Faculty of Engineering and Computing

Supervisor: Prof. Liam P. Barry

September 2021

Declaration

I hereby certify that this material, which I now submit for assessment on the programme of study leading to the award of Master of Engineering is entirely my own work, and that I have exercised reasonable care to ensure that the work is original, and does not, to the best of my knowledge, breach any law of copyright, and has not been taken from the work of others save and to the extent that such work has been cited and acknowledged within the text of my work.

Signed: _____________________ (Paul Sheridan)

ID No.: _________________

Date: ______________

For Michelle and my boys,

Ryan & Ethan.

"I think it's much more interesting to live not knowing than to have answers which might be wrong. I have approximate answers, and possible beliefs, and different degrees of uncertainty about different things, but I am not absolutely sure of anything. There are many things I don't know anything about, such as whether it means anything to ask "Why are we here?" I might think about it a little bit, and if I can't figure it out then I go on to something else. But I don't have to know an answer. I don't feel frightened by not knowing things, by being lost in the mysterious universe without having any purpose - which is the way it really is, as far as I can tell."

Richard P. Feynman

Table of Contents

Acknowledgements

I would like to thank my supervisor Prof. Liam Barry for giving me the opportunity to pursue a Masters in his research group. Without his patience, support and guidance the completion of this work would have been impossible.

A special thanks goes to Dr. Seán P. Ó Duill for the help provided and theoretical discussions during the writing of this thesis. My appreciation also extends to Dr. Yi Lin for his help, and valuable time and assistance.

Finally, I would like to express my immense gratitude to my parents and sister for their encouragement and support throughout my studies. Lastly, I would like to thank Michelle, my partner and best friend, for your unconditional support and love when it is needed most. I'll always be thankful to you all.

List of Figures

List of Acronyms

AON	Active Optical Network
APD	Avalanche Photodiode
ASE	Amplified Spontaneous Emission
AWG	Arbitrary Waveform Generator
AWG	Arrayed Waveguide Grating
B2B	Back-to-Back
BER	Bit-Error Ratio
BERT	Bit-Error Ratio Tester
CO	Central Office
CW	Continuous Wave
DFB	Distributed Feedback
DM	Directly Modulated
DML	Directly Modulated Laser
DMT	Discrete Multi-Tone
DP-QPSK	Dual Polarization Quadrature Phase Shift Keying
DSH	Delayed Self-Heterodyne
DWDM	Dense Wavelength Division Multiplexing
EAM	Electro-Absorption Modulator
EC	External Cavity
EM	Externally Modulated
EML	Electro-Absorption Modulated Laser
ER	Extinction Ratio
FEC	Forward-Error Correction
FP	Fabry-Pérot
FSR	Free Spectral Range
FWHM	Full Width at Half Maximum
FM	Frequency Modulation
FTTH	Fibre-to-the-Home
IM/DD	Intensity-Modulation and Direct-Detection
IL	Injection-Locking
ILM	Integrated Laser Modulator
ISI	Inter-Symbol Interference

MAC	Medium Access Control
MLM	Multi-Longitudinal Mode
MPN	Mode Partition Noise
NRZ	Non-Return to Zero
ODN	Optical Distribution Network
OFDM	Orthogonal Frequency Division Multiplexing
OLT	Optical Line Terminal
ONU	Optical Network Unit
OOK	On-Off-Keying
OSA	Optical Spectrum Analyser
PIC	Photonic Integrated Circuit
PM	Phase Modulation
PON	Passive Optical Network
PPG	Pulse Pattern Generator
PRBS	Pseudorandom Binary Sequence
PtP	Point-to-Point Network
QAM	Quadrature Amplitude Modulation
RBW	Resolution Bandwidth
RIN	Relative Intensity Noise
RMS	Root Mean Squared
RN	Remote Node
RTO	Real-Time Oscilloscope
SM	Single-Mode
SMSR	Side-Mode Suppression Ratio
SNR	Signal-to-Noise
SS-FP	Self-Seeded Fabry-Pérot
SSMF	Standard Single-Mode Fibre
TBPF	Tunable Bandpass Filter
TDM	Time Division Multiplexing
TDMA	Time Division Multiple Access
TWDM	Time and Wavelength Division Multiplexing
TEC	Thermoelectric Cooler
TLS	Tunable Laser Source
VOA	Variable Optical Attenuator

VNA	Vector Network Analyser
WDM	Wavelength Division Multiplexing

Development of high capacity transmission systems for future optical access networks

Paul D. Sheridan

Abstract

The cost-sensitivity of NG-PON2 and future optical access networks, employing wavelength division multiplexing (WDM) technology, may preclude the use of conventional $LiNbO_3$-based intensity and I/Q modulators, as they are currently too expensive for use in the access domain. Cost-effective directly modulated lasers (DMLs) and electro-absorption modulated lasers (EMLs) will need to be employed and, thus, are expected to be integral components in the realisation of tunable laser sources for future optical access networks. The limitations of DMLs and EMLs as transmitters merit thorough investigation to further understand how these devices can be adapted or optimised for use as tunable laser sources in future optical access networks.

In this thesis, the transmission performance of a directly modulated DFB laser (DML) and an externally modulated DFB laser monolithically integrated with an EAM (EML), are investigated. The performance of both devices under 12.5 Gbit/s NRZ-OOK modulation are evaluated for transmission over standard single-mode fibre (SSMF) in an IM/DD test-bed, with a view to further understanding the limitations of DMLs and EMLs in 10 Gbit/s IM/DD systems. Particular attention is given to the frequency chirp of the devices and how the chirp affects the performances of the devices for transmission over SSMF up to 50 km in length. Numerical models, which were developed in MATLAB, are utilised to simulate the characteristics and transmission performances of both the DML and EML. The latter half of this thesis is focused on the development of a self-seeded Fabry-Pérot (SS-FP) laser. The SS-FP laser is optimised and characterised, and the transmission performance of the directly modulated SS-FP laser over SSMF is evaluated in an IM/DD test-bed. Two intensity modulation (IM) formats are assessed, 12.5 Gbit/s NRZ-OOK and 12.5 Gbaud/s (25 Gbit/s) multilevel PAM-4, both IM formats are compatible with 10G class optical components and legacy PON deployments. The SS-FP laser holds potential for photonic integration, justifying its consideration as a candidate tunable laser source for next generation PONs and future optical access networks.

Introduction

The last decade has seen an incessant growth in data traffic and bandwidth demands. This growth has largely been driven by the rise of the ‘Internet of Things’ era, which has heralded unprecedented levels of device connectivity. It has also been driven by the continuous evolution of multimedia services such as high-definition video, online gaming and virtual and augmented reality applications. Fibre-to-the-Home (FTTH) has been deemed a future-proof optical access solution to meet the projected data rate and bandwidth requirements of end-users and the ever-increasing global data traffic demand. Passive optical networks (PONs) are considered to be the most cost-efficient and reliable network architecture for the delivery of FTTH and ubiquitous fibre-based connectivity. The introduction of a hybrid of time and wavelength division multiplexing (TWDM) technology to PONs, reflected in the recent NG-PON2 standard, will see future PONs exploit both the time and wavelength domains in order to deliver the capacity required to support the relentless growth in global traffic. However, with the introduction of WDM technology to NG-PON2, the wide scale deployment of these networks will require substantial financial investment and, thus, will be a highly cost-sensitive undertaking. As a result, the realisation of NG-PON2 and future WDM access networks presents significant challenges, particularly with regard to the development of cost-effective tunable optical sources, which must also meet stringent performance requirements. Hence, reducing the cost and complexity of tunable optical sources for NG-PON2 and future WDM access networks, while meeting the specified performance requirements, has been the focus of considerable research efforts in recent years.

Directly modulated lasers (DMLs) are attractive candidates for tunable optical sources in NG-PON2 and future WDM access networks, employing intensity modulation and direct detection (IM/DD), due to their cost-effectiveness and ability to achieve 12.5 Gbit/s data rates. However, DMLs produce instantaneous frequency chirp and when an optical signal that is transmitted from a DML propagates in optical fibre, the phase to intensity modulation (PM-IM) conversion of the signal, which occurs as a result of the interaction between the intrinsic chirp of the laser and the chromatic dispersion in the optical fibre, can severely degrade the signal quality. Consequently, this imposes significant limitations on the modulation rates that can be applied to DMLs and the transmission distances that they can achieve. External modulators offer an alternative solution for intensity modulation of lightwaves and can be relatively chirp free. However, traditional $LiNbO_3$-based intensity and I/Q modulators, which are employed extensively in core and metro transport networks, are currently too expensive to be employed in the access domain. Electro-absorption modulators (EAMs) are a cost-effective external intensity modulation solution. Moreover, EAMs can be monolithically integrated with lasers and packaged in a single device to produce electro-absorption modulated lasers (EMLs) or integrated laser modulators (ILMs), which are compact and cost-effective. EAMs are not entirely free of chirp, however, through careful optimisation of the bias voltage applied to the EAM it can exhibit zero or even negative chirp, which can actually aid signal transmission over optical fibre and extend transmission distances. Furthermore, EAMs tend to suffer from high insertion losses, leading to a significant reduction in the transmitted signal optical power when compared with DMLs. Considering the cost-sensitivity of NG-PON2 and future WDM optical access networks, DMLs and EMLs will be integral components in the realisation of cost-effective tunable laser sources (TLSs) for future networks. Thus, the limitations of DMLs and EMLs warrant thorough investigation to understand how these sources may be adapted or optimised for future tunable laser developments.

Wavelength locked Fabry-Pérot (FP) lasers could potentially be used to realise a cost-effective tunable laser source (TLS) for future ‘colourless’ WDM PONs and optical access networks. Self-seeded Fabry-Pérot (SS-FP) lasers are capable of producing a widely tunable, single-wavelength source exhibiting a high side-mode suppression ratio (SMSR) of >40 dB. Furthermore, when the FP laser is directly modulated, it can achieve multi-gigabit optical signal transmission over standard single-mode fibre (SSMF) distances which meet the requirements specified in recent PON standards. Moreover, SS-FP lasers hold potential for photonic integration. Indeed, for their practical and cost-effective wide scale deployment in PONs, the development of an SS-FP laser photonic integrated circuit (PIC) would be more of a necessity than a convenience. This justifies the consideration of SS-FP lasers as candidate tunable optical sources for future optical access networks and, hence, further study of SS-FP lasers is warranted.

Main Contributions

The main contributions of this work are:

- An experimental demonstration of error-free 12.5 Gbit/s NRZ-OOK optical transmission over 50 km of standard single-mode fibre (SSMF) with a directly modulated DFB laser (DML), without the use of optical or electronic dispersion compensation, is presented. The transmission performance of the DML is numerically modelled and the simulated results obtained from the model agree well with the experimental results. From the numerical model of the DML, key device parameters, such as the chirp or alpha parameter, α, and gain compression factor, ϵ, of the DFB laser, which enabled the enhanced transmission performance of the DML for transmission over 50 km of SSMF, are estimated. Furthermore, the magnitude and characteristics of the DML chirp are determined from the model. The transmission performance of an EML modulated with a 12.5 Gbit/s NRZ-OOK signal is also experimentally evaluated, and the results obtained are compared with the results of the DML transmission experiments. The EML is also numerically modelled, and from the model the range of alpha parameter, α_{EAM}, values exhibited by the EML are estimated. Furthermore, the magnitude and characteristics of the EML chirp are determined from the model.

- The first successful demonstration of error-free 12.5 Gbit/s NRZ-OOK optical signal transmission over 25 km of SSMF with a directly modulated (DM) self-seeded FP (SS-FP) laser in an IM/DD test-bed, without optical or electronic dispersion compensation, is presented. Furthermore, error-free 12.5 Gbit/s NRZ-OOK signal transmission over 25 km of SSMF with the DM SS-FP laser operating at different wavelengths is experimentally demonstrated. To the best of the author's knowledge, this work represents (at the publication date) the highest reported transmission rate and distance attained with a directly modulated self-seeded FP laser source. Moreover, 25 Gbit/s 4- level Pulse Amplitude Modulation (PAM-4) optical signal transmission in a back-to-back (b2b) configuration is experimentally demonstrated with the DM SS-FP laser with the aid of adaptive equalisation. The adaptive equalisation is employed in the offline digital processing of the received signal to produce a transmission performance below the 7% Forward Error Correction (FEC) limit.

Thesis structure

This thesis is structured as follows:

Chapter 1 describes the evolution of optical access networks. The different access network topologies are introduced and a description of the topologies is provided. Passive optical networks (PONs) are given particular attention, along with the technologies used to increase the capacity of PONs, including time division multiplexing (TDM) and wavelength division multiplexing (WDM), as the next generation of passive optical networks (NG-PON2) will employ a hybrid of the two multiplexing technologies. The roadmap towards the realisation of next-generation PONs, and the challenges that this presents, are also discussed.

Chapter 2 examines the characteristics and transmission performances of a directly modulated DFB laser (DML) and an electro-absorption modulated laser (EML). The performances of both transmitters under 12.5 Gbit/s NRZ-OOK modulation, transmitting over SSMF in an IM/DD test-bed are evaluated, with a view to better understanding the limitations of DMLs and EMLs in 10G IM/DD links. Particular attention is given to the frequency chirp of the devices and how the chirp affects the transmission performance of the devices over different SSMF distances. Numerical models are utilised to simulate the characteristics and transmission performances of both devices.

Chapter 3 is focused on the development of a tunable self-seeded Fabry-Pérot (SS-FP) laser. The SS-FP laser is optimised and characterised. The optimisation is performed by measuring the SMSR of the directly modulated (DM) SS-FP laser and the BER performance of the DM SS-FP laser for back-to-back (b2b) transmission. The characterisation includes large-signal modulation analysis (extinction ratio, ER power penalty, Q-factor), analysis of the influence of the seed signal optical power on the SMSR of the SS-FP laser and classification of the feedback regime, relative intensity noise (RIN) measurements and an evaluation of the performance of the different wavelength channels of the DM SS-FP laser and its tuning range. The experimental implementation of the DM SS-FP laser in a 12.5 Gbit/s NRZ-OOK and a 25 Gbit/s PAM-4 IM/DD transmission system is also demonstrated, to analyse the influence of the extinction ratio (ER), ER power penalty and Q-factor of the signal transmitted from the DM SS-FP laser on the transmission performance.

Chapter 4 concludes the thesis with a summary of the research and highlights the main contributions of this study. Finally, some future research lines are also proposed and discussed.

Chapter 1 Optical Access Networks

1.1 Introduction

The demand for high speed communications and media-rich applications and services, by residential and business consumers alike, continues to grow year on year. As shown in Figure 1.1, global IP traffic will increase at a Compound Annual Growth Rate (CAGR) of 26% from 2017 to 2022 and has been forecasted to reach 4.8 ZB per year by 2022, which will be a threefold increase on the 2017 annual run rate of 1.5 ZB per year [1]. The number of devices connected to IP networks globally is expected to be more than three times the global population by 2022 at 28.5 billion, having increased by over 10 billion from 2017 [1]. In the era of the so called “Internet of Things” (IoT), the relentless growth in global IP traffic shows no sign of abating and network providers are continuously being forced to increase the bandwidth provision of optical transport networks.

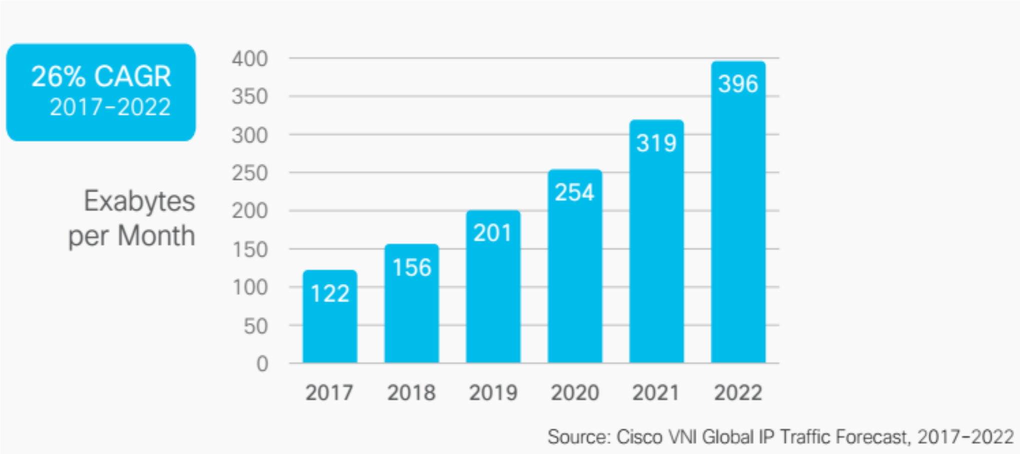

Figure 1.1: Cisco VNI monthly IP traffic forecast up to 2022 [1].

The transmission speed and throughput “bottleneck” of the internet is currently the access network, which covers the last span of the communications network between subscribers and the central office node. Access networks, and intra-data centre networks, typically fall under the “short-haul” networks category. The term “last mile” is often used when referring to access networks. In reality, several tens of kilometres of optical fibre can be deployed in optical access networks to connect subscribers to the optical line terminal (OLT) at the interface to the “long-haul” core and metro transport networks, as shown in Figure 1.2, which span transmission distances of hundreds or thousands of kilometres. In recent years, access networks have seen significant adoption of optical networking technologies in place of electrical as a means to increasing capacity and throughput. However, access networks, at present, still rely largely on copper-based communications. This presents a major obstacle considering that digital subscriber line (DSL) technologies are fast approaching their capacity limit and soon will not be capable of meeting the predicted bandwidth and data rate demands of end-users. Optical fibre communication is the obvious solution to the bottleneck problem. Broadband optical access networks, and Fibre-to-the-Home (FTTH) networks in particular, have been deemed a "future-proof" solution to meet the projected increase in bandwidth and data rate demands of end-users. In the next generation of fibre-based access networks, the optical transmission will be terminated closer than ever before to the subscriber premises, thus, exploiting the superior performance of optical fibre communications.

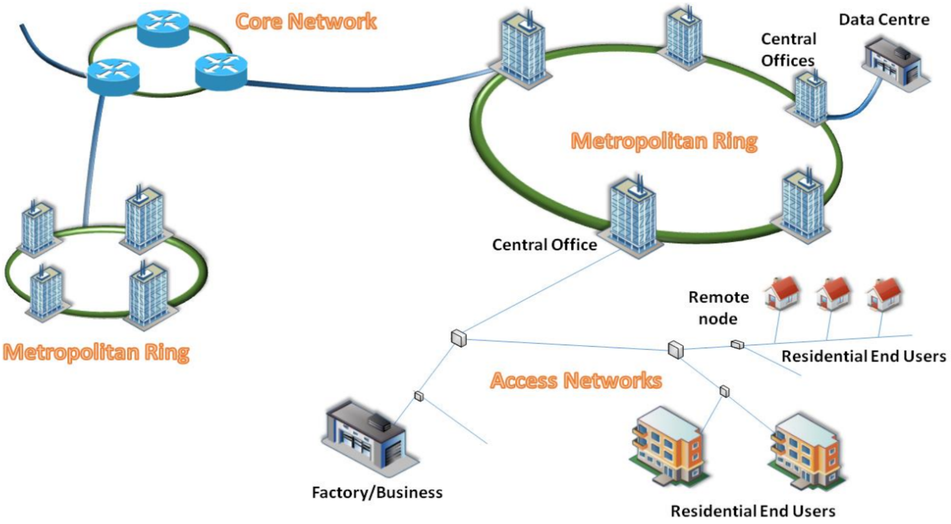

Figure 1.2: Illustration of network topologies which includes core, metropolitan and access networks [2].

Future access networks will need to be capable of offering Internet-Protocol-TV, Video-on-Demand, Voice-over-IP and High-Speed Internet Access, combined with guaranteed Quality of Service. Yet in order for an end-to-end solution for ubiquitous high-speed broadband optical access to be realised, cost-effective components and technologies for use in the optical access network physical layer must be made readily available to service providers. Passive optical networks (PONs) have been deemed the most cost effective architecture for future optical access networks and have become the preferred solution for network providers due to the potential bandwidth they can provide and their scalability.

This chapter explores the current state of optical access networks and the future of optical access. In section 1.2 an overview of optical access networks is provided. In section 1.3, passive optical networks (PONs) are discussed, including different PON multiplexing technologies and the recent PON standard NG-PON2. Finally, a summary of the chapter is presented in section 1.4, which addresses some of the challenges facing the realisation of NG-PON2 and future optical access networks.

1.2 Optical Access Networks Overview

Optical access networks are categorised based on the proximity of the fibre termination point to the end-user or subscriber. The “Fibre-to-the-x” or FTTX designation is typically used to indicate the fibre termination point, where “X” can signify either “Home”, “Buildling” or ”Curb”. Fibre-to-the-Home or Building (FTTH or FTTB) are considered the most future-proof solutions because they connect the end-users as close as possible to the fibre network. In the case of FTTH or FTTB, the fibre is terminated at the optical network unit (ONU), which is located at the dwelling or premises. With FTTB, the ONU is located at the building and coaxial or copper (e.g. twisted copper pair) cables are employed to connect multiple end-users in the building to the fibre terminal or ONU. In the case of Fibre-to-the-Curb (FTTC), the fibre network or optical distribution network (ODN) will extend from the central office (CO), where the optical line terminal (OLT) is located, to a point typically within 300 metres of the subscribers and, as in the case of FTTB, copper or coaxial cables will form the remainder of the connection from the ONU to the subscribers. Fibre-to-the-Node is similar to FTTC, however, the ONU can be situated at a distance greater than 1 km from the subscribers. Figure 1.3 illustrates the main network architectures used in fibre-based access to date including Point-to-Point (PtP) networks, Active Optical Networks (AONs) and Passive Optical Networks (PONs) [3].

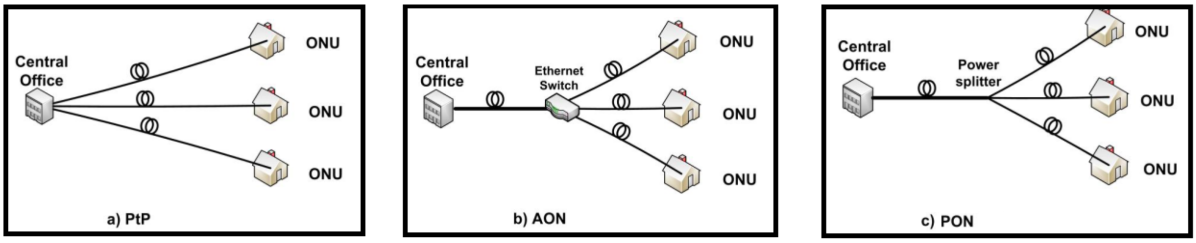

Figure 1.3: Basic FTTH access network architectures: a) point-to-point (P2P); b) active optical network (AON); c) passive optical network (PON) [3].

The point-to-point (PtP) architecture is the most straightforward deployment for fibre-based access. In a PtP system, as shown in Figure 1.3 (a), each subscriber ONU has a dedicated fibre connection to the OLT located at the CO and there are no additional components in the ODN between the OLT and ONU. Typically, only one fibre link is used to connect the OLT to the ONU, which utilises bi-directional downstream and upstream transmission, where transmission downstream and upstream is over the same fibre using two different wavelengths. In some cases, two separate fibre links are employed for downstream and upstream transmission. The advantage of the PtP architecture is that operators can expand the network as the number of subscribers increases and, as each subscriber link is independent of one another, any repair or maintenance work required on one subscriber’s link will not affect other subscribers in the network. This also makes it easy to upgrade the transmission speed line by line or perform component upgrades on a per-user basis [4]. Although it is the simplest architecture of the three, it is also the least cost efficient. PtP deployments require a high number of fibres and, more importantly, a high number of transceivers, as each subscriber in the network requires their own dedicated transceiver at the OLT [5]. As thousands of subscribers can be connected to an OLT, this can lead to significant issues regarding power consumption and space to house the components, coupled with the initial costs for deployment and the cost for maintenance and repairs, the running costs over the lifetime of a PtP access network can be considerable. Despite the cost factor, PtP architectures have been used in many fibre-based access deployments, particularly in Europe.

Active optical networks (AONs), shown in Figure 1.3 (b), are the second type of optical access network architecture. In AONs, a single feeder fibre connects the OLT to an active electrical switch in the ODN located at a remote node (RN), which is situated in close proximity to the ONUs. Distribution fibres are employed to connect the ONUs to the active switch at the RN and all of the ONUs are connected to the OLT through the feeder fibre. As active components are used at the RN, AON architectures can provide greater transmission distance than PtP [5]. Furthermore, the use of multiplexing at the RN allows for a single feeder fibre to be employed in this architecture, thus, reducing the amount of fibre required when compared with PtP. The number of transceivers required at the OLT is also reduced, however, transceivers are required for the active Ethernet switch at the RN. At the RN the incoming optical signal from the OLT is converted to the electrical domain and the Ethernet switch forwards the electrical signal to a transceiver where electro-optical conversion takes place and the optical signal is then transmitted through the distribution fibre to the subscribers ONU. Due to the active Ethernet switch element at the RN, a greater number of transceivers may be required in an AON than in a PtP network having the same number of end users [5]. Further costs are incurred in AONs due to the expensive housing required for the Ethernet switch, as the components need to withstand a wider range of temperatures than in-door equipment, consequently, if the RN is not temperature controlled, it can result in a higher rate of component failures [6]. The electrical power consumption at the RN is also considerable and the supply and maintenance of power is considered one of the main operational costs contributing to the high operating expenditure (OPEX) over the lifetime of an AON [7].

Passive optical networks (PONs), illustrated in Figure 1.4, historically have been the most widely deployed fibre-based access networks globally. Current growth in FTTH connections in Europe is running close to 20% annually [9]. Ultimately, FTTH is the end goal for service providers and given the cost sensitivity of new optical access deployments, PONs, employing a point-to-multipoint topology, have been deemed the most cost effective architecture to realise FTTH.

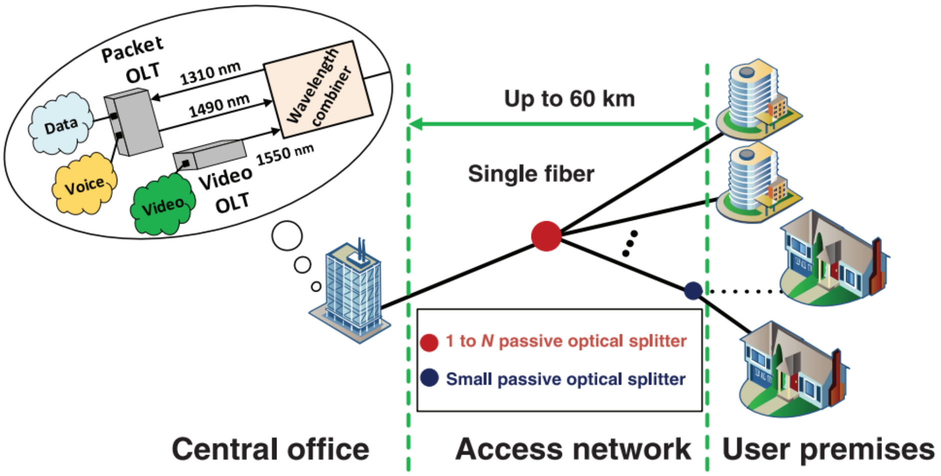

Figure 1.4: PON topology point-to-multipoint (P2MP) scheme [8].

1.3 Passive Optical Networks (PONs)

PONs typically employ a tree-like, point-to-multipoint topology, where only the OLT, located in the central office (CO), and the ONUs require active components and passive optical components are used at the remote node (RN) in the ODN to connect each subscriber ONU to the OLT. The passive optical components can include power or wavelength splitters/combiners, which interconnect the different fibre sections from each subscriber ONU to the remote node (RN). The fact that the components used in the ODN are passive results in a more cost effective network when compared with AONs. The initial cost for deployment of PONs is lower than AONs, and given the lower energy consumption and improved reliability of PONs, the costs for running and maintaining the network over its lifetime are considerably lower. The key elements of a PON are displayed in Figure 1.5. It shows the optical line terminal (OLT) located in the central office (CO), which serves as the interface between the access network and the metropolitan and core networks, the optical network unit (ONU), which, in the case of FTTH or FTTB, is located at the subscriber's premises and connects to the PON equipment at the subscriber side. Also shown is the optical distribution network (ODN), which connects the OLT to the ONU and comprises the fibres and the passive optical power splitter in the remote node [10].

The operation of a typical PON may be described as follows. For downstream transmissions, multiple data streams, each of which are assigned to a subscriber, are encoded and multiplexed in an optical signal that is transmitted from the OLT through the feeder fibre down to the passive splitter located in the ODN. The passive splitter produces replicas of the multiplexed signal and each replica is then transmitted to the different ONUs. When the optical signal is detected by the photo-receiver at the subscriber's ONU, the data that was destined for the subscriber is extracted from the multiplexed data stream and sent to the subscriber.

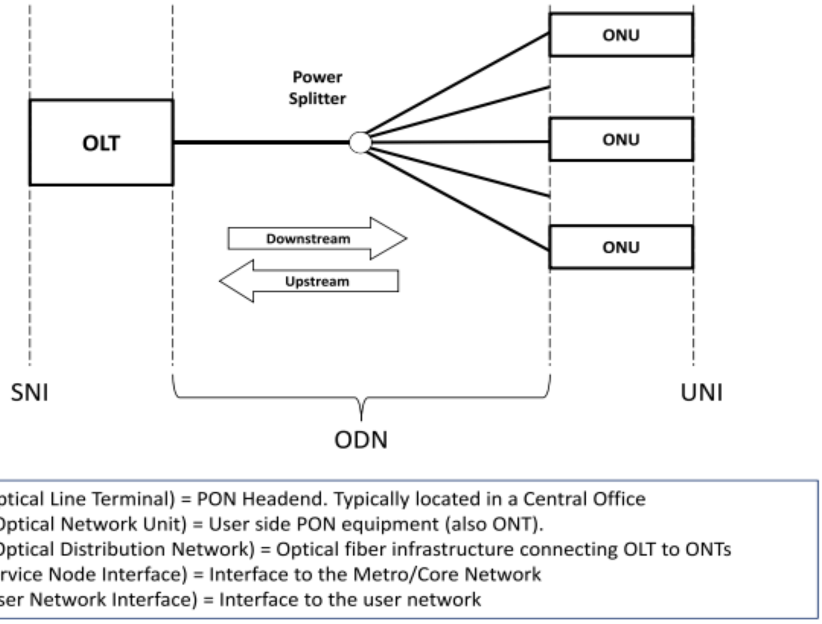

OLT (Optical Line Terminal) = PON Headend. Typically located in a Central Office
ONU (Optical Network Unit) = User side PON equipment (also ONT).
ODN (Optical Distribution Network) = Optical fiber infrastructure connecting OLT to ONTs
SNI (Service Node Interface) = Interface to the Metro/Core Network
UNI (User Network Interface) = Interface to the user network

Figure 1.5: PON Architecture and Terminology [10].

For upstream transmissions, each ONU encodes the subscriber's information in an optical signal which is then transmitted to the passive component at the RN in the ODN and transmitted upstream through the feeder fibre to the receiver at the OLT [11]. As shown in Figure 1.5, multiple subscriber ONUs are connected to the same OLT via the feeder fibre, which is shared among all of the subscribers. The number of ONUs serviced per OLT, is defined by the splitting ratio, typically 1:32 (15-dB loss) or 1:64 (18-dB loss). In typical PONs, the standardised distance between the ONU and OLT is 20 or 40 km. Given that there is no amplification or dispersion compensation between the multiple ONUs and OLT, the PON requires high optical power budgets, between 20 to 40 dB. In order to meet the power budget requirements, PONs require high power transmitters and very sensitive receivers, such as avalanche photodiodes (APDs). Forward error correction (FEC) codes can be employed to enhance receiver sensitivity, where a pre-FEC bit-error ratio (BER) of 10^{-3} is generally sufficient to obtain error-free transmission. The pre-FEC back-to-back (b2b) receiver sensitivity, $P_{Pre-FEC}$, is defined as the optical power on the receiver for a BER of $1\text{x}10^{-3}$ when the transmitter is connected directly to the receiver (b2b). The transmission power penalty, P_{PEN}, is the difference in power between the b2b receiver sensitivity and the sensitivity after transmission. The power budget, PB, of a PON may be defined by equation 1.1, where P_{Tx} is the fibre coupled transmitted signal optical power.

$$PB = P_{Tx} - P_{Pre-FEC} - P_{PEN} \qquad 1.1$$

Through the implementation of an appropriate multiplexing technology, or a combination of different multiplexing technologies, and the use of statistical aggregation of the data traffic based on end-user requirements, various types of PONs can be realised. Current PON standards, Ethernet PON (EPON) IEEE 802.3ah and Gigabit PON (GPON) ITU-T G.984, both employ time division multiplexing or multiple access (TDM/TDMA) technology, which allows the communications channel to be shared among all of the subscriber ONUs and a single wavelength channel is employed for both downstream and upstream transmissions. The majority of currently deployed PONs are G-PON systems with asymmetric speeds of 2.5 Gbit/s and 1.25 Gbit/s in the downstream and the upstream respectively. The next-generation ITU-T PON standard (NG-PON2) will be a time and wavelength division multiplexed (TWDM) PON. The NG-PON2 standard was finalised in 2015 in the ITU-T G.989 series of recommendations [12]. NG-PON2 will stack multiple TDM-PONs on a dense wavelength division multiplexed (DWDM) wavelength grid. The initial implementations of NG-PON2 will employ four wavelength channels with a fixed 100 GHz spacing between 1596 and 1603 nm and utilise standard on-off-Keying (OOK) modulation to achieve an aggregated capacity of 40 Gbit/s (4×10 Gbit/s) in the downstream direction. For transmission in the upstream direction, four wavelengths, each with a bit rate of 2.5 Gbit/s, will be employed to achieve an aggregated capacity of 10 Gbit/s with channel spacings of 200, 100 and 50 GHz.

Various multiplexing technologies were considered [10] prior to finalisation of the NG-PON2 standard, including time division multiplexing (TDM-PON), wavelength division multiplexing (WDM-PON) and orthogonal frequency division multiplexing (OFDM-PON), however, as previously mentioned, it was a hybrid of time and wavelength division multiplexing (TWDM-PON) technology that was finally chosen [10]. The different multiplexing technologies considered for NG-PON2 and the TWDM technology, which was finally chosen, are discussed in the following sections.

1.3.1 Time Division Multiplexed PON (TDM-PON)

As previously mentioned, the method by which the communications channel is shared among end-user ONUs in existing PON deployments is based on time division multiplexing (TDM) technology. This is reflected by the previous PON standards, Ethernet PON (EPON) IEEE 802.3ah and Gigabit PON (GPON) ITU-T G.984, both of which use Time Division Multiple Access (TDMA) as a means for channel sharing. With TDMA, each subscriber is allocated a time slot in which they can access the available bandwidth. The allocation of time slots is carried out in the medium access control or MAC layer which schedules what ONU has access to the network at any given time and dynamic bandwidth allocation algorithms at the OLT determine the amount of bandwidth that is made available to each ONU [6]. A passive power splitter is used to split the multiplexed signal transmitted from the OLT downstream to the ONUs, while also serving as a means to couple the upstream data from the subscribers into the feeder fibre back to the OLT. For downstream transmission, the multiplexed signal is transmitted to all of the subscribers and each subscriber ONU decodes only the data received within the timeslot that has been allocated to it by the OLT. For upstream transmission, the OLT assigns the time slots used by each subscriber to transmit their data in such a way so that there is no overlap of the data streams. As previously mentioned, typical downstream and upstream data rates for existing PON deployments are 2.5 Gbit/s and 1.25 Gbit/s, respectively. As an upgrade to EPON and GPON, 10 gigabit PON solutions are now available providing 10 Gbit/s aggregate data rates and symmetric transmission downstream and upstream over a single wavelength or channel. These 10 gigabit PON networks have been standardised by the IEEE and the ITU-T in 10G-EPON and XG-PON/XGS-PON, respectively. Both 10G-EPON and XG-PON/XGS-PON are also TDMA-based standards. A typical TDM-PON system is shown in Figure 1.6.

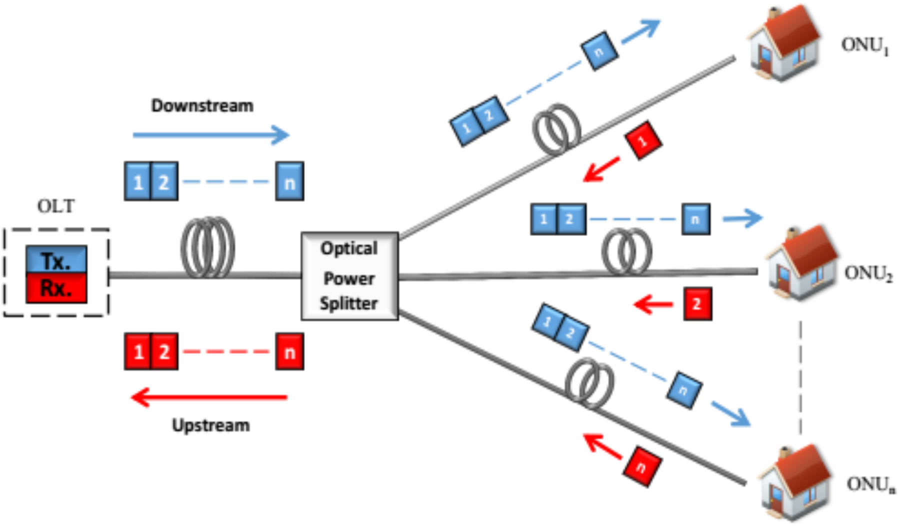

Figure 1.6: Typical TDM PON system configuration with power splitter as a passive remote terminal [13].

The time division multiplexing technology proposed for NG-PON2 was very similar to what is used in existing PON systems which employ a single wavelength for downstream transmission and a single wavelength for upstream transmission. To increase the downstream line rate of the PON to 40 Gbit/s the use of duobinary modulation was proposed, this would have also allowed 20 GHz bandwidth receivers to be used at the ONUs, while simultaneously reducing the dispersion power penalty [10]. To provide sufficient link budget, strong forward error correction (FEC) from low density parity check codes was also suggested, and the use of a bit-interleaving protocol was proposed in the downstream to reduce power consumption and the processing burden at the ONU [10]. In TDM-PON, the signals from the OLT incur high insertion losses at the passive power splitters located in the ODN. Ultimately, this sets a limit on the power budget of the link, and, consequently, a limit on the reach or transmission distance. As the number of ONUs which the OLT serves increases, it only further exacerbates the problem of limited optical power budget of the link. Additionally, as there are only two separate single wavelength channels used for both downstream and upstream transmission, which are shared among all of the ONUs, using this proposed technology would make it difficult to scale the network to higher line rates and bandwidths which will no doubt be a requirement in the near future.

It is universally recognised that TDM technology exploits only a small fraction of the huge potential that fibre optic communications can offer access networks and PONs. As a result, wavelength division multiplexed (WDM) technology was also proposed for NG-PON2 as a means to enhance the available bandwidth and improve the quality of service, as WDM is generally considered to be a more efficient way of utilising the available spectrum and the large bandwidth offered by the fibre channel.

1.3.2 Wavelength Division Multiplexed PON (WDM-PON)

In wavelength division multiplexed (WDM) PONs, either one or two wavelength channels may be assigned to each individual end-user for downstream and upstream transmission, however, if wavelength reuse is implemented, only one wavelength channel is assigned to each subscriber for both downstream and upstream transmission [10]. The passive power splitter located at the RN in the ODN used in TDM-PONs is replaced with a passive wavelength division multiplexing and de-multiplexing component, typically an AWG (arrayed waveguide grating) based router [14]. The WDM-PON architecture is similar to the PtP architecture in that it can provide a PtP logical (virtual) link to each subscriber [15], that is, independent connections can be created between the OLT and each individual subscriber ONU. This means that in WDM-PONs there is no competition for bandwidth between individual subscribers and each ONU has its own dedicated bandwidth. It also results in the WDM-PON being transparent to modulation formats and bit rates and the data rate and bandwidth which the network operator can provide each subscriber is limited only by the data rate supported by the transceiver [15]. Additionally, the limits imposed on the optical power budget in WDM-PON are less strict than that of TDM-PON, as the AWG that replaces the passive power splitter introduces less losses (2.5-6 dB) and is independent of the number of channels or ONUs [15]. The basic architecture of a WDM-PON is shown in Figure 1.7.

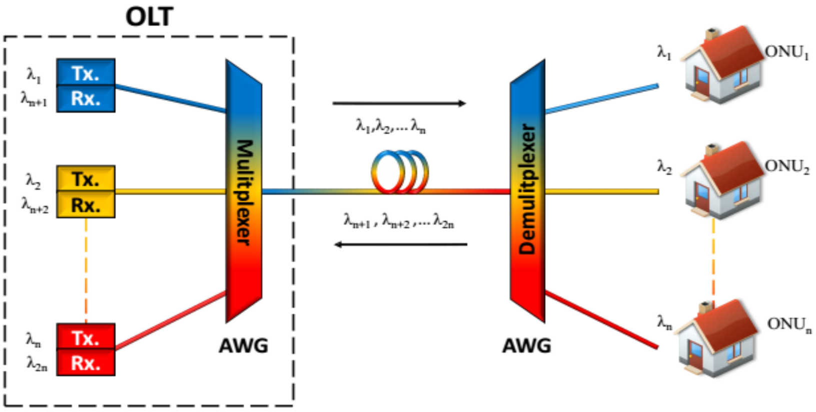

Figure 1.7: Basic WDM-PON system configuration with AWG at remote node [13].

One of the drawbacks of WDM-PONs is the necessity for either wavelength-selective or wavelength-specific (“coloured”) components at customer ONUs. The wavelength-specific or “coloured” operation is difficult for network operators to implement as it creates inventory management issues, and the wavelength selective operation is too expensive, considering the current state-of-the-art of available technology [15]. An alternative to this is to develop WDM-PONs using “colourless” components at the ONUs. In order to facilitate colourless operation, wavelength tunable transmitters and receivers are necessary and the use of colourless solutions, such as tunable transceivers, would increase capital expenditure [10]. The scaling of the number of end-users on a network could also pose problems in the future for WDM-PONs, as it would require dense wavelength division multiplexing (DWDM) technologies. Up until now DWDM has only been used in backbone and transport networks and the technology required to implement DWDM in optical access would be, at present, cost prohibitive [15]. Also, considering that each subscriber ONU has its own dedicated bandwidth, this means that it is not possible to utilise dynamic bandwidth allocation and statistical multiplexing. Another drawback of WDM-PONs is that a transceiver is required at the OLT for every subscriber ONU, similar to PtP fibre-based access, and this has associated issues regarding capital cost, power consumption and space to house the components. A future solution to this lies in silicon photonics or photonic integration, whereby multiple transceivers can be monolithically integrated providing a single packaged transceiver array [10], [15]. Field trials of WDM-PON systems are limited but some have been carried out in South Korea [16], Taiwan [17] and Austria [18].

A number of concepts regarding how WDM-PON could be implemented in NG-PON2 were studied including; externally seeded WDM-PON, wavelength re-use WDM-PON, tunable WDM-PON, ultra-dense coherent WDM-PON and self-seeded WDM-PON [10].

1.3.3 Hybrid TWDM-PON and NG-PON2

A number of technologies were considered for the next generation PON standard NG-PON2. The continuing use of TDM-PON was considered, which would require the replacement of old technologies with more advanced equipment and the implementation of complex modulation formats with digital signal processing techniques to replace the simple on-off keying (OOK) scheme. A number of WDM concepts were also considered, based on extensive academic research carried out in the community, as were OFDM PONs [15], [19]. However, it was a hybrid of time and wavelength division multiplexing (TWDM-PON) that was finally chosen for NG-PON2 and was first standardised by the ITU-T in 2013 in G.989.1 [20] – [22]. NG-PON2 is the first standard to be developed that provides transmission rates beyond 10 Gbit/s operation and was a big evolutionary jump from the previous PON standards, as it introduced multi-wavelength operation and WDM technology to increase the aggregate bandwidth to

40 Gbit/s. TWDM-PON was chosen for NG-PON2 primarily for its compatibility with pre-existing PON deployments, specifically in terms of the ODN equipment. Two other major factors which determined TDWM-PON being chosen were the relative complexity of the components that would be required in the systems and the industry wide support from major players. Figure 1.8 shows a basic schematic of the ITU-T standardised TWDM system architecture of NG-PON2 with high level features. NG-PON2 will stack multiple TDM-PONs, as per existing TDM-PONs, on a dense wavelength division multiplexed (DWDM) wavelength grid. For downstream transmission, initial implementations of NG-PON2 systems will use four wavelength channels, between 1596 and 1603 nm, with a channel spacing of 100 GHz and each wavelength capable of transmitting at 10 Gbit/s, using standard OOK modulation, to achieve an aggregated data rate of 40 Gbit/s.

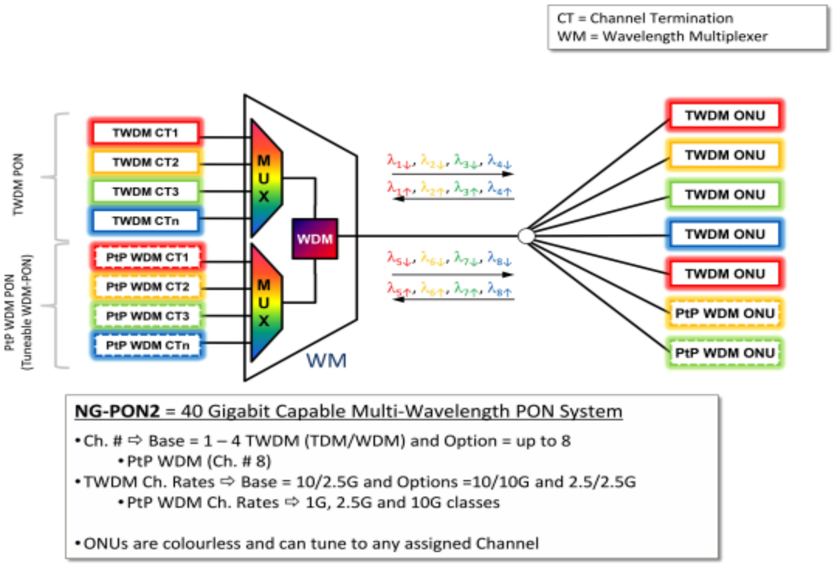

CT = Channel Termination
WM = Wavelength Multiplexer

NG-PON2 = 40 Gigabit Capable Multi-Wavelength PON System

- Ch. # ⇨ Base = 1 – 4 TWDM (TDM/WDM) and Option = up to 8
    - PtP WDM (Ch. # 8)
- TWDM Ch. Rates ⇨ Base = 10/2.5G and Options =10/10G and 2.5/2.5G
    - PtP WDM Ch. Rates ⇨ 1G, 2.5G and 10G classes

- ONUs are colourless and can tune to any assigned Channel

Figure 1.8: NG-PON2 system architecture and high level features. Note that the internal configuration of the WDM is just for illustration and is not defined by ITU-T recommendations [10].

In the upstream direction, four wavelengths with a bit rate of 2.5 or 10 Gbit/s can be used to establish an aggregated capacity of 10 or 40 Gbit/s, respectively. To account for the variation in the wavelength control capabilities of the different ONU transceiver technologies available, the upstream wavelength channels can be chosen in the narrow (1532-1540 nm), reduced (1528-1540 nm) or wide (1524-1544 nm) wavelength bands. The channel spacings will be 50, 100 and 200 GHz, as in dense WDM metro systems where volume manufactured C and L band multiplexers are utilised. NG-PON2 will be capable of serving multiple subscribers in homes, offices or via RF antennas from the same ODN. Subscribers will need to be able to receive information on any of the incoming wavelengths and will also need to be capable of transmitting their upstream bursts on one of the assigned wavelengths, thus, dynamic allocation of wavelength channels and time slots will be required. Fixed wavelength receivers and transmitters will be employed in the OLTs, as with legacy PONs, and passive power splitters will be utilised in the ODNs.

The most radical change to NG-PON2, when compared with legacy PONs, will be to the transceiver technologies employed at the ONUs. The ONUs will require tunable transceivers so that they can selectively transmit and receive in upstream and downstream wavelength channels, that is, the ONUs will need to be colourless, in order to avoid ONU inventory issues for network operators [10]. Tunable optical filters will need to be employed for wavelength selectivity at the ONUs, while tunable 'burst-mode' transmitters will also be required at the ONUs for selective upstream transmission to the OLT. Several technology options exist as possible solutions for implementation in the ONUs to achieve the required wavelength tunability, however, the availability of cost-effective tunable devices will most certainly be the driver for the successful and timely deployment of NG-PON2 networks.

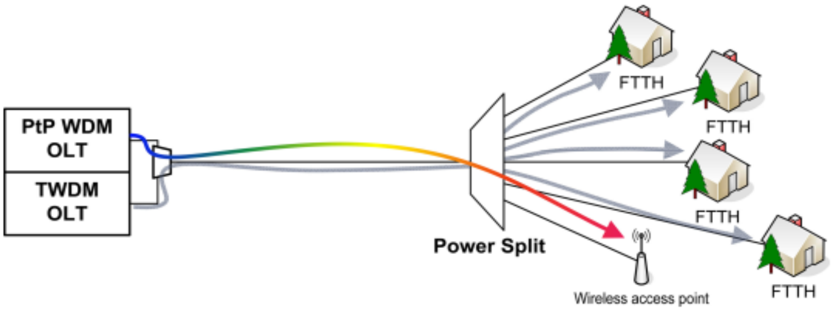

Figure 1.9: NG-PON2 architectural approach with TWDM-PON overlaid with PtP WDM PON to meet the diverse service requirements of FTTH and Wireless Backhaul [10].

An addition to the TWDM-PON technology in NG-PON2 is the Point-to-Point WDM Overlay (PtP WDM), which will serve as a dedicated wavelength channel provided to each ONU that will be directly linked to a single OLT. This will support potential high demand business and backhaul services, where TDM sharing is not desirable [10]. Figure 1.9 illustrates the NG-PON2 architectural approach with TWDM-PON overlaid with PtP WDM PON. As with TWDM-PON, cost effective tunable transceivers are also required for PtP WDM PON. The main difference between the PtP WDM and TWDM PON is that the transceivers in PtP WDM are operated in continuous mode, as opposed to burst mode operation for TWDM-PON. Bit-rate classes have been defined for PtP WDM spanning 1-10 Gbit/s [10].

Several technologies have the potential to impact the development of future high data rate single-wavelength channel PONs that could also serve as a per-wavelength upgrade for NG-PON2 [23], [24]. The technologies include advanced multi-level modulation formats beyond NRZ-OOK such as PAM formats [25] and optical duobinary format [26], [27], DSPs [28], multicarrier modulation techniques such as OFDM [29] and discrete multi-tone (DMT) modulation [30] and coherent detection [31], which would enable the use of higher-order modulation formats such as QAM [32], and DP-QPSK [33].

1.4 Summary

This chapter provided an overview of optical access networks and the evolution of PON architectures, from the widely deployed single channel E-PON and G-PON systems, to the migration towards 10G capable 10G-EPON and XG-PON, and the recently standardised NG-PON2. The ultimate goal for network operators is to have each end-user as close to the optical network as possible, thus, realising Fibre-to-the-Home or Premises (FTTH/-P) and this is reflected by the gradual replacement of copper cables in the access network domain with the superior performing and cost-comparable fibre-based PON technologies. Prior to the introduction of NG-PON2, legacy PON standards and deployments have been based on bi-directional TDM/TDMA technologies, where a single wavelength or channel is used to transmit data with the standard NRZ-OOK modulation format. To date, the transmission speeds and bandwidth that the legacy optical access technologies and TDM-based PONs provide have been sufficient. However, with the bandwidth and data rates that these legacy networks can provide fast approaching their limit, next generation PONs are required, which provide increased throughput and greater bandwidth flexibility.

The evolution of optical access networks and PONs has been predominantly driven by the cost of the optical networking components and the performance enhancement of legacy PONs has been largely limited by the availability of cost-effective optical components capable of operating beyond 10 Gbit/s. To overcome the bandwidth limitations of current 10G class optical components, wavelength division multiplexing (WDM) technology and more spectrally efficient modulation formats have been included in the recent NG-PON2 standardisation [12]. Thus, allowing the large bandwidth offered by the single-mode fibre to be further exploited. However, with the introduction of WDM technology to the recent NG-PON2 standard, and its anticipated implementation in future PONs and optical access networks, the availability of cost-effective “colourless” optical components and tunable transmitters that enable the realisation of wavelength agile, adaptive and reconfigurable PONs, which can support dynamic bandwidth allocation and network provisioning based on traffic and end-user demands, has never been more crucial.

References

[1] Cisco, 'Cisco Visual Networking Index: Forecast and Trends, 2017–2022', February 2019, White Paper.

[2] V. Vujicic, "Optical multicarrier sources for spectrally efficient optical networks," Ph.D. Thesis*,* Dept. Elect. Eng., Dublin City Univ., Dublin, Ireland, 2015.

[3] C. H. Lee and S. G. Mun, "WDM-PON Based on Wavelength Locked Fabry-Perot LDs," J. Opt. Soc. Korea, vol. 12, no. 4, pp. 326–336, 2008, doi: 10.3807/JOSK.2008.12.4.326.

[4] Y. Fujimoto, "Application of ethernet technologies to FTTH access systems," IEICE Trans. Commun., vol. E89-B, no. 3, pp. 661–667, 2006, doi: 10.1093/ietcom/e89-b.3.661.

[5] J. Chen, L. Wosinska, C. M. MacHuca, and M. Jaeger, "Cost vs. reliability performance study of fiber access network architectures," IEEE Commun. Mag., vol. 48, no. 2, pp. 56–65, 2010, doi: 10.1109/MCOM.2010.5402664.

[6] T. Koonen, "Fiber to the home/fiber to the premises: What, where, and when?," Proc. IEEE, vol. 94, no. 5, pp. 911–934, 2006, doi: 10.1109/JPROC.2006.873435.

[7] C. P. Larsen, A. Gavler., and K. Wang, "Comparison of active and passive optical access networks," 2010 9th Conf. Telecommun. Media Internet, CTTE 2010, pp. 1–5, 2010, doi: 10.1109/CTTE.2010.5557694.

[8] T. Horvath, P. Munster, V. Oujezsky, and N. H. Bao, "Passive optical networks progress: A tutorial," Electron., vol. 9, no. 7, pp. 1–31, 2020, doi: 10.3390/electronics9071081.

[9] FTTH Council Europe – Panorama, "New Market Panorama and Forecast data at the FTTH Conference 2019," FTTH Council Europe Conference – March 12-14th, 2019 –Amsterdam, https://www.ftthcouncil.eu/documents/PressReleases/2019/PR%20Market%20Panorama%20-%2014-03-2019%20V3.pdf

[10] D. Nesset, "NG-PON2 technology and standards," J. Light. Technol., vol. 33, no. 5, pp. 1136–1143, 2015.

[11] F. A. G. Uruñuela, "High-Capacity Multicarrier Electro-Optical Transceivers based on Analogue Signal Processing," Ph.D. Thesis*,* Dept. Elect. Eng., Dublin City Univ., Dublin, Ireland, 2016.

[12] ITU-T Telecommunication Standardization Sector of ITU: "40-Gigabit-capable passive optical networks 2 (NG PON2): Physical media dependent (PMD) layer specification, Corrigendum 1. Recommendation ITU-T G.989.2 (08/2019) – Corrigendum 1.

[13] E. Martin, "Photonic Generation of Millimetre Waves for Radio over Fibre Distribution Systems," Ph.D. Thesis, Dept. Elect. Eng., Dublin City Univ., Dublin, Ireland, 2015.

[14] I. M. M. Mohamed and M. S. Bin Ab-Rahman, “Options and challenges in next-generation optical access networks (NG-OANs),” Optik (Stuttg)., vol. 126, no. 1, pp. 131–138, 2015, doi: 10.1016/j.ijleo.2014.08.131.

[15] T. Muciaccia, F. Gargano, and V. Passaro, “Passive Optical Access Networks: State of the Art and Future Evolution,” Photonics, vol. 1, no. 4, pp. 323–346, 2014.

[16] C.-H. Lee et al., “WDM-PON experiences in Korea [Invited],” J. Opt. Netw., vol. 6, no. 5, p. 451, 2007, doi: 10.1364/jon.6.000451.

[17] S. Tu, H. Lin, C. Wang (et al.), “The Pilot Trial of Colorless WDM PON System in Taiwan,” The 16th Opto-Electronics and Communications Conference, pp. 2–3, OECC 2011.

[18] S. Pachnicke et al., “Field demonstration of a tunable WDM-PON system with novel SFP+ modules and centralized wavelength control,” 2015 Optical Fiber Communications Conference and Exhibition (OFC), Los Angeles, CA, 2015, pp. 1-3.

[19] N. Cvijetic, “OFDM for Next-Generation Optical Access Networks,” in Journal of Lightwave Technology, vol. 30, no. 4, pp. 384-398, Feb.15, 2012, doi: 10.1109/JLT.2011.2166375.

[20] W. Pöhlmann and T. Pfeiffer, “Demonstration of wavelength-set division multiplexing for a cost effective PON with up to 80 Gbit/s upstream bandwidth,” 2011 37th European Conference and Exhibition on Optical Communication, Geneva, pp. 1-3, 2011.

[21] ITU-T Telecommunication Standardization Sector, “ITU-T 40-Gigabit-capable passive optical networks (NG-PON2): General requirements,” ITU-T Recommendation G.989.1, 2013.

[22] Y. Luo et al., “Time- and Wavelength-Division Multiplexed Passive Optical Network (TWDM-PON) for Next-Generation PON Stage 2 (NG-PON2),” in Journal of Lightwave Technology, vol. 31, no. 4, pp. 587-593, Feb.15, 2013, doi: 10.1109/JLT.2012.2215841.

[23] P. Iannone, D. van Veen, A. Gnauck and V. Houtsma, “Extending capacity in access beyond NG-PON2: WDM vs. TDM,” 2015 European Conference on Optical Communication (ECOC), Valencia, 2015, pp. 1-3, doi: 10.1109/ECOC.2015.7341663.

[24] D. Zhang, D. Liu, X. Wu and D. Nesset, “Progress of ITU-T higher speed passive optical network (50G-PON) standardization,” in IEEE/OSA Journal of Optical Communications and Networking, vol. 12, no. 10, pp. D99-D108, October 2020, doi: 10.1364/JOCN.391830.

[25] J. Zhang et al., "Demonstration of 100-Gb/s/λ PAM-4 Transmission Over 45-km SSMF using one 10G-Class DML in the C-Band," 2019 Optical Fibre Communications Conference and Exhibition (OFC), San Diego, CA, USA, 2019, pp. 1-3.

[26] F. Qamar, M. K. Islam, S. Z. Ali Shah, R. Farhan and M. Ali, "Secure Duobinary Signal Transmission in Optical Communication Networks for High Performance & Reliability," in IEEE Access, vol. 5, pp. 17795-17802, 2017, doi: 10.1109/ACCESS.2017.2752002.

[27] Z. Li, L. Yi, X. Wang, and W. Hu, "28 Gb/s duobinary signal transmission over 40 km based on 10 GHz DML and PIN for 100 Gb/s PON," Opt. Express 23, 20249-20256 (2015).

[28] X. li, S. Zhou, F. Gao, m. luo, Q. Yang, Q. Mo, Y. Yu, and S. Fu, “4×28 Gb/s PAM4 Long-Reach PON Using Low Complexity Nonlinear Compensation,” in Optical Fibre Communication Conference, OSA Technical Digest (online) (Optical Society of America, 2017), paper M3H.4, 2017.

[29] Z. Zhang, Q. Zhang, J. Chen, Y. Li, and Y. Song, “Low-complexity joint symbol synchronization and sampling frequency offset estimation scheme for optical IM/DD OFDM systems,” Opt. Express, vol. 24, pp. 12577-12587, 2016.

[30] A. Udalcovs et al., "Towards 25+Gbpsλ IM-DD PON: NRZ, Duobinary, PAM4, and DMT Transmission and Optical Budget Comparison," 2019 21st International Conference on Transparent Optical Networks (ICTON), Angers, France, 2019, pp. 1-1.

[31] M. M. H. Adib et al., "Colorless Coherent Passive Optical Network using a Frequency Comb Local Oscillator," 2019 Optical Fibre Communications Conference and Exhibition (OFC), San Diego, CA, USA, 2019, pp. 1-3.

[32] Q. Zhou et al., "Symmetric Long-Reach 16-QAM Transmission using Lite Coherent Receiver for Next-Generation Optical Access Network," 2019 Optical Fiber Communications Conference and Exhibition (OFC), San Diego, CA, USA, 2019, pp. 1-3.

[33] S. Porto, D. Carey, N. Brandonisio, A. Naughton, C. Antony, P. Ossieur, N. Parsons, G. Talli, PD. Townsend, "Point-to-point overlay of a 100Gb/s DP-QPSK channel in LR-PONs for urban and rural areas," Opt Express, 5;26(3):3303-3319, 2018. doi: 10.1364/OE.26.003303.

Chapter 2 Direct vs External Modulation of Lasers for Next Generation PONs

2.1 Introduction

Current TDMA PONs employ direct modulation of single mode devices at 2.5 Gbit/s as this is the lowest cost option for a cost sensitive market such as access networks. For core and metropolitan networks, where per channel data rates are 10 Gbit/s and beyond, external modulation is typically employed, as the frequency chirp associated with direct laser modulation severely limits the transmission distances and data rates that can be achieved in the 1.55 μm window over standard single-mode fibre (SSMF) [1]. Moreover, external modulation, using IQ modulators, are required to generate spectrally efficient modulation formats, such as DP-QPSK, which are widely utilised in high capacity transmission systems. As optical access networks migrate towards higher data rates and potentially increased transmission distances [2], it is likely that external modulation will need to be considered and compared with direct modulation (DM) solutions in terms of system performance, complexity and cost.

Directly modulated tunable lasers, such as the thermally tunable DFB laser, are, at present, the most cost-effective tunable laser solution for NG-PON2 and IM/DD access networks. Furthermore, by employing DMLs, the insertion losses of external modulators can be avoided, thus, allowing the power budget of the access network to be maximised. However, it is difficult for standard DM DFB lasers to transmit beyond distances of ~15 km, due to the frequency chirp of DMLs, and the interplay between the chirp and the chromatic dispersion in standard single-mode fibre (SSMF) in the C-band. Techniques to overcome the transmission distance limitations, due to the chirp-dispersion interaction, have been developed [3] – [13], yet the majority of the techniques are too impractical or complex to be employed in the field. The limited extinction ratios (~8-10 dB) and modulation bandwidths (~10 GHz) of DMLs pose additional challenges for optical access networks, however, solutions to enhance data rates using advanced modulation formats can overcome the bandwidth limitation [14]. A cost-effective DML that achieves 12.5 Gbit/s C-band transmission over SSMF distances >15 km remains challenging, as the intrinsic chirp of DMLs ultimately limits the reach of the link and the data rates that can be employed.

Currently, the most promising alternatives to the cost-effective directly modulated (DM) thermally tunable DFB laser are the tunable externally modulated laser (EML) [15] – [17], which comprise an electro-absorption modulator (EAM) monolithically integrated with a thermally tunable DFB laser. Thus, tunable EMLs seem to be the most viable near-term alternative to DM thermally tunable DFB lasers. The implementation of tunable EMLs in future optical access will significantly enhance the data rate and reach that can be achieved due to the reduced frequency chirp of EMLs. Key considerations for tunable EMLs in future PONs will be the footprint of the devices, the cost and power consumption, hence, photonic integration will be imperative [18]. Nonetheless, the frequency chirp of EMLs, albeit greatly reduced when compared to DMLs, can also limit the transmission distances that these optical sources can achieve. More importantly, the limited optical power of EMLs, due to insertion or coupling losses (in the range of 3-5 dB power loss), is an additional disadvantage.

In this chapter, two single-channel C-band transmitters, a directly modulated multiple quantum well (MQW) DFB laser (DML) and an electro-absorption modulated (EAM) laser (EML), are experimentally characterised and the transmission performances of both devices modulated with standard NRZ-OOK modulation at a rate of 12.5 Gbit/s in an IM/DD test-bed are evaluated. The transmission performances of the DML and EML are evaluated for back-to-back (b2b) transmission and SSMF transmission. Measurements of the bit-error ratio (BER) performance as a function of received signal optical power and eye diagrams of the received signals are used to assess the transmission performance. Numerical models developed in MATLAB are employed to simulate the characteristics and transmission performances of both devices in the IM/DD test-bed. The numerical models are employed to estimate the chirp or alpha parameters, α, of the DML and EML, along with the magnitude of the frequency chirp exhibited by the devices under large signal 12.5 Gbit/s NRZ-OOK modulation. Particular attention is given to the frequency chirp of the DML and EML, as the interplay between the chirp of transmitted optical signals and the chromatic dispersion in optical fibre results in dispersive optical pulse broadening and inter-symbol interference (ISI), which can severely limit the transmission performance of PON links.

2.2 Direct Modulation of DFB Laser (DML)

This section presents the experimental characterisation and transmission performance evaluation of the DML, as well as the numerical modelling that was carried out to assess the chirp characteristics of the DML. The DML is a C-band (1537-1565 nm) InGaAsP/InP multi-quantum well (MQW) distributed feedback (DFB) laser with a 3-dB electrical bandwidth rating of 10 GHz, a typical linewidth rating of 1 MHz and an average relative intensity noise (RIN) of -150 dBc/Hz. Figure 2.1 shows an image of the DFB laser. The device is housed within a 7 pin butterfly package and contains a thermo-electric cooler (TEC), thermistor, back facet monitor detector, bias tee and an internal optical isolator.

(a) (b)

Figure 2.1: (a) Image of InGaAsP/InP multi-quantum well (MQW) DFB laser diode housed in a 7 pin butterfly package and (b) schematic of laser.

A polarization maintaining (PM) pigtailed fibre provided the output from the laser. The RF input to the device was a K-type connector, which enabled the direct modulation of the laser. The DFB laser was mounted on a printed circuit board for safety and ease of use.

2.2.1 Device Characterisation

Experimental characterisation of the MQW DFB laser was carried out to determine the optimal drive settings to directly modulate the laser with the 12.5 Gbit/s NRZ-OOK signal before its implementation in the IM/DD test-bed. It allowed for important parameters, such as the laser threshold current, I_{th}, and the modulation bandwidth, $f_{3\ dB}$, to be ascertained. It also allowed the extinction ratios, ER, and the 3-dB bandwidths, Δv_{3dB}, of the optical signals transmitted from the DFB laser under large-signal modulation, to be determined. The static characterisation of the MQW DFB laser was performed with the laser dc biased. Static characterisation includes measurement of the optical power output from the laser as a function of varying dc bias current and capturing the optical spectrum of the lightwave output from the laser during continuous wave (CW) operation. The P-I curve of the DFB laser and the optical spectrum captured from the laser are shown in Figure 2.2 and Figure 2.3, respectively.

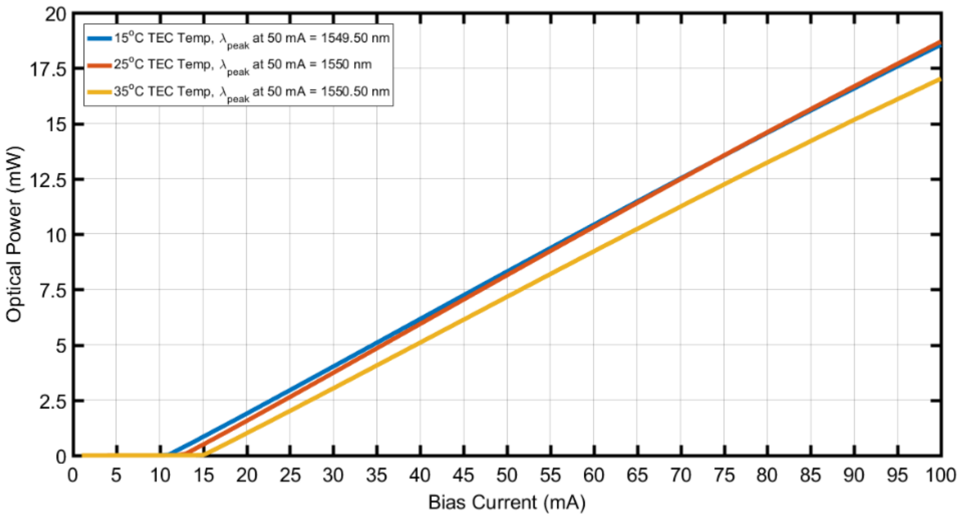

Figure 2.2: P-I curves for 15°C (blue curve), 25 °C (red curve) and 35 °C (yellow curve) TEC temperatures.

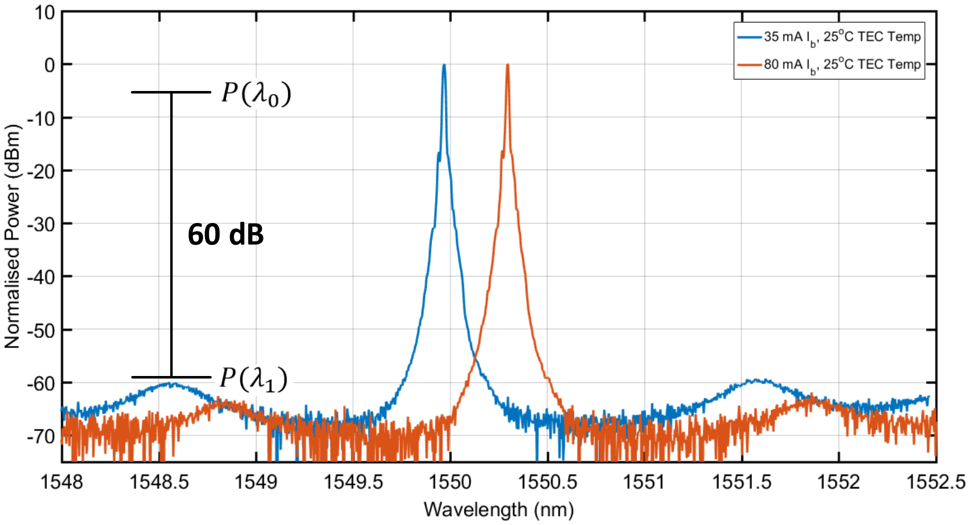

Figure 2.3: Optical spectra captured from DFB laser at 35 mA bias (blue spectrum) and 80 mA bias (red spectrum).

It may be observed in the P-I curve shown in Figure 2.2 that the threshold currents, I_{th}, for the DFB laser at 15, 25 and 35°C thermoelectric cooler (TEC) temperatures are 11, 13 and 15 mA respectively, indicating a ~0.2 mA variation in I_{th} per 1 degree change in temperature. The slope efficiencies, $\frac{dP}{dI}$, extracted from the P-I curves for the DFB laser operating at 15, 25 and 35°C TEC temperatures are 0.21, 0.216 and 0.202 mW/mA, respectively. The optical spectra shown in Figure 2.3 were captured with the Yokogawa OSA using a 0.02 nm/~3 GHz spectral resolution. In the spectra captured from the DFB laser biased at 35 and 80 mA, side modes appear ~1.5 nm from the main lasing mode. However, the modes are supressed significantly and the side-mode suppression ratio (SMSR), which provides an indication of the degree of single-mode operation of the laser, is ~60 dB. In general, an SMSR of >30 dB is required for optimal single-mode laser operation. For fibre optic communications, single-mode lasers typically require SMSR values of 40 dB or higher for optimal signal transmission. The peak wavelengths, λ_{peak}, of the spectra for the DFB laser biased at 35 and 80 mA are 1549.97 and 1550.29 nm, respectively, and this corresponds to a wavelength shift of ~7 pm per 1 mA change in the dc bias current. The wavelength shift is essentially due to heating of the device with increasing bias current. Varying the dc bias current to the laser enables the wavelength to be detuned. However, a more efficient method of wavelength detuning is achieved through variation of the device temperature, which is the detuning method employed with thermally tunable DFB lasers. Typically, a ~0.1 nm change in the λ_{peak} of the lasing mode is observed for a 1°C change in temperature.

Small-signal analysis of the MQW DFB laser was also performed to determine the 3-dB modulation bandwidth, f_{3dB}. The results of the small-signal analysis are shown in Figure 2.4. From Figure 2.4, the measured values of $f_{3\ dB}$ for the DFB laser biased at 30, 40, 50 and 60 mA are ~8, 10, 12 and 14 GHz, respectively, and the corresponding relaxation oscillation frequencies, f_R, occur at ~6, 8, 9 and 11 GHz, respectively.

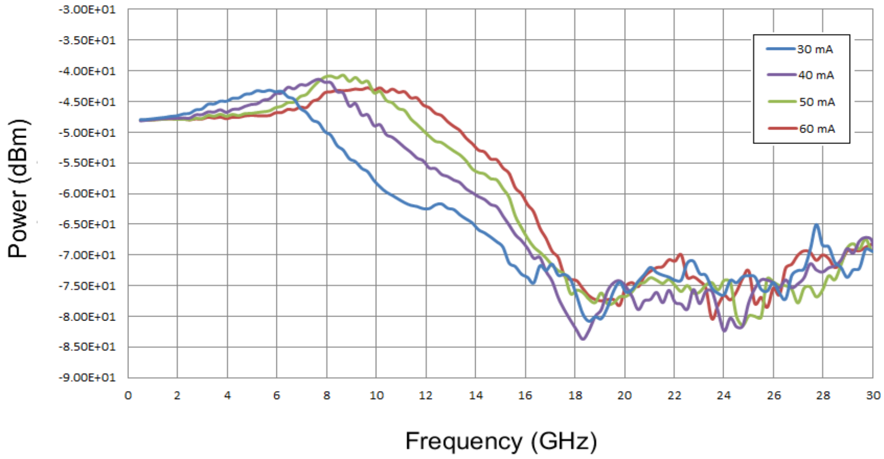

Figure 2.4: DFB laser IM frequency response for 30 mA (blue), 40 mA (purple), 50 mA (green) and 60 mA (red) bias currents.

For the small-signal modulation response of a DFB laser, the relaxation oscillation frequency, f_R, and the modulation bandwidth, $f_{3\,dB}$, increases with increasing photon density or output optical power due to the increase in the dc bias current applied to the laser. The flattening of the response and the reduction in the amplitude of the RO peak is a result of the increase in the damping rate and the K-factor, which can be attributed to the decrease in the differential gain, $\frac{dg}{dN}$, occurring as a result of increasing gain compression. The increased damping of the RO frequency, and the flattening of the modulation response at higher laser bias currents and output optical power, ultimately imposes a limit on the modulation bandwidth of the laser.

2.2.1.1 Large-signal intensity modulation (IM) analysis

Optical waveform analysis

The large-signal analysis of the DFB laser involved directly modulating the laser with a 12.5 Gbit/s NRZ-OOK signal and capturing optical eye diagrams and spectra at the output of the DML for different laser bias currents, I_b, and modulating signal amplitudes, I_m. From the captured eye diagrams and spectra, the extinction ratios, ER, ER power penalties, δ_{ER}, and the optical bandwidths, Δv_{3dB}, of the signals transmitted from the DML, were determined. A detailed qualitative analysis of the optical spectra was also carried out. The experimental setup employed to perform the large-signal modulation analysis is shown in Figure 2.5. The baseband 12.5 Gbit/s NRZ-OOK signal used to directly modulate the laser was generated using a pulse pattern generator (PPG) employing a pseudo random binary sequence (PRBS) of word length 2^{15}-1. A dc block was employed at the RF input to the laser via the bias tee to remove any parasitic dc signal that may have been present in the modulating signal output from the PPG.

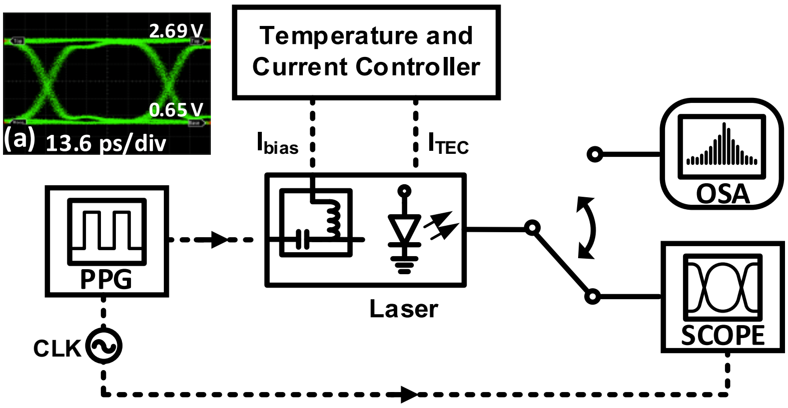

Figure 2.5: Schematic of experimental set up for large-signal modulation analysis of laser, inset (a) showing eye diagram of 12.5 Gbit/s NRZ modulating signal.

The optical eye diagrams were captured with the dc coupled photodetector integrated in the sampling oscilloscope. Three different modulating signal amplitudes, 2 V_{pp} (40 mA), 1 V_{pp} (20 mA) and 0.5 V_{pp} (10 mA), were evaluated with laser bias currents ranging from 20 to 90 mA. The laser bias current was swept from 20 to 90 mA in increments ranging from 2.5 to 10 mA for the three different modulating signal amplitudes. Eye diagrams were captured at each incremental change to the laser bias current. Considering that the photodetector (PD) employed to detect the optical signals was dc coupled and the measurement was limited only by the intrinsic thermal noise of the PD, the extinction ratio, ER, in decibels, and the ER power penalty, δ_{ER}, could be calculated using equations 2.1 and 2.2 [19] – [21]

$$ER\ (dB) = 10\log_{10}\left(\frac{P_1}{P_0}\right) \quad 2.1 \qquad\qquad \delta_{ER}\ (dB) = 10\log_{10}\left(\frac{ER+1}{ER-1}\right) \quad 2.2$$

where P_1 and P_0 are the average optical powers of the “1” and “0” binary levels of the transmitted signal waveform, respectively. Following analysis of the data extracted from the eye diagrams, the extinction ratios, ER, and ER power penalties, δ_{ER}, of the transmitted optical signals, were calculated. Figure 2.6 shows the measured extinction ratios, ER, (blue curves) and ER power penalties, δ_{ER}, (red curves) of the optical signals transmitted from the DML as a function of laser bias current for the 2 V_{pp} (magenta dots), 1 V_{pp} (cyan dots) and 0.5 V_{pp} (yellow dots) modulating signal amplitudes. From Figure 2.6, it can be observed that the 35 mA laser bias and the 2 V_{pp} modulating signal amplitude produce the optical signal transmitted from the DML exhibiting the highest ER and lowest ER power penalty, δ_{ER}. This is due to the DML being driven with the largest modulating signal amplitude as close as possible to the threshold of 13 mA without the optical signal being affected by the spontaneous emission noise of the laser below threshold. As a result, the lowest possible optical power is being transmitted in the “0” or “off” level of the signal waveform for the 2 V_{pp} modulating signal amplitude. It may also be observed that the ER and ER power penalty, δ_{ER}, decreases and increases for increasing laser bias current and decreasing modulating signal amplitude, respectively.

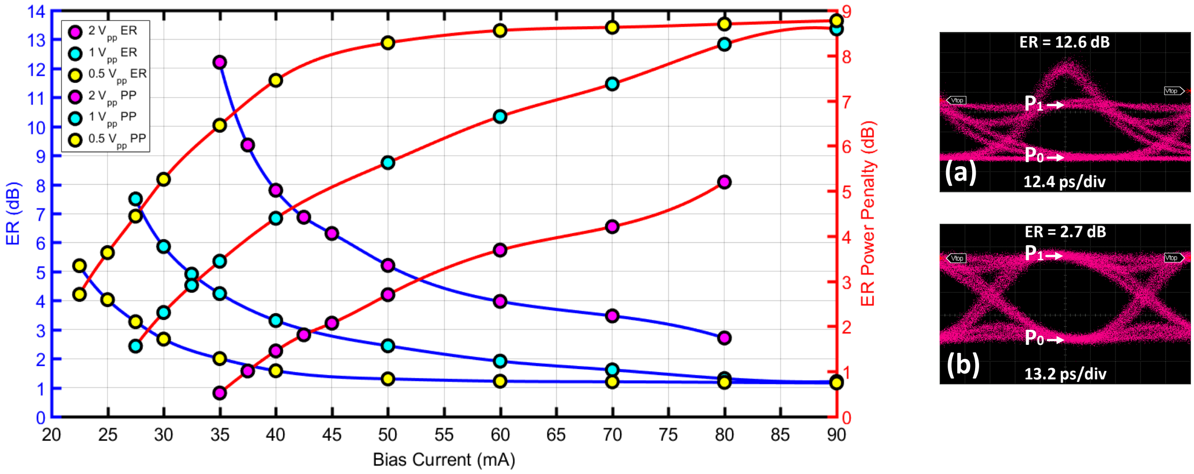

Figure 2.6: DFB laser optical extinction ratio, ER, (blue curves) and ER power penalty, δ_{ER}, (red curves) as a function of dc laser bias for 0.5 V_{pp} (yellow dots), 1 V_{pp} (cyan dots), 2 V_{pp} (magenta dots), modulating signal amplitudes. Insets (a) and (b) show the optical eye diagrams captured from the DML for the 2 V_{pp} modulating signal amplitude when biased at 35 and 80 mA, respectively. The "1" and "0" binary levels, P_1 and P_0, of the transmitted signal waveforms, which were used in the calculations of the extinction ratios, are illustrated in insets (a) and (b).

The ER measurements of the transmitted signals provide an indication as to which DML bias current and modulating signal amplitude would yield the highest SNR at the photodetector in the IM/DD test-bed and, consequently, produce the lowest BER for b2b transmission. Following the time-domain analysis of the optical signal waveforms transmitted from the DML under large-signal modulation, optical spectral analysis of the signals was carried out. Analysis of the optical spectrum of a signal transmitted from a DML provides an insight into the frequency chirp properties of the signal.

DML frequency chirp

When a laser is directly modulated, the time-varying injection current modulates the carrier density, which, in turn, modulates the gain of the laser resulting in the intensity modulation of the optical signal output from the DML. However, variations in the carrier density also causes variations in the refractive index of the active region, Δn. As a result, the instantaneous phase of the optical signal output from the DML will also be modulated, following the profile of the carrier density variation. The variation in the instantaneous phase of the optical signal, $\Delta\phi(t)$, causes changes in the instantaneous frequency of the signal, $\Delta\nu(t) = \frac{1}{2\pi}\frac{d\phi(t)}{dt}$, about the unmodulated carrier, which is known as frequency chirp. The frequency chirp causes the instantaneous frequency of the optical pulses, which represent the bits or symbols in the transmitted signal, to vary in time over the duration of each pulse. In IM/DD links employing DMLs, the frequency chirp leads to undesirable spectral components in the modulated optical signal which broadens the width of the optical signal spectrum. The spectral broadening can severely degrade the transmission performance of high-speed fibre optic communications links due to the temporal broadening of the transmitted optical pulses, which occurs as a result of the interplay of the DML chirp and the chromatic dispersion in standard single-mode fibre (SSMF). The broadened spectrum of the transmitted optical signal also reduces the bandwidth efficiency of the optical fibre link when wavelength division multiplexing (WDM) is employed. Therefore, the frequency chirp of a DML is an extremely important laser parameter in fibre optic communications. From the single-mode laser rate equations A.2 and A.3, shown in Appendix A [22], and the expression for the steady-state output optical power equation A.4, an equation for the frequency chirp, or the instantaneous frequency deviation, Δv, of a directly modulated single-mode laser can be derived, and is given as [23] – [26]

$$\Delta v(t) = \frac{1}{2\pi}\frac{d\phi(t)}{dt} = \frac{\alpha}{4\pi}\left(\frac{d}{dt}[\ln P(t)] + \kappa P(t)\right) \qquad 2.3$$

Equation 2.3 provides the large-signal expression for the frequency chirp in relation to the DML output optical power. The first term in equation 2.3, $\frac{d}{dt}[\ln P(t)]$, represents the device structure-independent transient or derivative chirp. The transient chirp is proportional to the derivative of the logarithm of the optical power output from the DML and leads to frequency excursions at the transitions between the “low” and “high” power levels of the optical signal waveform, or at the rising and falling edges of the optical pulses that comprise the transmitted signal. The second term in the equation, i.e. $\kappa P(t)$, represents the structure-dependent and frequency-independent adiabatic chirp. The parameter κ in equation 2.3 is the adiabatic chirp coefficient and it is related to the gain compression factor, ε, the laser active layer volume, V, and the confinement factor, Γ, by $\kappa = \frac{2\Gamma}{\eta h v V}\varepsilon$ [27]. The adiabatic chirp is directly proportional to the optical signal power output from the DML and generates a frequency or wavelength shift (offset) between the steady-state “high” and “low” power levels of the optical signal waveform. Both the transient and adiabatic chirp are a result of variations in the refractive index of the active region of the laser due to the injection current, which produces a variation in the optical path length of the laser cavity. It is clear from equation 2.3 that both the transient and adiabatic chirp components are scaled by the parameter, α, which is known as the linewidth enhancement factor, or the Henry alpha factor. The magnitude of the chirp exhibited by a DML is largely dependent on the linewidth enhancement factor, α, which provides a measure of the coupling strength between the intensity and frequency modulation (FM) of the laser. The linewidth enhancement factor, α, relates the real part of the refractive index, n', of the laser active region, to the imaginary part of the refractive index, n'', as shown in equation 2.4 [28], [29]. Through the Kramers-Kronig relation, any variation in the gain (or absorption) of the laser active region, due to variations in the imaginary part of the refractive index, $\Delta n''$, resulting from changes to the carrier density, will be accompanied by variations in the real part of the refractive index, $\Delta n'$, or the real part of the refractive index, n', undergoing some modulation.

$$\alpha = \left(\frac{\Delta n'}{\Delta n''}\right) = -\frac{dn'/_{dN}}{dn''/_{dN}} = -\frac{4\pi}{\lambda}\left(\frac{dn/_{dN}}{dg/_{dN}}\right) \qquad 2.4$$

Variation in the refractive index, Δn, where $\Delta n = \Delta n' + i\Delta n''$, of the active region alters the phase of the frequency components of the optical pulse and hence results in frequency chirp.

Optical spectrum analysis

To perform the large-signal optical spectral analysis of the DML, the output of the DML was connected to the Apex OSA, which was set to its highest resolution of 0.16 pm, corresponding to a bandwidth of ~20 MHz. As the 2 V_{pp} 12.5 Gbit/s NRZ-OOK modulating signal yielded the highest extinction ratio for the 35 mA laser bias current, optical spectra were only captured from the DML for the 2 V_{pp} modulating signal amplitude when biased at 35, 50, 65 and 80 mA. Figure 2.7 shows the optical spectra captured from the large-signal analysis of the DML. Figure 2.7 insets (b) and (c) show the optical eye diagrams of the signals transmitted from the DML modulated with the 2 V_{pp} signal and biased near threshold at 35 mA (~3x I_{th}) and well above threshold at 80 mA (~6x I_{th}), respectively. The overshoot following the "0" to "1" bit transitions in the eye diagram shown in Figure 2.7 inset (b) is indicative of a DML that is being driven near threshold, where the transient chirp is large and the damping of the relaxation oscillation, γ_R, is low. The ER measured from the eye diagram of the signal transmitted from the DML biased at 35 mA is 12.6 dB, and was the highest ER obtained. In contrast, the eye diagram of the signal transmitted from the DML biased at 80 mA exhibits no overshoot and the upper and lower levels of the eye are more defined and the crossings are more symmetrical than in the eye captured from the DML biased at 35 mA. The considerable reduction in the overshoot is a result of the increase in bias current, the increase in output optical power (photon number) and the increase in the damping of the relaxation oscillations. The ER of the signal transmitted from the DML biased at 80 mA is 2.7 dB, and the ~10 dB reduction in ER is due to the large increase in the optical power being transmitted in the "0" or "off" level of the signal waveform, which is a consequence of the DML being driven well above threshold.

Figure 2.7 inset (a) shows the electrical spectrum of a 12.5 Gbit/s NRZ-OOK signal simulated in MATLAB using a 2^{15}-1 PRBS pattern length. A 2nd order Butterworth low pass filter (LPF) was employed to reduce the bandwidth of the electrical signal. Thus, the simulated electrical signal essentially represents an ideal spectrum of a 12.5 Gbit/s NRZ-OOK data signal. The envelope of the double sideband spectrum approximates a sinc^2(f) function and the spectral nulls that occur at intervals of 12.5 GHz are characteristic of the NRZ data format. The 3, 10 and 20 dB electrical bandwidths of the NRZ-OOK signal spectrum are ~10, 15 and 20 GHz, respectively. For an EML that is modulated with a 12.5 Gbit/s NRZ-OOK signal, the optical spectrum of the signal transmitted from the EML would exhibit similar bandwidths as the spectrum of the electrical modulating signal. However, the bandwidths of the optical spectrum captured from a DML that is modulated with a 12.5 Gbit/s NRZ-OOK signal can vary significantly to the bandwidths of the spectrum of the electrical modulating signal, depending on the bias current applied to the DML, the modulating signal amplitude and the large-signal modulation dynamics of the DML.

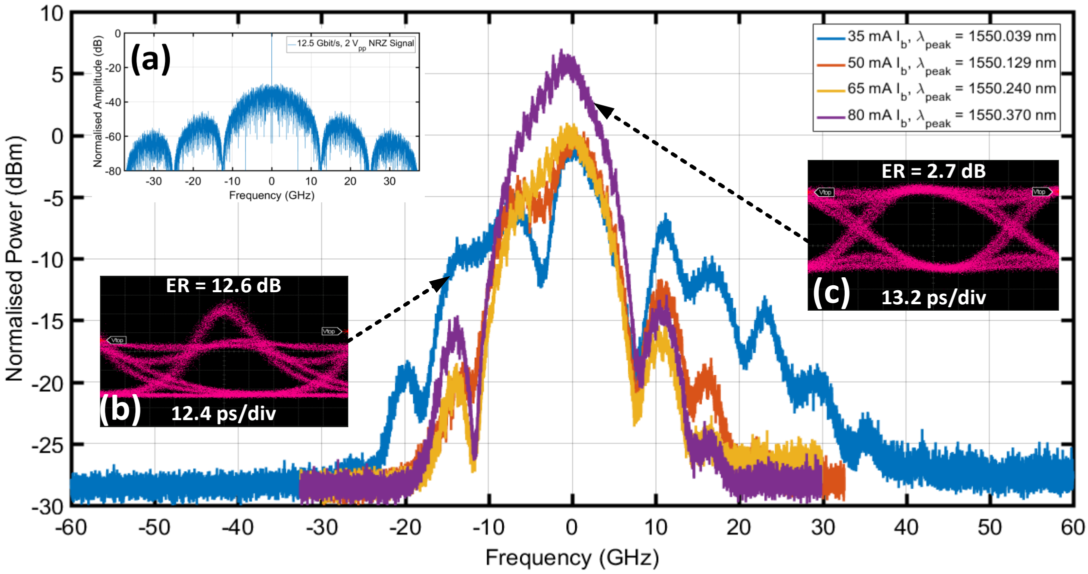

Figure 2.7: Optical spectra captured from the DFB laser for the 2 V_{pp} modulating signal amplitude and 35 mA (blue spectrum), 50 mA (red spectrum), 65 mA (yellow spectrum) and 80 mA (purple spectrum) laser bias currents, inset (a) shows the double sided spectrum of an simulated (ideal) 12.5 Gbit/s ZRZ modulating signal and insets (b) and (c) show the optical eye diagrams captured from the DML for the 2 V_{pp} modulating signal amplitude and biased at 35 and 80 mA, respectively.

The optical bandwidths of the spectra shown in Figure 2.7, captured from the DML biased at 35 mA (blue spectrum), 50 mA (red spectrum), 65 mA (yellow spectrum) and 80 mA (purple spectrum) when modulated with the 2 V_{pp} 12.5 Gbit/s NRZ-OOK signal, were measured at 3, 10 and 20-dB down from the spectral peaks to determine the degree of spectral broadening due to the direct modulation. To estimate the optical bandwidths of the spectrum captured from the DML biased at 35 mA, a peak finding and curve fitting algorithm was employed in MATLAB to approximate the spectral envelope. The 3, 10 and 20-dB optical bandwidths (blue curves), measured from the spectra, and the extinction ratios ER (red curve), measured from the optical eye diagrams, of the signals transmitted from the DML for the 2 V_{pp} modulating signal amplitude, are displayed in the graph shown in Figure 2.8 as a function of laser bias current. Analysis of the optical spectra shown in Figure 2.7 reveals further insights into the properties of the signals transmitted from the DML as the bias current to the laser was increased. The following analysis of the spectra is similar to the method of analysis employed in previous work [30], [31]. The optical power of the spectra have been normalised and the peak frequencies of each of the spectra have been normalised with respect to their nominal zero frequencies, which corresponds to the peak or centre frequency of the spectrum during continuous wave (CW) operation of the laser.

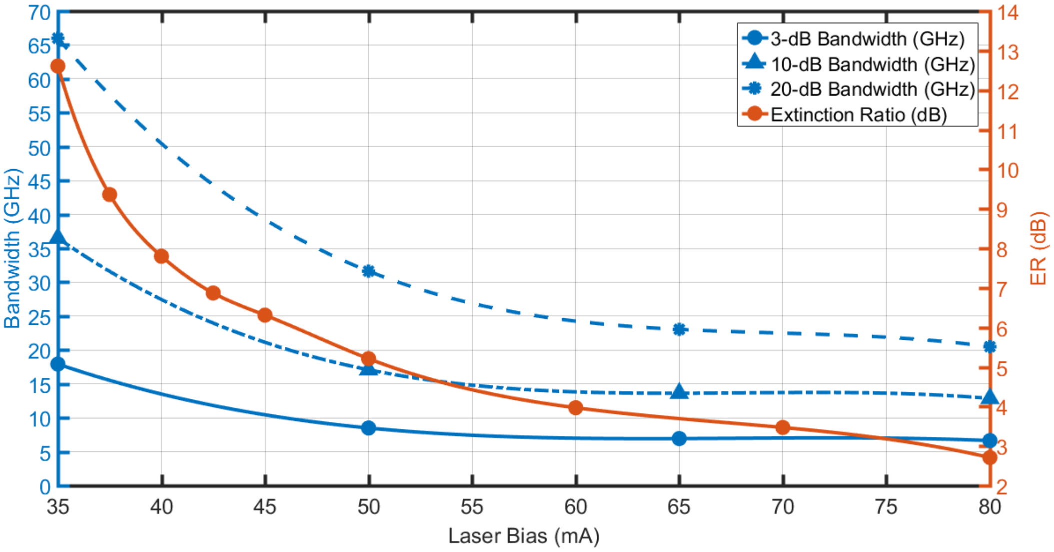

Figure 2.8: Graph of 3-dB (solid blue curve with dots), 10-dB (dashed blue curve with triangles) and 20-dB (dashed blue curve with asterisks) optical bandwidths and ERs (red curve) of transmitted optical signals from DML as a function of laser bias current for 2 V_{pp} modulating signal amplitude.

The peak wavelengths of the four modulated signal spectra in nanometres (nm), prior to being centred at their respective nominal zero frequencies, are shown in the legend in Figure 2.7. The peaks of the modulated signal spectra were normalised with respect to their nominal zero frequencies so that the relative spectral bandwidth variation of the four spectra with increasing laser bias could be determined. Furthermore, this allowed any discernible offset of the peak frequencies of the modulated signal spectra from their respective nominal zero frequencies to be identified, as an offset would indicate the presence of adiabatic chirp in the transmitted signal [31]. Numerical modelling of the spectra of optical signals transmitted from adiabatic chirp dominated DMLs in previous work [31], displayed two distinct peaks corresponding to the frequencies of the “1” and “0” bits, which, consequently, allowed the magnitude of the adiabatic chirp to be quantified.

For the optical spectrum captured from the DML biased at 35 mA, the estimated optical bandwidths of the signal 3, 10 and 20-dB down from the spectral peak are ~18, 36.5 and 66 GHz, respectively. The 3-dB bandwidth, Δv_{3dB}, is ~8 GHz higher than the 10 GHz electrical bandwidth of the 12.5 Gbit/s NRZ-OOK modulating signal. Thus, indicating significant broadening of the optical spectrum due to the high frequency content of the signal, which may be attributed to frequency chirp as a result of the direct modulation. Based on the appearance of the spectrum, the frequency chirp is predominantly transient in nature, which is due to the laser being driven near threshold. The peaks and dips that appear in the spectrum on the higher frequency side of the peak from ~+10 to +30 GHz are indicative of transient chirp. The peaks and dips represent the average of many brief, high-power, high-frequency, excursions that occur during the under-damped transition between the "0" and "1" binary levels [32], which correlates with the overshoot observed in the eye diagram captured from the DML biased at 35 mA shown in Figure 2.7 inset (b). There is no measureable offset of the peak of the spectrum from the nominal zero frequency, which is typical of DMLs that are transient chirp dominated [31]. Moreover, two distinct peaks corresponding to the frequencies of the "1" and "0" bit levels cannot be discerned. Thus, any adiabatic chirp in the signal spectrum is masked by the transient chirp and, hence, the magnitude of the adiabatic chirp cannot be ascertained. In view of the eye diagram of the transmitted signal and the width and characteristics of the optical spectrum, it may be concluded that the optical signal output from the DML when biased at 35 mA and modulated with the 2 V_{pp} 12.5 Gbit/s NRZ-OOK signal, is transient chirp dominated.

As the bias current to the DML is increased from 35 mA to 50, 65 and 80 mA, the 3-dB bandwidth, Δv_{3dB}, of the optical signal spectrum reduced from ~18 GHz to 8.5, 6.9 and 6.6 GHz, respectively. The 3-dB bandwidth of the spectrum captured from the DML biased at 80 mA is approximately half the data rate of the 12.5 Gbit/s NRZ-OOK modulating signal and the significant reduction in the 3-dB bandwidth, by ~3.4 GHz below the ~10 GHz bandwidth of the 12.5 Gbit/s NRZ-OOK modulating signal, can be attributed to the enhancement of the non-linear gain compression due to gain saturation that occurs with increasing bias current to the laser well above threshold. This leads to a reduction in the differential gain and, consequently, an increase in the damping. The most notable difference between the spectra captured from the DML biased at 80 mA and 35 mA, is that the peaks and dips that were observed in the spectrum captured from the DML biased at 35 mA, which appeared on the higher frequency side of the peak from ~10 to 30 GHz, are no longer visible. Thus, indicating a reduction in the transient chirp as the bias current to the laser is increased. The reduction in the overshoot observed in the eye diagram captured from the DML biased at 80 mA, shown in Figure 2.7 inset (c), is further indication of the reduction in the transient chirp. This can be attributed to saturation in the optical power output from the laser as the bias current is increased above threshold, which results in the $\frac{d}{dt}[\ln P(t)]$ term in equation 2.3 approaching zero.

As before with the spectrum captured from the DML biased at 35 mA, there is no measureable offset of the peak of the spectra captured from the DML biased at 50, 65 and 80 mA from their respective nominal zero frequencies. Moreover, peaks corresponding to the "1" and "0" bits cannot be discerned, as the adiabatic chirp is still being masked by the transient chirp, thus, the magnitude of the adiabatic chirp of the transmitted signal cannot be established. A final observation of note in the spectrum captured from the DML biased at 80 mA, is that there is an asymmetry between the upper and lower side-bands (UPS and LPS) of the two sided signal spectrum. This asymmetry, or partial suppression of the shorter wavelength (higher frequency) side-band, in the spectrum of a signal transmitted from a DML has been reported in previous work [33], [34]. It suggests mixed frequency modulation and amplitude or intensity modulation (FM and IM) of the DML, as opposed to pure IM. For full suppression or cancellation of one of the side-bands to occur, it would require a particular balance between the IM and FM and for the IM and FM to be in phase, furthermore, the peak-to-peak chirp would need to be less than half the bitrate [34].

2.2.2 Transmission Performance Evaluation of DML

This section details the experimental work carried out to evaluate the transmission performance of the DML under 12.5 Gbit/s NRZ-OOK modulation in an IM/DD test-bed. The results obtained from the transmission experiments are analysed and discussed. The experimental setup of the IM/DD test-bed is shown in Figure 2.9. The transmission performance of the DML was evaluated for back-to-back (b2b) transmission initially to establish a performance baseline and to allow the minimum receiver sensitivities for error-free transmission, i.e. for a 10^{-10} BER, to be ascertained, where the transmission performance of the link is limited only by the performance of the transmitter and the photodetector. Having ascertained the minimum receiver sensitivities attainable for b2b transmission, various lengths of standard single-mode fibre (SSMF) were added to the link, to evaluate the effects of the interplay between the frequency chirp of the DML and the chromatic dispersion (CD) in the optical fibre on the link performance. To evaluate the transmission performance of the DML in the IM/DD test-bed, the 12.5 Gbit/s NRZ-OOK signal with a PRBS of word length 2^{15}-1, which was employed in the large-signal analysis, was again generated using the PPG and used to directly modulate the DFB laser via the bias tee. A dc block was also employed at the RF input to the laser via the bias tee.

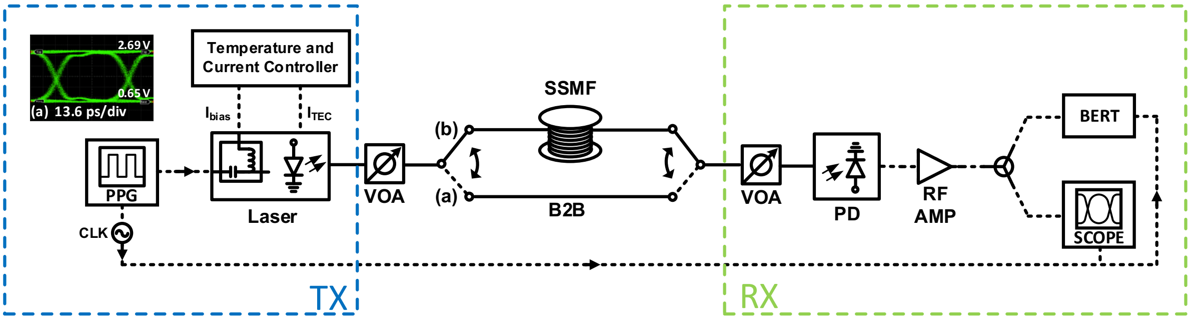

Figure 2.9: Experimental setup of IM/DD test-bed, inset (a) shows the eye diagram of the modulating signal from PPG.

Path (a) in the experimental setup of the IM/DD test-bed in Figure 2.9 indicates the optical path taken by the transmitted signal for b2b transmission. The APD and trans-impedance amplifier were operated at the recommended settings to minimise the shot noise. For a fixed DML bias and modulating signal amplitude, the optical signal output from the laser was transmitted to a variable optical attenuator (VOA), which allowed the optical power of the signal incident on the APD to be measured and varied. Following opto-electrical conversion of the signal by the APD, the electrical signal was amplified by a 10G class RF amplifier. The amplified electrical signal was then split using a 3-dB RF splitter, where one output of the splitter diverted half of the signal to the sampling scope for eye diagram generation and the second output of the RF splitter directed the other half of the signal to the BERT for bit-error ratio (BER) detection and counting. To generate the characteristic BER curves, the received optical power at which the BER result began to increase above error-free performance, i.e. >1x10^{-10}, was recorded along with the BER result. The received optical power was then reduced in increments of 1 dB and for each incremental reduction in the received power both the BER result and the corresponding received power were recorded. The BER measured as a function of received optical power for b2b transmission for different DML bias currents and modulating signal amplitudes, are shown in Figure 2.10.

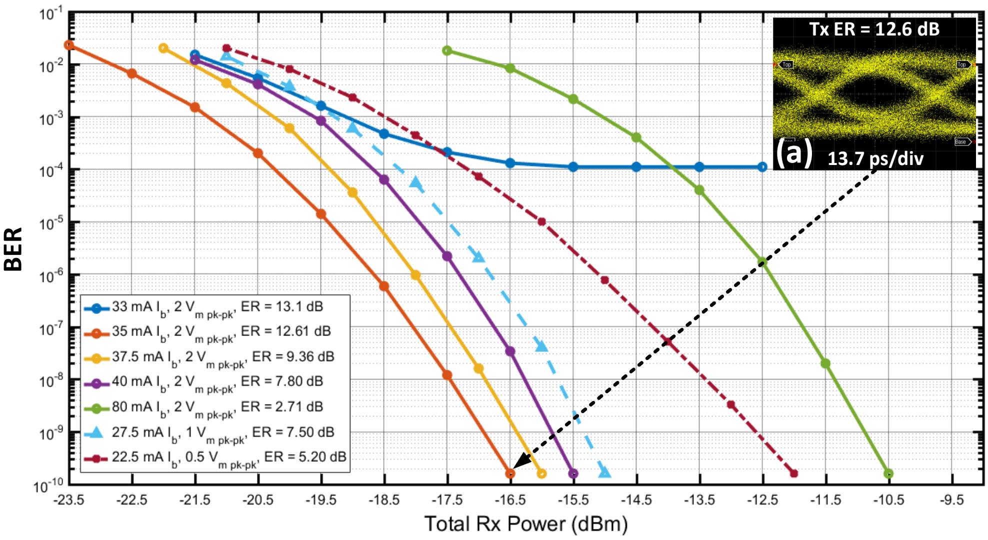

Figure 2.10: BER results for DML for b2b transmission in IM/DD test-bed using 12.5 Gbit/s NRZ-OOK modulation and various DML bias currents and modulating signal amplitudes, inset (a) shows the eye diagram of the electrical signal captured at the receiver for error-free transmission for the a DML bias of 35 mA and 2 V_{pp} modulating signal amplitude.

It can be observed in the BER results shown in Figure 2.10 that the DML for the 35 mA bias and 2 V_{pp} modulating signal amplitude, which also yielded the transmitted signal exhibiting the highest ER and lowest ER power penalty, δ_{ER} , produced the best b2b transmission performance. The received signal eye diagram shown in Figure 2.10 inset (a) was captured for error-free transmission with the DML for the 35 mA bias and 2 V_{pp} signal amplitude. The overshoot observed in the eye diagram of the optical signal transmitted from the DML, shown in Figure 2.7 inset (b), for the 35 bias and 2 V_{pp} modulating signal amplitude has been removed from the received signal eye diagram due to the low-pass filtering (LPF) effect of the APD. It may also be observed in the BER results that the receiver sensitivity degrades with decreasing transmitted optical signal ER, due to either the increasing laser bias or the decreasing amplitude of the modulating signal. The calculated transmitted signal ER power penalties, δ_{ER} , shown in the graph in Figure 2.6, correlate well with the reduction in receiver sensitivities observed in Figure 2.10. The poor transmission performance of the DML, when biased at 33 mA and modulated with the 2 V_{pp} signal (blue solid BER curve), is due to the DML being modulated near threshold and the resultant spontaneous emission noise of the laser destroying the quality of the transmitted signal.

Following the b2b transmission experiments, the transmission performance of the DML, biased at 35 mA and modulated with the 2 V_{pp} 12.5 Gbit/s NRZ-OOK signal, for transmission over 12.5, 25 and 37.5 km of SSMF, was evaluated. For the fibre transmission experiments, a second VOA was added to the experimental setup, as shown in Figure 2.9, to limit the optical power of the signal input to the fibre to <5 dBm. The second VOA was added to ensure that non-linear fibre effects would not affect the optical signal transmission [35]. Fibre attenuation was not considered an issue considering the high optical power of the signal transmitted from the DML and the transmission distances concerned. Path (b) in the experimental setup of the IM/DD test-bed shown in Figure 2.9 indicates the optical path taken by the signal transmitted from the DML for transmission over the SSMF. Using the BER measurement process that was employed before with the b2b transmission experiments, the BER was measured as a function of received optical power for transmission over 12.5 and 25 km of SSMF. The BER results for 12.5 km (red curve) and 25 km (yellow curve) SSMF transmission are shown in the graph displayed in Figure 2.11, along with the BER curve for b2b transmission (blue curve).

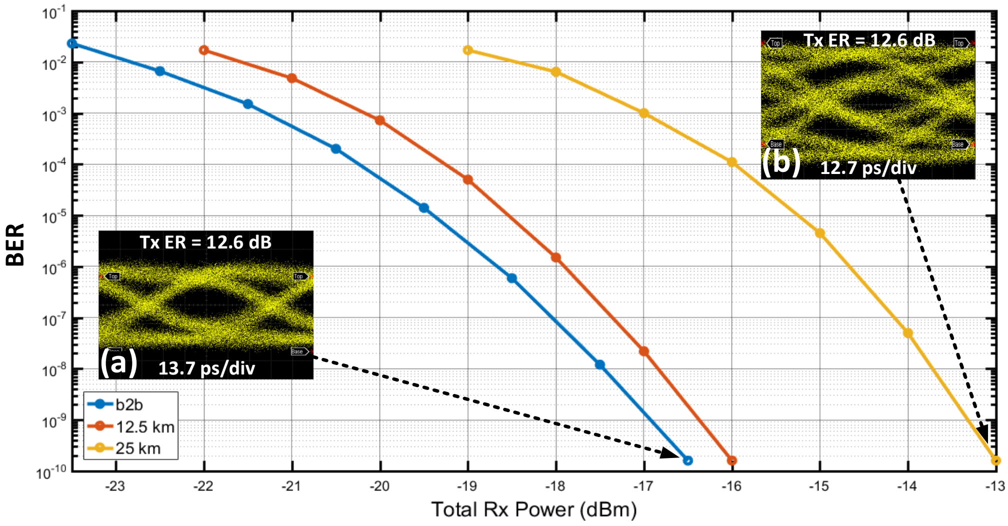

Figure 2.11: BER results for DML biased at 35 mA and modulated with the 2 V_{pp} 12.5 Gbit/s NRZ-OOK signal for b2b transmission (blue curve) and transmission over 12.5 km (red curve) and 25 km (yellow curve) of SSMF in IM/DD test-bed, inset (a) and (b) show the eye diagrams of the electrical signals captured at the receiver for error-free transmission for b2b transmission and transmission over 25 km of SSMF, respectively.

The effect of the chromatic dispersion (CD) in the SSMF on the transmission performance of the DML is evident from the BER results shown in Figure 2.11 and manifests as a receiver sensitivity penalty. A 0.5 dB receiver sensitivity penalty is incurred for transmission over 12.5 km of SSMF relative to b2b transmission at a BER of 10^{-9}. This is typical for a DML, as the accumulated CD over the 12.5 km of SSMF is low enough such that dispersive pulse broadening is negligible and significant ISI does not occur. However, for 25 km SSMF transmission, the accumulated CD increased such that the dispersive pulse broadening was no longer negligible, thus, a receiver sensitivity penalty, or dispersion power penalty, of 3.5 dB is incurred. The dispersive pulse broadening may be attributed to the interplay between the transient chirp dominated signal transmitted from the DML modulated near threshold and the CD in the fibre. The transient chirp of the optical pulses, which comprise the transmitted signal, exhibit blue- and red-shifted chirp at the rising and falling edges of the optical pulses respectively. The frequency dependent CD of the SSMF causes the rising edges of the pulses to travel faster in the fibre than the falling edges, hence, results in dispersive pulse broadening, which causes the energy of the “1” bits to spread into adjacent “0” bits and, in turn, produces ISI and closure of the eye diagram of the received signal. The effect of the dispersive pulse broadening and ISI on the transmission performance of the DML over 25 km of SSMF can be observed in the received signal eye diagram shown in Figure 2.11 inset (b) captured for error-free transmission. The multiple traces, or rising and falling double edges, are indication of dispersive pulse broadening, which results in the eye exhibiting a number of different traces for the “1” and “0” bits. The eye also appears asymmetric, further indication of dispersive pulse broadening. Furthermore, the eye does not appear to exhibit more noise than the eye diagram of the electrical signal captured for b2b transmission, shown in Figure 2.10 inset (a). Thus, the eye closure may be attributed entirely to dispersive pulse broadening and ISI due to the interplay between the transient chirp dominated DML and the CD in the SSMF.

Considering that 25 km SSMF transmission was achieved with the DML modulated near threshold, it indicates that the DML exhibits relatively low transient chirp, which can sometimes be the case with strained MQW DFB lasers [33], [36] – [40]. The low transient chirp of the strained MQW DFB laser may be attributed to an enhanced differential gain, $\frac{dg}{dN}$, and low differential index, $\frac{dn}{dN}$, and, given equation 2.4, results in a reduced phase-amplitude coupling coefficient or alpha parameter, α, value. Alpha parameter, α, values as low as 1 can be realised with strained MQW DFB laser diode designs. Hence, despite being modulated near threshold, a MQW DFB laser, such as the DML evaluated in this study, can exhibit relatively low transient chirp, and, as per equation 2.3, is due to the dependence of the magnitude of the transient chirp on the alpha parameter, α. Transmission over 37.5 km of SSMF was also attempted, however, the degree of dispersive pulse broadening and ISI was too great and signal transmission was not possible due to severe distortion of the received signal. Consequently, a BER measurement could not be acquired with the BERT, as it was unable to detect a signal. The electrical signal captured at the receiver for optical signal transmission over 37.5 km of SSMF, with the DML biased at 35 mA and modulated with the 2 V_{pp} 12.5 Gbit/s NRZ-OOK signal, is shown Figure 2.12 inset (a).

To ensure that a more suitable bias current for the DML when modulated with the 2 V_{pp} 12.5 Gbit/s NRZ-OOK signal was not being overlooked for transmission over 37.5 km of SSMF, a sweep of the laser bias current was performed for transmission over the 37.5 km of SSMF. To perform the bias current sweep, the amplitude of the modulating signal applied to the DML was maintained at 2 V_{pp} and the optical power of the signal at the receiver was kept constant at -14.5 dBm using the VOA at the input to the photodetector. The DML bias current was increased from 35 to 80 mA in 5 mA increments and at each incremental step in the bias current the BER was measured. BER results could not be acquired for the 35 and 40 mA DML bias current settings due to the degree of signal distortion, hence, the BER measurements begin at a laser bias of 45 mA. The results of the DML bias sweep are shown in Figure 2.12.

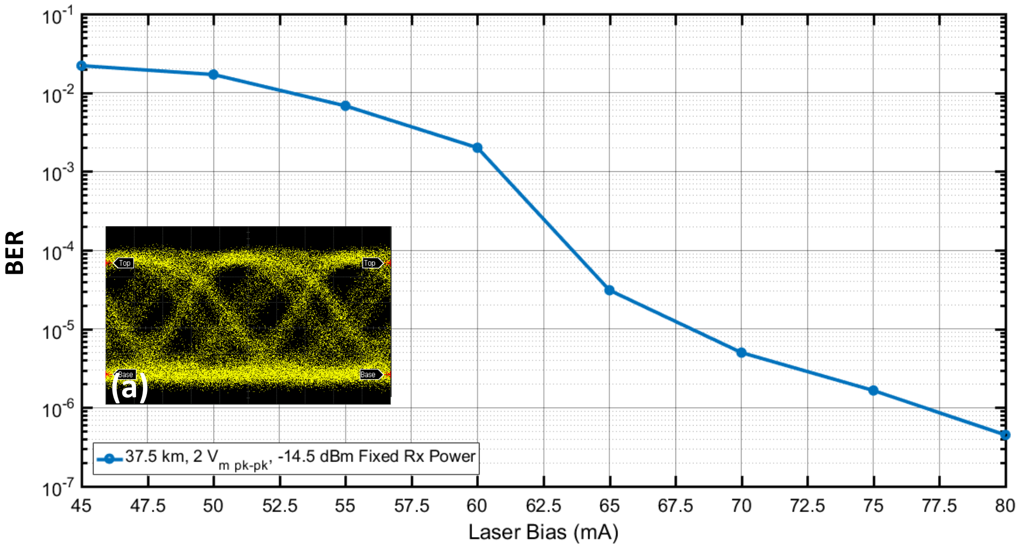

Figure 2.12: BER as a function of laser bias current for transmission over 37.5 km of SSMF at a fixed received optical power of -14.5 dBm for the DML modulated with a 2 V_{pp} 12.5 Gbit/s NRZ signal.

It can be observed in the results shown in Figure 2.12 that the BER reduces as the DML bias is increased to 80 mA bias. For transmission over 37.5 km of SSMF, the DML biased at 80 mA and modulated with the 2 V_{pp} signal produces the lowest BER of 4.50 x 10^{-7} at a fixed received optical power of -14.5 dBm. As the DML bias current was increased from 45 to 80 mA, the ER of the transmitted signal reduces from 6.3 to 2.7 dB and the 3-dB bandwidth of the signal spectrum, Δf_{3dB}, also reduces as shown in Figure 2.8. Having ascertained that 12.5 Gbit/s NRZ-OOK optical signal transmission over 37.5 km of SSMF could be achieved with the DML, BER measurements as a function of received optical power were acquired for transmission over 37.5 km of SSMF with the DML biased at 80 mA and modulated with the 2 V_{pp} 12.5 Gbit/s NRZ-OOK signal. Transmission experiments for 12.5, 25 and 50 km of SSMF transmission were also carried out. The BER results for transmission over 12.5 km (blue curve), 25 km (yellow curve), 37.5 km (purple curve) and 50 km (green curve) of SSMF, along with the BER results for b2b transmission (red curve), are shown in Figure 2.13. BER results were obtained for transmission over second SSMF reels of 37.5 km (dashed purple curve) and 50 km (dashed green curve) lengths, and these results are also shown in Figure 2.13. Furthermore, BER measurements were acquired for transmission over 50 km of SSMF with the DML biased at 80 mA, however, a 1 V_{pp} modulating signal amplitude was employed (dashed magenta curve). For all of the transmission experiments performed with the DML biased at 80 mA, the optical power of the signal input to the fibre was maintained below 5 mW using the VOA at the input to the fibre.

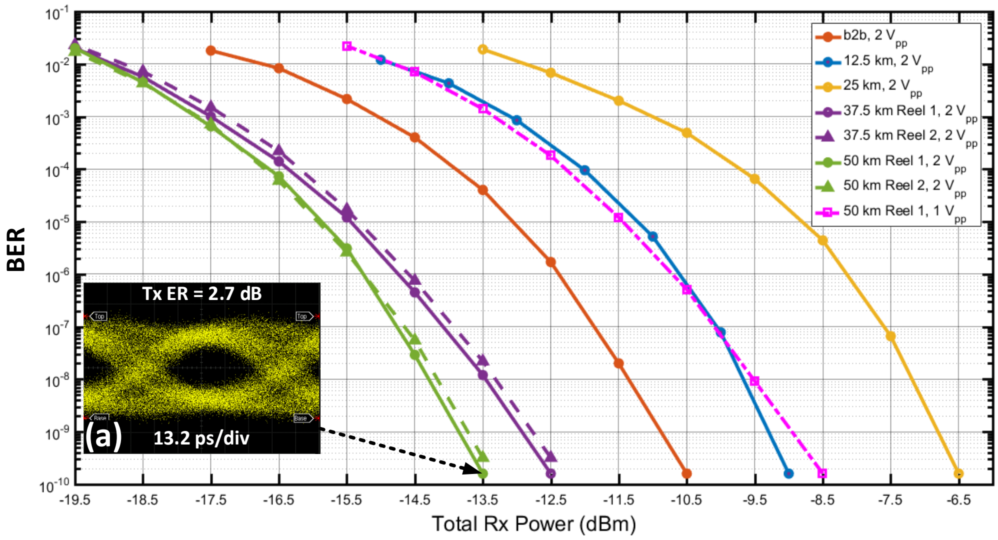

Figure 2.13: BER results for DML biased at 80 mA and modulated with the 2 V_{pp} 12.5 Gbit/s NRZ-OOK signal for b2b transmission (red curve) and transmission over 12.5 km (blue curve), 25 km (yellow curve), 37.5 km (purple curve), 37.5 km Reel 2 (dashed purple curve), 50 km (green curve) and 50 km Reel 2 (dashed green curve), and also for the DML modulated with the 1 V_{pp} 12.5 Gbit/s NRZ-OOK signal over 50 km of SSMF (dashed magenta curve), inset (a) shows the eye diagram of the electrical signal captured at the receiver for error-free transmission for transmission over 50 km Reel 1 of SSMF.

From the BER results shown in Figure 2.13, acquired with the DML biased at 80 mA and modulated with the 2 V_{pp} 12.5 Gbit/s NRZ-OOK signal, it can be observed that a dispersion power penalty of 1.5 and 6 dB is incurred for DML transmission over 12.5 and 25 km of SSMF, respectively. However, for transmission over 37.5 and 50 km of SSMF, there is an improvement in receiver sensitivity, relative to b2b transmission, of 2 and 3.5 dB, respectively. Figure 2.13 inset (a) shows the eye diagram of the received signal captured for error-free transmission over 50 km of SSMF at a received power of -13.5 dBm. The eye is open, however, it exhibits significant timing jitter and the crossings of the eye are not well defined. The enhanced transmission performance of the DML biased at 80 mA and modulated well above threshold, and the improvement in receiver sensitivities for transmission over 37.5 and 50 km of SSMF relative to the b2b transmission performance, may be attributed to the change in the frequency chirp characteristics of the DML at the higher bias current and the subsequent favourable interplay between the DML chirp and the accumulated CD of the fibre over the 37.5 and 50 km distances.

When the DML is biased at 80 mA and modulated well above threshold, the transient chirp of the transmitted signal reduces considerably and this was demonstrated in the spectra shown in Figure 2.7 and in the optical bandwidth measurements displayed in the graph in Figure 2.8. Thus, the adiabatic chirp becomes the dominant chirp component in the transmitted signal [27], [41]. Assuming that the signal transmitted from the DML biased at 80 mA and modulated well above threshold is adiabatic chirp dominated, then the optical frequency of the "1" bit or "high" binary level of the signal waveform output from the DML will be blue-shifted relative to the "0" bit or "low" binary level. Considering the ~6.6 GHz bandwidth measured 3-dB down on the optical spectrum of the signal transmitted from the DML biased at 80 mA and the enhanced transmission performance for transmission over 37.5 and 50 km of SSMF, it may be inferred that the frequency modulation of the DML, or the optical frequency difference between the "0" and "1" binary levels of the signal waveform transmitted from the DML, is approximately half the bandwidth of the modulating signal. This mode of operation of the DML creates what is known as the minimum shift keying (MSK) condition [38], [42] – [45], which results in a continuous phase shift, $\Delta\emptyset$, that occurs during each "0" bit in the transmitted signal waveform. Considering that a 12.5 Gbit/s NRZ-OOK modulating signal is being employed, where the bit period, T_b, of the signal waveform is 80 ps, then the total phase shift or slip that occurs during each "0" bit is [45]

$$\Delta\emptyset = \Delta\omega . T_b = 2\pi \times 6\ \mathrm{GHz} \times 80\ \mathrm{ps} = \pi \qquad 2.5$$

Thus, the phase varies slowly with a total shift of π during each "0" bit that is transmitted due to the frequency modulation (FM) of the DML and the output optical signal becomes line-coded, similar to optical duobinary (DB) modulation format [46]. When the mixed IM and FM optical signal output from the DML biased at 80 mA is transmitted over the 37.5 and 50 km of SSMF, the accumulated CD in the fibre over these distances results in the "1" bits overlapping and interfering destructively in the "0" bit slots separating them due to the π phase shift and because the blue-shifted "1" bits travel faster in SSMF than the red-shifted "0" bits. This FM to AM conversion results in optical pulse compression and produces an open received signal eye diagram and error-free transmission for transmission over 37.5 and 50 km of SSMF. Furthermore, it allows transmission beyond the dispersion limited link length of a DML, which is typically transient chirp dominated, to be achieved without the use of optical or electrical dispersion compensation. The 1 dB improvement in the receiver sensitivity observed as the transmission distance is extended from 37.5 to 50 km of SSMF may be attributed to the increase in the accumulated CD over the 50 km of SSMF, which, consequently, produces more favourable FM to AM conversion. Figure 2.14 shows the best BER results achieved with the DML for b2b transmission and for transmission over 12.5, 25, 37.5 and 50 km of SSMF.

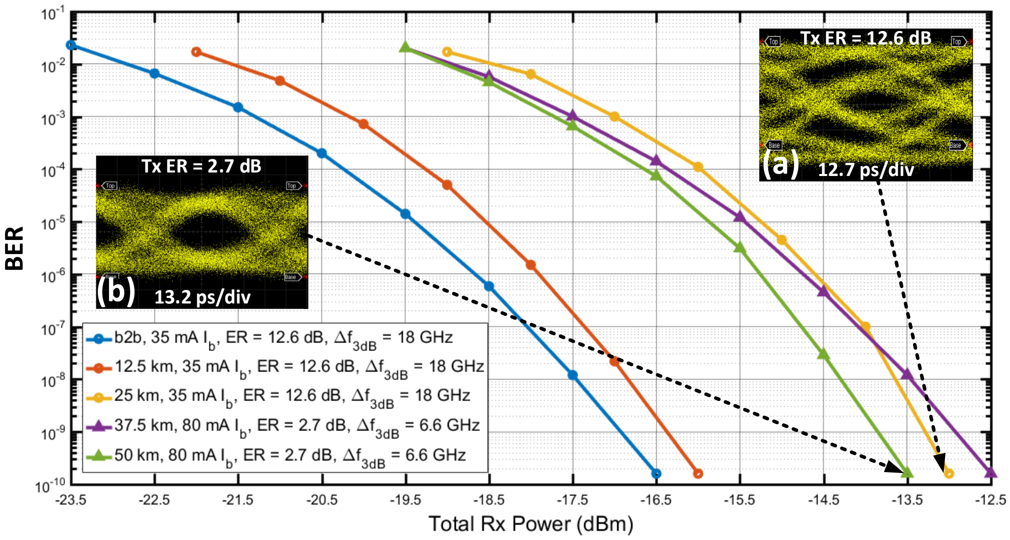

Figure 2.14: Best BER results obtained for DML modulated with the 2 V_{pp} 12.5 Gbit/s NRZ-OOK signal for b2b transmission (blue curve) and for transmission over 12.5 km (red curve), 25 km (yellow curve), 37.5 km (purple curve) and 50 km (green curve), insets (a) and (b) show the eye diagrams of the electrical signals captured at the receiver for error-free transmission for transmission over 50 and 25 km of SSMF, respectively.

The DML biased at 35 mA and modulated with the 2 V_{pp} 12.5 Gbit/s NRZ-OOK signal yielded the best transmission performance for b2b transmission and for transmission over 12.5 km and 25 km of SSMF. When biased at 35 mA and modulated near threshold, the signal transmitted from the DML exhibited the highest ER of 12.6 dB, however, at this bias the DML is transient chirp dominated, evidenced by the large overshoot observed in the eye diagram of the transmitted optical signal [47] and by the ~18 GHz 3-dB bandwidth of the optical spectrum. Transmission over 37.5 km of SSMF was not possible with the DML biased at 35 mA, as the received signal was too severely distorted due to the dispersive pulse broadening and ISI. When the DML was biased at 80 mA and modulated well above threshold with the 2 V_{pp} 12.5 Gbit/s NRZ-OOK signal, error-free transmission over 37.5 and 50 km of SSMF was achieved. From the BER results shown in Figure 2.14, it can be observed that for transmission over 37.5 and 50 km of SSMF with the DML biased at 80 mA, a 0.5 dB and 1 dB improvement in the receiver sensitivity was attained when compared with transmission over 25 km of SSMF with the DML biased at 35 mA. Despite the 2.7 dB ER of the signal transmitted from the DML biased at 80 mA, which was ~10 dB lower than the ER of the signal transmitted from the DML biased at 35 mA, the FM-AM conversion that occurred for the adiabatic chirp dominated signal transmitted from the DML biased at 80 mA for transmission over 37.5 and 50 km of SSMF, resulted in the enhanced transmission performance of the DML. The enhanced transmission performance can be attributed, in part, to the minimum shift keying (MSK) condition, which was established as a result of the mixed FM and IM of the DML when biased at 80 mA and modulated well above threshold, where the adiabatic chirp and optical frequency difference between the transmitted “1” and “0” bits is approximately half the rate of the modulating data signal [48], [49]. The enhanced transmission performance of the DML biased at 80 mA is only made possible by the accumulated CD of the SSMF over the 37.5 and 50 km distances, which enables the FM to AM conversion and the opening of the received signal eye diagram.

2.2.3 Numerical Modelling and Simulation of DML IM/DD Transmission

In order to estimate the linewidth enhancement factor or alpha parameter, α, of the MQW DFB laser, and estimate the magnitude of the frequency chirp exhibited by the DML when biased at 35 and 80 mA, and modulated with the 2 V_{pp} 12.5 Gbit/s NRZ-OOK signal, a numerical model was developed in MATLAB to simulate the transmission performance of the DML. The single-mode laser rate equations, equations A.1 – A.3, were solved numerically using the MATLAB ODE45 solver. The static and small-signal modulation characteristics of the MQW DFB laser were first modelled by appropriately varying typical DFB laser parameters. The P-I curve and small-signal intensity modulation response simulation results generated by the model are shown in Figure 2.15 and Figure 2.16, respectively. The small-signal response was determined for laser bias currents ranging from 30 to 80 mA in 10 mA increments.

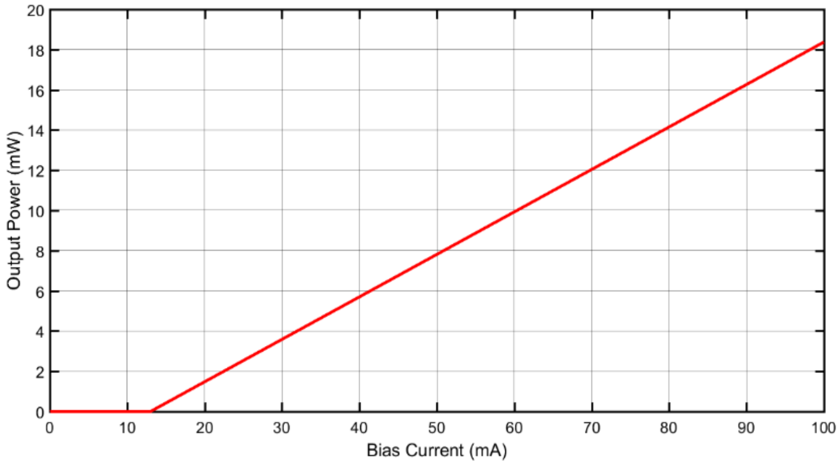

Figure 2.15: Simulated P-I curve of DFB laser.

The simulated P-I curve and small-signal modulation response agree well with the experimental results displayed in Figure 2.2 and Figure 2.4, respectively. The model parameters employed to generate the simulated results are provided in Table B.1 shown in Appendix B. Having yielded accurate simulated results for the P-I curve and small-signal modulation response of the MQW DFB laser, the parameter values were employed to simulate the transmission performance of the MQW DFB laser in a numerical model of the IM/DD transmission link. A description of the numerical model of the IM/DD transmission link is provided in Appendix C.

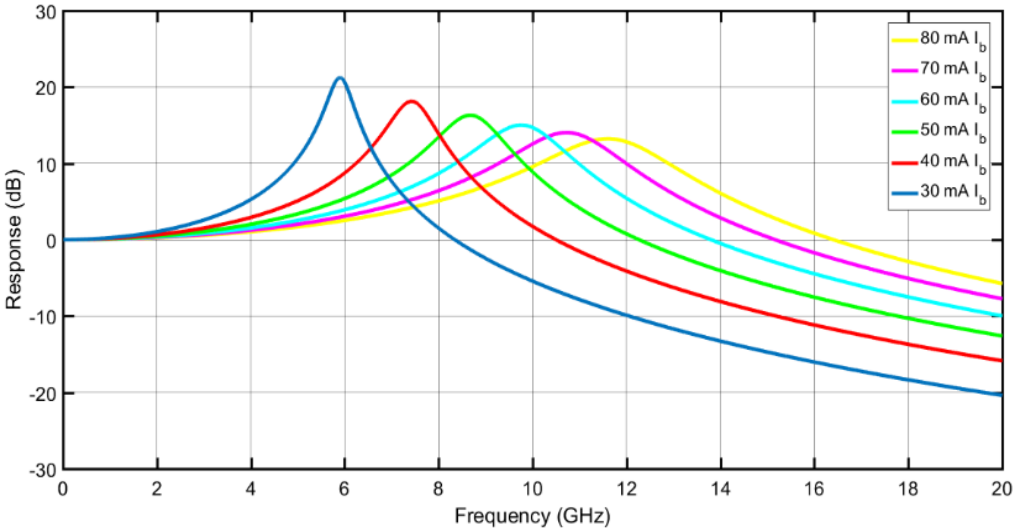

Figure 2.16: Simulated small-signal intensity modulation response of DFB laser.

To estimate the alpha parameter, α, of the MQW DFB laser that was experimentally evaluated, and to estimate the magnitude of the frequency chirp exhibited by the DML when biased at 35 and 80 mA and modulated with the 2 V_{pp} 12.5 Gbit/s NRZ-OOK signal, the DFB laser parameters listed in Table B.1 shown in Appendix B were utilised in the IM/DD transmission system model. The alpha parameter, α, and gain compression factor, ϵ, values were varied for transmission over 12.5, 25, 37.5 and 50 km of SSMF until the simulated BER results matched the BER results obtained experimentally. When varying the value of the alpha parameter, it was found that a low alpha parameter, α, value of 1.6 was required to simulate the transmission performance of the DML biased at 35 mA and modulated near threshold. Moreover, with the alpha parameter, α, value fixed at 1.6, a high gain compression factor, ϵ, value of $10\text{x}10^{-23}$ m^3 was required to simulate the transmission performance of the DML biased at 80 mA and modulated well above threshold. An alpha parameter, α, value of 1.6 and a gain compression factor, ϵ, value of $10\text{x}10^{-23}$ m^3, produced the simulated BER results and the received signal eye diagrams shown in Figure 2.17. The simulated results shown in Figure 2.17 agree well with the BER results obtained experimentally, shown in Figure 2.13 and Figure 2.14. Furthermore, it can be observed that the enhanced transmission performance of the DML biased at 80 mA was attained and the 3 dB improvement in receiver sensitivity for transmission over 50 km of SSMF, relative to the b2b transmission performance, demonstrates this. The enhanced transmission performance of the DML biased at 80 mA is further evidenced by the simulated received signal eye diagrams obtained for error-free transmission over 50 and 25 km of SSMF shown in Figure 2.17 insets (a) and (c), respectively. The eye diagram obtained for transmission over 50 km of SSMF with the DML biased at 80 mA shown in Figure 2.17 inset (a), is more open and less distorted than the eye diagram obtained for transmission over 25 km of SSMF shown in Figure 2.17 inset (c).

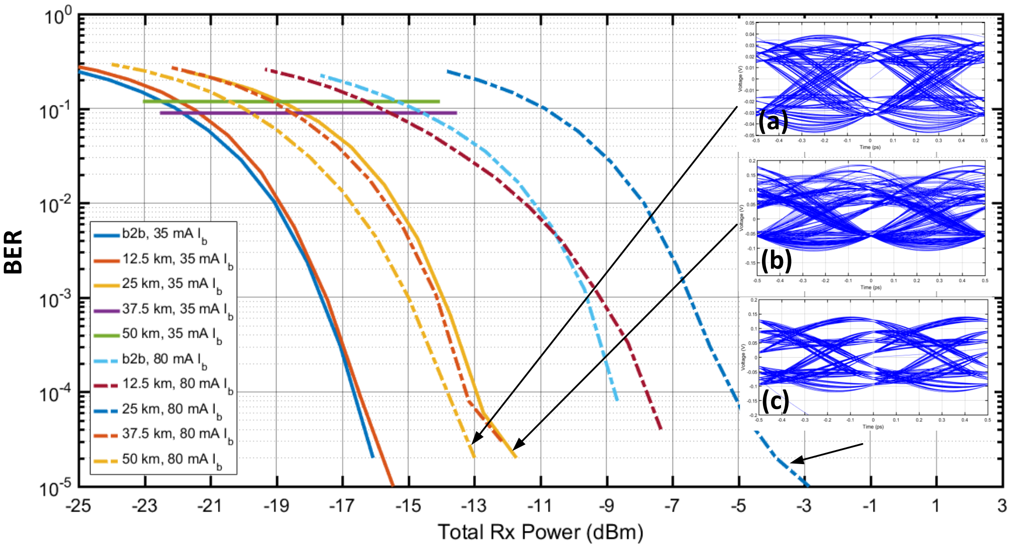

Figure 2.17: Simulated BER results for transmission over 0, 12.5, 25, 37.5 and 50 km of SSMF with the DML modulated with a 2 V_{pp} 12.5 Gbit/s NRZ-OOK signal when biased at 35 mA (solid curves) and 80 mA (dashed curves). Insets (a) and (c) show received signal eye diagrams for error-free transmission over 50 and 25 km of SSMF, respectively, with the DML biased at 80 mA and inset (b) shows the received signal eye diagram for error-free transmission over 25 km of SSMF with the DML biased at 35 mA.

The simulated received signal eye diagram obtained for error-free transmission over 25 km of SSMF with the DML biased at 35 mA, shown in Figure 2.17 inset (b), also appears less open than the eye obtained for transmission over 50 km of SSMF with the DML biased at 80 mA. Figure 2.18 shows the simulated optical spectra and eye diagrams of the signals transmitted from the DML biased at 35 mA and 80 mA and modulated with the 2 V_{pp} 12.5 Gbit/s NRZ-OOK signal.

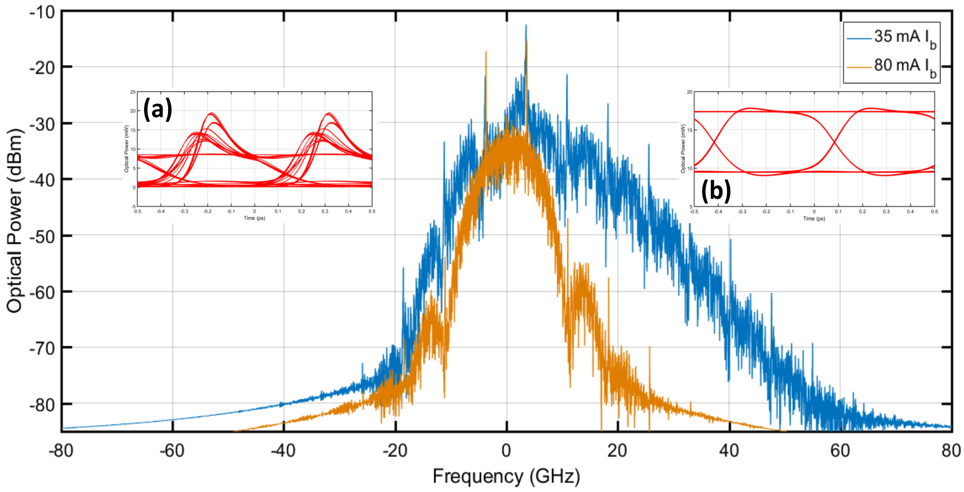

Figure 2.18: Simulated optical spectra generated for DML modulated with the 2 V_{pp} 12.5 Gbit/s NRZ-OOK signal when biased at 35 mA (blue spectrum) and 80 mA (brown spectrum), insets (a) and (b) show the transmitted signal eye diagrams obtained for the DML biased at 35 and 80 mA, respectively.

The simulated eye diagrams of the signals transmitted from the DML biased at 35 and 80 mA agree well with the experimental results shown in Figure 2.7 insets (b) and (c) in terms of overshoot and ER. The ER calculated from the simulated eye diagrams of the signals transmitted from the DML biased at 35 and 80 mA are 12.55 and 2.65 dB, respectively. The similated optical spectrum generated for the DML biased at 35 mA (blue spectrum) exhibits a similar 3-dB bandwidth (~18 GHz) as the spectrum obtained experimentally and shown in Figure 2.7. However, the simulated optical spectrum generated for the DML biased at 80 mA (brown spectrum) has a slightly larger 3-dB bandwidth (~9 GHz) than the experimentally measured spectrum, which was ~6.6 GHz, also shown in Figure 2.7. This discrepancy between the 3-dB bandwidths of the spectrum obtained experimentally and the spectrum obtained from the numerical model for the DML biased at 80 mA, may be attributed to the fact that the mixed frequency and intensity modulation (FM/IM) of the DML [33], [34], which induced partial suppression of the USB, was not reproducible in the simulated spectrum. It must be stated that the partial side-band suppression was reproducible when an alpha parameter with a negative value was employed, i.e. α = -1.6. However, it is well known that negative alpha parameter values are not considered in the context of MQW DFB lasers, as quantum well semiconductor materials have a large density of states at high energy and, as a result, the maximum gain incurs a blue shift with increasing carrier density [50]. Figure 2.19 and Figure 2.20 show the simulated chirp and optical power waveforms output from the DML modulated with the 2 V_{pp} 12.5 Gbit/s NRZ-OOK signal when biased at 35 and 80 mA, respectively.

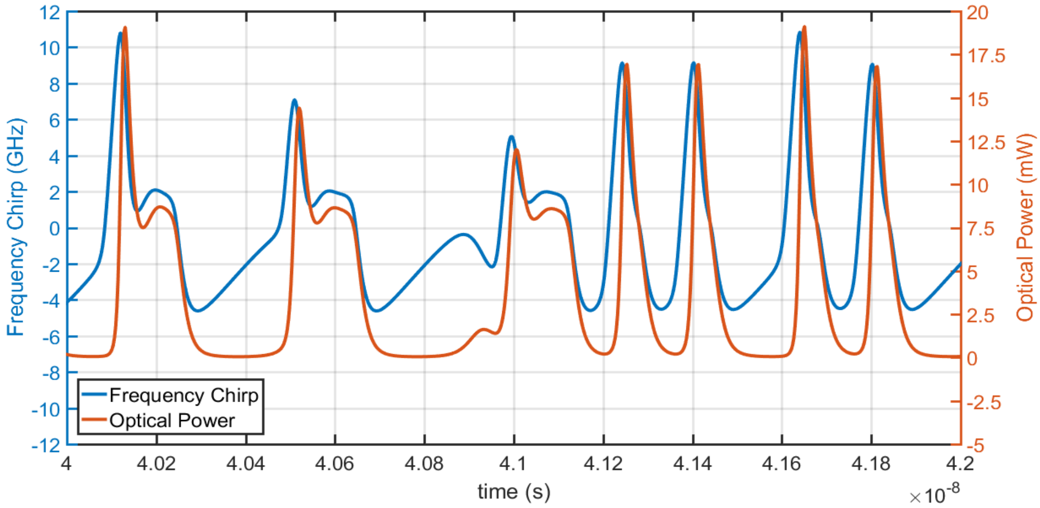

Figure 2.19: Simulated chirp and optical power waveform for DML modulated with a 2 V_{pp} 12.5 Gbit/s NRZ-OOK signal and biased at 35 mA.

In the simulated frequency chirp and power waveforms of the signal transmitted from the DML biased at 35 mA shown in Figure 2.19, it can be observed that the overshoot in the rising edge follows the frequency chirp. The peak-to-peak magnitude of the transient chirp is ~11 GHz, which comprises the ~9 GHz and 2 GHz blue- and red-shifted transient chirp in the rising and falling edges of the signal waveform, respectively. When biased at 35 mA and modulated near threshold, the DML is said to be transient chirp dominated.

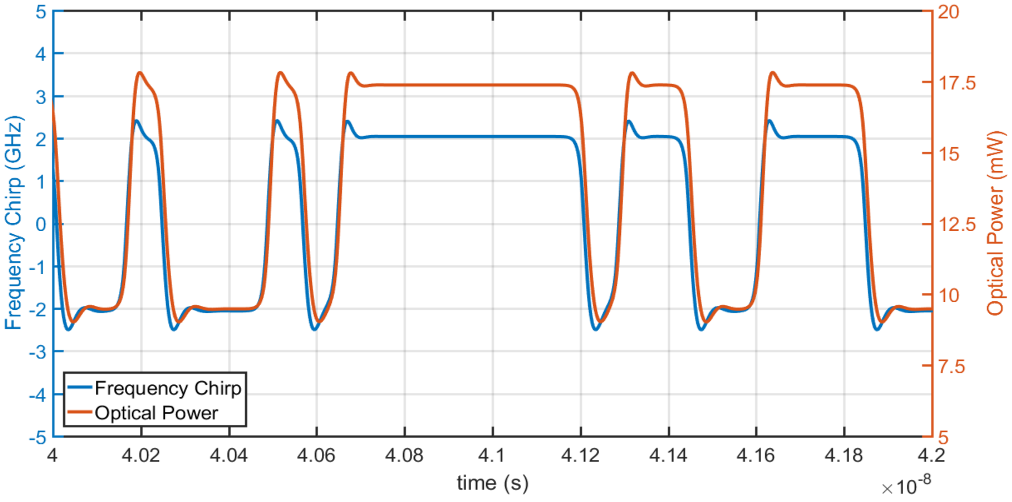

Figure 2.20: Simulated chirp and optical power waveform for DML modulated with a 2 V_{pp} 12.5 Gbit/s NRZ-OOK signal and biased at 80 mA.

In contrast to the DML biased at 35 mA, the chirp waveform of the DML biased at 80 mA exhibits only a small transient chirp of ~0.5 GHz at turn-on (blue-shifted) and turn-off (red-shifted). However, there is a well defined blue-shifted and red-shifted adiabatic chirp in the steady-state “1” and “0” levels of the signal waveform, respectively, exhibiting a peak-to-peak magnitude of 4 GHz. Therefore, the DML biased at 80 mA is said to be operating in an adiabatic chirp dominated regime and the adiabatic chirp is effectively the frequency modulation (FM) of the DML. The effects of the DML chirp on optical pulse propagation in 50 km of SSMF in both the transient and adiabatic chirp dominated DML regimes can be observed in Figure 2.21 and Figure 2.22, respectively.

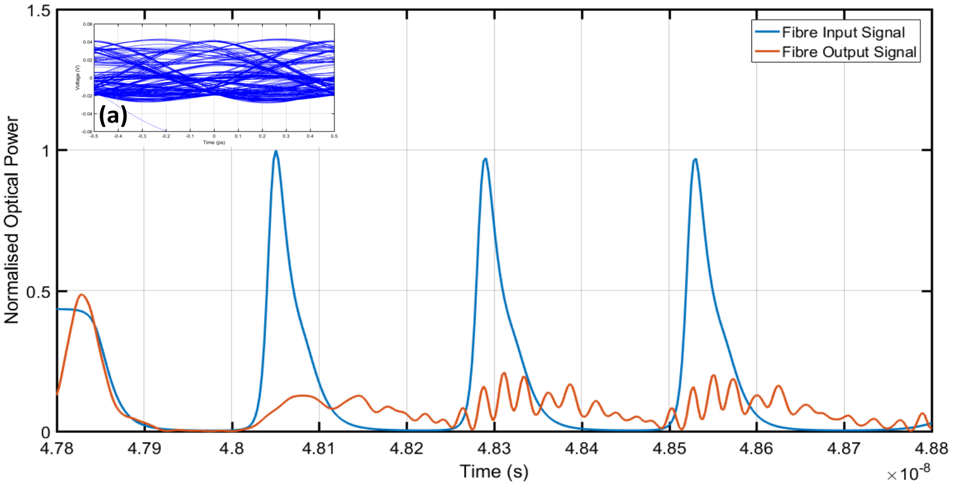

Figure 2.21: Simulated optical pulse propagation over 50 km of SSMF, signal transmitted from transient chirp dominated DML biased at 35 mA and modulated with 2 V_{pp} 12.5 Gbit/s NRZ-OOK signal. Inset (a) shows the eye diagram of the received signal.

In Figure 2.21, the chromatic dispersion (CD) accumulated over the 50 km SSMF distance causes the optical pulses that comprise the transient chirp dominated signal to be broadened in time, resulting in ISI. The ISI is depicted in the simulated received signal eye diagram displayed in Figure 2.21 inset (a). In contrast to the optical pulse broadening that was observed for signal transmission with the transient chirp dominated DML biased at 35 mA, pulse compression was observed for optical signal transmission over 50 km of SSMF with the adiabatic chirp dominated DML biased at 80 mA, as shown in Figure 2.22, where the optical pulse width of ~80 ps was effectively halved.

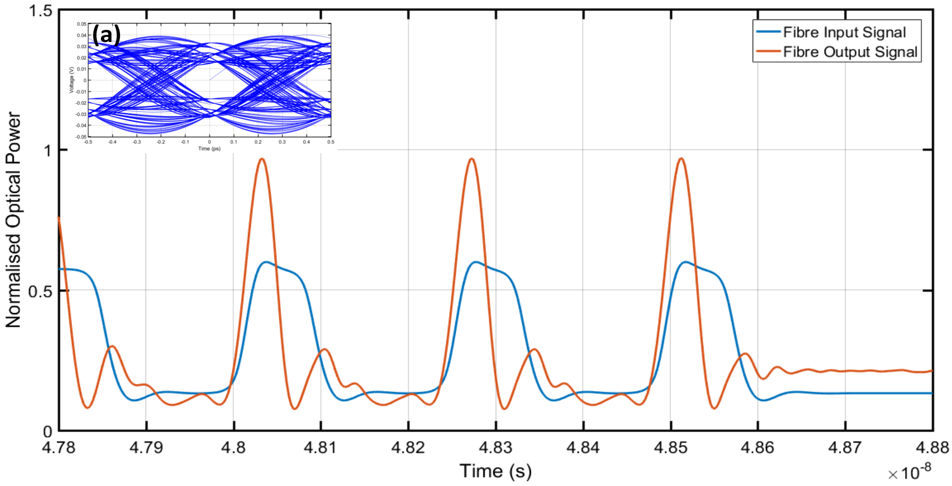

Figure 2.22: Simulated optical pulse propagation over 50 km of SSMF, signal transmitted from adiabatic chirp dominated DML biased at 80 mA and modulated with 2 V_{pp} 12.5 Gbit/s NRZ-OOK signal. Inset (a) shows the eye diagram of the received signal.

As previously mentioned, the origin of the pulse compression is in the minimum shift keying (MSK) condition, which is established as a result of the mixed FM and IM of the DML when biased at 80 mA and modulated well above threshold. When the adiabatic chirp dominated signal is transmitted over 50 km of SSMF, the accumulated CD in the fibre interacts favourably with the optical signal, resulting in FM to AM conversion of the signal. The CD causes the “1” bits to travel faster in SSMF than the “0” bits and, in the region where the “1” and “0” bit signal levels with different optical frequencies overlap, the “1” bits interfere destructively in the middle of the “0” bit slots. Hence, the optical fibre converts the frequency modulation (FM) of the optical signal into amplitude or intensity modulation (AM/IM), resulting in an open received signal eye diagram, which can be observed in Figure 2.22 inset (a).

2.3 External Modulation of EML

This section presents the experimental characterisation and transmission performance evaluation of the EML, as well as the numerical modelling that was carried out to assess the chirp characteristics of the EML. Figure 2.23 (a) and (b) shows an image and a schematic of the EML, respectively. The EML was mounted on a printed circuit board (PCB) for safety.

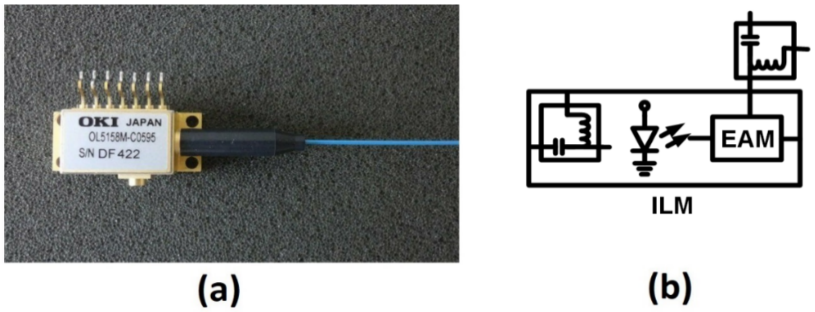

Figure 2.23: (a) Image of EML transmitter and (b) schematic of EML.

The EML is a C-band transmitter and comprised a DFB laser monolithically integrated with an MQW electro-absorption modulator (EAM). The EML is housed within a 7 pin butterfly package and contains a thermo-electric cooler (TEC), thermistor, back facet monitor detector, a bias tee and an internal optical isolator. A polarization maintaining (PM) pigtailed fibre provided the output from the laser. The EML was rated for 40 Gbit/s operation with a 3-dB electrical bandwidth of > 32 GHz.

2.3.1 Device Characterisation

Experimental characterisation of the EML was carried out to establish the performance of the device under various operating parameters and, furthermore, to determine the operating parameters that should be employed to optimise the b2b transmission performance of the EML in the IM/DD test-bed. Static characterisation includes measurements of the P-I curve, optical spectrum and the continuous wave (CW) optical power transmitted from the DFB laser in isolation under dc bias. The static power transfer characteristics of the EML, with the DFB laser and EAM dc biased, are measured to determine the static extinction ratio (SER) of the EAM and the sensitivity of the EAM to variations in the EML TEC temperature and in the wavelength of the lightwave input to the EAM. Dynamic characterisation of the EML includes a large-signal analysis using a 2 V_{pp} 12.5 Gbit/s NRZ-OOK signal to modulate the EAM. Eye diagrams and spectra of the transmitted optical signals are used to qualitatively and quantitatively analyse the large-signal modulation characteristics of the EML. The extinction ratio, ER, the ER power penalty, δ_{ER} , and Q-factor, Q, of the signals transmitted from the EML under large-signal modulation for different EAM bias voltages are calculated from the captured eye diagrams. The optical spectrum and the 3-dB optical bandwidth, Δv_{3dB}, of the signals transmitted from the EML at various EAM bias voltages are also presented and analysed. Due to the EML being rated for 40 Gbit/s operation, a small-signal analysis of the EML was not carried out considering that only 12.5 Gbit/s modulation was being employed. The results of the static characterisation of the isolated DFB laser in the EML are shown in Figure 2.24, Figure 2.25 and Figure 2.26, which include the P-I curve, optical spectra for a fixed device TEC temperature and varying laser bias current, and optical spectra for a fixed laser bias current and varying device TEC termperature, respectively.

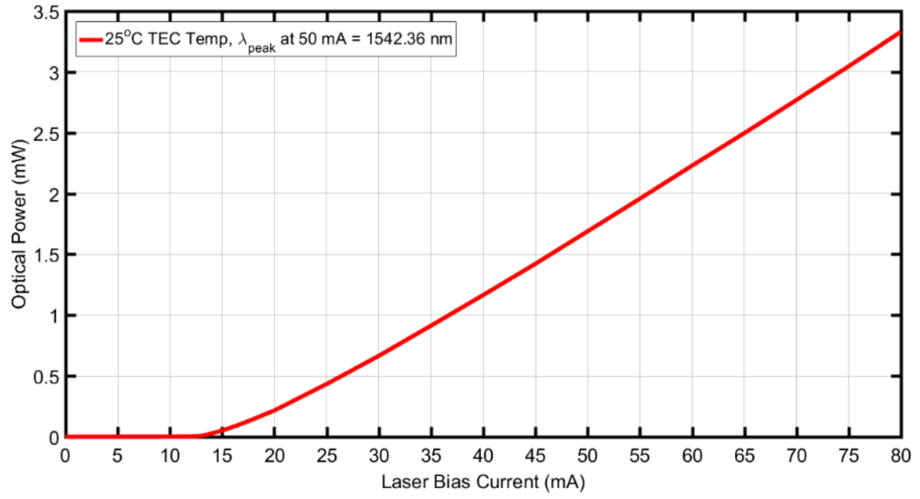

Figure 2.24: P-I curve for DFB laser in EML at 25^{o}C TEC temperature.

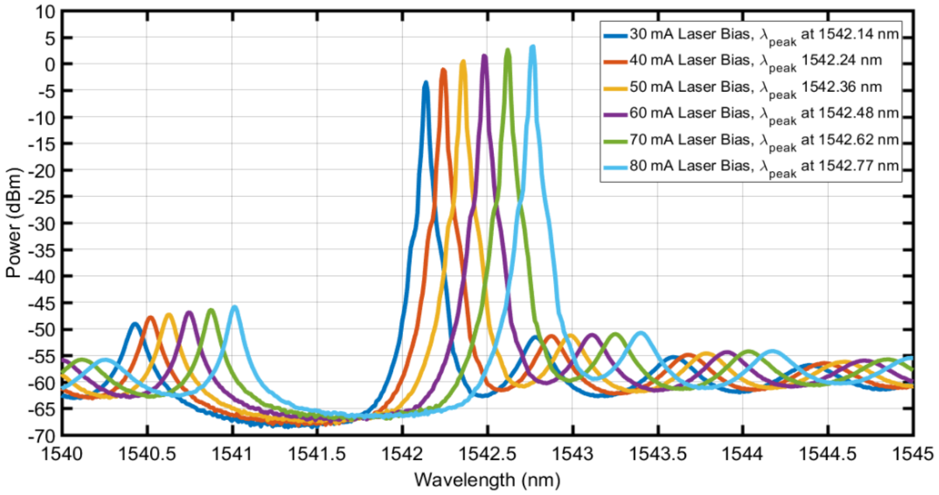

Figure 2.25: Optical spectra captured from EML for DFB laser in isolation using a fixed TEC temperature of 25 ^{o}C while sweeping the laser bias from 30 mA to 80 mA.

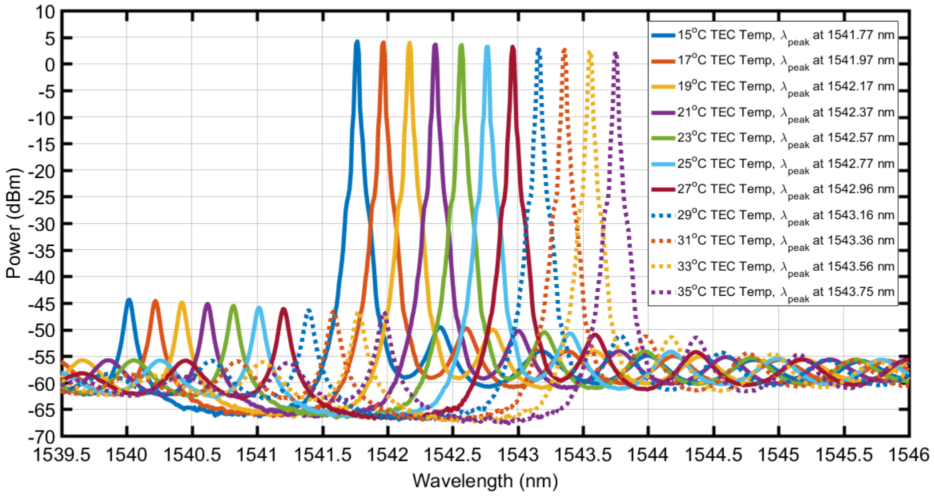

Figure 2.26: Optical spectra captured from EML for DFB laser in isolation for a fixed laser bias of 80 mA while sweeping the TEC temperature from 15^{o}C to 35^{o}C.

Figure 2.24 displays the P-I curve of the isolated DFB laser, that is, with no reverse voltage applied to the EAM. The threshold current of the DFB laser is 13 mA and the slope efficiency is ~0.052 mW/mA. At the maximum applied bias current of 80 mA, the optical power of the CW signal output from the DFB laser in the EML is ~3.4 mW. Figure 2.25 shows the spectra recorded for a fixed TEC temperature of 25°C while sweeping the DFB laser bias from 30 to 80 mA in 10 mA increments. The wavelengths range from 1542.14 nm (at 30 mA) to 1542.77 nm (at 80 mA) with an average shift in peak wavelength of 0.013 nm per 1 mA change in bias current. As the laser bias is increased from 30 to 80 mA, a ~7 dB increase in the optical power of the mode is observed. Side-modes appear at the shorter and longer wavelength sides of the main lasing mode ~1.75 nm and 0.65 nm away from the main mode, respectively, the SMSR is ~50 dB. Figure 2.26 shows the spectra recorded for a fixed DFB laser bias of 80 mA and the device TEC temperature was varied from 15 to 35°C in 2°C incremental steps. The peak wavelengths range from 1541.77 nm (at 15°C) to 1543.75 nm (at 35°C), with an average change in wavelength of 0.09 nm per 1°C change in TEC temperature, resulting in a tuning range of 1.98 nm. The tuning range achieved by varying the TEC temperature, while maintaining the DFB laser bias at 80 mA, is 1.26 nm larger than the tuning range observed when varying the DFB laser bias from 20 to 80 mA while keeping the TEC temperature fixed at 25°C. A ~2 dB reduction in the optical power of the CW signal output from the EML was observed when the TEC temperature was raised from 15 to 35°C.

2.3.1.1 EAM transfer function and SER

The principle of operation of an EAM is based on the optical absorption properties of semiconductor materials, specifically the fact that the effective bandgap, E_g, energy of the material can be reduced with an external electric field induced by an applied voltage. The degree of absorption that an EAM exhibits is dependent on the structure of the semiconductor device, the magnitude of the electric field or applied voltage, and the wavelength of the lightwave input to the device. The absorption of an EAM is, in part, due to the absorption edge of the semiconductor material being shifted or broadened to lower energies (longer wavelengths) when an electric field is applied. As a result, EAMs are inherently wavelength dependent and the wavelength of the input lightwave must be carefully chosen so that the lightwave will incur adequate absorption when an external electric field is applied. Since an EAM's absorption properties can be varied with an external electric field, it enables the device to be used as an intensity modulator (IM). When an EAM is modulated with a voltage signal, the optical absorption of the EAM varies in accordance with the applied time varying voltage and this allows the continuous wave (CW) optical field that is Input to the device to be intensity modulated. The transfer function of an EAM determines the optical power output from the device as a function of applied dc voltage. Furthermore, it indicates the modulation efficiency or the static "on-off" extinction and the linearity of the EAM. The EAM power transfer function may be represented in terms of the bias-dependent absorption coefficient as [51], [52]

$$P_{out}(V) = P_{in}.\, e^{[-\Gamma a_{abs}(V)L]} = f(V) \qquad 2.6$$

where P_{in} represents the optical power input to the EAM, P_{out} is the optical power output from the EAM, a_{abs} is the voltage dependent absorption coefficient, Γ is the optical confinement factor and L is the length of the EAM. The static "on-off" extinction ratio (ER) as a function of the reverse voltage applied to the EAM may be defined as [53]

$$ER = \left(\frac{P_{on}}{P_{off}}\right) = \left(\frac{P_{out}(V=0)}{P_{out}(V)}\right) = \left(\frac{P_{in}.\, e^{[-\Gamma a_{abs}(0)L]}}{P_{in}.\, e^{[-\Gamma a_{abs}(V)L]}}\right) \qquad 2.7$$

where $P_{out}(V)$ represents the transmitted optical power at the output of the EAM for a given bias voltage and $P_{out}(V = 0)$ represents the maximum transmitted optical power at zero bias. The static "on-off" extinction ratio in dB is expressed in equation 2.8.

$$ER_{dB} = 10\log_{10}(ER) = 4.343[a_{abs}(V) - a_{abs}(0)]\Gamma L = 4.343[\Gamma \Delta a_{abs} L] \qquad 2.8$$

The absorption coefficient, a_{abs}, is a function of the wavelength and the applied voltage and may be expressed as [54], [55]

$$a_{abs}(\lambda, V) = \frac{a_p(V) \times [\Delta\lambda(V)/2]^2}{\left[\lambda - \lambda_p(V)\right]^2 + [\Delta\lambda(V)/2]^2} \qquad 2.9$$

where $a_p(V)$ is the peak absorption coefficient, $\lambda_p(V)$ is the wavelength with the peak absorption coefficient and $\Delta\lambda(V)$ represents the spectral broadening.

Static power transfer characterisation

Static power transfer characterisation of the EAM was carried out to establish the static extinction ratio (SER) of the EAM for various DFB laser bias currents and TEC temperatures. Unlike the previous characterisation of the isolated DFB laser within the EML, the static power transfer characterisation of the EAM, within the EML, involved having both the DFB laser and the EAM dc biased. A reverse voltage was applied to the EAM via a bias tee as shown in Figure 2.23 (b). While maintaining the device

TEC temperature at 25°C and for a fixed DFB laser bias, the reverse voltage to the EAM was varied from 0 to 3 V and the optical power of the CW signal output from the EML was measured. This was performed for different DFB laser bias currents ranging from 30 to 80 mA in 10 mA increments. The resultant absorption curves that were generated are shown in Figure 2.27.

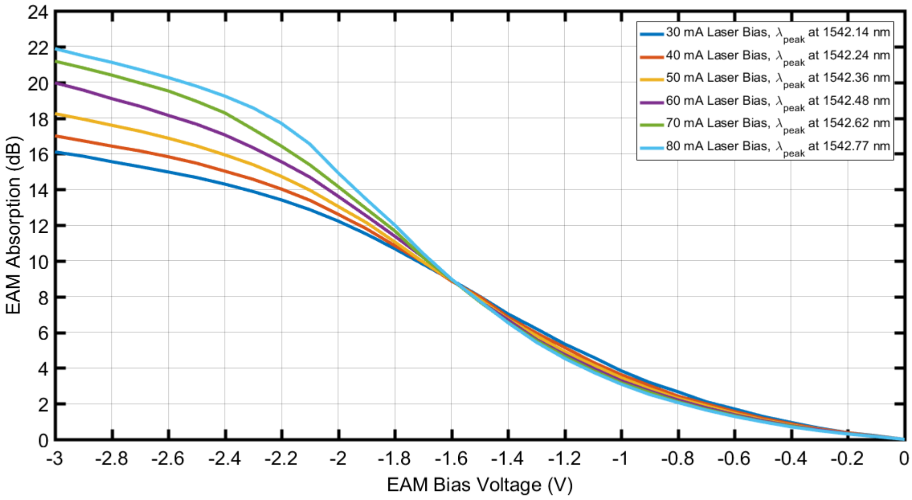

Figure 2.27: EAM absorption profile for a fixed TEC temperature of 25°C and DFB bias currents ranging from 30 to 80 mA.

It can be observed in Figure 2.27 that as the DFB laser bias current was increased from 30 to 80 mA, the absorption efficiency of the EAM also increased with increasing EAM reverse voltage. This can be attributed to the wavelength of the input lightwave shifting to longer wavelengths with increasing DFB laser bias and to the absorption edge of the EAM shifting to longer wavelengths as the EAM reverse voltage was increased. Thus, the EAM absorption increases at higher EAM reverse voltages when the wavelength of the input lightwave is higher and, hence, produces a greater SER. For a fixed 25°C TEC temperature, the highest SER of 22 dB is achieved at a DFB laser bias of 80 mA and an input wavelength of 1542.77 nm. The linear region of the absorption curve attained for the 80 mA DFB laser bias, ranges from ~-1.1 to -2.1 EAM bias voltage and corresponds to an SER of 12.8 dB. Having established that the 80 mA DFB laser bias yielded the highest SER, a sweep of the device TEC temperature from 15 to 35°C in 2°C increments was performed while maintaining the laser bias at 80 mA. For each TEC temperature setting, the optical power of the lightwave output from the EML was measured as a function of EAM reverse voltage. The resultant absorption curves are shown in Figure 2.28. It can be observed in Figure 2.28 that a ~2 dB increase and decrease in the SER of the EAM occurs with a 10°C increase and decrease of the device TEC temperature, respectively. Although the EML exhibited a ~2 dB higher SER when operated at the 35 °C TEC temperature, it was decided that the EML would be operated at room temperature, i.e., 25 °C, for the remainder of the experiments.

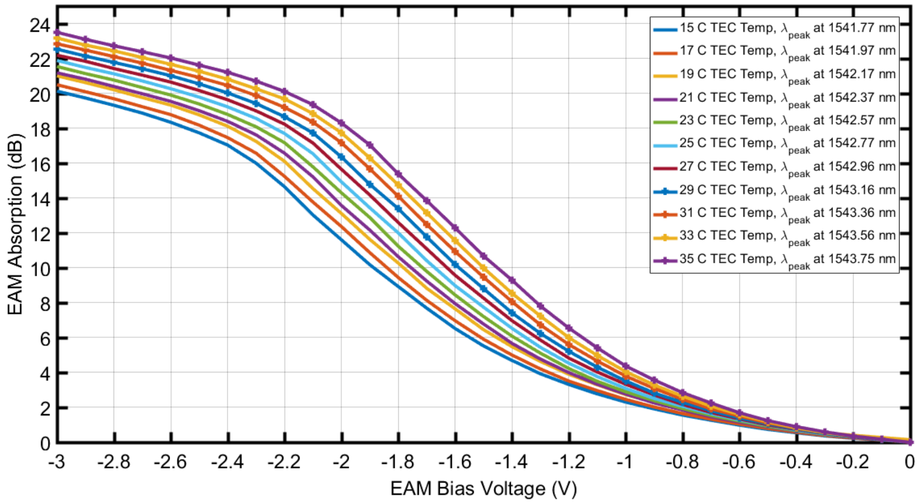

Figure 2.28: EAM absorption profile for a fixed DFB laser bias of 80 mA and TEC temperatures ranging from 15°C to 35°C.

Furthermore, it was decided that the 80 mA DFB laser bias would be employed for the remainder of the experiments, since the 80 mA DFB laser bias yielded the highest output optical power and highest SER for the 25°C device TEC temperature, thus, would be the optimal DFB laser bias current to operate the EML in order to achieve the best possible b2b transmission performance.

2.3.1.2 Frequency chirp of electro-absorption modulated laser (EML)

A consequence of the change in the EAM's absorption, resulting from the modulating voltage signal, is the variation in the refractive index (RI) of the semiconductor material, and the variation in the RI introduces a frequency chirp to the transmitted optical signal. Similar to DMLs, the EAM chirp is due to the variation in the imaginary part of the refractive index, $\Delta n''$, which is accompanied by a variation in the real part of the refractive index, $\Delta n'$, and is described by the Kramers-Kronig relations [56]. The variation in the RI causes the phase variation or frequency chirp of the transmitted optical signal. Like DMLs, the chirp or alpha parameter of an EAM, α_{EAM}, determines the magnitude of the frequency chirp exhibited by the modulator and is given by [57], [58]

$$\alpha_{EAM}(\lambda, V) = \frac{\Delta n'}{\Delta n''} = \frac{4\pi}{\lambda_0}\frac{\Delta n'(\lambda_0, \Delta V)}{\Delta\alpha_{abs}(\lambda, \Delta V)} \qquad 2.10$$

The numerator in equation 2.10, which denotes the change in the real part of the refractive index, $\Delta n'$, as a function of the input wavelength of the lightwave and the applied voltage, can be ascertained from measurements of the change in the absorption coefficient, $\Delta\alpha_{abs}$, through the Kramers–Kronig relation and can be expressed as [59] – [61]

$$\Delta n'(\lambda_0, \Delta V) = \frac{\lambda_0^2}{2\pi^2} PV \int_0^{\infty} \frac{\Delta\alpha_{abs}(\lambda, \Delta V)}{\lambda_0^2 - \lambda^2} d\lambda \quad 2.11$$

where λ_0 is the free-space wavelength of the input lightwave and PV represents the Cauchy principal value. For an MQW EAM, the absorption coefficient, α_{abs}, for an input lightwave with wavelength λ_0, increases with increasing electric field magnitude as the exciton peak shifts to longer wavelengths. As α_{abs} increases, $\Delta n'$ increases initially and then decreases. Eventually, $\Delta n'$ becomes negative for high electric field magnitudes, which is what produces the negative chirp or alpha parameter, α_{EAM}, of an MQW EAM. The frequency chirp of EAMs has been shown to be primarily transient in nature [62] that is, the rising and falling edges of the optical pulses that are transmitted from an EAM exhibit frequency excursions and the magnitude of the excursions are dependent on the alpha parameter value, α_{EAM}. However, when an EAM is integrated with a laser diode to form an integrated laser modulator (ILM) or EML, an adiabatic chirp component may also be introduced to the transmitted optical signal. The adiabatic chirp of an EML has been attributed to carrier density fluctuations, resulting from optical feedback into the laser cavity, and electrical crosstalk due to the integration of the laser and modulator sections on the same chip [63], [64].

Wavelength variation as a function of EAM reverse voltage

Optical spectra were captured from the EML for the 80 mA DFB laser bias, the 25°C TEC temperature and for EAM bias voltages of 0, -1.5 and -3 V. The spectra, captured with the Yokogawa AQ6370 OSA using a resolution of 0.02 nm, are shown in Figure 2.29. This was carried out to gain an insight into the degree of wavelength variation in the CW signal output from the EAM resulting from the variation in EAM bias voltage.

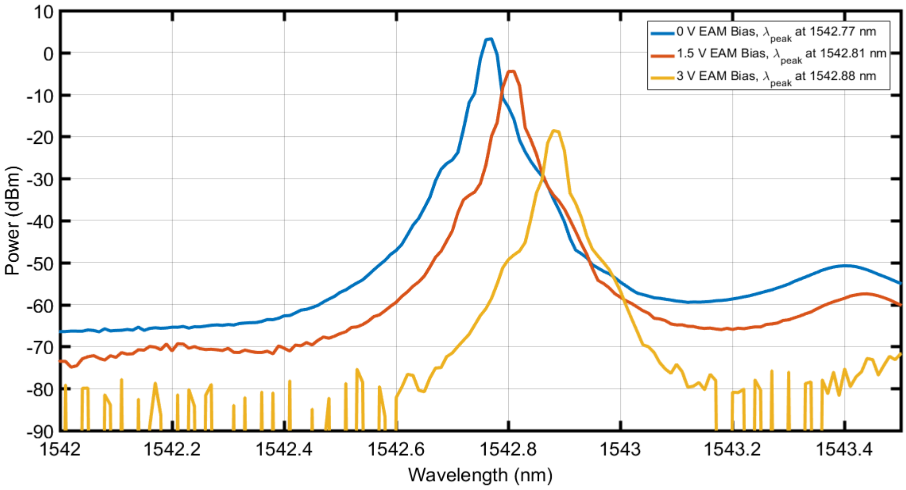

Figure 2.29: Optical spectra recorded for a fixed DFB laser bias of 80 mA and TEC temperature of 25°C for EAM reverse voltages of 0 V (blue spectrum), 1.5 V (red spectrum) and 3 V (yellow spectrum).

It can be observed in Figure 2.29 that the wavelength of the lightwave output from the EML varies from 1542.81 to 1542.77 nm as the bias voltage to the EAM is increased from -1.5 to 0 V, which corresponds to a blue-shift in the peak wavelength of 0.04 nm. However, when the bias voltage to the EAM is lowered from -1.5 to -3 V, the wavelength of the lightwave output from the EML experiences a red-shift of ~0.08 nm, which corresponds to a wavelength excursion that is a factor of two times greater than what is observed when the EAM bias voltage is increased from -1.5 to 0 V. The wavelength excursion of the lightwave output from the EML, due to the variation in the bias voltage applied to the EAM, is the origin of the transient chirp of the EML. Thus, the voltage applied to the EAM, and the wavelength of the input lightwave, influences both the SER and the frequency chirp of the EML.

2.3.1.1 Dynamic characterisation

Optical waveform analysis

For the large-signal modulation analysis of the EML, the experimental procedure, described in section 2.2.1.2, and setup, shown in Figure 2.5, which was used in the large-signal modulation analysis of the DML, was employed. To optimise the extinction ratio, ER, of the optical signals transmitted from the EML, the maximum amplitude of 2 V_{pp} for the 12.5 Gbit/s NRZ-OOK modulation signal was employed. With the modulating signal applied to the EAM and the DFB laser bias and the device TEC temperature set to 80 mA and 25°C, respectively, optical eye diagrams and spectra were captured at the output of the EML for EAM reverse voltages ranging from 1 to 2 V in 0.1 V increments. The extinction ratio, ER, and power penalty, δ_{ER} , of the optical signals transmitted from the EML for the different EAM reverse voltages were calculated from the captured eye diagrams. In addition to the ER and ER power penalty, δ_{ER} , the Q-factor, Q, of the signals transmitted from the EML was also ascertained. The Q-factor takes into account the average noise in both the "on" and "off" binary levels and combines the two signal-to-noise ratios (SNRs) of the two possible signal levels into a single quantity. The Q-factor, Q, may be expressed as [20], [21], [65]

$$Q = \frac{P_1 - P_0}{\sigma_1 + \sigma_0} \qquad 2.12$$

where P_1 and P_0 is the average optical power in the upper and lower rails or in the"on" and "off" state levels of the signal, respectively, and σ_1 and σ_0 are the standard deviations of the noise in the "on" and "off" state levels of the signal, respectively. Figure 2.30 shows the ER, δ_{ER} , and the Q of the optical signals transmitted from the EML as a function of EAM bias voltage.

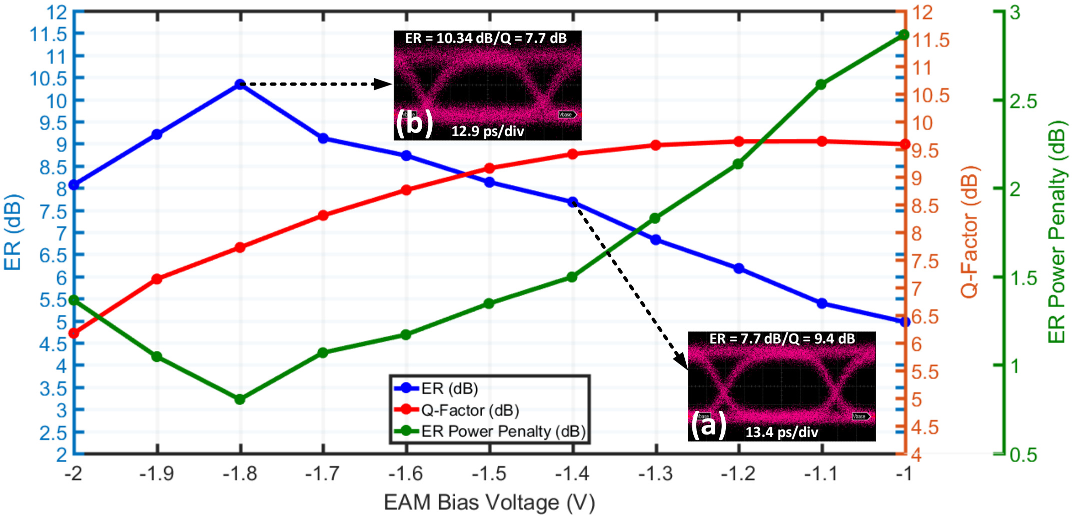

Figure 2.30: ER, δ_{ER}, and Q of the signals transmitted from the EML as a function of EAM bias voltage. Insets (a) and (b) show the captured transmitted signal eye diagrams for EAM bias voltages of -1.4 and -1.8 V, respectively.

The relevance of evaluating both the ER and Q-factor metrics to ascertain the optimum EML operating parameters, which would yield the best b2b transmission performance, can be observed in the results shown in Figure 2.30. As the EAM reverse voltage is increased from 1 to 2 V, the ER of the transmitted signal increases before peaking at 10.3 dB for an EAM reverse voltage of 1.8 V, it then decreases to 8.1 dB for the EAM reverse voltage of 2 V. It may also be observed that the ER power penalty, δ_{ER}, decreases and increases in accordance with increasing and decreasing ER. However, as the EAM reverse voltage is increased, the signal level in the "on" and "off" state power levels decreases due to the increase in the absorption of the EAM at the higher reverse voltage. From the graph shown in Figure 2.30, and the eye diagrams shown in Figure 2.30 insets (a) and (b), the reduction in the SNR in the "on" and "off" state power levels results in the closure of the eye diagram and a gradual reduction in the Q-factor, of the transmitted signal. With increasing EAM reverse voltage up to 1.8 V, the increase in the ER is offset by a decrease in the Q-factor, which is a result of the steeper gradient of the absorption curve shown in Figure 2.27. Thus, there is a trade-off between the ER and the Q-factor, Q, of the signals transmitted from the EML with increasing EAM reverse voltage, and a combination of both the ER and Q-factor, Q, of the transmitted optical signal will influence the transmission performance of the EML. The variation in the ER, δ_{ER}, and Q, of the signals transmitted from the EML is a result of the EAM power transfer curve and the absorption characteristics of the EAM.

Optical spectrum analysis

The optical spectra captured from the EML modulated with the 2 V_{pp} 12.5 Gbit/s NRZ-OOK signal for EAM reverse voltages ranging from 1 to 2 V in 0.1 V incremental steps are shown in Figure 2.31. The frequency axis has been normalised to determine if there is any bandwidth variation with increasing

EAM reverse voltage. It can be observed from the spectra shown in Figure 2.31 that the eleven spectra of the transmitted signals exhibit a similar 3-dB optical bandwidth, Δv_{3dB}, of ~12 GHz.

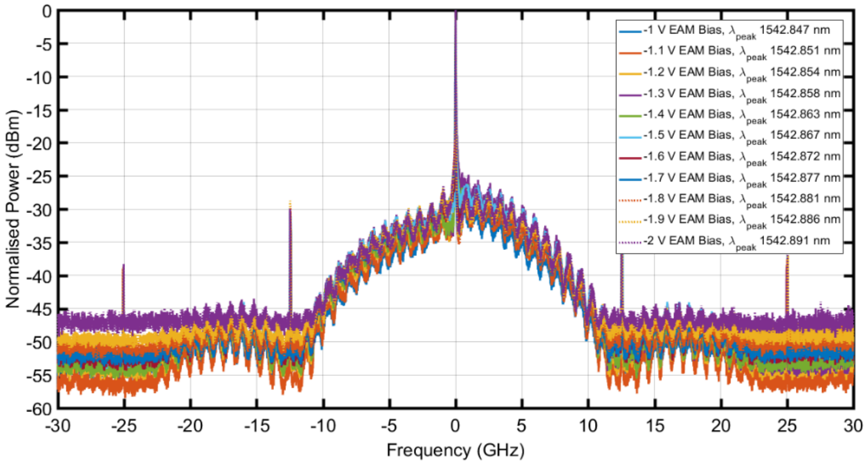

Figure 2.31: Optical spectra captured from the EML for a 12.5 Gbit/s NRZ-OOK modulating signal with a 2 V_{pp} modulating signal amplitude, a fixed DFB laser bias current of 80 mA and a fixed device TEC temperature of 25°C. The eleven different spectra correspond to EAM bias voltage settings ranging from -1 to -2 V increasing in increments of 0.1 V.

Unlike the optical spectra captured from the DML shown in Figure 2.7, the spectra captured from the EML resemble a typical double sideband NRZ-OOK spectrum with an envelope approximating a sinc^2(*f*) function. The sinc^2(*f*) shape of the spectra is due to the rectangular pulses that were used to modulate the EML. The spectral nulls, which occur at intervals of ~12.5 GHz, are characteristic of the NRZ data format. The tones, which occur at the null points, are due to the large carrier signal as a result of the high DFB laser bias employed. The ripples in the spectra are a result of the repetitive nature of the PRBS pattern, i.e. PRBS 2^{15}-1. While the spectra captured from the EML exhibit very little distortion, there is a small frequency chirp present in the signals, as evidenced by the asymmetry between the upper and lower sidebands about the carrier. As the EAM reverse voltage increases from 1 to 2 V the asymmetry shifts, which indicates that the alpha parameter, α_{EAM}, is changing.

2.3.2 Transmission Performance Evaluation of EML

This section deals with the experimental work carried out to evaluate the transmission performance of the EML in the IM/DD test-bed shown in Figure 2.9, when modulated with the 2 V_{pp} 12.5 Gbit/s NRZ-OOK signal with a PRBS of word length 2^{15}-1. The BER results obtained from the EML transmission experiments are presented, analysed and discussed. The experiments were carried out with the EML DFB laser bias current fixed at 80 mA, the device TEC temperature set at 25°C and for different EAM bias voltages ranging from -1 to -2 V. Similar to the DML transmission experiments in section 2.2.2, the b2b transmission performance of the EML was evaluated first to establish the minimum receiver sensitivities attainable for error-free transmission, i.e. for a 10^{-10} BER, where the performance of the link is limited only by the ER and Q of the transmitted signal and the SNR of the photodetector (PD).

Following the b2b transmission experiments, transmission experiments over 25 and 50 km of SSMF were performed to determine the effect of the frequency chirp of the EML and the CD in the fibre on the transmission performance. The experimental procedure, described in section 3.2.2, and setup, shown in Figure 2.9, which were utilised to acquire the BER results in the transmission experiments with the DML, were used to evaluate the transmission performance of the EML. Figure 2.32, Figure 2.33 and Figure 2.34 display the BER results of the transmission experiments with the EML for b2b transmission and transmission over 25 km and 50 km of SSMF, respectively. For the b2b transmission, the transmission performance of the EML was evaluated for EAM reverse voltages ranging from 1 to 2 V increasing in 0.2 V increments. For transmission over 25 and 50 km of SSMF, the performance of the EML was evaluated for 1.4, 1.6, 1.8 and 2 V EAM reverse voltages.

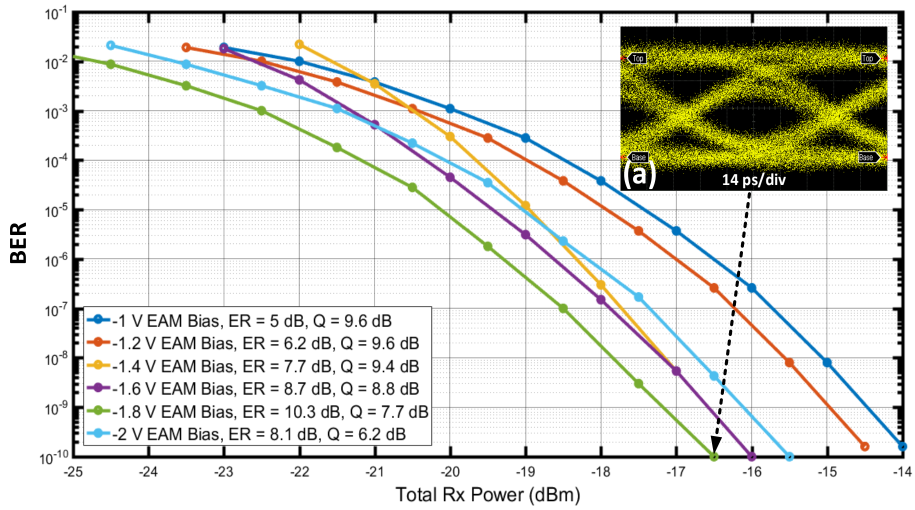

Figure 2.32: BER results for b2b transmission with EML (EML) in IM/DD test-bed using 12.5 Gbit/s NRZ-OOK modulation, inset (a) shows the eye diagram of the received signal captured for error-free transmission at a received power of -16.5 dBm with the EML for -1.8 V EAM bias voltage.

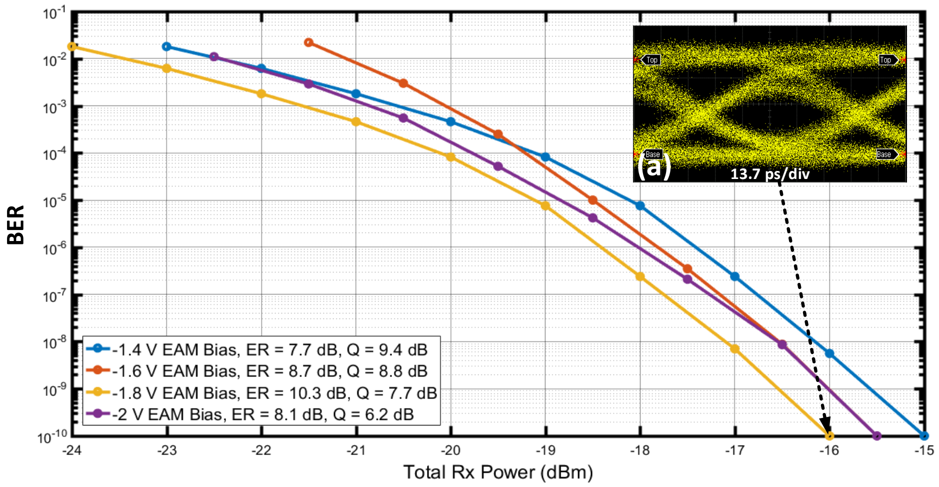

Figure 2.33: BER results for 25 km SSMF transmission with EML in IM/DD test-bed using 12.5 Gbit/s NRZ-OOK modulation, inset (a) shows the eye diagram of the received signal captured for error-free transmission at a received power of -16 dBm with the EML for -1.8 V EAM bias voltage.

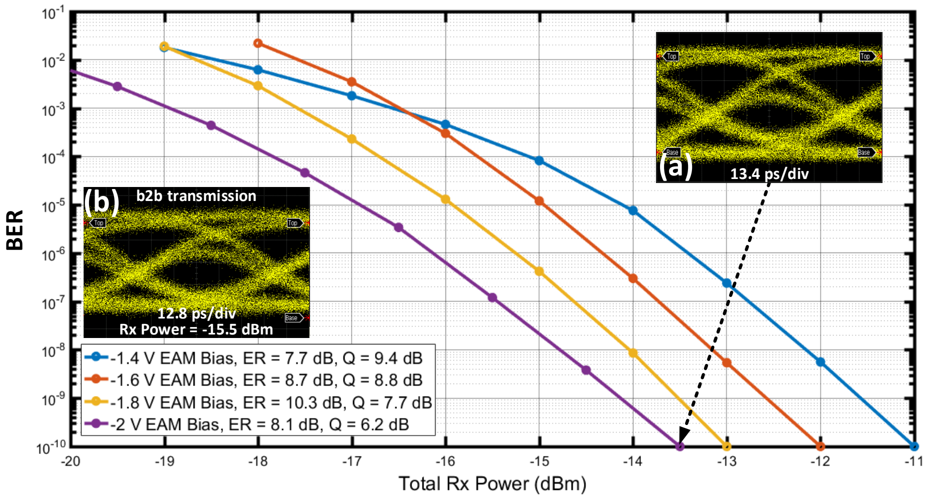

Figure 2.34: BER results for 50 km SSMF transmission with EML (EML) in IM/DD test-bed using 12.5 Gbit/s NRZ-OOK modulation. Inset (a) shows the eye diagram of the received signal captured for error-free 50 km SSMF transmission at a received power of -13.5 dBm, with the EML for -2 V EAM reverse voltage. Inset (b) shows the eye diagram of the received signal captured for error-free b2b transmission at a received power of -15.5 dBm with the EML for -2 V EAM bias voltage.

It can be observed in Figure 2.32 that the EAM bias voltage of -1.8 V yields the best b2b transmission performance with the EML in the IM/DD test-bed. For the -1.8V EAM bias voltage, the signal output from the EML exhibited the highest ER of 10.3 dB and a moderate Q-factor, Q, of 7.7 dB. It may also be observed that as the ER of the transmitted signal decreases, with increasing or decreasing EAM bias voltage, a receiver sensitivity penalty is incurred. The dependence of the EML b2b transmission performance on both the ER and the Q-factor, Q, of the transmitted signal is apparent when the performance of the EML for the EAM bias voltages of -1.4 and -2 V are compared. Although the ER of the signal transmitted from the EML for the -2 V EAM bias voltage is ~0.5 dB higher than the ER of the signal transmitted from the EML for the -1.4 V EAM bias voltage, the EML at the -1.4 V EAM bias voltage provides a ~0.5 dB improvement in receiver sensitivity. This may be attributed to the 3.2 dB higher Q-factor, Q, of the signal transmitted from the EML for the -1.4 V EAM bias voltage compared to the signal transmitted from for the -2 V EAM bias voltage. The received signal eye diagram shown in Figure 2.32 inset (a), captured for error-free transmission at a received optical power of -16.5 dBm with the EML for the -1.8 V EAM bias voltage, is a clear and open eye. However, there is a slight closure of the eye in the upper level due to amplitude variations or incomplete extinctions and the crossing point is slightly below 50%. This may be attributed to the asymmetric bias point of the EAM or the nonlinear EAM power transfer function, shown in Figure 2.27, and also to the internal capacitance of the EML. It may be concluded from the evaluation of the b2b transmission performance of the EML that a combination of both the ER and the Q-factor, Q, of the transmitted signal influences the b2b transmission performance.

From the BER results displayed in Figure 2.33, attained for transmission over 25 km of SSMF with the EML, it can be observed that the -1.8 V EAM bias voltage again produces the best BER performance, with error-free transmission achieved at a receiver sensitivity of -16 dBm. The eye diagram of the received signal captured for error-free transmission over 25 km of SSMF with the EML for the -1.8 V EAM bias voltage is shown in Figure 2.33 inset (a). The eye is relatively unchanged from the eye obtained for b2b transmission shown in Figure 2.32 inset (a). Relative to the b2b transmission performance of the EML for the -1.8 V EAM bias voltage, only a 0.5 dB receiver sensitivity penalty is incurred following transmission over 25 km of SSMF. Furthermore, a 0.5 and 1 dB receiver sensitivity penalty is incurred for 25 km SSMF transmission with the EML for the EAM bias voltages of -1.6 and -1.4 V, respectively. However, for transmission over 25 km of SSMF with the EML for the -2 V EAM bias voltage, no receiver sensitivity penalty is incurred relative to the b2b transmission performance. Thus, indicating that that the frequency chirp of the EML at the -2 V EAM bias voltage interacts favourably with the accumulated chromatic dispersion (CD) of the SSMF over the 25 km distance, unlike what is observed for 25km SSMF transmission with the EML for the -1.4, -1.6 and -1.8 V EAM bias voltages.

The favourable interaction of the CD in the optical fibre with the frequency chirp of the EML at the -2 V EAM bias voltage is more apparent for EML transmission over 50 km of SSMF. Figure 2.34 shows the BER results obtained from the 50 km SSMF transmission experiments with the EML. It can be observed in Figure 2.34 that the best transmission performance was attained with the EML for the -2 V EAM bias voltage, with error-free transmission achieved at a receiver sensitivity of -13.5 dBm. The eye diagram of the received signal captured for error-free transmission over 50 km of SSMF with the EML for the -2 V EAM bias voltage is shown in Figure 2.34 inset (a). Also shown in Figure 2.34 inset (b) is the received signal eye diagram for b2b transmission with the EML for the -2 V EAM bias voltage. On comparison of the two eye diagrams, the effect of the chromatic dispersion (CD) in the fibre can be observed in the apparent closure of the eye shown in Figure 2.34 inset (a), captured following 50 km SSMF transmission, and the reduction in the amplitude of the upper level eye component exhibiting incomplete extinction. Nonetheless, a clear and open received signal eye diagram was captured for 50 km SSMF transmission with the EML for the -2 V EAM bias voltage. Relative to b2b transmission, the receiver sensitivity penalty incurred for 50 km SSMF transmission with the EML for the -2 V EAM bias voltage was 2 dB. The receiver sensitivity penalties incurred for 50 km SSMF transmission with the EML for -1.8, -1.6 and -1.4 V EAM bias voltages were 3.5, 4 and 5 dB, respectively. It is clear from the BER results shown in Figure 2.34 that the frequency chirp generated by the EML for the -2 V EAM bias voltage interacts favourably with the accumulated chromatic dispersion (CD) in the SSMF over the 50 km distance. This resulted in the EML for the -2 V EAM bias voltage outperforming the EML for the -

1.8 V EAM bias voltage for transmission over 50 km of SSMF, unlike what was observed previously for b2b transmission and for transmission over 25 km of SSMF.

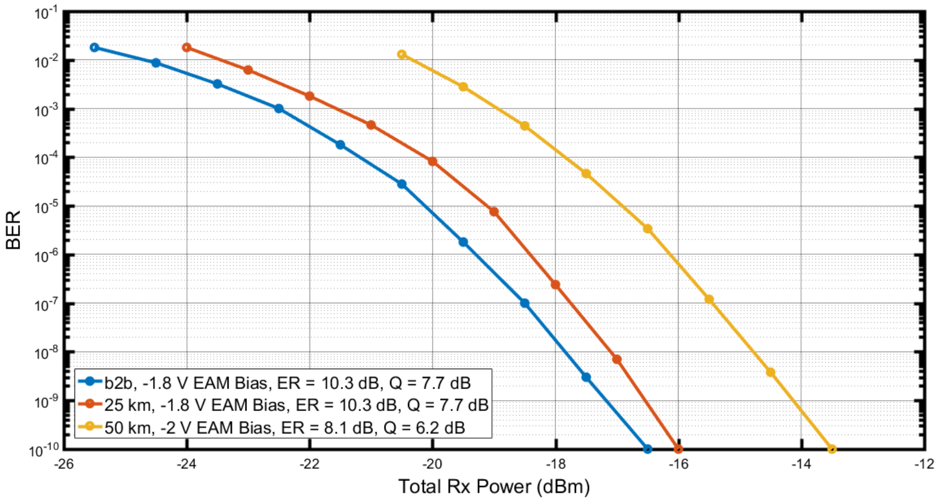

Figure 2.35: Best transmission performance achieved with EML (EML) in IM/DD test-bed using 12.5 Gbit/s NRZ-OOK modulation for b2b transmission and transmission over 25 and 50 km of SSMF.

Figure 2.35 shows the best BER results and transmission performances achieved with the EML for b2b transmission and for transmission over 25 and 50 km of SSMF.

2.3.3 Numerical Modelling and Simulation of EML IM/DD Transmission

This section discusses the numerical modelling that was carried out to simulate the performance of the EML transmitter externally modulated with a 2 V_{pp} 12.5 Gbit/s NRZ-OOK signal in the IM/DD test-bed. The purpose of the numerical model was to estimate the alpha parameter, α_{EAM}, values of the EAM integrated in the EML that was experimentally evaluated and, moreover, to determine the type of transient chirp and to estimate the peak-to-peak magnitude of the chirp exhibited by the EML. The EML numerical model was developed in MATLAB and is based on models described in previous studies [54], [60], [66] – [68]. Previous studies have shown that there can be an adiabatic chirp component in the overall chirp of EMLs [60], [64], however, the magnitude of the adiabatic chirp is typically quite small in comparison to the transient chirp. Thus, only the transient chirp was considered in the model employed in this study. To model the modulated optical signal output from the EML, the EAM power transfer curve shown in Figure 2.36, which was obtained experimentally for an 80 mA DFB laser bias current and a 25°C device TEC temperature over a 0 to -3 V EAM bias voltage range, was utilised. EAM alpha parameter, α_{EAM}, values were extracted from previous work [66] and the values were used to generate an EAM alpha parameter, α_{EAM}, function (red), which was fitted to the graph of the EAM power transfer function (blue) over the 0 to -3 V EAM bias voltage range, as shown in Figure 2.36.

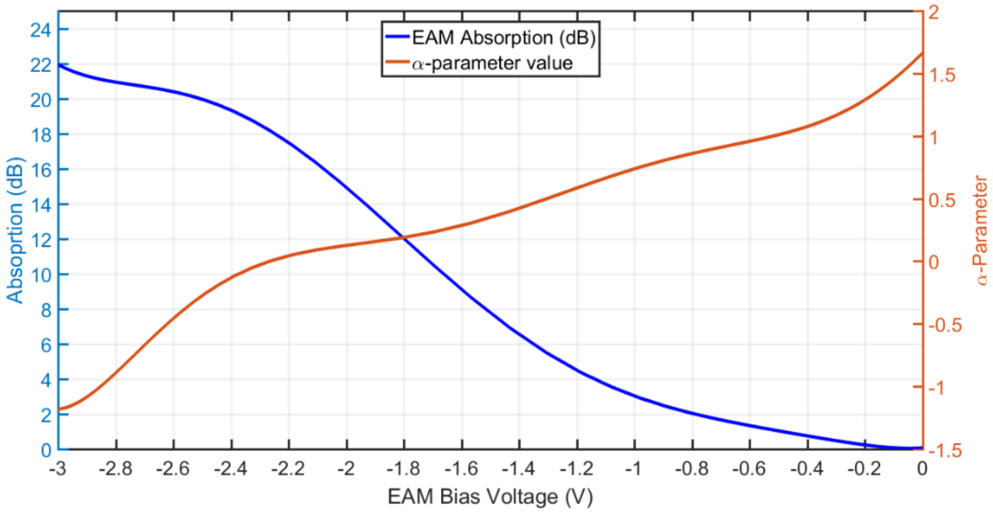

Figure 2.36: EAM power transfer curve and alpha parameter, α_{EAM}, curve used to model the signal transmitted from EML.

The optical power of the CW field input to the EAM was set to 3.3 mW in the model, as this was the experimentally measured optical power output from the EML for the 80 mA DFB laser bias and the 25°C device TEC temperature when no bias voltage was applied to the EAM. By applying polynomial interpolation to both the EAM power transfer and alpha parameter functions, the optical field, E_{out}, of the modulated signal output from the EML could be modelled using equation 2.13 [60], [66]

$$E_{out}(V) = P_{out}(V)^{(1+\alpha_{EAM}j)/2} \qquad 2.13$$

$$\Delta v(t) = \frac{1}{2\pi}\frac{d\phi(t)}{dt} = \frac{\alpha_{EAM}}{4\pi}\left(\frac{d}{dt}[\ln P_{out}(t)]\right) \qquad 2.14$$

where P_{out} is the voltage-dependent optical power of the signal transmitted from the EML and α_{EAM} is the alpha parameter. Using the IM/DD model described in section 2.2.3, the additive white Gaussian noise (AWGN) and the range of EAM alpha parameter, α_{EAM}, values were varied until the transmission performance and BER results generated by the model agreed with the experimental results attained for b2b transmission and transmission over 25 and 50 km of SSMF.

Figure 2.37, Figure 2.38 and Figure 2.39 show the simulated BER results generated by the model for b2b transmission and transmission over 25 and 50 km of SSMF, respectively, for EML EAM bias voltages of -1.4, -1.6, -1.8 and -2 V. The modified EAM alpha parameter, α_{EAM}, curve, which shows the range of alpha parameter, α_{EAM}, values that yielded the simulated BER results obtained from the model for EML transmission over 25 and 50 km of SSMF, is displayed in Figure 2.40. The alpha parameter values shown in Figure 2.40 were generated by multiplying the alpha parameter values shown in Figure 2.36 by 0.42. Also shown in Figure 2.40 insets (a) and (b) are the simulated eye diagrams of the optical signals transmitted from the modelled EML for EAM bias voltages of -1.4 and -2 V, respectively.

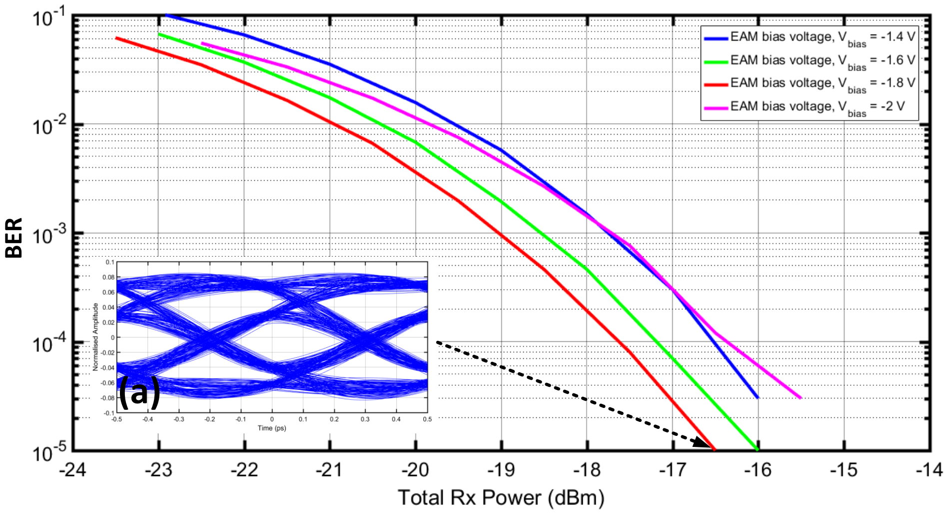

Figure 2.37: Simulated EML transmission performance for b2b transmission for EAM bias voltages of -1.4 V (blue), -1.6 (green), -1.8 (red) and -2 V (magenta). Inset (a) shows the received signal eye diagram for the -1.8 V EAM bias voltage.

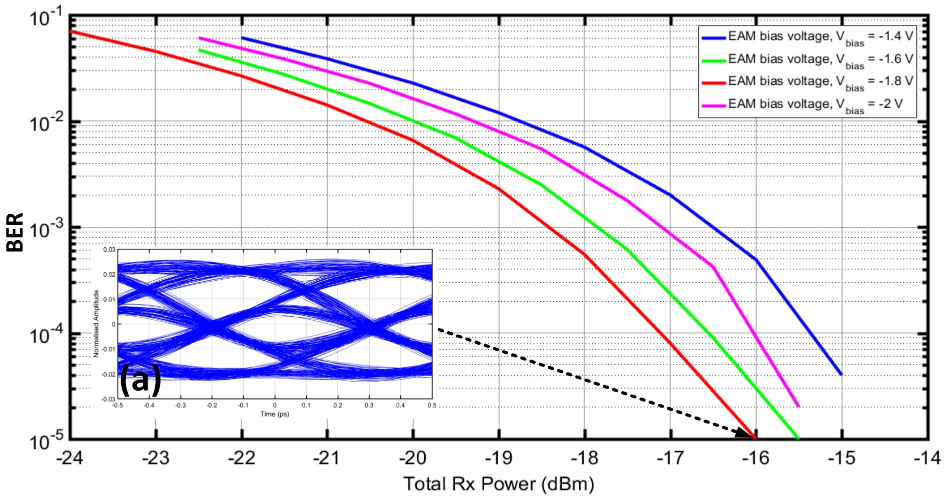

Figure 2.38: Simulated EML transmission performance for 25 km SSMF transmission for EAM bias voltages of -1.4 V (blue), -1.6 (green), -1.8 (red) and -2 V (magenta). Inset (a) shows the received signal eye diagram for the -1.8 V EAM bias voltage.

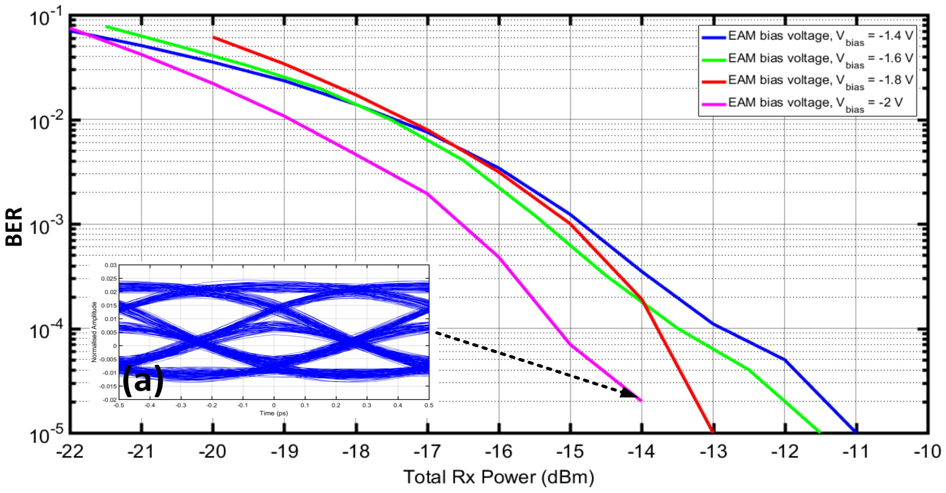

Figure 2.39: Simulated EML transmission performance for 50 km SSMF transmission for EAM bias voltages of -1.4 V (blue), -1.6 (green), -1.8 (red) and -2 V (magenta). Inset (a) shows the received signal eye diagram for the -2 V EAM bias voltage.

It can be observed in Figure 2.40 that the alpha parameter, α_{EAM}, values of the EAM, integrated in the EML that was experimentally evaluated, estimated from the model, range from 0.7 to -0.7 over the 0 to 3 V EAM reverse voltage range.

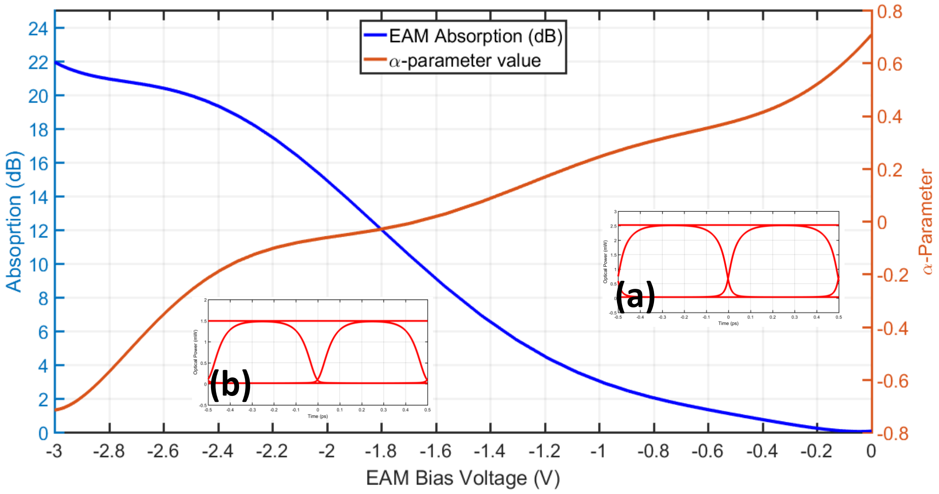

Figure 2.40: EAM power transfer curve and modified alpha parameter, α_{EAM}, curve used to model the signal field transmitted from the EML. Insets (a) and (b) show the simulated optical eye diagrams of the signals transmitted from the EML for EAM bias voltages of -1.4 and -2, respectively.

The optical power and frequency chirp waveforms of the signals transmitted from the EML for the -1.4 and -2 V EAM bias voltages are shown in Figure 2.41 and Figure 2.42, respectively. The frequency chirp waveforms, shown in Figure 2.41 and Figure 2.42, were generated using equation 2.14, which describes the transient chirp of an EAM. The output power, P_{out}, and alpha parameter, α_{EAM}, values were obtained from polynomial interpolation of the curves shown in Figure 2.40.

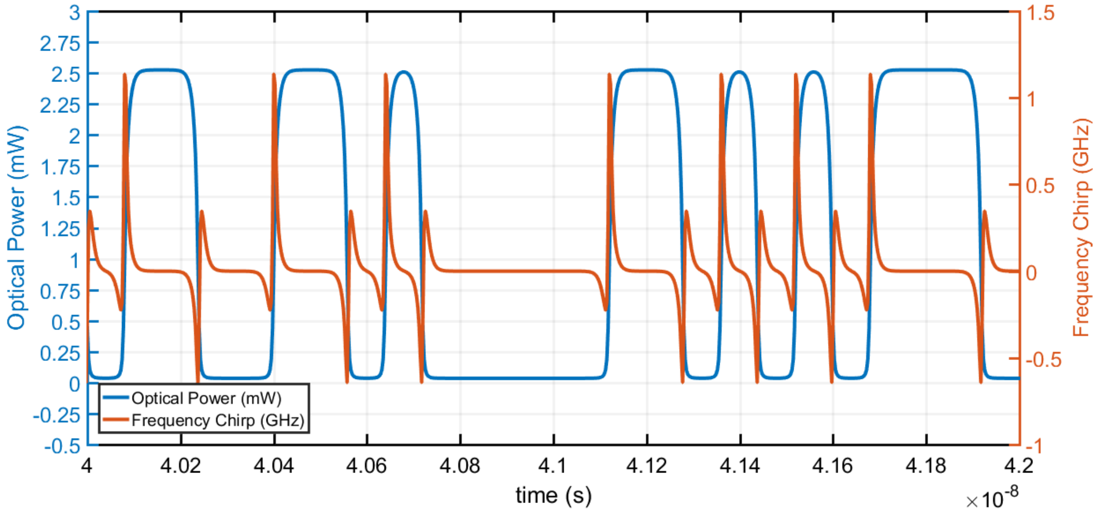

Figure 2.41: Optical power and frequency chirp waveforms of signal transmitted from EML for -1.4 EAM bias voltage.

From the optical power and chirp waveforms displayed in Figure 2.41, which were generated from the modelled EML for the -1.4 EAM bias voltage, it can be observed that the rising and falling edges of the optical pulses exhibited blue- and red-shifted chirp, respectively. This is due to the alpha parameter,

α_{EAM}, values, shown in Figure 2.40, being primarily positive within the on/off EAM modulation voltage swing. At the rising edge of the pulse, the magnitude of the blue-shifted chirp was ~1.1 GHz, while at the falling edge, the magnitude of the red-shifted chirp was ~0.6 GHz. Thus, the EML exhibited a peak-to-peak transient chirp of ~1.7 GHz when the EAM was biased at -1.4 V.

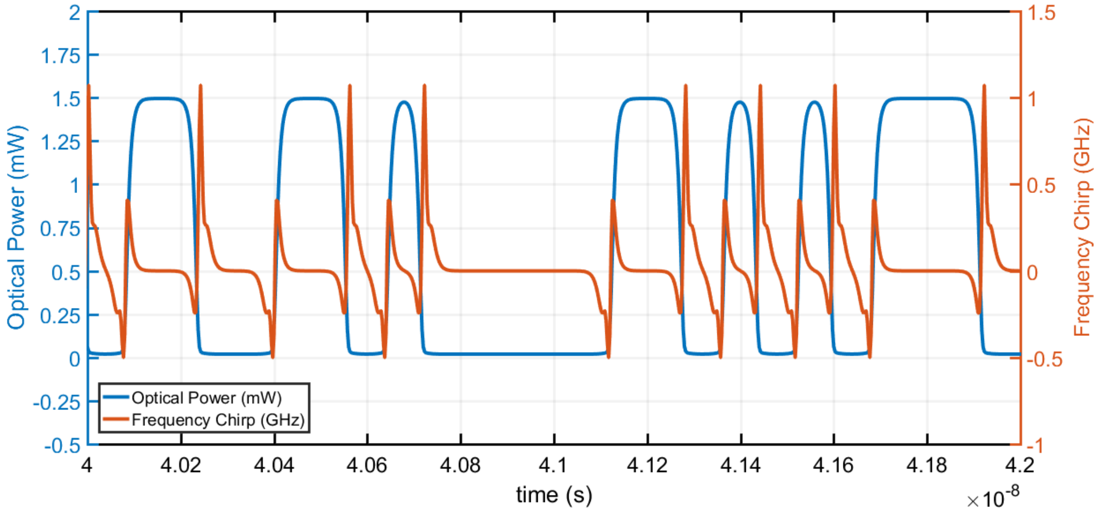

Figure 2.42: Optical power and frequency chirp waveforms of signal transmitted from EML for -2 EAM bias voltage.

In the optical power and chirp waveforms displayed in Figure 2.42, generated from the EML model for the -2 V EAM bias, the inverse was observed in the chirp waveform, where the rising and falling edges of the optical pulses exhibited red-shifted and blue-shifted chirp, respectively. This is due to the alpha parameter, α_{EAM}, values being primarily negative within the on/off EAM modulation voltage swing. At the rising edge of the optical pulse, the magnitude of the red-shifted chirp was ~0.5 GHz, while at the falling edge, the magnitude of the blue-shifted chirp was ~1.1 GHz. Thus, the EML exhibited a peak-to-peak transient chirp of ~1.6 GHz when the EAM was biased at -2 V.

From the simulated results, when the EAM exhibited positive alpha parameter values, the rising edge of the transmitted optical pulses experienced a blue-shift or positive chirp and the falling edge of the pulses experienced a red-shift or negative chirp, thus, the output of the EML is said to be positively chirped. Similar to what is observed with transient chirp dominated DMLs, when the EML is positively chirped, the optical pulses, which comprise the signal transmitted from the EML, will experience dispersive pulse broadening when propagating over SSMF at 1.55 μm. The pulse broadening can lead to a reduction in the pulse peak power, deformation of the pulse and ISI, which subsequently leads to a reduction in the receiver sensitivity and errors in the received signal. However, as the EAM bias voltage is reduced, and the absorption of the EAM increases, the alpha parameter, α_{EAM}, values decrease to low positive values or negative values. For high EAM reverse voltages, where the optical absorption is high and the alpha parameter values are negative, the EML becomes negatively chirped. When negatively chirped, the rising and falling edges of the optical pulses, which comprise the signal transmitted from the EML, are red-shifted and blue-shifted, respectively. For transmission over SSMF at 1.55 μm, the favourable interaction of the negatively chirped optical pulses with the CD in the fibre can result in pulse compression, therefore, extending the transmission distance of the EML, which is what was observed in this study for transmission over 50 km of SSMF with the EML for the -2 V EAM bias voltage. In general, EAM alpha parameter, α_{EAM}, values are small and positive (~0.5-2) for low EAM bias voltages (high reverse voltages), particularly when the detuning energy is large [57], [69]. The alpha parameter, α_{EAM}, value decreases with increasing EAM reverse voltage, or as the wavelength of the input lightwave decreases, both of which results in larger “on” state optical loss [57], [69]. Hence, for EAM-based EMLs, there is a trade-off between the optical loss or transmitted signal power and the alpha parameter value, α_{EAM}, of the EAM, which determines the type of transient chirp and the magnitude of the frequency chirp exhibited by the EML. Typically, after compromising ~3 dB of the transmitted signal optical power, a small positive to negative alpha parameter, α_{EAM}, value may be achieved within the on/off EAM modulation voltage swing [57], [69].

2.4 Conclusions

This chapter has experimentally investigated the characteristics and transmission performances of a directly modulated MQW DFB laser (DML) and an electo-absorption modulated laser (EML). Error-free 12.5 Gbit/s NRZ-OOK optical signal transmission is achieved with the DML and EML for transmission over 25 and 50 km of SSMF. A receiver sensitivity of -16 dBm is attained with the EML for 25 km SSMF transmission, which is 3 dB better than the receiver sensitivity attained with the DML, due to the additional chirp in the DML resulting in more broadening in the dispersive fibre. A receiver sensitivity of -13.5 dBm can be attained with both the DML and EML for transmission over 50 km of SSMF. The enhanced performance of the DML modulated well above threshold for transmission over 50 km of SSMF, may be attributed, in part, to the minimum shift keying (MSK) condition, which is established as a result of the mixed FM and AM of the DML. The favourable interaction of the adiabatic chirp dominated optical signal output from the DML with the accumulated chromatic dispersion in the SSMF over the 50 km distance, results in FM to AM conversion of the optical signal and in an open received signal eye diagram. Considering the cost-sensitivity of access networks, the DML would be the ideal choice over the EML. However, the ERs of the signals transmitted from the DML modulated well above threshold and the EML for the -2 V EAM bias voltage are 2.7 and 8.1 dB, respectively. In NG-PON2, a minimum ER of 6 dB has been specified for transmitters employed at the ONUs for upstream transmission [70], hence, would preclude the use of the DFB laser evaluated in this study, as a tunable DML in NG-PON2. Thus, a technique that increases the ER of the signal transmitted from the DML, which also maintains the chirp characteristics and transmission performance of the laser, is necessary.

References

[1] K. Sato, S. Kuwahara and Y. Miyamoto, "Chirp characteristics of 40-gb/s directly Modulated distributed-feedback laser diodes," in Journal of Lightwave Technology, vol. 23, no. 11, pp. 3790-3797, Nov. 2005, doi: 10.1109/JLT.2005.857753.

[2] G. Talli and P. D. Townsend, "Hybrid DWDM-TDM long-reach PON for next-generation optical access," in Journal of Lightwave Technology, vol. 24, no. 7, pp. 2827-2834, July 2006, doi: 10.1109/JLT.2006.875952.

[3] Y. Hong and K. A. Shore, "Locking characteristics of a side-mode injected semiconductor laser," in IEEE Journal of Quantum Electronics, vol. 35, no. 11, pp. 1713-1717, Nov. 1999, doi: 10.1109/3.798096.

[4] S. K. Hwang and J. M. Tian, "Chirp reduction in directly-modulated semiconductor lasers subject to external optical injection," 2005 IEEE LEOS Annual Meeting Conference Proceedings, Sydney, NSW, 2005, pp. 798-799, doi: 10.1109/LEOS.2005.1548249.

[5] L. Illing and M. B. Kennel, "Shaping current waveforms for direct modulation of semiconductor lasers," in IEEE Journal of Quantum Electronics, vol. 40, no. 5, pp. 445-452, May 2004, doi: 10.1109/JQE.2004.826446.

[6] H. Sung, E. K. Lau and M. C. Wu, "Optical Single Sideband Modulation Using Strong Optical Injection-Locked Semiconductor Lasers," in IEEE Photonics Technology Letters, vol. 19, no. 13, pp. 1005-1007, July1, 2007, doi: 10.1109/LPT.2007.898760.

[7] R. Heidemann, B. Wedding and G. Veith, "10-Gb/s transmission and beyond," in Proceedings of the IEEE, vol. 81, no. 11, pp. 1558-1567, Nov. 1993, doi: 10.1109/5.247727.

[8] B. Wedding, "New method for optical transmission beyond dispersion limit," in Electronics Letters, vol. 28, no. 14, pp. 1298-1300, 2 July 1992, doi: 10.1049/el:19920825.

[9] L.-S. Yan, Y. Wang, B. Zhang, C. Yu, J. McGeehan, L. Paraschis, and A. E. Willner, "Reach extension in 10-Gb/s directly modulated transmission systems using asymmetric and narrowband optical filtering," Opt. Express 13, 5106-5115 (2005).

[10] D. Mahgerefteh, Y. Matsui, X. Zheng and K. McCallion, "Chirp Managed Laser and Applications," in IEEE Journal of Selected Topics in Quantum Electronics, vol. 16, no. 5, pp. 1126-1139, Sept.-Oct. 2010, doi: 10.1109/JSTQE.2009.2037336.

[11] Y. Matsui et al., "Chirp-managed directly modulated laser (CML)," in IEEE Photonics Technology Letters, vol. 18, no. 2, pp. 385-387, Jan. 15, 2006, doi: 10.1109/LPT.2005.862358.

[12] S. Warm, C.-A. Bunge, T. Wuth and K. Petermann, "Electronic Dispersion Precompensation With a 10-Gb/s Directly Modulated Laser," in IEEE Photonics Technology Letters, vol. 21, no. 15, pp. 1090-1092, Aug.1, 2009, doi: 10.1109/LPT.2009.2022957.

[13] J. Tabares, A. Napoli, V. Polo, S. Calabrò, B. Sommerkorn-Krombholz, B. Spinnler, and J. Prat, "Digital Pre-emphasis for 10Gb/s with Low-cost Directly Phase-Modulated Lasers for PONs," in Advanced Photonics 2018 (BGPP, IPR, NP, NOMA, Sensors, Networks, SPPCom, SOF), OSA Technical Digest (online) (Optical Society of America, 2018), paper SpTh3G.2.

[14] C. Browning, K. Shi, P. M. Anandarajah, R. Phelan and L. P. Barry, "Direct modulation of a tuneable slotted Fabry-Pérot laser with adaptive modulation OFDM," 2012 38th European Conference and Exhibition on Optical Communications, Amsterdam, 2012, pp. 1-3.

[15] X. Yin et al., "40-Gb/s TDM-PON downstream with low-cost EML transmitter and 3-level detection APD receiver," 2016 Optical Fiber Communications Conference and Exhibition (OFC), Anaheim, CA, 2016, pp. 1-3.

[16] J. Verbist et al., "First real-time 100-Gb/s NRZ-OOK transmission over 2 km with a silicon photonic electro-absorption modulator," 2017 Optical Fiber Communications Conference and Exhibition (OFC), Los Angeles, CA, 2017, pp. 1-3.

[17] J. C. Velásquez, J. Tabares, and J. Prat, "Differential 8-APSK monolithically integrated dual-EML transmitter for flexible coherent PONs," Opt. Lett. 44, 2760-2763 (2019).

[18] C. Pinho, F. Rodrigues, A.M. Tavares, C. Rodrigues, C.E. Rodrigues and A. Teixeira, "Photonic Integrated Circuits for NGPON2 ONU Transceivers (Invited)," Appl. Sci. 2020, 10, 4024.

[19] M. Azadeh, "Fiber Optics Engineering," Springer US, 2009.

[20] C. DeCusatis, "Handbook of Fibre Optic Data Communication: A Practical Guide to Optical Networking, 4th Edition", Academic Press, 2013.

[21] R. Hui, "Introduction to Fibre-Optic Communications," 1st Edition, Academic Press, 2019.

[22] J. C. Cartledge and R. C. Srinivasan, "Extraction of DFB laser rate equation parameters for system simulation purposes," in Journal of Lightwave Technology, vol. 15, no. 5, pp. 852-860, May 1997, doi: 10.1109/50.580827.

[23] T. L. Koch and J. E. Bowers, "Nature of wavelength chirping in directly modulated semiconductor lasers," in Electronics Letters, vol. 20, no. 25, pp. 1038-1040, 6 December 1984, doi: 10.1049/el:19840709.

[24] R. Tucker, "High-speed modulation of semiconductor lasers," in Journal of Lightwave Technology, vol. 3, no. 6, pp. 1180-1192, December 1985, doi: 10.1109/JLT.1985.1074340.

[25] R. Nagarajan, J. E. Bowers, "Chapter 3 - High-Speed Lasers, In Optics and Photonics, Semiconductor Lasers I, Academic Press, 1999, Pages 177-290.

[26] P. Krehlik, "Characterization of semiconductor laser frequency chirp based on signal distortion in dispersive optical fiber," Opto-Electron. Rev. 14, 119–124 (2006).

[27] T. L. Koch and R. A. Linke, “Effect of nonlinear gain reduction on semiconductor laser wavelength chirping,” Appl. Phys. Lett. 48 (10). 10 March 1986.

[28] C. Henry, "Theory of the linewidth of semiconductor lasers," in IEEE Journal of Quantum Electronics, vol. 18, no. 2, pp. 259-264, February 1982, doi: 10.1109/JQE.1982.1071522.

[29] C. A. Green, N. K. Dutta, and W. Watson, "Linewidth enhancement factor in InGaAsP/InP multiple quantum well lasers," Applied Physics Letters, vol. 50, no. 20, pp. 1409, 1987.

[30] I. Tomkos, I. Roudas, R. Hesse, N. Antoniades, A. Boskovic, R. Vodhanel, "Extraction of laser rate equations parameters for representative simulations of metropolitan-area transmission systems and networks," Optics Communications, Volume 194, Issues 1–3, Pages 109-129, 2001.

[31] J. D. Downie, I. Tomkos, N. Antoniades and A. Boskovic, "Effects of filter concatenation for directly modulated transmission lasers at 2.5 and 10 Gb/s," in Journal of Lightwave Technology, vol. 20, no. 2, pp. 218-228, Feb. 2002, doi: 10.1109/50.983235.

[32] K. Hinton and T. Stephens, "Modeling high-speed optical transmission systems," in IEEE Journal on Selected Areas in Communications, vol. 11, no. 3, pp. 380-392, April 1993, doi: 10.1109/49.219553.

[33] M. Blez et al., "Very low chirping of InGaAs-InGaAlAs MQW DFB BRS lasers under 10 Gbit/s modulation," in IEEE Journal of Quantum Electronics, vol. 29, no. 6, pp. 1676-1681, June 1993, doi: 10.1109/3.234420.

[34] J. Binder and U. Kohn, "10 Gbit/s-dispersion optimized transmission at 1.55 µm wavelength on standard single mode fiber," in IEEE Photonics Technology Letters, vol. 6, no. 4, pp. 558-560, April 1994, doi: 10.1109/68.281826.

[35] S. Pato, R. Luis, P. Monteiro, H. Silva, "On the Impact of Nonlinear Effects in 10 Gbit/s Ethernet Passive Optical Networks,” Conference Paper, March 2006.

[36] G.-Y. Kim and Y.-G. Lee, "The influence of chirp and extinction ratio on directly modulated DFB lasers," Technical Digest. CLEO/Pacific Rim 2001. 4th Pacific Rim Conference on Lasers and Electro-Optics (Cat. No.01TH8557), Chiba, Japan, 2001, pp. II-II.

[37] S. J. Wang, L. J. P. Ketelsen, V. R. McCrary, Y. Twu, S. G. Napholtz and W. Werner, "Dynamic and CW linewidth measurements of 1.55- µm InGaAs-InGaAsP multiquantum well distributed feedback lasers," in IEEE Photonics Technology Letters, vol. 2, no. 11, pp. 775-777, Nov. 1990, doi: 10.1109/68.63217.

[38] S. Mohrdiek et al., "10-Gb/s standard fiber transmission using directly modulated 1.55-µm quantum-well DFB lasers," in IEEE Photonics Technology Letters, vol. 7, no. 11, pp. 1357-1359, Nov. 1995, doi: 10.1109/68.473497.

[39] P. A. Morton et al., "High-speed, low chirp, directly modulated 1.55-µm DFB laser sources for 10 Gbit/s local distribution," Optical Fiber Communications, OFC., San Jose, CA, USA, 1996, pp. 39-40, doi: 10.1109/OFC.1996.907622.

[40] P.–K. Lau and T. Makino, "Effects of laser diode parameters on power penalty in 10 Gb/s optical fiber transmission systems," in Journal of Lightwave Technology, vol. 15, no. 9, pp. 1663-1668, Sept. 1997, doi: 10.1109/50.622891.

[41] J. A. P. Morgado and A. V. T. Cartaxo, "Improved model to discriminate adiabatic and transient chirps in directly modulated semiconductor lasers," Journal of Modern Optics, 56:21, 2309-2317, 2009, DOI: 10.1080/09500340903348809.

[42] B. Wedding, "New method for optical transmission beyond dispersion limit," in Electronics Letters, vol. 28, no. 14, pp. 1298-1300, 2 July 1992, doi: 10.1049/el:19920825.

[43] B. Wedding, B. Franz and B. Junginger, "10-Gb/s optical transmission up to 253 km via standard single-mode fiber using the method of dispersion-supported transmission," in Journal of Lightwave Technology, vol. 12, no. 10, pp. 1720-1727, Oct. 1994.

[44] Y. Matsui et al., "Chirp-managed directly modulated laser (CML)," in IEEE Photonics Technology Letters, vol. 18, no. 2, pp. 385-387, Jan. 15, 2006, doi: 10.1109/LPT.2005.862358.

[45] D. Mahgerefteh, Y. Matsui, X. Zheng and K. McCallion, "Chirp Managed Laser and Applications," in IEEE Journal of Selected Topics in Quantum Electronics, vol. 16, no. 5, pp. 1126-1139, Sept.-Oct. 2010, doi: 10.1109/JSTQE.2009.2037336.

[46] T. Ono et al., "Characteristics of optical duobinary signals in terabit/s capacity, high-spectral efficiency WDM systems," in Journal of Lightwave Technology, vol. 16, no. 5, pp. 788-797, May 1998, doi: 10.1109/50.669006.

[47] R. S. Tucker, "Large-signal switching transients in index-guided semiconductor lasers," in Electronics Letters, vol. 20, no. 19, pp. 802-803, 13 September 1984.

[48] J. Yu et al., "Applications of 40-Gb/s Chirp-Managed Laser in Access and Metro Networks," in Journal of Lightwave Technology, vol. 27, no. 3, pp. 253-265, Feb.1, 2009.

[49] D. Mahgerefteh (Finisar Corporation), "Chirp Managed Laser (CML) and Applications," March 23, 2011. Available at: https://iee.ucsb.edu/sites/default/files/docs/mahgerefteh_daniel.pdf

[50] S. Melnik, G. Huyet, and A. V. Uskov, "The linewidth enhancement factor α of quantum dot semiconductor lasers," Opt. Express 14, 2950-2955, 2006.

[51] G.-W. Lee, and S.-K. Han, "Linear dual electroabsorption modulator for analog optical transmission," Microw. Opt. Technol. Lett., 22: 369-373, 1999.

[52] H.-D. Jung et al., "Nonlinearity suppression of electroabsorption modulator through dual-parallel modulation," Microw. Opt. Technol. Lett., 29: 2-5, 2001.

[53] F. Deshours, C. Algani, F. Blache, G. Alquié, C. Kazmierski and C. Jany, "New Nonlinear Electrical Modeling of High-Speed Electroabsorption Modulators for 40 Gb/s Optical Networks," in Journal of Lightwave Technology, vol. 29, no. 6, pp. 880-887, March15, 2011.

[54] Y. Kim, S. Hur, H. Jang and J. Jeong, "Theoretical and Experimental Study of Large Signal Chirp in Electro-Absorption Modulators Integrated DFB Lasers," Journal of The Korean Physical Society - J KOREAN PHYS SOC, 37, 2000.

[55] W.W. Feng and N.H. Zhu, "Analysis of chirp characteristics of DFB lasers and integrated laser-modulators," Opt Quant Electron 36, 1237–1245, 2004.

[56] J. A. J. Fells et al., "Chirp and system performance of integrated laser modulators," in IEEE Photonics Technology Letters, vol. 7, no. 11, pp. 1279-1281, Nov. 1995, doi: 10.1109/68.473471.

[57] G. L. Li and P. K. L. Yu, "Optical intensity modulators for digital and analog applications," in Journal of Lightwave Technology, vol. 21, no. 9, pp. 2010-2030, Sept. 2003.

[58] F. Devaux et al., "Electroabsorption modulators for high-bit-rate optical communications: a comparison of strained InGaAs/InAIAs and InGaAsP/InGaAsP MQW," Semiconductor Science and Technology 10 (1995): 887-901.

[59] G. B. Morrison, J. W. Raring, C. S. Wangb, E. J. Skogen, Y.-C. Chang, M. Sysak, L. A. Coldren, "Electroabsorption modulator performance predicted from band-edge absorption spectra of bulk, quantum-well, and quantum-well-intermixed InGaAsP structures," Solid-State Electronics, Volume 51, Issue 1, January 2007, Pages 38-47.

[60] R. Chen and J. C. Cartledge, "Measurement-based model for the modulation properties of an integrated laser modulator and its application to systems with tight optical filtering," in Journal of Lightwave Technology, vol. 23, no. 4, pp. 1683-1691, April 2005.

[61] T. Yamanaka, K. Wakita and K. Yokoyama, "Potential chirp-free characteristics (negative chirp parameter) in electroabsorption modulation using a wide tensile-strained quantum well structure," Appl. Phys. Lett. 68, 3114, 1996.

[62] P. Brosson and H. Bissessur, "Analytical expressions for the FM and AM responses of an integrated laser-modulator," in IEEE Journal of Selected Topics in Quantum Electronics, vol. 2, no. 2, pp. 336-340, June 1996, doi: 10.1109/2944.577390.

[63] Y. Kim, H. Lee, J. Lee, J. Han, T. W. Oh and J. Jeong, "Chirp characteristics of 10-Gb/s electroabsorption modulator integrated DFB lasers," in IEEE Journal of Quantum Electronics, vol. 36, no. 8, pp. 900-908, Aug. 2000.

[64] I. Garcés, A. Villafranca, and J. Lasobras "Characterization of the chirp behavior of integrated laser modulators (ILM) by measurements of its optical spectrum", Proc. SPIE 6997, Semiconductor Lasers and Laser Dynamics III, 69971S (8 May 2008).

[65] G.P. Agrawal, "Fibre-Optic Communication Systems," 4th edition, Wiley (2010).

[66] J. C. Cartledge and B. Christensen, "Optimum operating points for electroabsorption modulators in 10 Gb/s transmission systems using nondispersion shifted fiber," in Journal of Lightwave Technology, vol. 16, no. 3, pp. 349-357, March 1998, doi: 10.1109/50.661360.

[67] Y. Kim, S.K. Kim, J. Lee, Y. Kim, J. Kang, W. Choi and J. Jeong, "Characteristics of 10-Gb/s Electroabsorption Modulator Integrated Distributed Feedback Lasers for Long-Haul Optical Transmission Systems, Optical Fiber Technology, Volume 7, Issue 2, Pages 84-100, ISSN 1068-5200, 2001. https://doi.org/10.1006/ofte.2000.0352.

[68] M. Y. Jamro, J. M. Senior, "Optimising negative chirp of an electroabsorption modulator for use in high-speed optical networks," European Transactions on Telecommunications, 2007.

[69] F. Dorgeuille and F. Devaux, "On the transmission performances and the chirp parameter of a multiple-quantum-well electroabsorption modulator," in IEEE Journal of Quantum Electronics, vol. 30, no. 11, pp. 2565-2572, Nov. 1994, doi: 10.1109/3.333708.

[70] ITU-T Telecommunication Standardization Sector of ITU: 40-Gigabit-capable passive optical networks 2 (NG PON2): Physical media dependent (PMD) layer specification, Corrigendum 1. Recommendation ITU-T G.989.2 (08/2019) – Corrigendum 1.

Chapter 3 Self-Seeded Fabry-Pérot (SS-FP) Laser as a Tunable Laser Source (TLS) for Next Generation PONs

3.1 Introduction

The introduction of wavelength division multiplexing (WDM) technology to NG-PON2 heralds in a new era for optical access, and will serve to increase the transmission capacity and bandwidth efficiency of future access networks. However, the introduction of WDM technology to the access domain places greater demands on the tunable transmitters and the optical components that are required to realise these new networks. Tunable lasers are considered the most logical choice of transmitter for NG-PON2 and future optical access networks employing WDM, as they exhibit wideband wavelength tunability, fast switching times between wavelength channels, fine tuning granularity and excellent wavelength stability. Considering the potentially large numbers of subscriber ONUs in the NG-PON2 architecture, illustrated in Figure 3.1, cost-effective tunable lasers will be necessary. Not only will the tunable laser sources need to be cost-effective for wide-scale and mass deployment, they will also be required to meet certain performance parameters so that the technical requirements laid down in the NG-PON2 standard [1] are met.

Thus, the development of novel and cost-effective tunable lasers for future optical access networks is vitally important to support the ever growing data rate and bandwidth demands of end-users globally. The 'colourless' transmitters that are needed to realise these future networks must demonstrate the capability to operate at high bit rates (10+ Gbit/s per λ channel) and, moreover, exhibit low chirp, high output optical power (>+3 dBm), wide wavelength tuning ranges (>20 nm), fine wavelength granularity and fast switching speeds between stable wavelength channels. Furthermore, the tunable lasers that are proposed will need to exhibit low relative intensity noise (RIN), as the RIN of transmitters is one of the main limiting factors in the transmission performance of IM/DD links. Additionally, these novel tunable lasers will need to exhibit low power consumption and a small foot print.

Considering the number of wavelength channels (4-8) and channel spacing (50/100/200 GHz) specified for NG-PON2, directly modulated thermally tunable DFB lasers [2] have been identified as potential candidate transmitters for initial NG-PON2 deployments due to the relatively low cost of DFB lasers and their reasonable wavelength tuning range. However, the transmission distances and modulation rates that directly modulated (DM) DFB lasers can achieve are severely limited by the intrinsic chirp of the devices. Furthermore, as the number of subscribers and network capacity requirements increases, tunable lasers that exhibit wider tuning ranges and finer tuning granularity will be necessary. Verticalcavity surface-emitting lasers (VCSELs), which use micro electro-mechanical mirror systems (MEMs) to achieve wavelength tuning, offer an alternative to DM thermally tunable DFB lasers and have been successfully demonstrated for WDM-PON [3], [4]. However, there are concerns with VCSELs regarding their wavelength stability, switching time, reliability, cost-effectiveness and scalability. Other tunable laser technologies currently being considered for use in NG-PON2 and future optical access networks include directly modulated DBR lasers [5], [6], and DBR lasers without cooling, i.e. with no integrated TEC [7], and externally modulated lasers (EMLs) that comprise electro-absorption modulators (EAMs) monolithically integrated with laser arrays [8]. Similar to VCSELs, questions remain regarding the cost-effectiveness of DBR lasers and EMLs for optical access network applications.

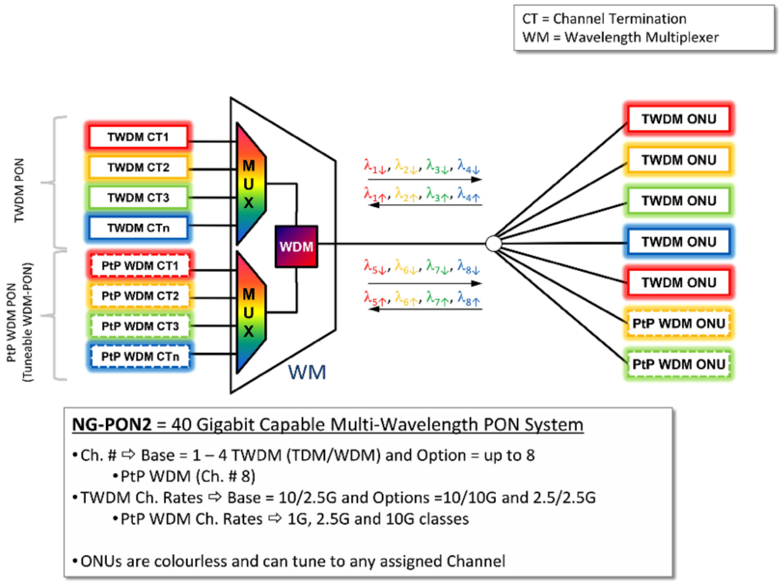

NG-PON2 = 40 Gigabit Capable Multi-Wavelength PON System

- Ch. # ⇨ Base = 1 – 4 TWDM (TDM/WDM) and Option = up to 8
  - PtP WDM (Ch. # 8)
- TWDM Ch. Rates ⇨ Base = 10/2.5G and Options =10/10G and 2.5/2.5G
  - PtP WDM Ch. Rates ⇨ 1G, 2.5G and 10G classes
- ONUs are colourless and can tune to any assigned Channel

Figure 3.1: NG-PON2 system architecture and high level features. Note that the internal configuration of the WDM is just for illustration and is not defined by ITU-T recommendations [9].

This chapter presents an experimental characterization of a self-seeded Fabry-Pérot (SS-FP) laser. The transmission performance of the directly modulated (DM) SS-FP laser is experimentally evaluated in an IM/DD test-bed, as NG-PON2 will utilise IM/DD transmission. The transmission performance of the DM SS-FP laser is evaluated with two intensity modulation formats, 12.5 Gbit/s NRZ-OOK modulation and 12.5 Gbaud/s (25 Gbit/s) 4-level pulse amplitude modulation (PAM-4), as the PAM-4 format will most likely replace the NRZ-OOK format to increase the capacity of future PONs. The proposed self-seeded Fabry-Pérot (SS-FP) laser could be a very promising candidate for cost-effective colourless ONUs in future bandwidth symmetric TWDM-PON.

3.2 Fabry-Pérot (FP) Laser as a Tunable Laser Source (TLS)

The wide multi-longitudinal mode (MLM) spectrum of a Fabry-Pérot (FP) laser makes it unsuitable for optical fibre communications, unless the FP laser is utilised in single-channel transmission systems over short distances (~500 m). This is due to the wavelength dependent chromatic dispersion of standard single-mode fibre (SSMF), which results in the optical signals transmitted from an FP laser becoming severely distorted when propagating in SSMF and, ultimately, destroys the received signal. Moreover, the wide multimode spectrum of an FP laser would preclude its use in NG-PON2 and optical access networks employing WDM, due to the specified wavelength channel spacing of 50, 100 or 200 GHz, where each channel requires its own assigned wavelength channel. However, it is the wide multi-mode spectrum, high output optical power, low power consumption and the cost-effectiveness of FP lasers which make them ideal components to help realise colourless PONs and future optical access networks. When an FP laser is injection-locked (IL) [10], self-seeded (SS) [11], or subjected to external injection with spectrally-sliced broadband light [12], single-mode operation with the FP laser can be achieved. Furthermore, the wavelength-locking (WL) techniques allow any of the longitudinal modes in the MLM spectrum of the FP laser to be accessed dynamically. When the wavelength locking techniques are employed to achieve single-mode (SM) operation with an FP laser, the main factor limiting the realisation of stable single-mode operation, and successful signal transmission, is the mode partition noise (MPN) and MPN-induced relative intensity noise (RIN) of the FP laser.

3.2.1 Mode Partition Noise (MPN) of an FP Laser

When multiple wavelengths satisfy the phase condition of an FP laser cavity, the number of longitudinal modes that lase is largely dependent on the length of the cavity and, furthermore, on the width of the semiconductor material gain curve. The longitudinal modes supported by the cavity will compete for the shared carrier density and the modes near the peak of the gain curve will consume the majority of the carriers, hence, will exhibit the highest optical powers. Although the carrier density along the cavity is non-uniform, the difference in the optical gain experienced by the modes at the peak of the gain curve is quite small. However, mode competition and random perturbations to the optical gain in the cavity, due to spontaneous emission, external reflections or temperature variations, results in random fluctuations in the instantaneous optical power distribution among the multiple longitudinal modes, which is known as mode partition noise (MPN) [13]. Under dc bias conditions the optical power output from an FP laser remains relatively constant, as the total photon number is stabilised due to the carrier-gain dynamic reaching an equilibrium. However, since there is only one carrier pool from which all of the lasing modes consume carriers, this stabilisation process is effective only for the total photon number, and the stabilisation process, via the carrier density, does not hold for a single longitudinal mode within the multimode spectrum [14]. Therefore, the relative intensity noise (RIN), which describes the fluctuations in the CW output optical power of a laser, is much higher for a single longitudinal mode within the multi-longitudinal laser spectrum when compared to the full spectrum, particularly at low frequencies. The MPN, σ_{mpn}, imposes a limit on the transmission performance of an FP laser in an IM/DD link through an MPN-induced power penalty, α_{mpn} [15] – [17].

3.2.2 FP Laser Characterisation and Directly Modulated (DM) Transmission Performance

The FP laser used in this work was packaged in a 7-pin butterfly package, which included an integrated thermo-electric cooler (TEC), a thermistor, a back facet monitor detector and an internal bias tee. The 7-pin butterfly package also comprised an integrated optical isolator and a polarization maintaining (PM) pigtailed fibre, which provided the optical output of the laser. The RF input to the laser was a k-type connector, which allowed it to be directly modulated via an external dc block. Before developing the self-seeded FP (SS-FP) laser scheme, basic static and dynamic characterisation of the FP laser was performed and the transmission performance of the directly modulated (DM) FP laser, for both b2b transmission and transmission over 1 km of SSMF, was evaluated. The P-I curve of the FP laser is shown in Figure 3.2. The P-I curve was produced from data acquired with the FP laser device TEC temperature set at 25°C.

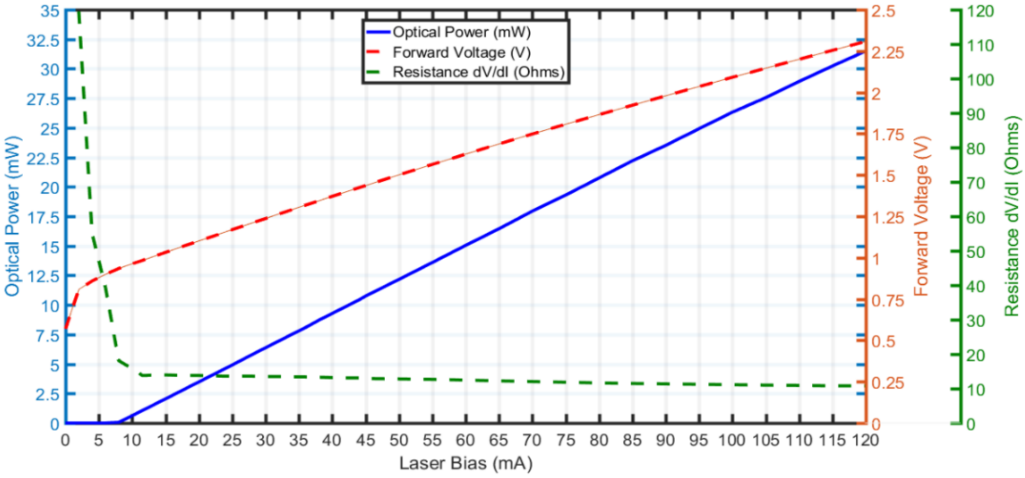

Figure 3.2: P-I, V-I and dynamic impedance curves for FP laser for a device TEC temperature of 25°C.

It can be observed from Figure 3.2 that the threshold current, I_{th}, of the FP laser is 8 mA and, at the maximum current rating of 120 mA, the output optical power from the laser is 31.5 mW. The slope efficiency, $\frac{dP}{dI}$, and the differential quantum efficiency, η_d, calculated from the P-I curve, are 0.2849 mW/mA (~28%) and ~72%. The MLM spectra captured from the FP laser for a 30 mA laser bias current and 15°C (red spectrum), 25°C (blue spectrum), and 35°C (yellow spectrum) device TEC temperatures, are shown in Figure 3.3.

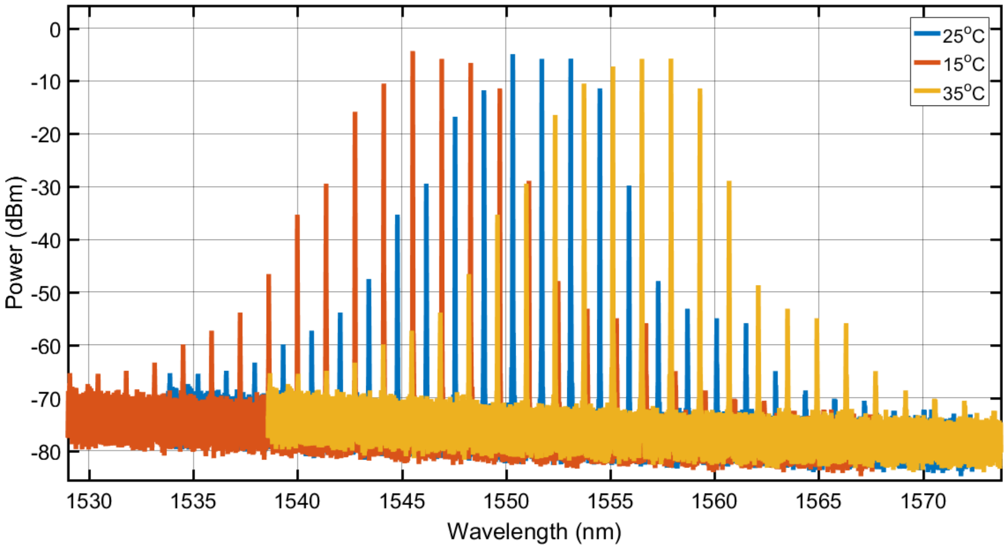

Figure 3.3: Free-running multimode FP laser spectrum biased at 30 mA and a device TEC temperature of 15°C (red), 25°C (blue) and 35°C (orange).

From the spectrum captured for the 25°C device TEC temperature, it can be observed that the spectrum is centred at 1553.1 nm and the spectral envelope, which exhibits 16 longitudinal modes above -60 dBm, spans ~21 nm. The free spectral range (FSR) of the multimode spectrum is 1.39 nm, which corresponds to 173.38 GHz. The 3-dB spectral width of the envelope is ~4 nm, which is a typical width for an FP laser [18]. Within the 3-dB spectral width of the envelope of the FP laser there are three modes with peak powers of ~-5 dBm. When the device TEC temperature is increased and decreased by 10°C, it results in a ~4.8 nm red- and blue-shift of the MLM spectrum, respectively, which corresponds to a 0.48 nm shift in wavelength per 1°C variation in the TEC temperature. The spectra captured for the 15 and 35°C TEC temperatures exhibit essentially the same span, FSR, number of modes and mode peak powers as the spectrum captured for the 25°C device TEC temperature. It can be observed in Figure 3.3 that by varying the TEC temperature of the FP laser, the multi-longitudinal mode spectrum of the CW optical field output from the laser covers virtually the entire C-band.

$$\Delta\nu = FSR = \frac{c}{2n_g L} \tag{3.1}$$

Using the measured FSR value of 1.39 nm, and a typical value of 3.6 for the group refractive index, n_g, [18], [19], the cavity length of the FP laser, estimated using equation 3.1, is ~240 μm. The small-signal modulation response of the FP laser is displayed in Figure 3.4 inset (a), and the experimental setup that was employed to obtain the results is shown in Figure 3.4 inset (b).

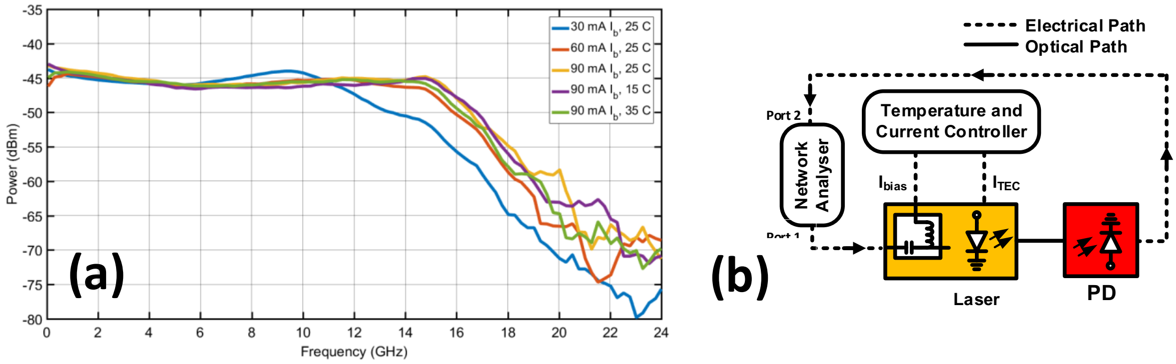

Figure 3.4: Inset (a) IM response of free-running FP laser for a device TEC temperature of 25°C and bias currents of 30 mA (blue), 60 mA (red), 90 mA (yellow), and for a 90 mA bias current when temperature controlled to 15°C (purple) and 35°C (green). Inset (b) Experimental setup for small-signal modulation response measurement.

It can be observed in Figure 3.4. that the 3-dB electrical bandwidths, f_{3dB}, of the FP laser for the 25°C device TEC temperature setting and with the FP laser biased at 30, 60, and 90 mA are ~12.5, 15.5 and 16 GHz, respectively, with the corresponding relaxation oscillation frequencies, f_R, occurring at ~9, 12 and 15 GHz, respectively. It can also be observed that the relaxation oscillation frequencies are pushed out to higher frequencies and the 3-dB bandwidth increases, with increasing dc bias current, I_b, to the FP laser. The results of the large-signal modulation analysis of the directly modulated free-running FP laser are shown in Figure 3.5.

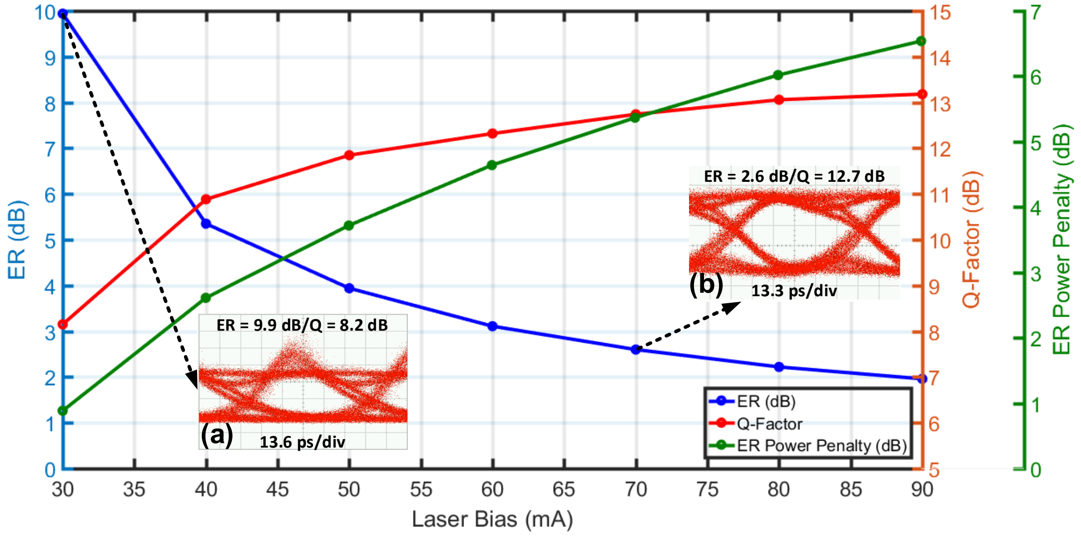

Figure 3.5: Extinction ratio, ER, ER power penalty, δ_{ER}, and Q-factor, Q, of optical signals transmitted from free-running FP laser directly modulated with a 2 V_{pp} 12.5 Gbit/s NRZ-OOK signal, as a function of laser dc bias current. Insets (a) and (b) show the eye diagrams of the optical signals captured for FP laser bias currents of 30 mA and 70 mA respectively.

The extinction ratio, ER, ER power penalty, δ_{ER}, and Q-factor, Q, of the signals transmitted from the free-running FP laser directly modulated with a 2 V_{pp} 12.5 Gbit/s NRZ-OOK signal with a PRBS word length of 2^{15}-1, as a function of FP laser bias current are displayed in Figure 3.5.The experimental procedure described in section 2.2.1.2 and setup shown in Figure 2.5, was employed to measure the large-signal modulation response of the FP laser. The FP laser device TEC temperature was maintained at 25°C.

3.2.2.1 Transmission performance evaluation of the directly modulated free-running FP laser

Following characterisation of the FP laser, an evaluation of its transmission performance under direct modulation was carried out. The experimental procedure described in section 2.2.2 and the setup of the IM/DD test-bed shown in Figure 2.9 was employed in the transmission experiments. The FP laser device TEC temperature was set at 25°C. A baseband 12.5 Gb/s NRZ-OOK signal, with a peak-to-peak modulation voltage swing of 2 V_{pp} and a PRBS word length of 2^{15}-1, was generated with the PPG to directly modulate the laser. The transmission performance of the directly modulated (DM) free-running FP laser for back-to-back (b2b) transmission and for transmission over 1 km of SSMF, was evaluated. The transmission performance of a single longitudinal mode, filtered from the multimode spectrum of the signal transmitted from the DM FP laser using a tunable optical bandpass filter (TBPF), was also evaluated for 1 km SSMF transmission. This was performed to demonstrate the effect of the mode partition noise (MPN) of the FP laser on its transmission performance over SSMF. The TBPF that was used exhibited a minimum 3-dB bandwidth of ~0.02 nm, an insertion loss of ~5 dB, a wavelength tuning range of 1450 to 1650 nm and a resolution of 5 pm. The spectrum of the single longitudinal mode at 1553.1 nm, filtered from the MLM spectrum of the DM FP laser biased at 30 mA (yellow spectrum), is displayed in Figure 3.6. A TBPF 3-dB bandwidth of 50 GHz was employed to filter the single longitudinal mode and a spectrum of the filter response (red spectrum), which was measured using the amplified spontaneous emission (ASE) output from an EDFA, is also shown in Figure 3.6.

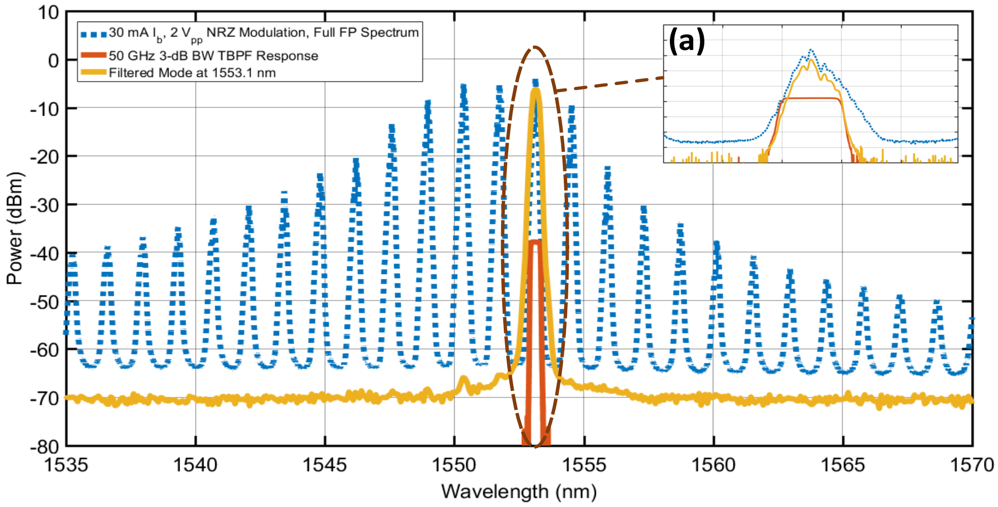

Figure 3.6: Directly modulated free-running FP laser spectrum (blue spectrum) at 30 mA FP laser bias, filter response (red spectrum) and filtered FP laser mode (yellow spectrum). Inset (a) shows an enhanced view of the longitudinal mode at 1553.1 nm, the filter response for a 3-dB bandwidth of 50 GHz and centred at 1553.1 nm, and the filtered longitudinal mode at 1553.1 nm.

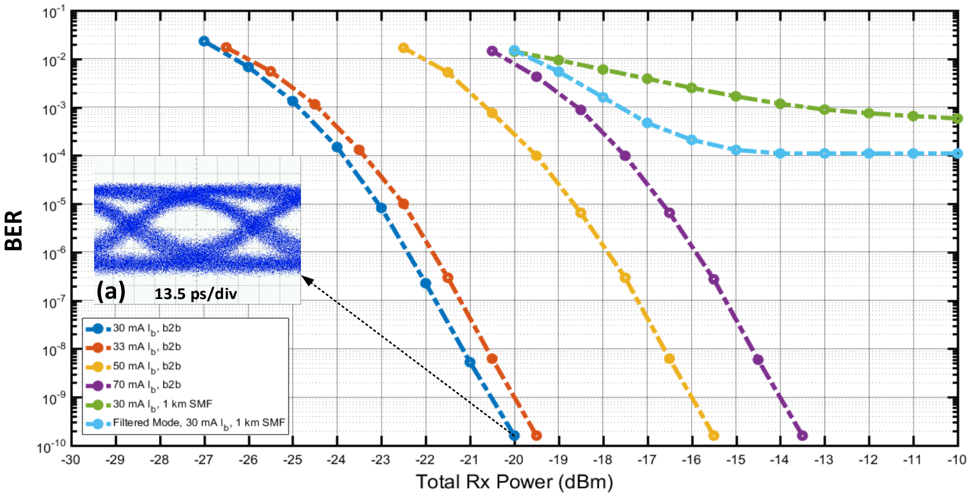

Figure 3.7: BER performance of directly modulated FP laser in IM/DD test-bed for b2b transmission and transmission over 1 km of SSMF. Inset (a) shows the eye diagram of the received electrical signal captured for error-free transmission in the b2b case at a received optical power of -20 dBm for the directly modulated free-running FP laser biased at 30 mA.

Figure 3.7 displays the bit-error ratio (BER) performance of the DM FP laser. It can be observed in the BER results shown in Figure 3.7 that the DM free-running FP laser biased at 30 mA produced the best transmission performance and the lowest receiver sensitivity of -20 dBm for error-free transmission in the IM/DD test-bed. This correlates well with the results obtained from the large-signal modulation analysis of the DM free-running FP laser shown in Figure 3.5, where the DM free-running FP laser biased at 30 mA exhibits the highest ER and the lowest ER power penalty, δ_{ER}, of 9.9 dB and 0.88 dB, respectively. It can be observed in the BER results displayed in Figure 3.7 that as the FP laser bias is increased, there is a degradation in the b2b transmission performance and in the receiver sensitivity attained, due to the decreasing ER and increasing ER power penalty, δ_{ER}, of the signal transmitted from the DM free-running FP laser. Considering that the DM free-running FP laser biased at 30 mA produced the best b2b transmission performance, the 30 mA FP laser bias was employed for optical signal transmission over 1 km of SSMF. The resultant BER curve (green curve) is displayed in Figure 3.7, it can be observed that a BER floor occurs at ~$1x10^{-3}$. The poor performance of the DM free-running FP laser for transmission over 1 km of SSMF, can be attributed to the MPN of the FP laser and the wide MLM spectrum of the transmitted signal, which experiences dispersive pulse broadening and signal waveform distortion when transmitted over SSMF due to the wavelength-dependent chromatic dispersion (CD) and attenuation of the optical fibre.

When a free-running FP laser is directly modulated, the total optical power of the signal transmitted from the laser remains relatively constant from pulse to pulse [20] – [22]. However, when the signal is transmitted over SSMF, the MPN of the FP laser, or the fluctuation in the instantaneous optical power distribution among the longitudinal modes within the MLM spectrum of the transmitted signal, causes the longitudinal modes from pulse to pulse to have different group velocities and group delays due to the CD of the optical fibre. Furthermore, the amplitudes from pulse to pulse will vary due to the wavelength-dependent attenuation of the optical fibre. Accordingly, the effects of the MPN of a multimode laser can manifest in the received electrical signal, having been transmitted over SSMF, in two ways [23]. The first is a result of the CD of the optical fibre, which transforms the spectral fluctuations into signal variations in line in time. If the fluctuations occur slower than the bit rate, this will be observed as timing jitter in the signal. This type of received signal distortion is dependent on the bit rate of the transmission system and the accumulated CD in the fibre channel. The second way in which the MPN of the FP laser can manifest in the received electrical signal is as variations in the signalling levels. This is due to the wavelength-dependent attenuation of the fibre, which exacerbates the intensity noise of the transmitted signal due to the fluctuating intensity of the longitudinal modes, thus, giving rise to variations in the received signal levels. This type of MPN-induced received signal distortion is independent of the bit rate and is effectively the intensity noise of the signal.

In the absence of the wavelength-dependent CD and attenuation of SSMF in the 1.5 μm window, the MPN would not pose a problem, as all of the modes would propagate at the same speed in the fibre and the fluctuation in the optical power distribution among the longitudinal modes would remain anti-correlated. Therefore, the resulting pulse-to-pulse noise would be zero and, in effect, the longitudinal modes would remain synchronized during transmission and detection. However, due to the CD and the wavelength-dependent attenuation of optical fibre, this is not the case, and for links that employ multimode lasers, such as FP lasers, the MPN causes the different modes to become desynchronized resulting in significant pulse distortions that produce fluctuations in the receiver photocurrent. The fluctuations in the receiver photocurrent reduces the signal-to-noise ratio (SNR) at the decision circuit resulting in noise penalties and errors at the receiver decision instant [24], which ultimately introduces an error floor [25]. Once an MPN-induced bit-error rate (BER) floor has been reached, the system SNR becomes independent of the received signal optical power. Hence, any increase in the signal optical power at the receiver will not improve the transmission performance or the receiver sensitivty [26].

In the absence of the MPN of the FP laser, where the optical power distribution among the longitudinal modes in the MLM spectrum of the transmitted optical signal remained constant, any power penalties incurred for signal transmission over SSMF with a DM free-running FP laser would be due to dispersive pulse broadening and inter-symbol interference (ISI), occurring as a result of the interplay of the chirp of the transmitted signal and the CD of the fibre. Previous studies [27], [28], have shown that even in transmission links where directly modulated single-mode DFB lasers with insufficient SMSR (</=30 dB) are employed, the main effect leading to power penalties or to the introduction of a BER floor is the MPN. Thus, in fibre optic communications links where directly modulated multimode lasers, such as

FP lasers, are employed, the power penalties incurred due to the signal-dependent MPN are more detrimental to the transmission performance of the link than the power penalties resulting from the interplay between the frequency chirp of the DM laser and the CD of the fibre.

The effect of the MPN of the FP laser on the transmission performance of the link is further evidenced by the BER results (light blue curve) shown in Figure 3.7, which were obtained from the transmission experiment with the single longitudinal mode filtered from the MLM spectrum of the DM FP laser. Transmission of the single longitudinal mode produced a marginal improvement in the performance of the link, which is demonstrated by the slight reduction in the BER floor to ~$1x10^{-4}$. By transmitting the filtered single longitudinal mode, the power penalty introduced by dispersive pulse broadening and the signal distortion occurring due to the combination of the MPN of the MLM spectrum of the transmitted signal and the wavelength-dependent CD and attenuation of the fibre, is negated. Thus, the intensity noise of the DM FP laser, due to the MPN, is the main factor limiting the transmission performance of the filtered single longitudinal mode [29] – [31].

It is evident from the results obtained from the transmission performance evaluation of the DM free-running FP laser that the MLM spectrum, and the MPN which is intrinsic to FP lasers, limits their use to transmission over very short-range SSMF links (<1 km). A more effective method to suppress all but one of the longitudinal modes of the MLM spectrum of an FP laser, reduce the MPN-induced RIN of the single longitudinal mode and attain stable single-mode operation, is self-seeding [11].

3.3 Self-Seeded FP Laser Optimisation, Characterisation and Transmission Performance Evaluation

As a means to extending the transmission distance of the DM FP laser, and exploit its MLM spectrum, a self-seeding scheme was developed, with a view to realising a cost-effective tunable laser source for NG-PON2 and future optical access networks. Unlike typical injection-locking (IL) schemes that require external injection from a 'master' laser into the gain section of a free-running 'slave' laser [32], [33], or external injection schemes that require a spectrally sliced broadband light source [34], self-seeding (SS), or self-injection locking (SIL), is achieved by feeding a portion of the optical carrier transmitted from the laser, called the 'seed signal', back into the gain section of the laser by employing an external cavity, which contains a reflective element or feedback loop [35], [36]. Thus, the self-seeding approach does not require an additional optical source or a 'master' laser to achieve wavelength-locking and, by implementing a self-seeding scheme, a single longitudinal mode (SLM) within the MLM spectrum of an FP laser can be wavelength-locked. Hence, stable single-mode operation of an FP laser can be achieved. Self-seeding results in the enhancement of the optical gain in the single longitudinal mode, while concurrently suppresses all other modes in the MLM spectrum, which is quantified by the side-mode suppression (SMSR) of the laser [37], [38]. As previously mentioned, the self-seeding scheme requires an external cavity to enable the portion of the optical carrier output from the laser, or seed signal, to be filtered or reflected and reinjected back into the gain section of the laser cavity. A number of different external cavity configurations can be implemented to achieve the seed signal feedback, including a simple Sagnac fibre loop [11], a fibre reflective mirror (FRM) [39], or a fibre Bragg grating (FBG) [40]. A directly modulated (DM) self-seeding FP laser transmitting 10 Gbit/s NRZ-OOK optical signals in the C-band over 20 km of SSMF was demonstrated in [40], and in [41], a DM self-seeding FP laser transmitting 2.5 Gbit/s NRZ-OOK signals in the C-band over 85 km of SSMF was demonstrated.

This section describes the experimental work performed to establish and optimise the operation of the directly modulated (DM) self-seeded FP (SS-FP) laser, which includes large-signal modulation analysis of the DM SS-FP laser. Furthermore, the dependence of the SMSR of the SS-FP laser on the seed signal optical power is investigated. The relative intensity noise (RIN) of the SS-FP laser is also characterised and compared with the RIN of the free-running FP laser and a single longitudinal mode filtered from the MLM spectrum of the FP laser. The different wavelength channels of the DM SS-FP laser are then characterised and the wavelength tuning range potential of the transmitter is evaluated. Finally, the transmission performance of the DM SS-FP laser is evaluated in IM/DD test-beds with two different IM formats, which include 12.5 Gbit/s NRZ-OOK format and 12.5 Gbaud/s (25 Gbit/s) PAM-4 format.

3.3.1 SS-FP Laser Design and Operation

A number of different external cavity (EC) configurations were investigated and evaluated during the process of establishing self-seeded FP laser operation. The EC configuration that was finally chosen for implementation in the self-seeded FP (SS-FP) laser scheme was a circulator-based fibre loop, which is essentially a passive optical circuit that enables the necessary filtering of a single longitudinal mode selected from the MLM spectrum of the free-running FP laser, and the reinjection of the filtered mode, or seed signal, back into the FP laser cavity. In the self-seeding scheme developed in this study, the selected single longitudinal mode was filtered with a tunable optical bandpass filter (TBPF), which was installed in the EC feedback loop. The TBPF used in the EC exhibited a minimum 3-dB bandwidth of ~0.02 nm and a ~5 dB insertion loss. A schematic of the SS-FP laser is shown in Figure 3.8. The length of the external cavity employed in the setup was ~10 m. A VOA was used initially in the setup to control the optical power of the reinjected seed signal, however, it was ultimately removed, as the insertion loss of the VOA was too large and when the VOA was used it resulted in poor self-seeding performance of the SS-FP laser.

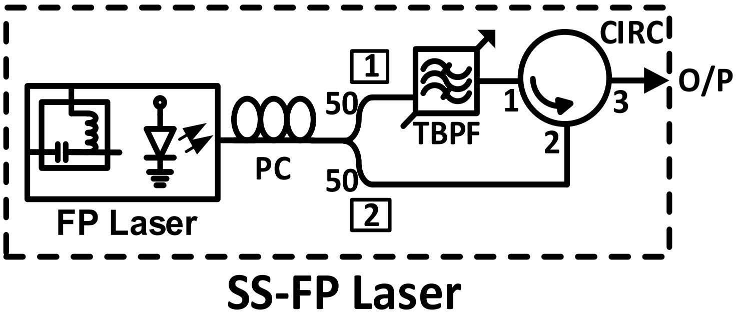

Figure 3.8: Self-seeded FP (SS-FP) laser design.

The EC feedback loop comprises a polarisation controller (PC), a 3-port 3-dB (50:50) coupler, the TBPF and a 3-port circulator (CIRC). The polarisation controller is employed in the external cavity to enable the polarisation state of the reinjected seed signal to be adjusted to the TE mode of the FP laser for optimal self-seeding [42], [43]. The signal transmitted from the MLM FP laser propagates through the PC, which maintains a fixed polarisation state for the signal transmitted from the FP laser and the reinjected seed signal. The signal then travels through the first arm of the 3-dB coupler which is input to the TBPF. Through appropriate detuning of the centre frequency of the TBPF passband and adjustment of the TBPF 3-dB bandwidth, a single longitudinal mode can be filtered from the MLM spectrum of the signal transmitted from the FP laser. The filtered single longitudinal mode, or seed signal, then travels to port 1 of the circulator, which redirects or reinjects the seed signal back into the FP laser cavity via port 2 of the circulator, the second arm of the 3-dB coupler and the PC. The circulator supports optical signal transmission in one direction only, which is indicated by the curved arrow within the circulator in the schematic shown in Figure 3.8. The reinjection of the filtered single longitudinal mode back into the FP laser cavity enables self-seeding of a selected FP laser longitudinal mode, thus, resulting in single-mode operation. When single-mode operation is established, the self-seeded mode is transmitted from the FP laser back through the external cavity and is output from port 3 of the circulator. When the FP laser is directly modulated, an intensity modulated (IM) signal that exhibits stable single-mode operation can be realised. Through appropriate detuning of the centre frequency of the TBPF passband and adjustment of the 3-dB bandwidth of the TBPF, any longitudinal mode within the MLM spectrum of the signal output from the FP laser, shown in Figure 3.3 can be accessed dynamically and self-seeded.

3.3.2 Optimising the Directly Modulated SS-FP Laser

To determine the directly modulated (DM) SS-FP laser operating parameters that would produce the best transmission performance with the SS-FP laser in the IM/DD test-bed, a number of experiments were performed to optimise and characterise the DM SS-FP laser. The experiments that were carried out are described in this section, including an analysis and discussion of the results obtained. Figure

3.9 shows the experimental setup employed to establish the optimal operating parameters of the DM SS-FP laser and to assess the large-signal modulation characteristics of the transmitter. The FP laser device TEC temperature was maintained at 25°C throughout the experiments.

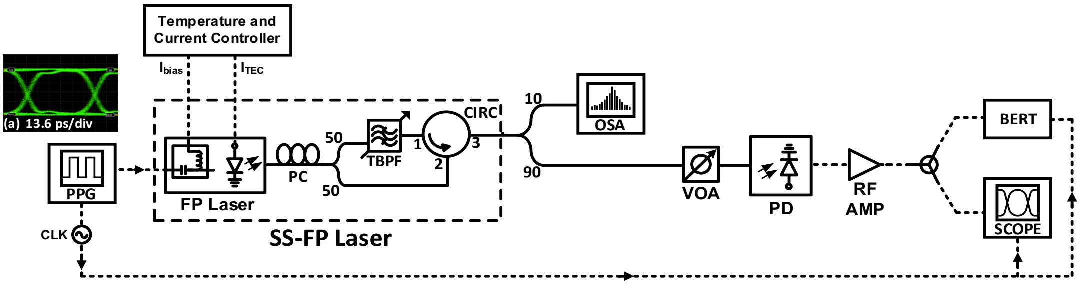

Figure 3.9: Experimental setup used to establish optimal operating parameters of SS-FP laser and characterise the laser.

The side-mode suppression ratio (SMSR) of the directly modulated (DM) SS-FP laser and bit-error ratio (BER) performance for back-to-back (b2b) transmission of 12.5 Gbit/s NRZ-OOK optical signals were the metrics employed to ascertain the optimal operating parameters of the DM SS-FP laser. Measuring the SMSR provided an indication of the degree of single-mode operation that had been established with the DM SS-FP laser and the effectiveness of the self-seeding of the selected mode. Two different OSAs were employed in the experimental setup shown in Figure 3.9. The Yokogawa AQ 6370 OSA, with a spectral resolution setting of 0.5 nm/62.4 GHz, was used during the optimisation of the SMSR and the BER performance of the DM SS-FP laser. The Yokogawa OSA allowed for the SMSR of the DM SS-FP laser to be monitored in real-time during optimisation. The second type of OSA employed was the high resolution Apex OSA with a resolution setting of 0.16 pm/20 MHz. The Apex OSA was used to further investigate the spectral properties of the signals transmitted from the optimised DM SS-FP laser. The 3-dB bandwidth of the TBPF and the centre frequency of the TBPF passband were adjusted and tuned to maximise the SMSR and minimise the BER, which was measured with the BERT. This was carried out for various FP laser bias currents and modulating signal amplitudes. The eye diagram of the received electrical signal for b2b transmission was observed on the sampling oscilloscope and provided an indication of the quality of the signal transmitted from the DM SS-FP laser in real-time. By adjusting the 3-dB bandwidth of the TBPF and detuning the centre frequency of the TBPF passband appropriately, the quality of the signal transmitted from the DM SS-FP laser could be optimised. The bandwidth of the TBPF and the centre frequency of the TBPF passband were measured at different stages during the experiments by observing the optical response of the TBPF on the OSA using the ASE output from an EDFA. The optical power of the signal incident on the APD receiver was maintained at -14 dBm throughout the experiments using the VOA at the input to the APD, shown in Figure 3.9. The optical extinction ratio, ER, ER power penalty, δ_{ER}, and Q-factor, Q, of the signals transmitted from the DM SS-FP laser were measured for various FP laser bias currents and modulating signal amplitudes.

The 3-dB bandwidths of the optical spectra, Δv_{3dB}, of the signals transmitted from the DM SS-FP laser for the optimised operating parameters were also measured.

The operating parameters that produced the best b2b transmission performance and BER results with the DM free-running FP laser, shown in Figure 3.7, were evaluated first, that is, the 30 mA FP laser bias and the 2 V_{pp} modulating signal amplitude. A baseband 12.5 Gbit/s NRZ-OOK signal with a PRBS word length of 2^{15}-1 was generated with the PPG and used to directly modulate the FP laser. With the FP laser biased at 30 mA and modulated with a 2 V_{pp} 12.5 Gbit/s NRZ-OOK signal, the mode at 1553.1 nm was selected for self-seeding. The PC in the external cavity of the SS-FP laser was adjusted to maximise the SMSR and optical power of the signal output from port 3 of the circulator. Figure 3.10 shows the spectrum of the signal transmitted from the DM SS-FP laser for the 30 mA FP laser bias and the 2 V_{pp} modulating signal amplitude, having optimised the bandwidth of the TBPF and the centre frequency of the TBPF passband. Figure 3.10 insets (a) and (b) show the eye diagrams of the transmitted optical signal and the received electrical signal for b2b transmission, respectively, captured with the sampling scope. The transmitted optical signal was detected using the dc coupled photodiode integrated in the sampling scope. The eye diagram of the transmitted optical signal is the time-domain representation of the spectrum shown in Figure 3.10. The maximum SMSR and minimum BER result, attainable with the DM SS-FP laser for the 30 mA FP laser bias and 2 V_{pp} modulating signal amplitude, are 21.2 dB and 2.14x10^{-6}, respectively. The ER and Q-factor, Q, of the signal transmitted from the DM SS-FP laser for the 30 mA FP laser bias and 2 V_{pp} modulating signal amplitude, are 7.8 and 1.6 dB, respectively.

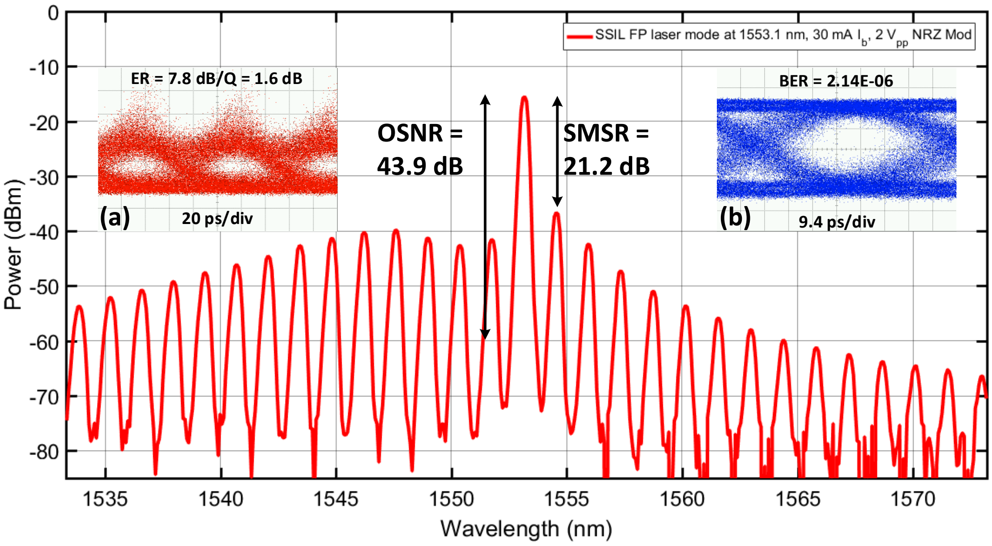

Figure 3.10: DM SS-FP laser spectrum for the 30 mA FP laser bias and the 2 V_{pp} modulating signal amplitude, exhibiting an SMSR of 21.2 dB and an OSNR of 43.9. Insets (a) and (b) show the eye diagrams of the transmitted optical and received electrical signals, respectively.

Comparing the eye patterns of the signals transmitted from the DM SS-FP laser and the DM free-running FP laser, shown in Figure 3.10 inset (a) and Figure 3.5 inset (a), respectively, it can be observed that through self-seeding the ER and Q of the signal transmitted from the DM SS-FP laser decreased by 2.1 and 6.6 dB, respectively. The reduction in the ER and the Q of the self-seeded signal can be attributed to the low SMSR and the sub-optimal self-seeding that was established. To investigate if a more suitable FP laser bias current and modulating signal amplitude could yield a higher SMSR and lower BER result for b2b transmission with the DM SS-FP laser, the SMSR of the DM SS-FP laser and the BER performance of the DM SS-FP laser for b2b transmission of 12.5 Gbit/s NRZ-OOK optical signals were measured for different FP laser bias currents and modulating signal amplitudes. The SMSR and BER results obtained from the sweeps of the FP laser bias, with a fixed modulating signal amplitude, and the sweeps of the modulating signal amplitude, with a fixed FP laser bias, are shown in Figure 3.11, Figure 3.12, Figure 3.13 and Figure 3.14.

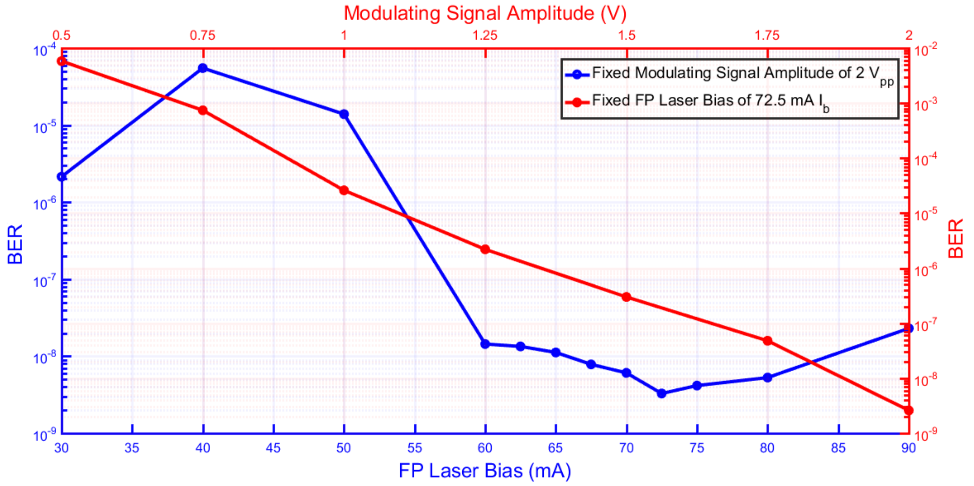

Figure 3.11: BER performance of DM SS-FP laser for b2b transmission, as a function of FP laser bias current for a fixed modulating signal amplitude of 2 V_{pp} (blue plot) and as a function of modulating signal amplitude for a fixed FP laser bias of 72.5 mA (red plot).

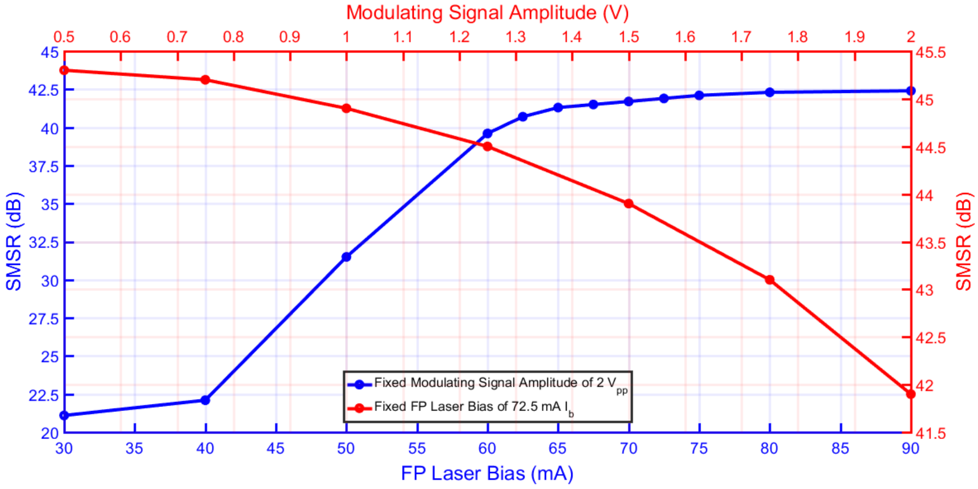

Figure 3.12: SMSR of DM SS-FP laser as a function of FP laser bias current for a fixed modulating signal amplitude of 2 V_{pp} (blue plot) and as a function of modulating signal amplitude for a fixed FP laser bias of 72.5 mA (red plot).

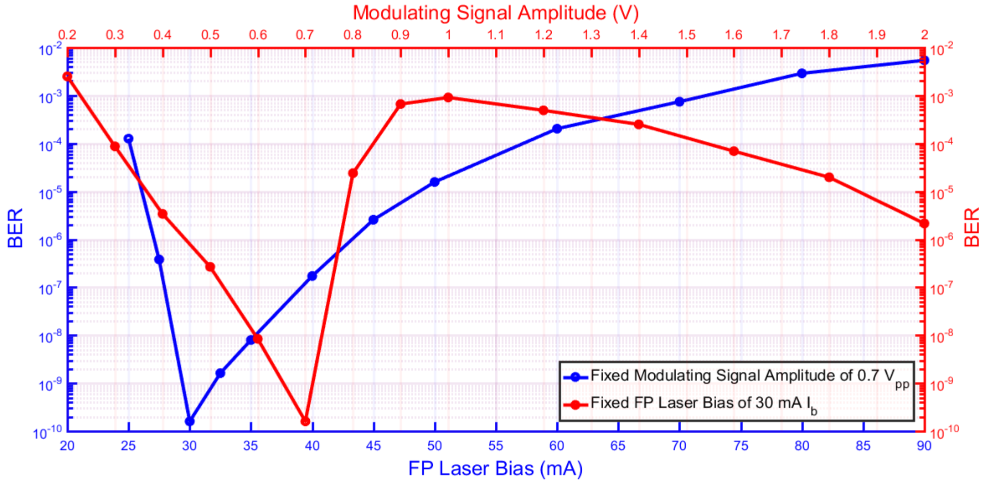

Figure 3.13: BER performance of DM SS-FP laser for b2b transmission, as a function of modulating signal amplitude for a fixed FP laser bias of 30 mA (red plot) and as a function of FP laser bias current for a fixed modulating signal amplitude of 0.7 V_{pp} (blue plot).

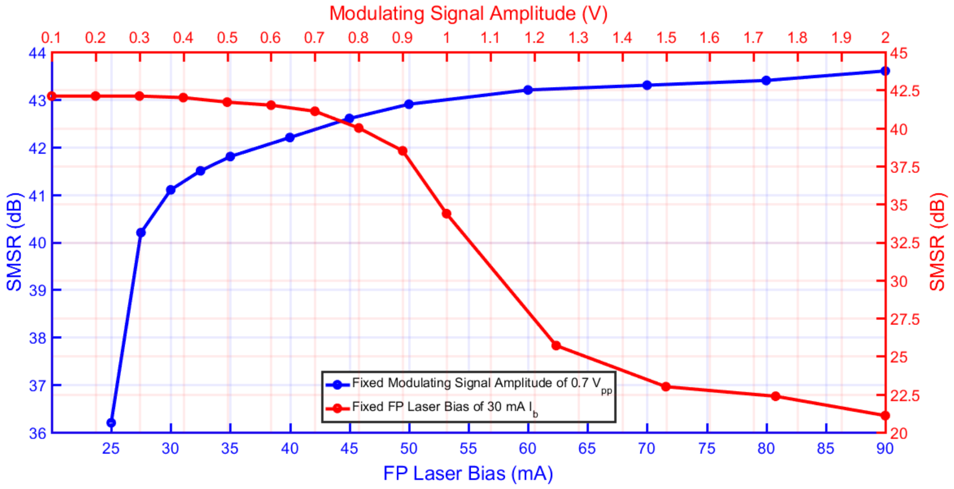

Figure 3.14: SMSR of DM SS-FP laser as a function of FP laser bias current for a fixed modulating signal amplitude of 0.7 V_{pp} (blue plot) and as a function of modulating signal amplitude for a fixed FP laser bias of 30 mA (red plot).

When the FP laser is directly modulated with a 2 V_{pp} 12.5 Gbit/s NRZ-OOK signal, an FP laser bias current of 72.5 mA yields the lowest BER of 3.28×10^{-9} for b2b transmission, and the DM SS-FP laser exhibits an SMSR of 42.1 dB. When the FP laser is directly modulated with a 0.7 V_{pp} 12.5 Gbit/s NRZ-OOK signal, an FP laser bias current of 30 mA yields the lowest BER of 1.60×10^{-10} for b2b transmission, and the DM SS-FP laser exhibits an SMSR of 41.1 dB. Furthermore, from the FP laser bias current and modulating signal amplitude sweeps, it can be concluded that there is a direct correlation between the SMSR of the DM SS-FP laser and the b2b transmission performance of the transmitter. Moreover, it appears that an SMSR of ~40 dB is necessary for useful optical signal transmission with the DM SS-FP laser. Further sweeps of the FP laser bias current, with the modulating signal amplitude fixed, and sweeps of the modulating signal amplitude, with the FP laser bias current fixed, could potentially allow an FP laser bias and modulating signal amplitude combination, which yields better b2b transmission performance, to be identified. Figure 3.15 displays the optical spectrum of the signal transmitted from the DM SS-FP laser for the 72.5 mA FP laser bias and 2 V_{pp} modulating signal amplitude, which yields the lowest BER result shown in the graph displayed in Figure 3.11.

As shown in Figure 3.15, the longitudinal mode selected for self-seeding occurs at 1559.6 nm. The eye diagram of the optical signal transmitted from the DM SS-FP laser for the 72.5 mA FP laser bias and the 2 V_{pp} modulating signal amplitude is shown in Figure 3.15 inset (a). Figure 3.15 inset (b) displays the eye diagram of the received electrical signal following b2b transmission captured at a received power of -14 dBm. The ER and the Q-factor, Q, of the signal transmitted from the DM SS-FP laser for the 72.5 mA FP laser bias and the 2 V_{pp} modulating signal amplitude, were 2.8 and 7.4 dB, respectively. Thus, the increase in the FP laser bias from 30 to 72.5 mA results in a 5 dB reduction in the ER and a 5.8 dB increase in the Q-factor, Q, of the signal transmitted from the DM SS-FP laser when the 2 V_{pp} modulating signal amplitude is employed.

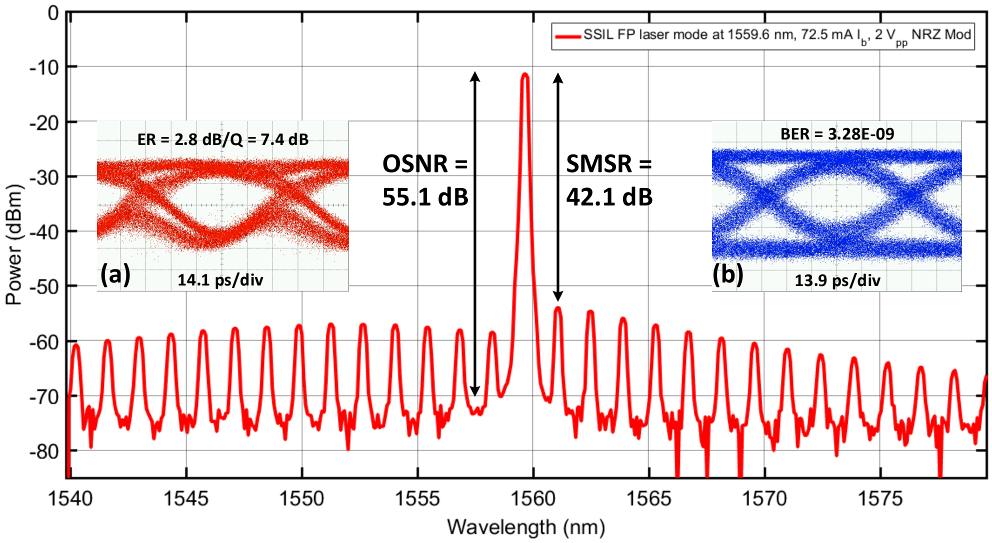

Figure 3.15: Spectrum of mode at 1559.6 nm captured from DM SS-FP laser for 72.5 mA FP laser bias and 2 V_{pp} modulating signal amplitude, exhibiting an SMSR of 42.1 dB and an OSNR of 62.1 dB. Insets (a) and (b) show the eye diagrams of the transmitted optical and received electrical signals, respectively.

Figure 3.16 shows the high resolution spectrum of the signal transmitted from the DM SS-FP laser for the optimal FP laser bias of 72.5 mA with the 2 V_{pp} modulating signal amplitude (purple spectrum), showing the self-seeded mode at 1559.6 nm/192.218 THz, and was captured with the Apex OSA. Also shown in Figure 3.16 are the spectra of the mode at 1559.6 nm captured from the free-running FP laser biased at 72.5 mA in CW operation (blue spectrum) and directly modulated with the 2 V_{pp} 12.5 Gbit/s NRZ-OOK signal (red spectrum). The spectrum of the optical response of the TBPF for the optimised filter settings, which yielded the lowest BER result attainable for b2b transmission with the DM SS-FP laser for the 2 V_{pp} modulating signal amplitude, was also captured and is shown in Figure 3.16 (yellow spectrum). Figure 3.16 insets (a) and (b) display the eye diagrams of the optical signals transmitted from the DM SS-FP laser and the DM free-running FP laser, respectively, for the 72.5 mA

FP laser bias and 2 V_{pp} modulating signal amplitude. The 3-dB bandwidths of the optical spectra shown in Figure 3.16 captured from the DM SS-FP laser and the DM free-running FP laser mode at 1559.6 nm are 11.8 and 8.4 GHz, respectively, and the bandwidths measured 20-dB down from the peaks are 21.3 and 13.4 GHz, respectively. Thus, through self-seeding, the 3-dB bandwidth, Δv_{3dB}, of the signal transmitted from the DM SS-FP laser increases by ~3.4 GHz, and the 20-dB bandwidth increases by ~8 GHz. The increased bandwidth at the base of the DM SS-FP laser spectrum can be attributed to the additional spectral content introduced by the modes that form in the external cavity of the SS-FP laser, and the tones that appear at the peak of the spectrum, and at the peaks of both of the side modes, are a manifestation of the external cavity side modes.

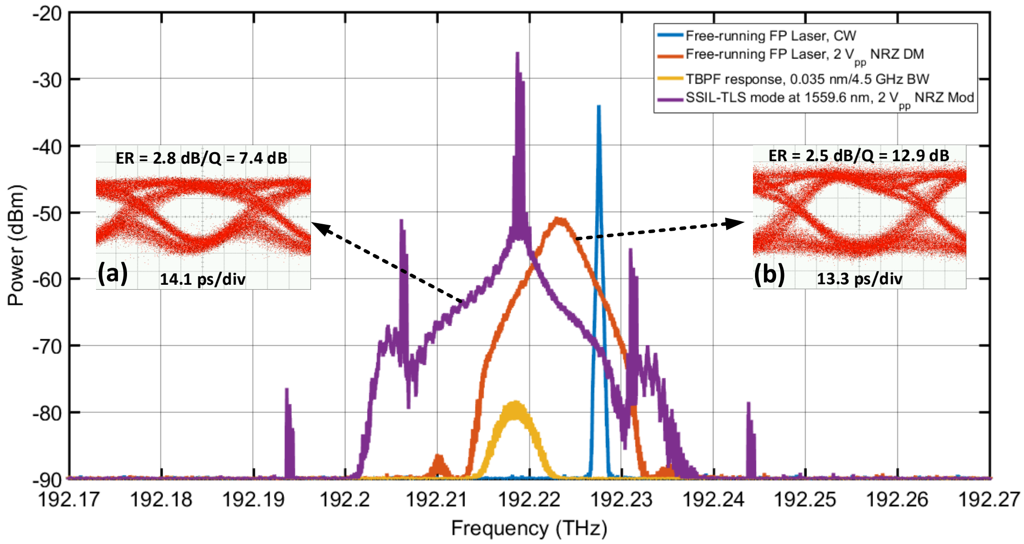

Figure 3.16: Spectra captured of the mode at 1559.6 nm, for the 72.5 mA FP laser bias, from the DM SS-FP laser (purple spectrum), the DM free-running FP laser (red spectrum) and the free-running FP laser during CW operation (blue spectrum). Also shown is the spectrum of the optimised TBPF optical response (yellow spectrum). Insets (a) and (b) show the eye patterns of the optical signals transmitted from the DM SS-FP laser and the DM free-running FP laser, respectively.

The 3-dB bandwidth of the TBPF and the centre frequency of the TBPF passband, having optimised the TBPF to yield the highest BER result attainable for b2b transmission with the DM SS-FP laser for the 72.5 mA FP laser bias and 2 V_{pp} modulating signal amplitude, are 4.5 GHz/0.035 nm and 192.2185 THz/1559.645 nm, respectively. It can be observed in Figure 3.16 that the centre frequency of the TBPF passband is negatively detuned by ~5 GHz with respect to the peak frequency of the DM free-running FP laser spectrum. The ~5 GHz red-shift in the peak frequency of the spectrum of the signal transmitted from the DM SS-FP laser observed in Figure 3.16, is due to the self-seeding [44] – [47]. Comparing the eye diagrams of the signals transmitted from the DM SS-FP laser and the DM free-running FP laser, shown in Figure 3.16 insets (a) and (b), respectively, it can be observed that through self-seeding the ER of the signal transmitted from the DM SS-FP laser increases by 0.3 dB, however, the Q reduces by 5.5 dB.

Optical Eye diagrams of the self-seeded signals output from the SS-FP laser under direct modulation with the 2 V_{pp} 12.5 Gbit/s NRZ-OOK signal were captured for FP laser bias currents ranging from 40 to 90 mA, in increments ranging from 2.5 to 10 mA. The extinction ratios, ER, ER power penalties, δ_{ER} , and Q-factors, Q, of the transmitted signals were calculated from the data extracted from the captured eyes. Figure 3.17 shows the results of the eye diagram analysis. It can be observed in Figure 3.17 that the 72.5 mA FP laser bias, which produced the best b2b transmission performance with the DM SS-FP laser using the 2 V_{pp} modulating signal amplitude, also yielded the highest transmitted signal Q of 7.4 dB.

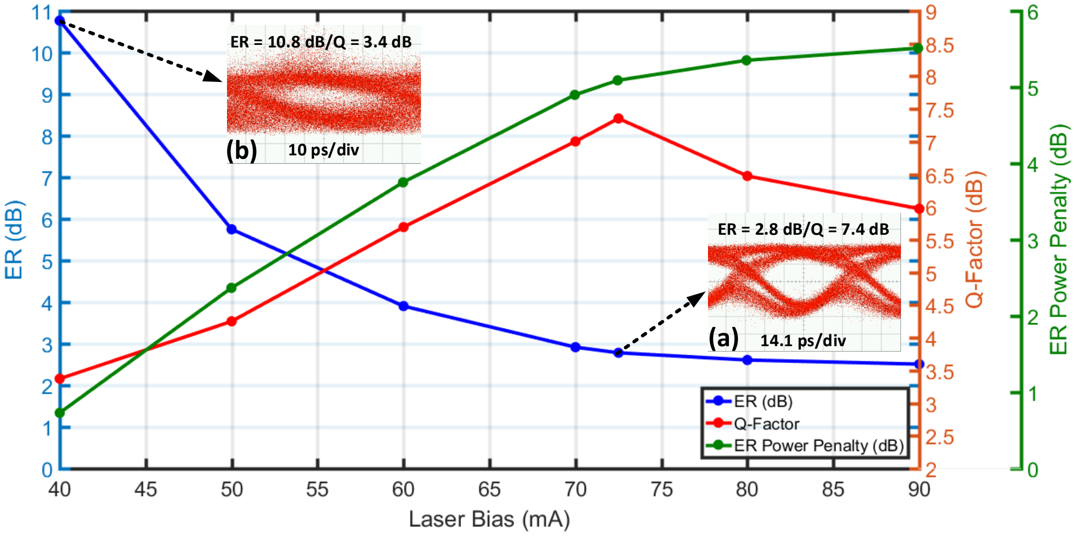

Figure 3.17: Extinction ratio, ER, ER power penalty, δ_{ER}, and Q-factor, Q, of optical signals transmitted from DM SS-FP laser as a function of FP laser bias current. Insets (a) and (b) show the eye diagrams of the optical signals transmitted from the DM SS-FP laser for FP laser bias currents of 72.5 mA and 40 mA respectively.

Based on the results shown in Figure 3.17, and the BER results obtained from the b2b transmission experiments with the DM SS-FP laser shown in Figure 3.11, the Q of the transmitted signal is the characteristic that determines the transmission performance of the DM SS-FP laser when modulated with the 2 V_{pp} signal. However, it must be stated that the low ER (2.8 dB) and the high power penalty, δ_{ER} , (5.1 dB) of the signal transmitted from the DM SS-FP laser for the 72.5 mA FP laser bias and 2 V_{pp} modulating signal amplitude, would preclude the use of the SS-FP laser in NG-PON2 applications based on current standards [1].

Figure 3.18 shows the spectrum of the self-seeded signal transmitted from the DM SS-FP laser for the optimal FP laser bias of 30 mA when employing the 0.7 V_{pp} modulating signal amplitude, which yields the lowest BER result and error-free transmission for b2b transmission at a received optical power of -14 dBm. The spectrum was captured with the Yokogawa OSA. The longitudinal mode at 1553.1 nm was selected for self-seeding. Figure 3.18 insets (a) and (b) show the eye diagrams of the transmitted optical signal and the received electrical signal for b2b transmission, respectively, captured when the

30 mA FP laser bias and 0.7 V_{pp} modulating signal amplitude were employed to operate the DM SS-FP laser. The ER, ER power penalty, δ_{ER}, and the Q-factor, Q, of the signal transmitted from the DM SS-FP laser for the 30 mA FP laser bias current and 0.7 V_{pp} modulating signal amplitude, are 3.9, 3.8 and 5.3 dB, respectively. The eye diagram of the received signal was captured for b2b transmission at the fixed received optical power of -14 dBm and for a BER of 1.60x10^{-10}. As previously mentioned, the maximum SMSR and minimum BER result for b2b transmission attained with the DM SS-FP laser for the 30 mA FP laser bias and 0.7 V_{pp} modulating signal amplitude, having optimised the 3-dB bandwidth of the TBPF and the centre frequency of the TBPF passband, are 41.1 dB and 1.6x10^{-10}, respectively.

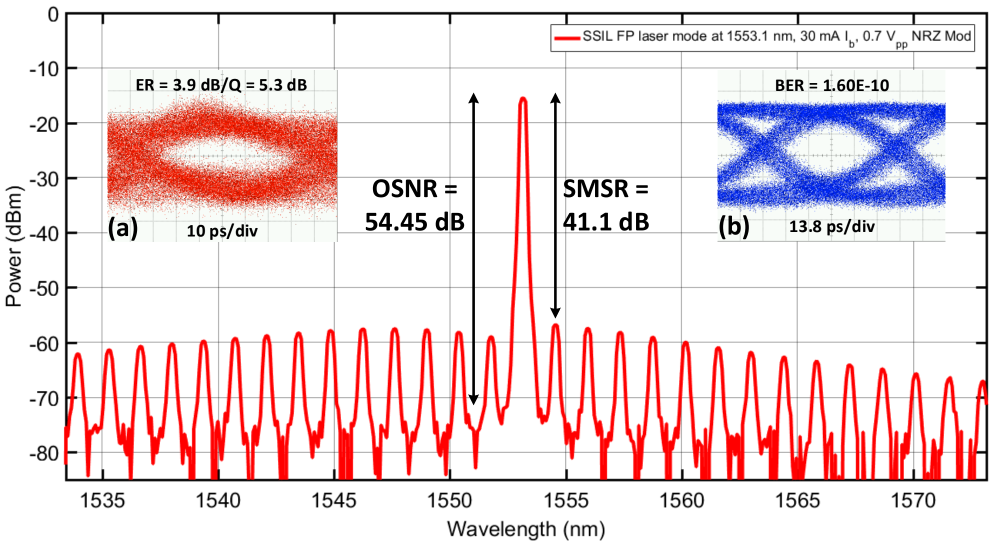

Figure 3.18: Spectrum of mode at 1553.1 nm captured from DM SS-FP laser for 30 mA FP laser bias and 0.7 V_{pp} modulating signal amplitude, exhibiting an SMSR of 41.1 dB and an OSNR of 56.5 dB. Insets (a) and (b) show the eye diagrams of the transmitted optical and received electrical signals, respectively.

Decreasing the FP laser bias from 72.5 to 30 mA and reducing the modulating signal amplitude from 2 to 0.7 V_{pp}, increases the ER of the signal transmitted from the DM SS-FP laser from 2.8 to 3.9 dB and decreases the BER for b2b transmission from 3.28x10^{-9} to 1.6x10^{-10}, however, the Q-factor, Q, of the transmitted signal decreases slightly from 7.4 to 5.3 dB. The increase in the ER of the transmitted signal, coupled with only a slight decrease in the Q-factor, Q, results in the DM SS-FP laser, for the 30 mA FP laser bias and 0.7 V_{pp} modulating signal amplitude, yielding better transmission performance than the DM SS-FP laser for the 72.5 mA FP laser bias and 2 V_{pp} modulating signal amplitude.

Figure 3.19 shows the high resolution optical spectrum of the signal transmitted from the DM SS-FP laser for the 30 mA FP laser bias and 0.7 V_{pp} modulating signal amplitude (purple spectrum), showing the self-seeded mode at 1553.1 nm/193.023 THz, and was captured with the Apex OSA. Also displayed in Figure 3.19 are the spectra of the mode at 1553.1 nm captured from the free-running FP laser biased at 30 mA in CW operation (blue spectrum) and under direct modulation with the 0.7 V_{pp} 12.5 Gbit/s NRZ-OOK signal (red spectrum). The spectrum of the optical response of the TBPF for the optimised filter settings, which yields the lowest BER result for b2b transmission with the DM SS-FP laser for the 30 mA FP laser bias and 0.7 V_{pp} modulating signal amplitude, is also shown (yellow spectrum). Figure 3.19 inset (a) shows the eye diagram of the optical signal transmitted from the DM SS-FP laser for the 30 mA FP laser bias and 0.7 V_{pp} modulating signal amplitude, which was shown previously in Figure 3.18 inset (a) and corresponds to the DM SS-FP laser spectrum (purple spectrum).

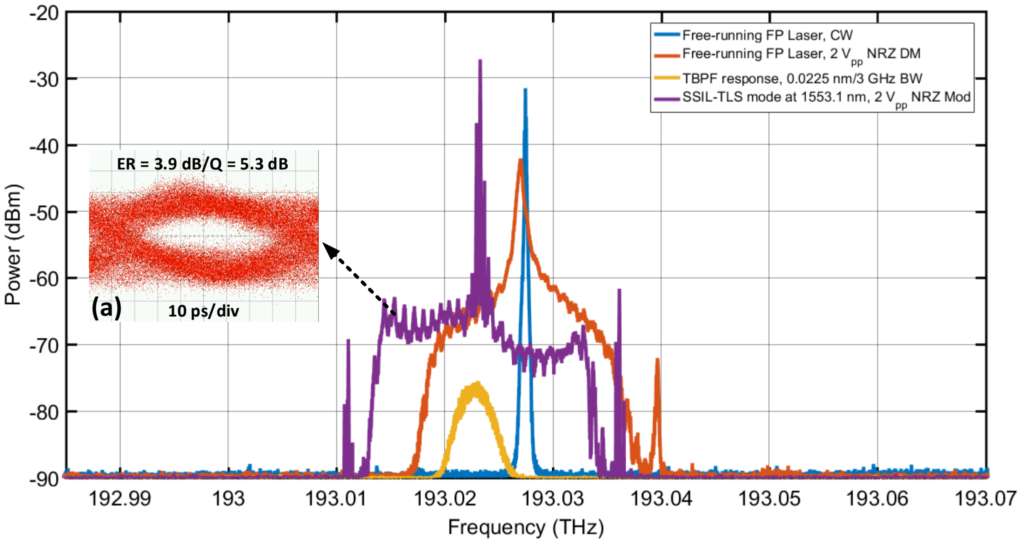

Figure 3.19: Spectra captured of the mode at 1553.1 nm, for the 30 mA FP laser bias, from the DM SS-FP laser (purple spectrum), the DM free-running FP laser (red spectrum) and the free-running FP laser during CW operation (blue spectrum). Also shown is the spectrum of the optimised TBPF optical response (yellow spectrum). Insets (a) shows the eye pattern of the optical signal transmitted from the DM SS-FP laser.

The 3-dB bandwidths, Δv_{3dB}, of the optical spectra of the signals transmitted from the DM SS-FP laser and the DM free-running FP laser mode at 1553.1 nm, for the 30 mA FP laser bias current and 0.7 V_{pp} modulating signal amplitude, are ~8 GHz and the 20-dB bandwidths of both spectra are ~20 GHz. Therefore, self-seeding results in no significant broadening or reduction in the optical bandwidth of the DM SS-FP laser spectrum when compared with the DM free-running FP laser mode spectrum. The tones observed in the spectrum of the signal transmitted from the DM SS-FP laser for the 72.5 mA FP laser bias and 2 V_{pp} modulating signal amplitude shown in Figure 3.16, which are a manifestation of the external cavity side modes, are still visible in the spectrum of the signal transmitted from the DM SS-FP laser for the 30 mA FP laser bias and 0.7 V_{pp} modulating signal amplitude. The 3-dB bandwidth of the TBPF and the centre frequency of the TBPF passband, having optimised the TBPF to yield the lowest BER result and error-free transmission for b2b transmission with the DM SS-FP laser for the 30 mA FP laser bias current and 0.7 V_{pp} modulating signal amplitude, are ~0.02 nm/3 GHz and ~1553.14 nm/193.023 THz, respectively. The centre frequency of the TBPF passband is negatively detuned by ~4 GHz with respect to the peak of the spectrum of the signal transmitted from the DM free-running FP laser. The peak of the DD SS-FP laser spectrum is red-shifted by ~4 GHz with respect to the peak of the DM free-running FP laser spectrum, thus, indicating that optimal self-seeding was successfully established.

During the optimisation and characterisation of the SS-FP laser under direct modulation with the 12.5 Gbit/s NRZ-OOK signal, the FP laser bias current that yielded the best b2b transmission performance with the DM SS-FP laser, when the 0.7 V_{pp} modulating signal amplitude was employed, was 30mA. For the 30 mA FP laser bias and 0.7 V_{pp} modulating signal amplitude, the DM SS-FP laser also exhibits a high SMSR of 41.1 dB. Furthermore, the signal transmitted from the DM SS-FP laser for the 30 mA FP laser bias and the 0.7 V_{pp} signal amplitude exhibits the highest ER of 3.9 dB, the lowest ER power penalty, δ_{ER}, of 3.8 dB and a moderate Q-factor, Q, of 5.3 dB. The 3-dB bandwidth, Δv_{3dB}, of the spectrum of the optical signal transmitted from the DM SS-FP laser for the 30 mA FP laser bias and 0.7 V_{pp} modulating signal amplitude is ~8 GHz and is similar to the 3-dB bandwidth, Δv_{3dB}, of the spectrum of the DM free-running FP laser mode at 1553.1 nm for the same FP laser bias and modulating signal amplitude. The TBPF 3-dB bandwidth and passband centre frequency for the optimised DM SS-FP laser, using the 30 mA FP laser bias and 0.7 V_{pp} signal amplitude, are ~0.02 nm/3 GHz and ~1553.14 nm/193.023 THz, respectively.

3.3.3 Dependence of SS-FP Laser SMSR on Seed Signal Optical Power

To investigate the dependence of the SMSR of the SS-FP laser on the optical power of the seed signal reinjected back into the FP laser cavity, the optical power of the seed light was reduced using different optical attenuators at the output of the TBPF and the SMSR of the SS-FP laser was measured with the FP laser in continuous wave operation. The FP laser was biased at 30 mA, the device TEC temperature set at 25°C and the 3-dB bandwidth of the TBPF and the centre frequency of the TBPF passband were set to ~0.02 nm/3 GHz and ~1553.14 nm/193.023 THz, respectively. Thus, the FP laser longitudinal mode selected for self-seeding was the mode at 1553.1 nm. Optical spectra of the lightwaves output from the SS-FP laser were captured with the Yokogawa OSA for 0, 1 and 5-dB attenuation of the optical power of the reinjected seed signal. Figure 3.20 displays a blue spectrum, a red spectrum and a yellow spectrum, which correspond to the reinjected seed signal attenuated by 0, 1 and 5 dB, respectively. Figure 3.20 inset (a) displays the external cavity (EC) of the SS-FP laser and also shows the optical power of the FP laser longitudinal mode at 1553.1 nm, which was measured at various points in the passive optical circuit that forms the EC. The optical power of the longitudinal mode, within the MLM spectrum of the CW free-running laser, was measured at three points before input to the TBPF. The optical power of the filtered single longitudinal mode, or seed signal, was measured at the output of the TBPF. Assuming the same loss in optical power is incurred for the reinjected seed signal, when transmitted through the 3-dB coupler, the PC and back into the FP laser cavity, as is incurred by the optical signal initially transmitted from the free-running FP laser (~3.8-dB), then the estimated optical powers of the seed signals reinjected back into the FP laser cavity for 0, 1 and 5-dB attenuation are -20.4 dBm (9.1 μW), -21.4 dBm (7.2 μW) and -25.4 dBm (2.9 μW), respectively.

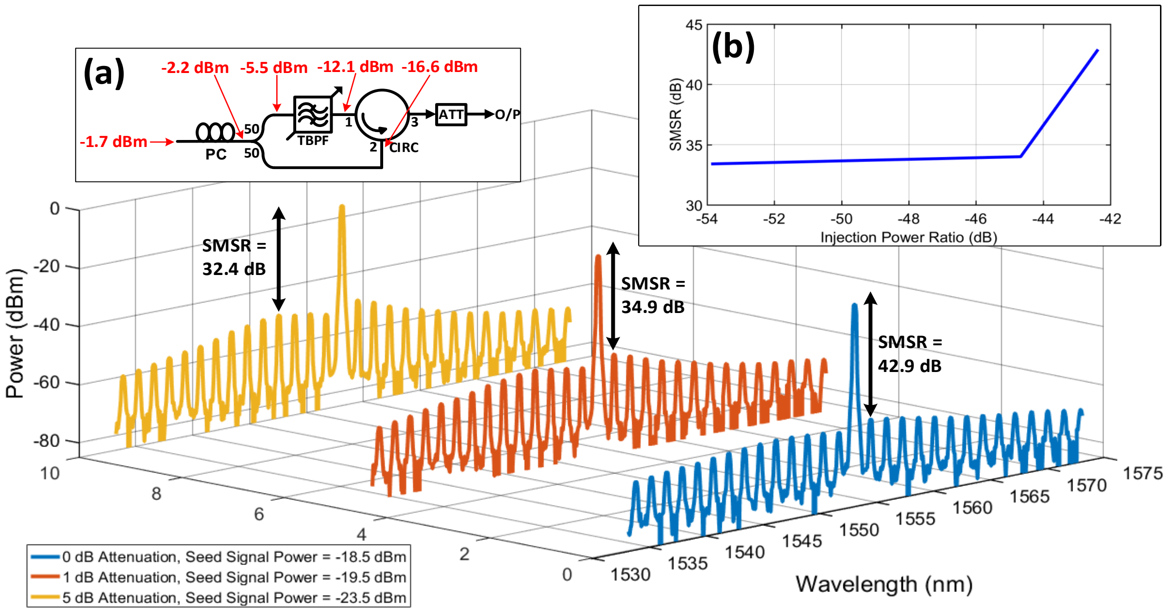

Figure 3.20: Spectra of the CW output from the SS-FP laser showing SMSR for 0 dB (blue spectrum), 1 dB (red spectrum) and 5 dB (yellow spectrum) attenuation of the optical power of the seed signal. Inset (a) shows the external cavity (EC) of the SS-FP laser and the optical power of the mode at 1553.1 nm measured at different stages throughout the EC. Inset (b) shows the SMSR of the SS-FP laser as a function of seed signal injection power ratio (IPR).

Using the estimated optical powers of the seed signals, the injection power ratios (IPRs) can be calculated. In the case of the self-seeded regime, the IPR can be defined as the ratio of the power of the reinjected mode or seed signal, to the power of the same longitudinal mode in the MLM spectrum of the optical signal initially transmitted from the free-running FP laser into the EC of the SS-FP laser [48]. From the estimated optical powers of the reinjected seed signals attenuated by 0, 1 and 5 dB, the corresponding injection power ratios are 1.43%, 1.15% and 0.46%, respectively. Thus, the self-seeded regime implemented in this study, where the CW SS-FP laser for the 30 mA FP laser bias exhibits an SMSR of 42.9 dB, can be categorised as a ‘weak’ feedback regime [45]. The graph displayed in Figure 3.20 inset (b) shows the exponential-like increase in the SMSR of the SS-FP laser with increasing IPR. As shown in Figure 3.20 inset (b), in order to achieve an SMSR of ~40 dB, which is necessary to achieve error-free 12.5 Gbit/s NRZ-OOK signal transmission with the DM SS-FP laser for b2b transmission, an IPR of >-43 dB is required.

3.3.4 Relative Intensity Noise (RIN) of the SS-FP Laser

The intensity noise of a semiconductor laser is due to the random spontaneous emission of photons that occurs in the cavity when the laser is biased above threshold. When carriers randomly recombine in the cavity of the laser to generate photons, it results in instantaneous time variations in the carrier and photon densities described by Langevin noise [49], [50]. During lasing, the photons that originate from stochastic spontaneous emission each adds a small field component with a random phase to the coherent field that has been established through stimulated emission, which randomly perturbs the amplitude of the coherent field resulting in intensity noise. This occurs even when the laser is biased above threshold with a constant dc current that exhibits negligible current fluctuations. The random fluctuations in the intensity or amplitude of the laser output optical power at a specific frequency is quantified by the relative intensity noise or RIN, which is a measure of the intensity noise of the laser normalised to the average output power level or, a measure of the fluctuation in the optical power output from the laser about its mean steady-state value. The RIN can be statistically described with a power spectral density which depends on the noise frequency. It is typically analysed and presented in the frequency domain as a PSD over a specific noise frequency range and the RIN PSD is represented in logarithmic scale with units of dBc/Hz. The RIN may be described as an inverse carrier-to-noise-ratio relationship. It is defined mathematically as the ratio of the mean-square optical power fluctuations, or the intensity noise, $\langle \Delta P(t)^2 \rangle$, of the lightwave output from the laser diode with respect to time (ac component), to the square of the average optical power, P_0^2, of the lightwave output from the laser (dc component) and is given as [14], [51] – [53]

$$RIN = \frac{\langle \Delta P(t)^2 \rangle}{P_0^2} \qquad 3.2$$

The laser RIN is an important parameter to characterise, particularly when intensity modulation (IM) formats are being employed with lasers for signal transmission in optical fibre communications links. It is most likely that the IEEE 802.3 GBase standard will be adopted In NG-PON2, in which case the upper limit of the allowable transmitter RIN is determined by the data rate employed. In the current standards, the maximum permissible transmitter RIN in Gigabit Ethernet ranges from -128 to -132 dBc/Hz, depending on the IEEE 802.3 Physical Layer specification [54], [55]. Therefore, it is necessary to characterise the RIN of a laser diode prior to its implementation in an IM/DD link, particularly if the laser is being directly modulated.

Characterisation of the RIN can be performed by detecting the CW laser output optical power with a high-speed, wide bandwidth, photodiode (PD) and then capturing the spectrum of the signal output from the PD with an electrical spectrum analyser (ESA). The RIN measurement can then be extracted from the electrical spectrum of the optical power fluctuations, which is the frequency noise spectrum associated with the total power. Through the square-law relationship, the photocurrent generated by the PD is proportional to the incident optical power, and the electrical power generated at the output of the PD is proportional to the square of the photocurrent and, thus, to the square of the incident optical power. The Fourier transform (FT) of the term $\langle \Delta P(t)^2 \rangle$ in equation 3.2 is the electrical noise power spectral density (PSD), or the PSD of the frequency noise, in units of W/Hz, and the FT of P_0^2 is proportional to the average electrical power generated at the output of the PD corresponding to the PSD of the dc photocurrent in Watts. The RIN can be expressed in terms of power in dBc as a function of frequency in Hz through equation 3.3 [51] – [53].

$$RIN_{dBc}(f) = 10\log_{10}\left(\frac{\langle |\Delta P(f)^2| \rangle}{\langle P_0^2 \rangle}\right) \qquad 3.3$$

The experimental setup used for the RIN measurement is shown in Figure 3.21. For a fixed laser bias, the CW optical signal output from the laser under test (LUT) was passed through the optical isolator, which limited any optical feedback into the laser cavity that may have occurred due to back reflections. The VOA at the input to the PD ensured that a fixed optical power of 1 dBm was incident on the PD throughout the experiment and also ensured that saturation of the PD was avoided. It was necessary to employ a wide bandwidth PD (~20 GHz), as the RIN is typically measured from dc up to 20 GHz. The PD employed also displayed the generated photocurrent, therefore, it was not necessary to separate the dc and ac components of the generated photocurrent with a bias tee. The electrical RF amplifier employed exhibited low noise, a known high gain and a passband spectrum which covered the spectral range of interest. The high bandwidth ESA was used to capture the noise spectrum of the RF amplified photocurrent. The dc blocks employed at the input to, and output from, the RF amplifier ensured that only the amplified AC component of the electrical signal was captured by the ESA. When measuring the RIN, the noise power spectrum captured by the ESA is the total noise power of the experimental setup used to characterise the RIN, which comprises noise contributions from three different sources, including the shot, thermal and laser intensity noise. Thus, in order to extract the laser intensity noise or RIN from the total frequency noise spectrum, the thermal noise contribution from the PD and the RF amplifier combination, and the shot noise contribution due to the average optical power incident on the PD, must be determined and subtracted from the total noise power [51] – [53].

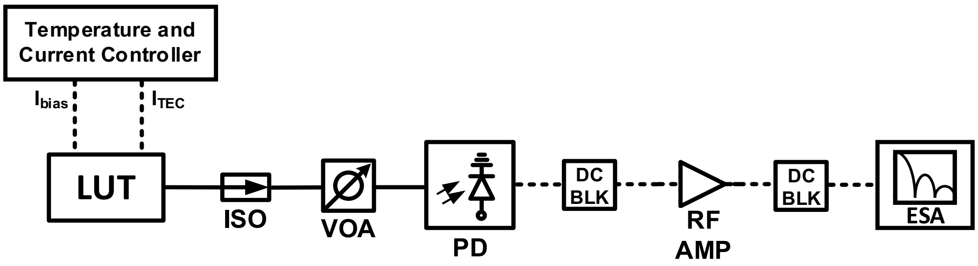

Figure 3.21: Experimental setup for RIN measurement.

The RIN of the SS-FP laser was measured for the 30 mA FP laser bias and 25°C device TEC temperature, with the mode at 1553.1 nm self-seeded. The RIN of the SS-FP laser was measured for 0, 1 and 5 dB attenuation of the optical power of the seed signal. The spectra of the lightwaves output from the SS-FP laser for the 0, 1 and 5 dB attenuation of the seed signal power, or the 1.45%, 1.15% and 0.46% injection power ratios (IPRs), were shown in Figure 3.20. The SMSR of the SS-FP laser corresponding to the 0, 1 and 5 dB attenuation of the seed signal power were 42.9, 34.9 and 32.4 dB, respectively. The RIN of the full MLM spectrum of the free-running FP laser and the RIN of the single longitudinal mode at 1553.1 nm filtered from the MLM spectrum of the free-running FP laser, were also measured for comparison with the RIN of the SS-FP laser for the 0, 1 and 5 dB attenuation of the seed signal optical power. For the characterisation of the RIN of the filtered single longitudinal mode at 1553.1 nm, the VOA was removed from the setup and a TBPF was inserted between the ISO and PD in order to filter the single longitudinal mode from the MLM of the free-running FP laser. An EDFA was initially employed at the output of the TBPF to amplify the power of the filtered mode prior to detection with the PD. However, when the EDFA was employed to amplify the filtered mode, the relaxation oscillation (RO) peak of the resultant RIN spectrum was obscured by the ASE noise of the EDFA. Subsequently, it was discovered that the filtered longitudinal mode had sufficient optical power to measure the noise spectrum without requiring the EDFA. Figure 3.22 displays the results obtained from the experimental characterisation of the RIN.

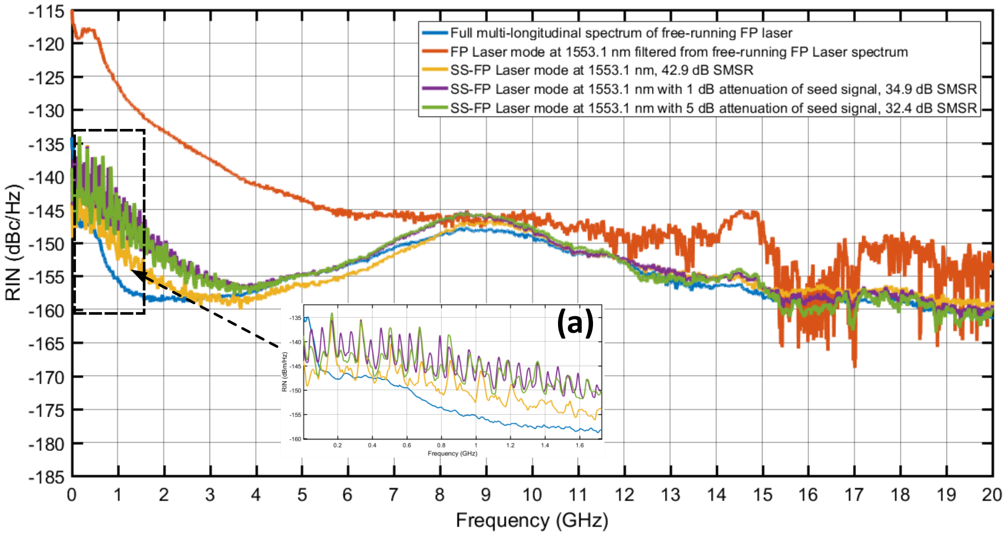

Figure 3.22: RIN PSD for SS-FP laser for 0 dB (yellow), 1 dB (purple) and 5 dB (green) attenuation of the seed signal optical power and the RIN PSD of the full multi-longitudinal mode spectrum of the free-running FP laser (blue) and the RIN PSD of the filtered single longitudinal mode at 1553.1 nm (brown). Inset (a) shows an enhanced view of the selected area.

Through self-seeding of the selected FP laser mode, the RIN observed in the single longitudinal mode filtered from the MLM spectrum of the free-running FP laser (red RIN spectrum), particularly at low frequencies, has been significantly reduced. The averaged RIN of the SS-FP laser for the 1.45% (yellow RIN spectrum), 1.15% (purple RIN spectrum) and 0.46% (green RIN spectrum) injection power ratios

(IPRs), are -146.5, -145.5 and -145 dBc/Hz, respectively, which are on par with the averaged RIN of the full MLM spectrum free-running FP laser. Furthermore, the RO frequency peak of the RIN spectra of the SS-FP laser is also ~9 GHz. Although the low frequency RIN of the SS-FP laser and the full spectrum free-running FP laser is similar, the RIN spectra of the SS-FP laser exhibit sharp noise peaks from dc to ~2 GHz. As the IPR or seed signal optical power of the SS-FP laser decreases, the baseline RIN of the SS-FP laser over the 0 to ~3 GHz range increases and the magnitude and frequency of the sharp noise peaks also increase. The sharp noise peaks observed at low frequencies in the RIN spectra captured from the SS-FP laser, shown in Figure 3.22 inset (a), can be attributed to the external cavity modes.

The formation of the external cavity modes is due to the excessive length of the external cavity of the SS-FP laser, which was calculated to be ~10 m, and was unavoidable considering off-the-shelf optical components were employed to construct the cavity. The RIN of semiconductor lasers subjected to optical feedback from external cavities and the beating among longitudinal external cavity modes. that occurs in self-seeding lasers, which are particularly sensitive to RIN at low frequencies, has been studied extensively [56] – [72]. The low frequency RIN observed in self-seeding lasers employing external cavities, ocurring as a result of the presence of the external cavity modes, can be exacerbated by fluctuations in the optical power of the reinjected seed light. Thus, the optical path of the feedback loop, which forms the external cavity and enables the self-seeding, must be stable so that the low frequency RIN, due to the external cavity modes, is minimised. In the self-seeding scheme developed in this study, it is suspected that the external cavity of the SS-FP laser was adversely affected by environmental noise. Variations in the refractive index of the SSMF in the external cavity, due to temperature and acoustic fluctuations, causes perturbations in the optical phase, frequency and power of the reinjected seed light and the external cavity modes, thus, resulting in the the sharp noise peaks observed at low frequencies in the RIN spectrum of the SS-FP laser.

3.3.5 SS-FP Laser Channel Characterisation and Wavelength Tuning Range

Before evaluating the transmission performance of the directly modulated (DM) SS-FP laser over SSMF in an IM/DD test-bed, the transmission performance of 18 SS-FP laser modes or wavelength channels, spanning 23 nm (1537.99 to 1561.59 nm), were evaluated for b2b transmission. The b2b transmission performance analysis of the 18 channels of the SS-FP laser, was performed with the FP laser biased at 30 mA, the laser TEC temperature set at 25°C and the FP laser directly modulated with the 12.5 Gbit/s NRZ-OOK signal using the 0.7 V_{pp} signal amplitude. The experimental setup shown in Figure 3.9 was employed for the analysis. Each of the 18 SS-FP laser channels was accessed by manually detuning the TBPF passband centre wavelength, while the TBPF bandwidth was maintained at ~0.02 nm/3 GHz and the SS-FP laser was directly modulated. A tuning step of ~1.39 nm/173.38 GHz, which is the FSR of the

MLM spectrum of the FP laser measured in section 3.2.2, was employed to access each of the SS-FP laser channels. The BER measurements were acquired for a fixed received optical power of -14 dBm, which was maintained at -14 dBm using the VOA at the input to the APD receiver. The BER result for each of the 18 DM SS-FP laser channels was recorded as well as the SMSR of the DM SS-FP laser, which was measured with the Yokogawa OSA using a spectral resolution setting of 0.5 nm. The spectra of the optical signals output from the DM SS-FP laser at each of the 18 operating wavelengths or channels were captured with the Yokogawa OSA. Figure 3.23 displays the SMSR and BER performance for b2b transmission of the 18 channels of the directly modulated SS-FP laser.

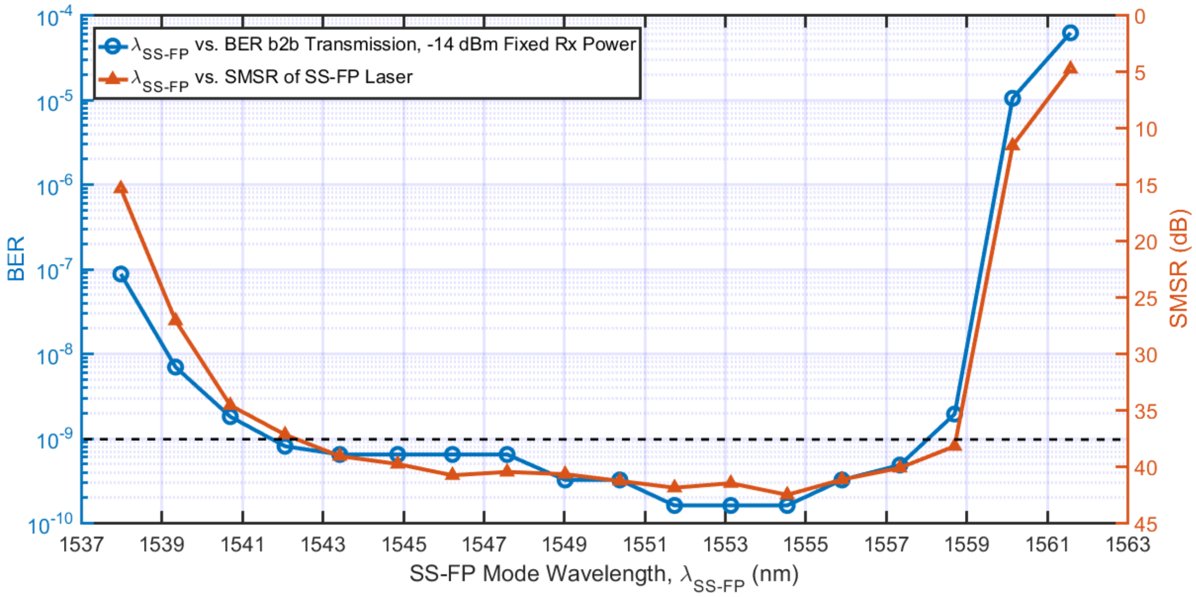

Figure 3.23: BER measurements for b2b transmission and SMSR of 18 SS-FP IL modes or wavelength channels, with the SS-FP laser directly modulated with the 12.5 Gbit/s NRZ-OOK signal using the 0.7 V_{pp} signal amplitude.

It can be observed in Figure 3.23 that 12 of the 18 DM SS-FP laser channels produce error-free, or near error-free, transmission performance for b2b transmission at a fixed received power of -14 dBm. The 12 channels span ~15 nm from 1542.07 to 1557.35 nm with SMSRs ranging from 37.2 to 42.5 dB. Further to what was observed previously in section 3.3.2, as the SMSR decreases, the b2b transmission performance degrades. Figure 3.24 displays the spectra of the 12 optical signals transmitted from the DM SS-FP laser, which all produce near error-free b2b transmission performance at a received optical power of -14 dBm. The 12 channels span a wavelength range of 15 nm, from 1542.07 to 1557.35 nm, and the corresponding SMSR of the different DM SS-FP laser channels are also shown. To optimise the SMSR and the BER performance for b2b transmission of all 12 channels of the DM SS-FP laser, the centre frequency of the TBPF passband was negatively detuned by ~4 GHz with respect to the peak of the spectrum of the mode transmitted from the DM free-running FP laser, and this was consistent for all 12 channels.

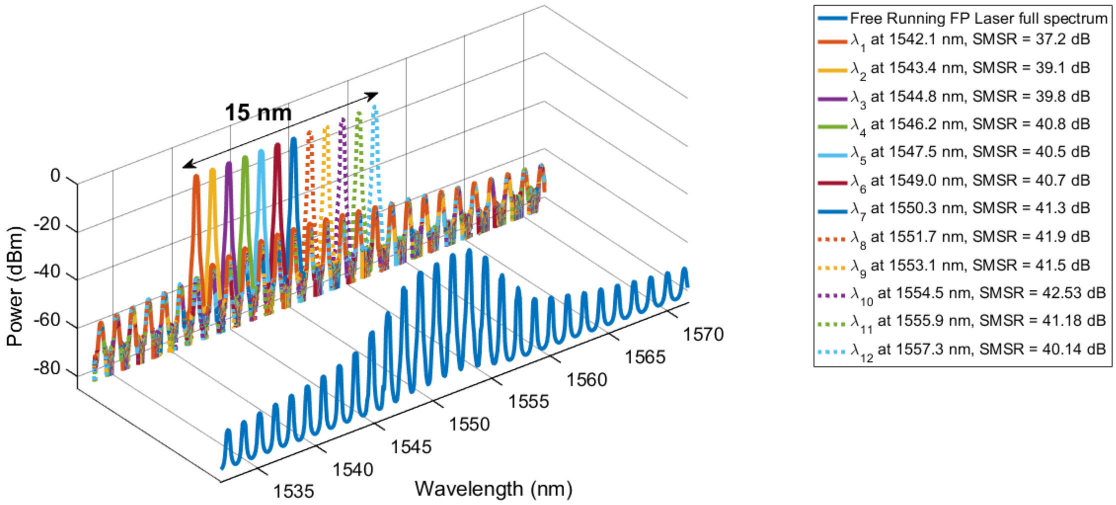

Figure 3.24: Spectra of the optical signals transmitted from the DM SS-FP laser at the 12 different operating wavelengths or channels spanning a wavelength range of 15 nm.

The ~4 GHz negative detuning, or the detuning of the centre frequency of the TBPF passband, is necessary in order to compensate for the shifting of the cavity resonances of the FP laser towards lower frequencies, which occurs as a result of the refractive index variation within the active region of the FP laser due to the seed signal being re-injected back into the laser cavity. The reinjection of the seed signal back into the FP laser cavity reduces the threshold carrier density in the gain section of the laser which, as a result, reduces the threshold gain in the cavity. The reduction in the threshold gain results in an increase in the refractive index of the gain section and this causes the red-shift in the operating frequency or increase in the lasing wavelength [44]. The red-shift in the operating frequency is accompanied by a reduction in the lasing threshold, which compensates for the gain reduction to some extent [44] – [46]. Moreover, the red-shift is an indication that wavelength-locking through self-seeding is successfully established [47]. In the experiments, when no detuning of the TBPF centre frequency was performed, the quality of the resulting eye diagrams of both the transmitted optical signal and received electrical signal that were observed degraded significantly. The eye diagrams exhibited more distortion, noise and timing jitter and, consequently, the resultant BER for b2b transmission increased by over two orders of magnitude to >1x10^{-7}. Thus, the detuning of the centre frequency of the TBPF passband with respect to the peak frequency of the spectrum of the signal transmitted from the DM free-running FP laser, is necessary to establish optimal self-seeding and to optimise the quality of the signal transmitted from the DM SS-FP laser. Figure 3.25 displays a graph showing the peak optical powers and the SMSRs of the 12 DM SS-FP laser modes or channels displayed in Figure 3.24.

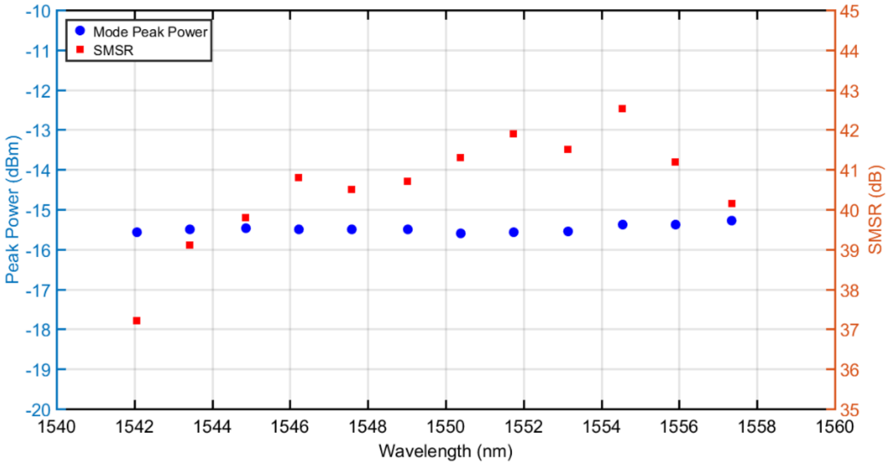

Figure 3.25: Peak optical power and SMSR of DM SS-FP laser IL modes or wavelength channels in the wavelength range of 1542.07 to 1557.35 nm with a tuning step of ~1.39 nm.

From analysis of the results shown in Figure 3.23 and Figure 3.25, it is clear that the b2b transmission performance of the DM SS-FP laser is, in part, dependent on the SMSR, as degradation in the BER performance of the laser is observed as the SMSR decreases. This is particularly evident in the poor performance of the channels at both ends of the spectrum, since the output power and, hence, the SMSR of the DM SS-FP laser is influenced by the gain profile of the FP laser. Output optical power and wavelength stability analysis of the 12 different DM SS-FP laser modes or channels was not performed. However, a short-term stability analysis of the SS-FP laser channel at 1553.14 nm was performed for an observation time of 30 minutes. The variation in the wavelength, optical power and SMSR of the channel at 1553.14 nm observed during the 30 minute time frame were 0.01 nm, 0.67 dB, and 1.2 dB respectively.

Considering that the minimum FWHM or 3-dB bandwidth of the TBPF is ~0.02 nm/3 GHz and the FSR of the MLM spectrum of the FP laser is 1.39 nm/173.38 GHz, the tuning range of the SS-FP laser, in its current form, is therefore dependent on the wavelength range and resolution of the TBPF, and the gain profile and the operating temperature range of the FP laser. The wavelength range of the TBPF is 1450 to 1650 nm and the resolution is 5 pm, hence, the gain profile and operating temperature range of the FP laser are the factors currently limiting the tuning range of the SS-FP laser. The gain profile of the FP laser is such that 12 DM SS-FP laser operating wavelengths or channels produce near error-free transmission performance for b2b transmission at a received optical power of -14 dBm, with the SMSR of the DM SS-FP laser ranging from 37.2 dB to 42.53 dB. From Figure 3.3 it can be observed that up to 30 SS-FP laser channels, over a wavelength tuning range of ~27 nm, could potentially be exploited for signal transmission by varying the temperature of the FP laser device TEC temperature by +/- 10^{o}C. The wavelength shift of the longitudinal modes of the MLM spectrum of the FP laser, as a result of temperature variation, is determined by the linear relation $\Delta\lambda/\Delta T_{(°\mathrm{C})}$, which, from section 3.2.2, is

0.48 nm/1°C. Figure 3.26, shows the full MLM spectra of the FP laser biased at 30 mA and directly modulated with the 0.7 V_{pp} 12.5 Gbit/s NRZ-OOK signal, for 24, 25 and 26°C device TEC temperatures, respectively. The spectra were captured with the Apex OSA using a spectral resolution setting of 0.16 pm/20 MHz. Figure 3.26 inset (a) shows an enhanced view of 3 adjacent modes or channels within the DM free-running FP laser spectrum centred at 1551.7 nm, which exhibit a channel spacing of 1.39 nm/173 GHz. Figure 3.26 inset (b) displays an enhanced view of 3 adjacent modes or channels in the DM free-running FP laser spectra centred at 1553.1 nm for 24, 25 and 26°C device TEC temperatures, respectively.

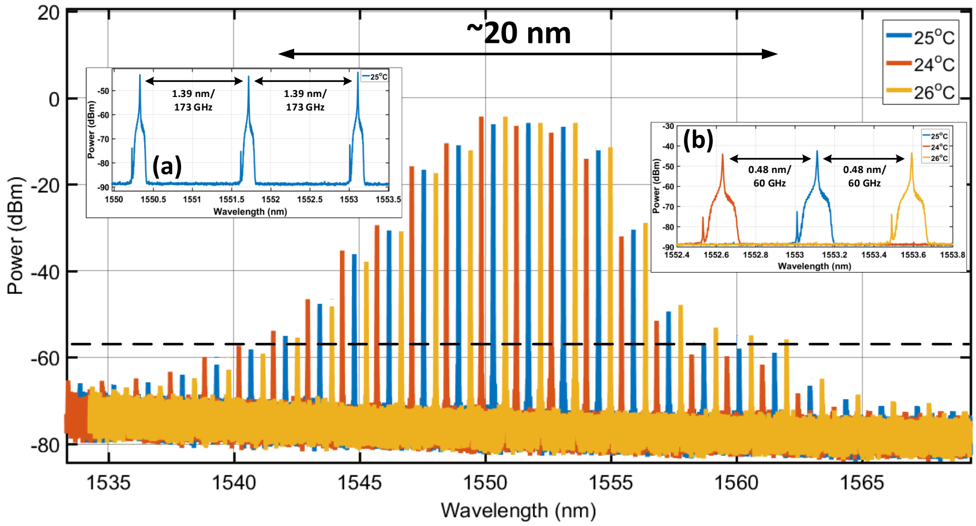

Figure 3.26: full multi-longitudinal mode spectra of the FP laser biased at 30 mA and directly modulated with the 0.7 V_{pp} 12.5 Gbit/s NRZ-OOK signal, for 24°C, 25°C and 26°C device TEC temperatures, respectively.

If the 12 SS-FP laser channels that produced error-free transmission for b2b transmission at a received optical power of -14 dBm are considered, then up to 50 SS-FP laser channels, spanning a wavelength tuning range of ~20 nm, could potentially be utilised for signal transmission through variation of the FP laser device TEC temperature by +/-1°C. Moreover, variation in the FP laser device TEC temperature by 1°C corresponds to a wavelength shift of the longitudinal modes by ~0.3 nm/50 GHz, which is one of the channel spacings requirements that tunable laser sources must meet to be suitable for use at the ONUs in NG-PON2, which has been specified in the recent ITU-T G989.2 recommendations [1].

3.3.6 Transmission Performance Evaluation of the Directly Modulated SS-FP Laser

To assess the suitability of the proposed SS-FP laser for potential use as a tunable laser source (TLS) in NG-PON2 or future IM/DD-based optical access networks, the transmission performance of the SS-FP laser under direct modulation (DM) is experimentally evaluated. The transmission performance of the DM SS-FP laser is assessed with two different intensity modulation (IM) formats, NRZ-OOK and PAM-4. The SS-FP laser is directly modulated with a 12.5 Gbit/s NRZ-OOK signal and the performance for transmission over 25 km of SSMF is assessed. Furthermore, the performances of 4 different SS-FP laser channels are evaluated. The performance of the SS-FP laser directly modulated with a 12.5 Gbaud/s (25 Gbit/s) PAM-4 signal is assessed for b2b transmission. In the PAM-4 transmission experiment, an adaptive equaliser is utilised in the offline digital processing of the received signal to compensate for the ISI resulting from the bandwidth limit and non-ideal channel frequency response characteristics of the transmission system. Error-free 12.5 Gbit/s NRZ-OOK optical signal transmission over 25 km of SSMF is attained with the DM SS-FP laser without electronic or optical dispersion compensation. For b2b transmission of the PAM-4 signal, performance below the 7% forward error correction (FEC) limit is attained. These experiments demonstrate that the SS-FP laser, with appropriate modifications and optimisation, could potentially be employed as a directly modulated tunable laser source (TLS) in NG-PON2 or IM/DD-based future optical access networks utilising WDM technologies.

3.3.6.1 12.5 Gbit/s NRZ-OOK transmission

The experimental setup employed to evaluate the transmission performance of the SS-FP laser directly modulated with the 12.5 Gbit/s NRZ-OOK signal is illustrated in Figure 3.27. With the FP laser device TEC temperature maintained at 25°C, the BER performance of the DM SS-FP laser is evaluated for the 30 and 72.5 mA FP laser biases with the 0.7 and 2 V_{pp} modulating signal amplitudes, respectively. For transmission with the DM SS-FP laser for the 30 mA FP laser bias and the 0.7 V_{pp} modulating signal amplitude, the lasing mode or wavelength channel at 1553.14 nm is utilised and for the 72.5 mA FP laser bias and the 2 V_{pp} modulating signal amplitude, the lasing mode or wavelength channel at 1559.6 nm is employed.

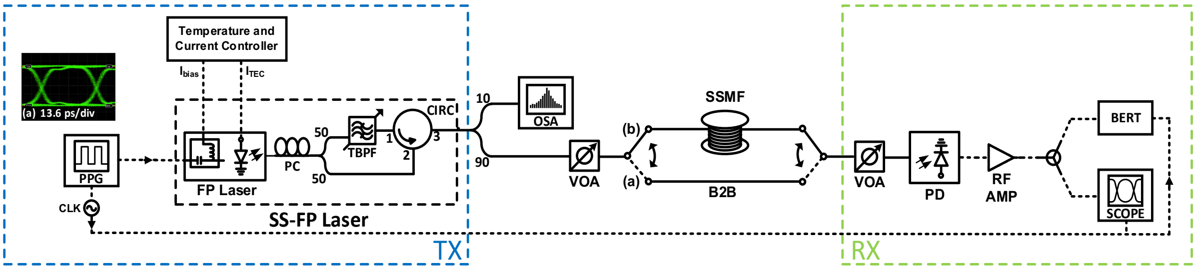

Figure 3.27: Experimental setup for 12.5 Gbit/s NRZ-OOK signal transmission with the DM SS-FP laser.

The TBPF 3-dB bandwidth and passband centre frequency utilised for the transmission experiments with the DM SS-FP laser for the 30 mA FP laser bias and the 0.7 V_{pp} modulating signal amplitude, were 0.02 nm/3 GHz and 1553.14 nm/193.023 THz, respectively. For the transmission experiments with the DM SS-FP laser for the 72.5 mA FP laser bias and 2 V_{pp} modulating signal amplitude, the TBPF 3-dB bandwidth and passband centre frequency were 4.5 GHz/0.035 nm and 192.2185 THz/1559.645 nm, respectively. The experimental procedure that was followed to acquire the BER measurements in the transmission experiments with the DML, which is described in section 2.2.2, is followed to acquire the BER results in the transmission experiments with the DM SS-FP laser. The transmission performance of the DM free-running FP laser for the 30 and 72.5 mA FP laser bias currents with the 0.7 and 2 V_{pp} modulating signal amplitudes, respectively, is also evaluated for b2b transmission. Figure 3.28 shows the BER results obtained from the transmission performance evaluation of the DM SS-FP laser and the DM free-running FP laser. Figure 3.28 inset (a) shows the eye diagram of the received signal captured following error-free transmission over 25 km SSMF attained with the DM SS-FP laser for the 30 mA FP laser bias and 0.7 V_{pp} modulating signal amplitude.

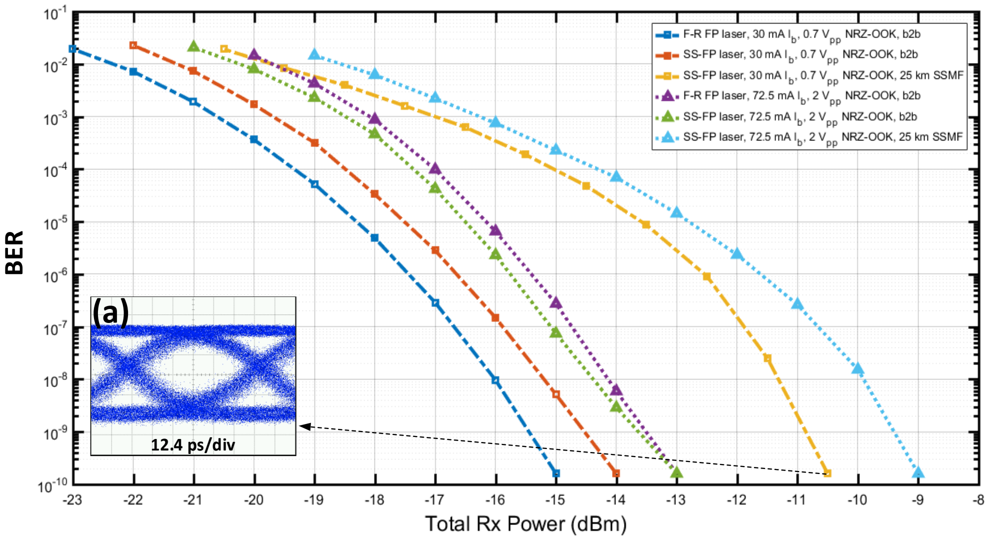

Figure 3.28: BER performance of DM SS-FP laser and DM free-running FP laser for 30 mA FP laser bias and 0.7 V_{pp} modulating signal amplitude, and for 72.5 mA FP laser bias and 2 V_{pp} modulating signal amplitude, for b2b transmission and transmission over 25 km of SSMF.

It can be observed in the BER results displayed in Figure 3.28 that the 30 mA FP laser bias and 0.7 V_{pp} modulating signal amplitude produce the best transmission performance with the DM SS-FP laser for b2b transmission and for transmission over 25 km of SSMF. Relative to the BER performance for b2b transmission with the DM free-running FP laser biased at 30 mA and modulated with the 0.7 V_{pp} signal amplitude, only a 1 dB power penalty is observed for transmission with the DM SS-FP laser operated at the same laser bias and modulating signal amplitude. For transmission over 25 km of SSMF with the DM SS-FP laser for the 30 mA FP laser bias and 0.7 V_{pp} modulating signal amplitude, a 3.5 dB power penalty is observed relative to b2b transmission. The receiver sensitivity penalty that is observed for transmission with the DM SS-FP laser for the 72.5 mA laser bias and 2 V_{pp} modulating signal amplitude operating parameters relative to the DM SS-FP laser for the 30 mA laser bias and 0.7 V_{pp} modulating signal amplitude parameters, may be attributed to the ER and ER power penalty, δ_{ER}, of the signal transmitted from the DM SS-FP laser for the higher bias and modulating signal amplitude, which were 1.1 dB lower and 1.3 dB higher, respectively. It is noteworthy that the DM SS-FP laser and the free-running FP laser for the 72.5 mA laser bias and 2 V$_{pp}$ modulating signal amplitude produced very similar b2b transmission performance, this can be attributed to the signals transmitted from the DM SS-FP laser and the free-running laser exhibiting similar ER and ER power penalty, δ_{ER}, metrics. However, the Q-factor, Q, of the signal transmitted from the DM free-running FP laser for the 72.5 mA bias and 2 V$_{pp}$ signal amplitude of 13 dB, was 5.6 dB higher than the Q of the signal transmitted from the DM SS-FP laser for the same bias current and modulating signal amplitude. Therefore, it may be inferred that once the Q-factor of the transmitted signal exceeds a certain threshold, the factors influencing the b2b transmission performance is the ER and ER power penalty, δ_{ER} of the transmitted signal.

To determine the variability in the BER performances of the different SS-FP laser modes or wavelength channels, 4 of the 12 wavelength channels that produced error-free transmission for b2b transmission with the DM SS-FP laser for the 30 mA FP laser bias and the 0.7 V$_{pp}$ modulating signal amplitude, shown in Figure 3.23 in section 3.3.5, were selected and the BER performance of each of the 4 channels were experimentally evaluated. With the FP laser biased at 30 mA and directly modulated with the 0.7 V$_{pp}$ 12.5 Gbit/s NRZ-OOK signal, the BER performance of the DM SS-FP operating at 1543.4 nm (λ_2), 1547.5 nm (λ_5), 1553.1 nm (λ_9) and 1557.3 nm (λ_{12}) were individually assessed for b2b transmission and for transmission over 25 km of SSMF.

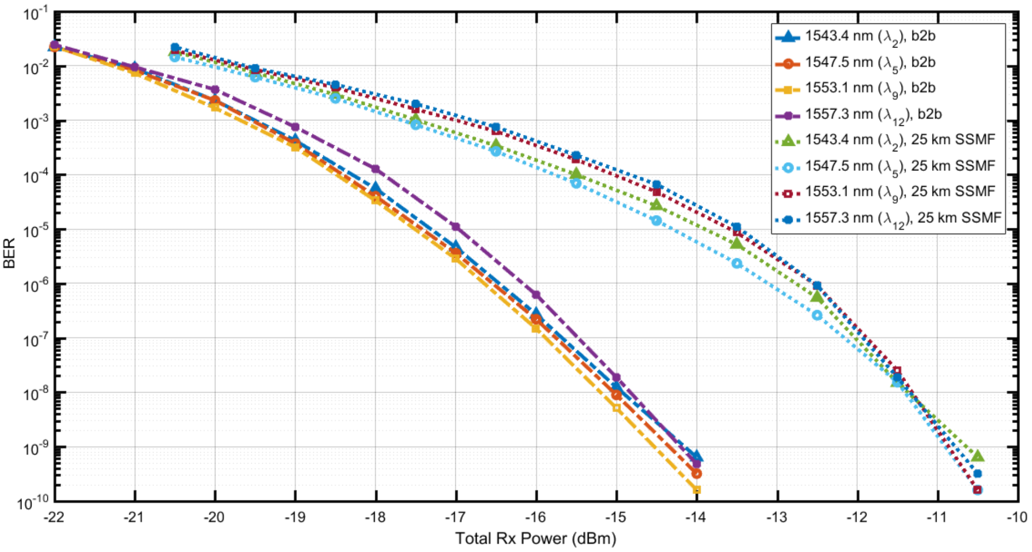

Figure 3.29: BER performance of DM SS-FP laser for 30 mA FP laser bias and 0.7 V$_{pp}$ modulating signal amplitude, operating at 1543.4 nm (λ_9), 1547.5 nm (λ_5), 1553.1 nm (λ_9) and 1557.3 nm (λ_{12}) channels, for b2b transmission and transmission over 25 km of SSMF.

Each of the 4 SS-FP laser wavelength channels were accessed by varying the TBPF passband centre frequency and the BER was measured as a function of received signal optical power. The BER results obtained from the experiments are shown in Figure 3.29. It can be observed in Figure 3.29 that the 4 channels of the DM SS-FP laser exhibit similar BER performance and the same receiver sensitivities are attained for both b2b transmission and for transmission over 25 km of SSMF without any dispersion compensation. Moreover, given that similar BER performance and receiver sensitivities are attained for b2b transmission with all 4 SS-FP laser channels, it suggests that the different channels exhibit similar levels of RIN.

3.3.6.2 12.5 Gbaud/s (25 Gbit/s) PAM-4 transmission

The experimental setup employed to evaluate the transmission performance of the SS-FP laser directly modulated with a 12.5 Gbaud/s (25 Gbit/s) PAM-4 signal is shown in Figure 3.30. Due to the reduced noise tolerance, increased SNR requirements and reduced optical power efficiency of PAM-4 optical signal transmission systems [73], the decision was made to employ the 72.5 mA FP laser bias and 2 V_{pp} modulating signal amplitude operating parameters when directly modulating the SS-FP laser in order to attain the highest receiver sensitivity. This decision was taken because the signal transmitted from the DM SS-FP laser with the FP laser biased at 72.5 mA and modulated with the 2 V_{pp} 12.5 Gbit/s NRZ-OOK signal exhibited the highest Q-factor of 7.4 dB observed in section 3.3.2. Furthermore, when the FP laser was biased at 72.5 mA and directly modulated with the 2 V_{pp} 12.5 Gbaud/s PAM-4 signal, the average optical power output from the DM SS-FP laser was +3.8 dBm, which was 4.3 dBm higher than the average power output from the DM SS-FP laser when the FP laser was biased at 30 mA and directly modulated with the 0.7 V_{pp} PAM-4 signal.

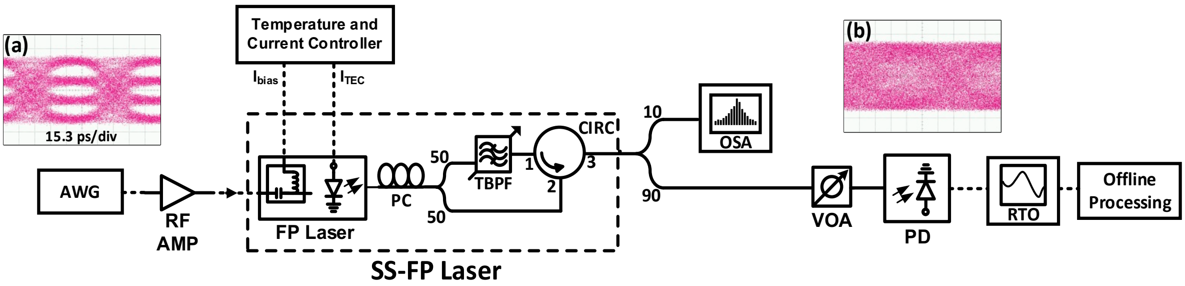

Figure 3.30: Experimental setup for 12.5 Gbaud/s PAM-4 signal transmission with the DM SS-FP laser. Insets (a) and (b) show the eye diagram of the amplified PAM-4 modulating signal output from the AWG and the electrical signal output from the APD following detection of the transmitted 12.5 Gbaud/s PAM-4 optical signal, both signals were captured with the sampling oscilloscope.

The maximum peak-to-peak (V_{pp}) amplitude of the PAM-4 modulating signal output from the arbitrary waveform generator (AWG, Tektronix AWG70002A) was 0.5 V_{pp}, thus, to generate the 2 and 0.7 V_{pp} modulating signals, the PAM-4 electrical signal output from the AWG needed to be amplified with an RF amplifier. With the FP laser was biased at 72.5 mA and the device TEC temperature set to 25°C. The wavelength channel at 1559.6 nm was selected for self-seeding, thus, the centre frequency of the TBPF passband was detuned to 192.2185 THz/1559.645 nm and the 3-dB bandwidth of the TBPF was adjusted to 4.5 GHz/0.035 nm. The 12.5 Gbaud/s PAM-4 signal used to directly modulate the SS-FP laser was produced by mapping a PRBS, or bit stream, to the PAM-4 symbols by means of Gray coding

[73] – [74][75] and then upsampling the resultant signal by a factor of 2. The PAM-4 electrical signal waveform, with a sequence length of 2^{15} symbols long and an amplitude of 0.3 V_{pp}, output from the AWG operating at 25 GSa/s was amplified to 2 V_{pp} with the RF amplifier and the amplified signal was used to directly modulate the SS-FP laser. During the experiment, the SMSR of the DM SS-FP laser was monitored with the Yokogawa OSA and was maintained above 40 dB throughout. The resultant PAM-4 optical signal transmitted from the DM SS-FP laser was detected with a 10G class APD photodetector (PD) with an integrated trans-impedance amplifier. The VOA at the input to the PD enabled the optical power of the received signal incident on the PD to be varied, which allowed the BER results to be measured as a function of the received optical power. The electrical signal output from the PD was captured with a real-time oscilloscope (RTO) operating at 100 Ga/s.

Digital processing of the received signal (downsampling, normalisation, adaptive equalisation, symbol synchronization, decoding), and BER calculations were performed offline using MATLAB. The symbol synchronization was realised with the aid of a $2^{\hat{}7}$ symbols long training sequence. The adaptive filter employed for channel equalisation was a 21 tap FIR (feed-forward) filter using a least-mean square (LMS) algorithm for tap weights adaptation. The feed-forward equalizer (FFE) was used to compensate for linear impairments and ISI induced by the limited bandwidth of the PD and, consequently, reduce the number of errors in the received signal. Figure 3.31 shows the BER results obtained from the b2b transmission experiment with the SS-FP laser directly modulated with the 12.5 Gbaud/s (25 Gbit/s) PAM-4 signal. Figure 3.31 inset (a) displays the eye diagram of the PAM-4 optical signal transmitted from the DM SS-FP laser which was captured with the dc-coupled photodetector integrated in the sampling oscilloscope. Also shown in Figure 3.31 insets (b) and (c) are the spectrum and eye diagram of the received electrical signal, respectively, generated following offline DSP in MATLAB.

It can be observed in Figure 3.31 that b2b transmission with the SS-FP laser directly modulated with the 12.5 Gbaud PAM-4 signal, yielded a BER of $3x10^{-3}$ for a received signal optical power of -7 dBm and the BER of $3x10^{-3}$ is slightly below the 7% FEC (BER = $3.8x10^{-3}$ [76]) limit. The extinction ratio, ER, of the transmitted PAM-4 optical signal, calculated with data extracted from the eye diagram shown in Figure 3.31 inset (a), is 2.65 dB. This is comparable to the 2.8 dB ER of the optical signal transmitted from the SS-FP laser with the laser biased at 72.5 mA and directly modulated with the 2 V_{pp} 12.5 Gbit/s NRZ-OOK signal, which was measured in section 3.3.2. The 3-dB bandwidth of the PAM-4 spectrum shown in Figure 3.31 inset (b) is ~11 GHz. Similarly, this is comparable to the 3-dB bandwidth of the optical spectrum of the signal transmitted from the SS-FP laser with the FP laser biased at 72.5 mA and directly modulated with the 2 V_{pp} 12.5 Gbit/s NRZ-OOK signal, which was also measured in section 3.3.2 and found to be 11.8 GHz. It is clear from the eye diagram shown in Figure 3.31 inset (c) that the received signal is heavily filtered by the APD at ~7 GHz, which negatively impacts the transmission performance.

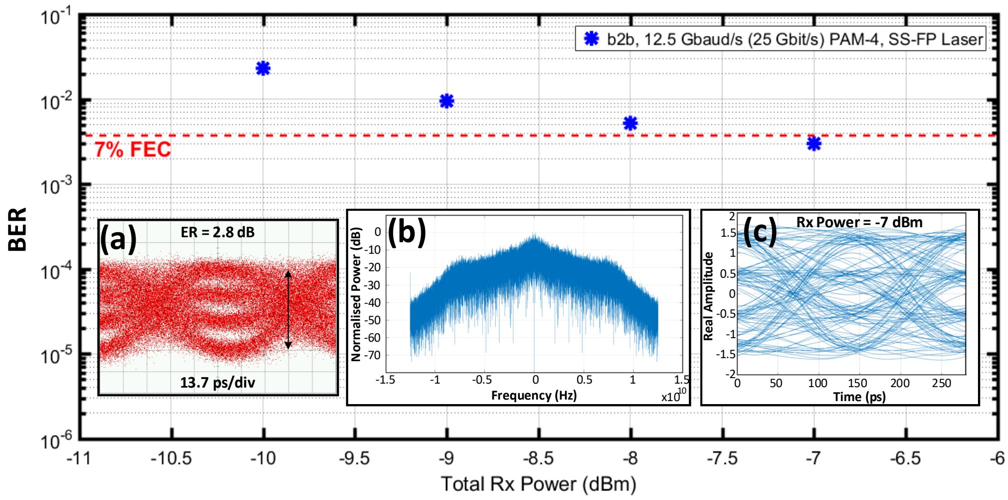

Figure 3.31: BER performance for b2b transmission of SS-FP laser for 72.5 mA FP laser bias and directly modulated with a 2 V_{pp} 12.5 Gbaud/s PAM-4 signal, inset (a) shows the eye diagram of the PAM-4 optical signal transmitted from the DM SS-FP laser and insets (b) and (c) display the spectrum and eye diagram of the transmitted optical and received electrical signals, respectively.

Figure 3.30 (b) shows the electrical signal output from the APD receiver following detection of the 12.5 Gbaud/s PAM-4 optical signal. The electrical signal was captured with the sampling oscilloscope having disconnected the RTO. It can be observed in Figure 3.30 (b) that the three eye diagrams and multiple symbol levels of the PAM-4 signal cannot be distinguished. This is due to the limited bandwidth of the APD employed, which was ~7 GHz. Although the ~7 GHz bandwidth of the APD was sufficient to detect 12.5 Gbit/s NRZ-OOK optical signal, a larger bandwidth is required to detect the 12.5 Gbaud/s PAM-4 optical signal to generate a clear and open eye diagram with the sampling scope. Nevertheless, some level of transmission performance is achieved when the APD is used for detection of the PAM-4 optical signal and adaptive equalisation is applied to the signal captured with the RTO offline, as evidenced by the BER results shown in Figure 3.30.

To investigate the detector bandwidth and electrical modulating signal noise limitations of the PAM-4 optical transmission system, the APD was removed from the setup and replaced with a 20 GHz PIN photodiode. Figure 3.32 (a), (b) and (c), display the eye diagrams of the 12.5 Gbaud/s PAM-4 electrical signal output from the AWG and amplified to 2 V_{pp} with the RF amplifier, the resultant PAM-4 optical signal transmitted from the DM SS-FP laser for the 72.5 mA FP laser bias, and the resultant electrical signal output from the 20 GHz PIN photodiode following detection of the PAM-4 optical signal at a received optical power of +3.8 dBm, all captured with the sampling oscilloscope.

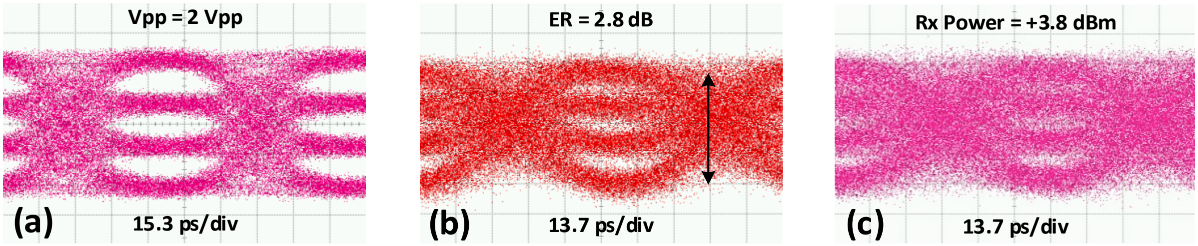

Figure 3.32: Eye diagrams of (a) 12.5 Gbaud/s PAM-4 electrical signal output from the AWG and amplified to 2 V_{pp} with the RF amplifier, (b) PAM-4 optical signal output from the DM SS-FP laser for 72.5 mA FP laser bias, (c) electrical signal output from the 20 GHz PIN photodiode following detection of PAM-4 optical signal at a received optical power of +3.8 dBm.

Figure 3.33 (a), (b) and (c) show the eye diagrams of the 0.5 V_{pp} 12.5 Gbaud/s PAM-4 electrical signal directly from the AWG with no amplification of the electrical signal with the RF amplifier, the resultant PAM-4 optical signal transmitted from the DM SS-FP laser for the 30 mA FP laser bias, and the resultant electrical signal output from the 20 GHz PIN photodiode following detection of the PAM-4 optical signal at a received signal optical power of -0.5 dBm, similarly, all eye diagrams were captured with the sampling scope.

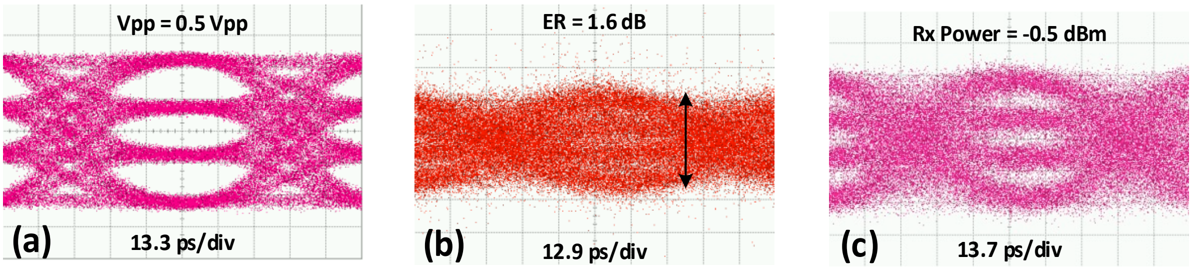

Figure 3.33: Eye diagrams of (a) 0.5 V_{pp} 12.5 Gbaud/s PAM-4 electrical signal direct from the AWG, (b) PAM-4 optical signal output from the DM SS-FP laser for 30 mA FP laser bias, (c) electrical signal output from the 20 GHz PIN photodiode following detection of PAM-4 optical signal at a received optical power of -0.5 dBm.

It is evident from Figure 3.32 (c) and Figure 3.33 (c) that employing a larger bandwidth photodetector for optical signal detection allows for the eye diagrams of the received 12.5 Gbaud/s PAM-4 signals to be captured with the sampling scope. Comparing the eye diagrams of the PAM-4 electrical modulating signals shown in Figure 3.32 (a) and Figure 3.33 (a), it is clear that the RF amplifier distorts the signal output from the AWG and adds considerable noise to the signal when amplifying it from 0.3 to 2 V_{pp}. Figure 3.32 (b) and Figure 3.33 (b) show the eye diagrams of the resultant optical signals transmitted from the DM SS-FP laser with the FP laser biased at 72.5 and 30 mA, respectively. It can be observed that the extinction ratio, ER, of the optical signal transmitted from the DM SS-FP laser for the 72.5 mA FP laser bias is 1.2 dB higher than the ER of the signal transmitted from the DM SS-FP laser for the 30 mA FP laser bias. Furthermore, the Q-factor, Q, of the three eyes of the optical signal transmitted from the DM SS-FP laser for the 72.5 mA FP laser bias is clearly higher than the signal transmitted from the DM SS-FP laser for the 30 mA FP laser bias. The higher ER and Q of the signal transmitted from the DM SS-FP laser for the 72.5 mA FP laser bias would suggest that the b2b transmission performance of the signal would be better than the signal transmitted from the DM SS-FP laser for the 30 mA FP laser bias. However, this is not the case, as demonstrated by the eye diagrams of the received signals detected with the 20 GHz PIN photodiode shown in Figure 3.32 (c) and Figure 3.33 (c).

The eye shown in Figure 3.33 (c), resulting from transmission with the DM SS-FP laser for the 30 mA FP laser bias and the 0.5 V_{pp} modulating signal direct from the AWG, i.e., with no amplification of the modulating signal with the RF amplifier, was captured at a received optical power of -0.5 dBm and exhibits a BER between ~$1x10^{-3}$ and $1x10^{-4}$. However, the eye shown in Figure 3.32 (c), resulting from transmission with the DM SS-FP laser for the 72.5 mA FP laser bias and the 2 V_{pp} signal amplitude, was captured at a received optical power of +3.8 dBm and exhibits a BER between ~$1x10^{-1}$ and $1x10^{-2}$. Thus, the DM SS-FP laser for the 30 mA FP laser bias and 0.5 V_{pp} modulating signal amplitude provides better transmission performance. This may be attributed to the noise in the 2 V_{pp} 12.5 Gbaud/s PAM-4 signal used to directly modulate the SS-FP laser with the FP laser biased at 72.5 mA, which is due to the noise contribution from the RF amplifier employed to increase the amplitude of the signal output from the AWG from 0.3 to 2 V_{pp}. Moreover, the received signal eye diagram shown in Figure 3.33 (c), resulting from optical transmission with the DM SS-FP laser for the 30 mA FP laser bias and the 0.5 V_{pp} signal amplitude, was generated without the use of offline digital processing and adaptive equalisation. This demonstrates that the DM SS-FP laser, for the 30 mA FP laser bias and 0.5 V_{pp} modulating signal amplitude, could produce better transmission performance than that attained with the DM SS-FP laser for the 72.5 mA FP laser bias and 2 V_{pp} modulating signal amplitude, which yielded a minimum BER of $3x10^{-3}$ at a received signal optical power of -7 dBm.

When compared with NRZ-OOK optical transmission, higher signal to noise ratio (SNR) is required for PAM-4 optical transmission to obtain the same performance due to the smaller difference in the amplitude levels of the symbols. Thus, the noise levels of the optical transmission system, which includes the noise of the transmitter and receiver, have a greater negative effect on PAM-4 optical transmission and reception. Consequently, the noise in the electrical drive signal, the RIN of the transmitter [77] and the timing jitter of the transmitted optical signal, all need to be minimised to ensure the optimal performance of IM/DD optical links utilising multilevel PAM signalling.

3.4 Conclusions

This chapter described the development and operation of a self-seeded Fabry-Pérot (SS-FP) laser, and has presented a detailed experimental characterisation of the SS-FP laser prior to an evaluation of its direct modulation transmission performance in a IM/DD test-bed. The SS-FP laser comprises a Fabry-Pérot (FP) laser, with a cavity length of ~240 m, and an external cavity based on a passive circulating fibre loop, which consists of a polarisation controller, a 3-port 3-dB (50:50) coupler, a tunable optical bandpass filter (TBPF) and a 3-port circulator. The optimal FP laser bias currents to operate the SS-FP laser directly modulated with a 12.5 Gbit/s NRZ-OOK signal are 30 and 72.5 mA for modulating signal amplitudes of 0.7 and 2 V_{pp}, respectively. The extinction ratio, ER, ER power penalty, δ_{ER}, and Q-factor, Q, of the signal transmitted from the DM SS-FP laser for the 30 mA FP laser bias and 0.7 V_{pp} modulating signal amplitude, are 3.9, 3.8 and 5.3 dB, respectively. The ER, δ_{ER}, and Q, of the signal transmitted from the DM SS-FP laser for the 72.5 mA FP laser bias and 2 V_{pp} modulating signal amplitude, are 2.8, 5.1 and 7.4 dB, respectively. The 3-dB optical bandwidths of the signals transmitted from the DM SS-FP laser for the 30 mA FP laser bias and 0.7 V_{pp} modulating signal amplitude, and the 72.5 mA FP laser bias and 2 V_{pp} modulating signal amplitude are 8 and 11.8 GHz, respectively.

The averaged RIN of the SS-FP laser is -146.5 dBc/Hz (dc-12 GHz), however, sharp noise peaks occur in the RIN spectrum at low frequencies (dc to ~1.6 GHz), which can be attributed to the beating of the longitudinal external cavity modes of the SS-FP laser. In the evaluation of the different wavelength channels of the SS-FP laser, 12 of the 18 channels of the SS-FP laser directly modulated with a 12.5 Gbit/s NRZ-OOK signal produced error-free b2b transmission performance. Furthermore, the 12 channels of the DM SS-FP laser exhibited only a slight variation in BER performance for b2b transmission, suggesting that the 12 channels exhibit similar levels of RIN. Moreover, the 12 channels of the DM SS-FP laser exhibit optical powers of ~-15.5 dBm, along with SMSRs ranging from 37.2 to 42.53 dB. The wavelength tuning range of the SS-FP laser, in its current form, is limited only by the wavelength range and resolution of the TBPF, and the gain profile and rated operating temperature range of the FP laser. The potential tuning range of future iterations of a practical tunable SS-FP laser was demonstrated to be ~27 nm, which could be achieved through variation of the FP laser device TEC temperature by +/-10^{o}C and would allow for up to 30 wavelength channels to be accessed dynamically and employed for signal transmission. Furthermore, it was shown that up to 36 channels, spanning a wavelength range of ~20 nm, could potentially be exploited for signal transmission by varying the FP laser device TEC temperature by +/-1^{o}C, which would result in a more efficient use of the available spectrum.

Finally, the transmission performance of the directly modulated SS-FP laser is evaluated in an IM/DD test-bed with two different intensity modulation (IM) formats. First, the SS-FP is directly modulated with a 12.5 Gbit/s NRZ-OOK signal and error-free transmission over 25 km of SSMF at a received optical power of -10.5 dBm is demonstrated with the SS-FP laser channel at 1553.1 nm for the 30 mA FP laser bias. The transmission performances of 3 additional channels of the SS-FP laser directly modulated with the 12.5 Gbit/s NRZ-OOK signal are then evaluated for transmission over 25 km of SSMF and error-free transmission is demonstrated with all 3 channels. Furthermore, the 4 channels of the SS-FP laser are shown to exhibit virtually no variability in transmission performance. The SS-FP laser is then directly modulated with a 12.5 Gbaud/s (25 Gbit/s) PAM-4 signal and the transmission performance for b2b transmission in an IM/DD test-bed is evaluated. The PAM-4 signal transmission experiments were performed with the DM SS-FP laser for an FP laser bias of 72.5 mA, as the 72.5 mA FP laser bias produced the highest, measureable, PAM-4 transmitted optical signal extinction ratio, ER, and Q-factor, Q. For b2b transmission, and with the aid of channel equalisation, the directly modulated SS-FP laser is shown to perform below the 7% FEC limit at a received power of -7 dBm.

The experimental results presented in this chapter clearly demonstrates that the proposed SS-FP laser, with the necessary and appropriate modifications and optimisation to increase the ER and reduce the beating among the external cavity modes of the SS-FP laser, has the potential to be employed as a directly modulated tunable laser source (TLS) for 12.5 Gbit/s NRZ-OOK and 25 Gbit/s PAM-4 optical signal transmission in NG-PON2 or future optical access networks employing WDM.

References

[1] ITU-T Telecommunication Standardization Sector of ITU: 40-Gigabit-capable passive optical networks 2 (NG PON2): Physical media dependent (PMD) layer specification, Corrigendum 1. Recommendation ITU-T G.989.2 (08/2019) – Corrigendum 1.

[2] S. Sakano, T. Tsuchiya, M. Suzuki, S. Kitajima and N. Chinone, "Tunable DFB laser with a striped thin-film heater," in IEEE Photonics Technology Letters, vol. 4, no. 4, pp. 321-323, April 1992, doi: 10.1109/68.127200.

[3] A. Gatto, P. Parolari, C. Neumeyr and P. Boffi, "Beyond 25 Gb/s Directly-Modulated Widely Tunable VCSEL for Next Generation Access Network," 2018 Optical Fiber Communications Conference and Exposition (OFC), San Diego, CA, 2018, pp. 1-3.

[4] P. Parolari, A. Gatto and P. Boffi, "Long Wavelength VCSELs Exploitation for Low-Cost and Low-Power Consumption Metro and Access Networks," 2018 20th International Conference on Transparent Optical Networks (ICTON), Bucharest, 2018, pp. 1-4.

[5] L. Yu et al., "A Widely Tunable Directly Modulated DBR Laser With High Linearity," in IEEE Photonics Journal, vol. 6, no. 4, pp. 1-8, Aug. 2014, Art no. 1501308.

[6] D.-B. Zhou et al., "Widely Tunable Two-Section Directly Modulated DBR Lasers for TWDM-PON System," Chinese Physics Letters, Volume 34, Number 3, 2017.

[7] L. Ponnampalam, C. C. Renaud, R. Cush, R. Turner, M. J. Wale and A. J. Seeds, "Simplified wavelength control of uncooled widely tuneable DSDBR laser for optical access networks," 39th European Conference and Exhibition on Optical Communication (ECOC 2013), London, 2013, pp. 1-3, doi: 10.1049/cp.2013.1677.

[8] A. Ramaswamy et al., "Optical transceivers using heterogeneous integration," 2015 International Conference on Photonics in Switching (PS), Florence, Italy, 2015, pp. 315-317, doi: 10.1109/PS.2015.7329038.

[9] D. Nesset, "NG-PON2 Technology and Standards," in Journal of Lightwave Technology, vol. 33, no. 5, pp. 1136-1143, 1 March1, 2015, doi: 10.1109/JLT.2015.2389115.

[10] K. Iwashita and K. Nakagawa, "Suppression of mode partition noise by laser diode light injection," in IEEE Journal of Quantum Electronics, vol. 18, no. 10, pp. 1669-1674, October 1982, doi: 10.1109/JQE.1982.1071415.

[11] M. Zhu, S. Xiao, M. Bi, H. Chen, and W. Hu, "Cost-effective tunable fibre laser based on self-seeded Fabry-Perot laser diode using a Sagnac loop reflector," Chin. Opt. Lett. 8, 1150-1151 (2010).

[12] Sang-Mook Lee, Ki-Man Choi, Sil-Gu Mun, Jung-Hyung Moon and Chang-Hee Lee, " Dense WDM-PON Based on Wavelength-Locked Fabry–Pérot Laser Diodes," in IEEE Photonics Technology Letters, vol. 17, no. 7, pp. 1579-1581, July 2005, doi: 10.1109/LPT.2005.848558.

[13] R. Hui, "Introduction to Fibre-Optic Communications," 1st Edition, Academic Press, 2019.

[14] K. Petermann, “Laser Diode Modulation and Noise”, Kluwer, 1988.

[15] G. P. Agrawal, P. J. Anthony and T. M. Shen, "Dispersion penalty for 1.3 mu m lightwave systems with multimode semiconductor lasers," in Journal of Lightwave Technology, vol. 6, no. 5, pp. 620-625, May 1988, doi: 10.1109/50.4046.

[16] S. Bottacchi, “Noise and Signal Interference in Optical Fibre Transmission Systems”, John Wiley and Sons, 2008.

[17] Q. Guo, L. Deng, J. Mu, X. Li, and W.-P. Huang, "Investigation of mode partition noise in Fabry-Perot laser diode,” Proc. SPIE 9288, Photonics North 2014, 928816 (25 September 2014); https://doi.org/10.1117/12.2075233

[18] J. Fu, Y. Xi, X. Li and W. Huang, "Narrow Spectral Width FP Lasers for High-Speed Short-Reach Applications," in Journal of Lightwave Technology, vol. 34, no. 21, pp. 4898-4906, 1 Nov.1, 2016, doi: 10.1109/JLT.2016.2602225.

[19] L. A. Coldren, S. W. Corzine and M. L. Mashanovitch, “Diode Lasers and Photonic Integrated Circuits,” 2nd Edition (Wiley Series in Microwave and Optical Engineering), New York, NY, USA: Wiley, 2012.

[20] K. Ogawa, "Analysis of mode partition noise in laser transmission systems," in IEEE Journal of Quantum Electronics, vol. 18, no. 5, pp. 849-855, May 1982, doi: 10.1109/JQE.1982.1071617.

[21] K. Ogawa and R. Vodhanel, "Measurements of mode partition noise of laser diodes," in IEEE Journal of Quantum Electronics, vol. 18, no. 7, pp. 1090-1093, July 1982.

[22] K. Ogawa, “Semiconductor laser noise: Mode partition noise,” in Semiconductors and Semimetals, Vol. 22, W. T. Tsang, Ed. New York: Academic, 1985, ch. 8.

[23] B. Hellström (1985), “Analysis of Mode Partition Noise in Optical Fibre Line Systems”, Journal of Optical Communications, 6(4), 132-136. doi: https://doi.org/10.1515/JOC.1985.6.4.132.

[24] P. Anandarajah, M. Rensing, and L. P. Barry, "Signal degradation due to output filtering of self-seeded gain-switched pulses exhibiting weak inherent side-mode-suppression ratios," Appl. Opt. 44, 7867-7871, 2005.

[25] Y. Okano, K. Nakagawa and T. Ito, "Laser Mode Partition Noise Evaluation for Optical Fibre Transmission," in IEEE Transactions on Communications, vol. 28, no. 2, pp. 238-243, February 1980, doi: 10.1109/TCOM.1980.1094649.

[26] M. Ramadan, "Parameters affecting mode partition noise in laser transmission systems," 1989 IEEE Global Telecommunications Conference and Exhibition 'Communications Technology for the 1990s and Beyond', Dallas, TX, USA, 1989, pp. 692-695 vol.2.

[27] R. Heidemann, "Investigations on the dominant dispersion penalties occurring in multigigabit direct detection systems," in Journal of Lightwave Technology, vol. 6, no. 11, pp. 1693-1697, Nov. 1988, doi: 10.1109/50.9986.

[28] R. H. Wentworth, G. E. Bodeep and T. E. Darcie, "Laser mode partition noise in lightwave systems using dispersive optical fibre," in Journal of Lightwave Technology, vol. 10, no. 1, pp. 84-89, Jan. 1992, doi: 10.1109/50.108741.

[29] M. Ohtsu, Y. Teramachi and T. Miyazaki, "Mode stability analysis of nearly single-longitudinal-mode semiconductor lasers," in IEEE Journal of Quantum Electronics, vol. 24, no. 5, pp. 716-723, May 1988, doi: 10.1109/3.187.

[30] M. Ohtsu and Y. Teramachi, "Analyses of mode partition and mode hopping in semiconductor lasers," in IEEE Journal of Quantum Electronics, vol. 25, no. 1, pp. 31-38, Jan. 1989, doi: 10.1109/3.16237.

[31] P. J. Herre and U. Barabas, "Mode switching of Fabry-Perot laser diodes," in IEEE Journal of Quantum Electronics, vol. 25, no. 8, pp. 1794-1799, Aug. 1989, doi: 10.1109/3.34037.

[32] L.Y. Chan, C.K. Chan, F. Tong, D.T.K. Tong, L.K. Chen, "Upstream traffic transmitter using injection-locked Fabry-Perot laser diode as modulator for WDM access networks," Electronics Letters, Volume 38, Issue 1, 3 January 2002.

[33] Z. Xu, Y. J. Wen, C. J. Chae, Y. Wang, and C. Lu, “10 Gb/s WDM-PON upstream transmission using injection- locked Fabry-Perot laser diodes,” in OFC06, JThB72 (2006).

[34] H. D. Kim, S.-G. Kang, and C. H. Lee, “A low-cost WDM source with an ASE injected Fabry-Perot semiconductor laser,” IEEE Photon. Technol. Lett. 12, 1067-1069 (2000).

[35] M. Presi, A. Chiuchiarelli, and E. Ciaramella, “Polarization independent self-seeding of Fabry-Peròt laser diodes for WDM-PONs,” in OFC/NFOEC, pp. 1-3, Mar. 2012.

[36] Y.C. Su, Y. C. Chi and G. R. Lin, “A Remote-free Self-feedback Colorless FPLD with FBG Based Single-mode Filter for Multi-channel 2.5 Gbit/s DWDM-PON,” JTu4A.57, CLEO 2014.

[37] M.M. Krstic, D.M. Gvozdić, "Side-Mode-Suppression-Ratio of Injection-Locked Fabry-Perot Lasers," Acta Physica Polonica A. 116. 664-, 2009, 10.12693/APhysPolA.116.664.

[38] K. Shortiss, M. Shayesteh, W. Cotter, A.H. Perrott, M. Dernaika, and F.H. Peters, "Mode Suppression in Injection Locked Multi-Mode and Single-Mode Lasers for Optical Demultiplexing," Photonics 6, no. 1: 27, 2019, https://doi.org/10.3390/photonics6010027.

[39] C. H. Yeh, F. Y. Shih, C. H. Wang, C. W. Chow, and S. Chi, "Cost-effective wavelength-tunable fibre laser using self-seeding Fabry-Perot laser diode," Opt. Express 16, 435-439 (2008).

[40] S. Hann, D. S. Moon, Y. Chung and C. S. Park, "Upstream signal transmission using a self-injection locked Fabry-Perot laser diode for WDM-PON," Optical Engineering 44(6), 060509 (1 June 2005). https://doi.org/10.1117/1.1920069.

[41] F. Y. Shih, C. H. Yeh, C. W. Chow, C. H. Wang, and S. Chi, “Utilization of self-injection Fabry–Perot laser diode for long-reach WDM-PON,” Opt. FiberTechnol., vol. 16, no. 1, pp. 46–49, 2010.

[42] M. Schell, D. Huhse, W. Utz, J. Kaessner, D. Bimberg and I. S. Tarasov, "Jitter and dynamics of self-seeded Fabry-Perot laser diodes," in IEEE Journal of Selected Topics in Quantum Electronics, vol. 1, no. 2, pp. 528-534, June 1995, doi: 10.1109/2944.401238.

[43] D. Huhse, M. Schell, W. Utz, J. Kaessner and D. Bimberg, "Dynamics of single-mode formation in self-seeded Fabry-Perot laser diodes," in IEEE Photonics Technology Letters, vol. 7, no. 4, pp. 351-353, April 1995, doi: 10.1109/68.376799.

[44] K. Petermann, "External optical feedback phenomena in semiconductor lasers," in IEEE Journal of Selected Topics in Quantum Electronics, vol. 1, no. 2, pp. 480-489, June 1995.

[45] P. Besnard, B. Meziane and G. M. Stephan, "Feedback phenomena in a semiconductor laser induced by distant reflectors," in IEEE Journal of Quantum Electronics, vol. 29, no. 5, pp. 1271-1284, May 1993, doi: 10.1109/3.236141.

[46] W. Liang, V. Ilchenko, D. Eliyahu et al., “Ultralow noise miniature external cavity semiconductor laser,” Nat Commun 6, 7371 (2015). https://doi.org/10.1038/ncomms8371.

[47] J. Connie, C. Hasnain and Z. Xiaoxue, "Ultrahigh-speed laser modulation by injection locking," in Optical Fibre Telecommunications VB: Components and Subsystems, I. P. Kaminow, T. Li, and A. E. Willner, eds. (Academic Press, Oxford, 2008), pp. 145-182.

[48] R. Tkach, A. Chraplyvy, "Regimes of feedback effects in 1.5-µm distributed feedback lasers," in Journal of Lightwave Technology, vol. 4, no. 11, pp. 1655-1661, November 1986, doi: 10.1109/JLT.1986.1074666.

[49] C. Henry, "Theory of the linewidth of semiconductor lasers," in IEEE Journal of Quantum Electronics, vol. 18, no. 2, pp. 259-264, February 1982, doi: 10.1109/JQE.1982.1071522.

[50] M. Ahmed, M. Yamada and M. Saito, "Numerical modeling of intensity and phase noise in semiconductor lasers," in IEEE Journal of Quantum Electronics, vol. 37, no. 12, pp. 1600-1610, Dec. 2001, doi: 10.1109/3.970907.

[51] D. Derickson, J. Vobis, L. Stokes, P. Hernday, V. McOmber, D.M. Barney, W. V. Sorin, J. Beller, C.M. Miller, S.W. Hinch and C. Hentschel, “Fibre Optic Test and Measurement”, Nova Jersey: Prentice Hall PTR, 1998.

[52] C. M. Miller, "Intensity modulation and noise characterization of high-speed semiconductor lasers," in IEEE LTS, vol. 2, no. 2, pp. 44-50, May 1991, doi: 10.1109/80.93288.

[53] Eagleyard-Photonics, “Relative Intensity Noise of Distributed Feedback Lasers,” Available On-line: https://www.toptica-eagleyard.com/fileadmin/downloads/documents/eyP_App_Note_RIN__1-6.pdf

[54] IEEE Standard for Ethernet," in IEEE Std 802.3-2018 (Revision of IEEE Std 802.3-2015), vol., no., pp.1-5600, 31 Aug. 2018, doi: 10.1109/IEEESTD.2018.8457469.

[55] IEEE Standard for Ethernet Amendment 9: Physical Layer Specifications and Management Parameters for 25 Gb/s and 50 Gb/s Passive Optical Networks," in IEEE Std 802.3ca-2020, vol., no., pp.1-267, 3 July 2020, doi: 10.1109/IEEESTD.2020.9135000.

[56] R. Lang and K. Kobayashi, "External optical feedback effects on semiconductor injection laser properties," in IEEE Journal of Quantum Electronics, vol. 16, no. 3, pp. 347-355, March 1980, doi: 10.1109/JQE.1980.1070479.

[57] B. Tromborg, J. Osmundsen and H. Olesen, "Stability analysis for a semiconductor laser in an external cavity," in IEEE Journal of Quantum Electronics, vol. 20, no. 9, pp. 1023-1032, September 1984, doi: 10.1109/JQE.1984.1072508.

[58] H. Sato, T. Fujita and K. Fujito, "Intensity fluctuation in semiconductor lasers coupled to external cavity," in IEEE Journal of Quantum Electronics, vol. 21, no. 1, pp. 46-51, January 1985, doi: 10.1109/JQE.1985.1072526.

[59] J. Mork and B. Tromborg, "The mechanism of mode selection for an external cavity laser," in IEEE Photonics Technology Letters, vol. 2, no. 1, pp. 21-23, Jan. 1990, doi: 10.1109/68.47029.

[60] J. Mork, M. Semkow and B. Tromborg, "Measurement and theory of mode hopping in external cavity lasers," in Electronics Letters, vol. 26, no. 9, pp. 609-610, 26 April 1990.

[61] D. Lenstra, “Statistical theory of the multistable external-feedback laser,” Opt. Commun., vol. 81, pp. 209-214, 1991.

[62] A. T. Ryan, G. P. Agrawal, G. R. Gray and E. C. Gage, "Optical-feedback-induced chaos and its control in multimode semiconductor lasers," in IEEE Journal of Quantum Electronics, vol. 30, no. 3, pp. 668-679, March 1994, doi: 10.1109/3.286153.

[63] Y. Kitaoka, H. Sato, K. Mizuuchi, K. Yamamoto and M. Kato, "Intensity noise of laser diodes with optical feedback," in IEEE Journal of Quantum Electronics, vol. 32, no. 5, pp. 822-828, May 1996, doi: 10.1109/3.493006.

[64] K. I. Kallimani and M. J. O'Mahony, "Relative intensity noise for laser diodes with arbitrary amounts of optical feedback," in IEEE Journal of Quantum Electronics, vol. 34, no. 8, pp. 1438-1446, Aug. 1998, doi: 10.1109/3.704337.

[65] S. G. Abdulrhmann, M. Ahmed, T. Okamoto, W. Ishimori and M. Yamada, "An improved analysis of semiconductor laser dynamics under strong optical feedback," in IEEE Journal of Selected Topics in Quantum Electronics, vol. 9, no. 5, pp. 1265-1274, Sept.-Oct. 2003.

[66] J. Poette, O. Vaudel, & P. Besnard, "Relative Intensity Noise of an injected semiconductor laser," Proceedings of SPIE - The International Society for Optical Engineering, 2006, 6054. 10.1117/12.660527.

[67] S. M. S. Imran, M. Yamada and Y. Kuwamura, "Theoretical Analysis of the Optical Feedback Noise Based on Multimode Model of Semiconductor Lasers," in IEEE Journal of Quantum Electronics, vol. 48, no. 4, pp. 521-527, April 2012, doi: 10.1109/JQE.2012.2186790.

[68] J. H. Lim, J. H. Song, R. K. Kim, K. S. Lee and J. R. Kim, "External cavity laser with high-sidemode suppression ratio using grating-assisted directional coupler," in IEEE Photonics Technology Letters, vol. 17, no. 11, pp. 2430-2432, Nov. 2005.

[69] H.-C. Kwon, S.-K. Han, “Performance analysis of a wavelength-locked Fabry-Perot laser diode by light injection of an external spectrally sliced Fabry-Perot laser diode,” Applied optics, 45, (2006), 6175-9. 10.1364/AO.45.006175.

[70] J. Sun, L. Huang, "Single-longitudinal-mode fibre ring laser using internal lasing injection and self-injection feedback," Opt. Eng. 46(7) 074201 (1 July 2007).

[71] M. Presi, A. Chiuchiarelli, R. Corsini and E. Ciaramella, "Self-seeding of semiconductor lasers for next-generation WDM Passive Optical Networks," 2013 15th International Conference on Transparent Optical Networks (ICTON), Cartagena, 2013, pp. 1-4.

[72] F. Wei, F. Yang, X. Zhang, D. Xu, M. Ding, L. Zhang, D. Chen, H. Cai, Z. Fang, and G. Xijia, "Subkilohertz linewidth reduction of a DFB diode laser using self-injection locking with a fibre Bragg grating Fabry-Perot cavity," Opt. Express 24, 17406-17415 (2016).

[73] K. Szczerba et al., "4-PAM for high-speed short-range optical communications," in IEEE/OSA Journal of Optical Communications and Networking, vol. 4, no. 11, pp. 885-894, Nov. 2012, doi: 10.1364/JOCN.4.000885.

[74] N. Benvenuto and G. Cherubini, ”Algorithms for Communications Systems and Their Applications”. Wiley, 2002.

[75] E. Agrell, J. Lassing, E. G. Strom and T. Ottosson, "On the optimality of the binary reflected Gray code," in IEEE Transactions on Information Theory, vol. 50, no. 12, pp. 3170-3182, Dec. 2004, doi: 10.1109/TIT.2004.838367.

[76] N. Eiselt et al., "Evaluation of Real-Time 8 × 56.25 Gb/s (400G) PAM-4 for Inter-Data Center Application Over 80 km of SSMF at 1550 nm," in Journal of Lightwave Technology, vol. 35, no. 4, pp. 955-962, 15 Feb.15, 2017, doi: 10.1109/JLT.2016.2617283.

[77] V. Vujicic, “Mitigation of relative intensity noise of quantum dash mode-locked lasers for PAM4 based optical interconnects using encoding techniques,” Opt. Express, vol. 25, pp. 20-29, 2017.

Chapter 4 Final Conclusions and Future Work

4.1 Final Conclusion

The principal challenge in realising NG-PON2 and future optical access networks utilising wavelength division multiplexing (WDM) technology is the development of innovative tunable laser technologies aimed at mass deployment in subscriber ONUs. Due to the highly cost-sensitive nature of the access domain, directly modulated tunable lasers are the ideal solution. However, the transmission distances (~15 km) and data rates (10 Gbit/s) achievable with directly modulated lasers (DMLs) are inhibited by the intrinsic frequency chirp of the devices and the interplay of the chirp with the chromatic dispersion (CD) in optical fibre. The directly modulated tunable lasers that have been identified thus far as being the most suitable to NG-PON2 are thermally tunable DFB lasers and DBR lasers without active cooling. However, the former are limited in their tuning range (~4nm) and the latter are still considered to be too expensive for access networks.

In this thesis, an in-depth experimental investigation of a directly modulated DFB laser (DML) and an electro-absorption modulated laser (EML) has been presented, with a special focus on the frequency chirp of both transmitters and the effects of the chirp on the transmission performance. Furthermore, an extensive experimental development and investigation of a self-seeded Fabry-Pérot (SS-FP) Laser has been presented, along with an examination of the transmission performance of the SS-FP laser in IM/DD transmission systems. The main results are outlined below.

In Chapter 2, the characteristics and transmission performances of a directly modulated MQW DFB laser (DML) and an electo-absorption modulated laser (EML) have been demonstrated. Error-free 12.5 Gbit/s NRZ-OOK optical signal transmission was achieved with the DML and EML for transmission over 25 and 50 km of SSMF. Although the ER of the optical signal transmitted from the DML modulated near threshold was 12.6 dB, which was 2.3 dB higher than the signal transmitted from the EML, a receiver sensitivity of -16 dBm was attained with the EML for 25 km SSMF transmission, which was 3 dB higher than the receiver sensitivity attained with the DML. This can be attributed to the transient chirp of the optical signal transmitted from the DML modulated near threshold. Considering that transmission over 25 km of SSMF was attained with the DML modulated near threshold, indicated that the MQW DFB laser was highly damped and exhibited a relatively low linewidth enhancement factor or alpha parameter, α, value. Error-free 12.5 Gbit/s NRZ-OOK optical transmission was also achieved with the DML and the EML for transmission over 50 km of SSMF and a receiver sensitivity of -13.5 dBm was attained with both the DML and EML. Transmission over 50 km of SSMF was achieved with the

DML only when it was modulated well above threshold and was not possible with the DML modulated near threshold, as the received signal was too distorted due to the dispersive pulse broadening and ISI resulting from the interplay of the transient chirp dominated signal and the chromatic dispersion in the optical fibre. Moreover, a 1 dB improvement in receiver sensitivity was attained for transmission over 50 km of SSMF with the DML modulated well above threshold when compared to transmission over 25 km SSMF with the DML modulated near threshold. From numerical modelling of the DML, the alpha parameter, α, and gain compression factor, ϵ, of the DML were estimated to be 1.6 and 10x10^{-23} m^3, respectively. From the numerical model of the EML, the estimated alpha parameter, α_{EAM}, values ranged from 0.8 to -0.8.

When modulated well above threshold, the 3-dB bandwidth of the spectrum of the optical signal transmitted from the DML was 6.6 GHz and the upper side-band (UPS) was partially supressed, which suggested mixed frequency and amplitude modulation (FM and AM) of the DML modulated well above threshold with the 2 V_{pp} 12.5 Gbit/s NRZ-OOK signal. The enhanced transmission performance of the DML, which allowed error-free transmission over 50 km of SSMF to be achieved without the use of electronic or optical dispersion compensation, may be attributed, in part, to the mixed FM and AM of the DML, as it enabled the minimum shift keying (MSK) condition to be established. The MSK condition of the DML, coupled with the favourable interaction of the adiabatic chirp dominated optical signal transmitted from the DML modulated well above threshold with the chromatic dispersion in the SSMF over the 50 km distance, resulted in FM to AM conversion of the optical signal and in an open received signal eye diagram and error-free signal transmission. However, the ER of the signal transmitted from the DML modulated well above threshold, which achieved error-free transmission over 50 km of SSMF, was 2.7 dB, which would preclude the use of the DFB laser in NG-PON2.

In Chapter 3 of this thesis, the development and operation of a self-seeded Fabry-Pérot (SS-FP) laser has been presented. Furthermore, an extensive experimental characterisation of the SS-FP laser, along with an evaluation of the transmission performance of the directly modulated SS-FP laser in an IM/DD test-bed, was demonstrated. Through large-signal modulation analysis of the SS-FP laser, two FP laser bias currents of 30 and 72.5 mA were found to produce the best b2b transmission performance with the SS-FP laser when directly modulated with the 12.5 Gbit/s NRZ-OOK signal using 0.7 and 2 V_{pp} signal amplitudes, respectively. The extinction ratio, ER, power penalty, δ_{ER}, and Q-factor, Q, of the signal transmitted from the directly modulated (DM) SS-FP laser for the 30 mA FP laser bias and 0.7 V_{pp} modulating signal amplitude, were 3.9, 3.8 and 5.3 dB, respectively. The ER, δ_{ER}, and Q, of the signal transmitted from the DM SS-FP laser for the 72.5 mA FP laser bias and the 2 V_{pp} modulating signal amplitude, were 2.8, 5.1 and 7.4 dB, respectively. The 3-dB optical bandwidths of the signals transmitted from the DM SS-FP laser for the 30 mA FP laser bias and 0.7 V_{pp} modulating signal amplitude, and the 72.5 mA FP laser bias and 2 V_{pp} modulating signal amplitude, were ~8 and 11.8 GHz, respectively. Through self-seeding, the 3-dB optical bandwidth, Δv_{3dB}, of the signal transmitted from the DM SS-FP laser for the 72.5 mA mA FP laser bias reduced by ~1 GHz, when compared with the DM free-running FP laser spectrum. The 3-dB optical bandwidth, Δv_{3dB}, of the signal transmitted from the DM SS-FP laser for the 30 mA mA FP laser bias was similar to the 3-dB optical bandwidth of the signal transmitted from the DM free-running FP laser when biased at 30 mA.

When the FP laser was biased at 30 mA, the averaged RIN of the SS-FP laser mode at 1553.14 nm was -146.5 dBc/Hz (dc-12 GHz). However, sharp noise peaks were observed in the RIN spectrum at low frequencies (dc to ~1.6 GHz), and this low frequency RIN can be attributed to the presence of the longitudinal modes that form within the external cavity of the SS-FP laser. When the FP laser was biased at 30 mA and directly modulated with the 0.7 V_{pp} 12.5 Gbit/s NRZ-OOK signal, 12 self-seeded modes or wavelengths channels of the SS-FP laser produced error-free b2b transmission performance and it may be inferred that the different channels exhibited similar RIN considering that there was only slight variation in the BER performance of the 12 channels for b2b transmission. Furthermore, the 12 channels exhibited similar peak optical powers (~-15.5 dBm) and SMSR (~40 dB) when the FP laser was directly modulated. The potential wavelength tuning range of future iterations of a practical tunable SS-FP laser could be up to ~27 nm, depending on the mechanism employed for filtering the single longitudinal mode from the MLM spectrum of the free-running FP laser before reinjection of the filtered mode back into the FP laser cavity.

Error-free 12.5 Gbit/s NRZ-OOK optical signal transmission over 25 km of SSMF in an IM/DD test-bed was experimentally demonstrated with the SS-FP laser under direct modulation. Of the 12 channels that produced error-free b2b transmission with the directly modulated SS-FP laser for the 30 mA FP laser bias, 4 were evaluated for transmission over 25 km of SSMF and all channels produced similar BER performance and receiver sensitivities (-10.5 dBm). When directly modulated with a 12.5 Gbaud/s PAM-4 signal, the SS-FP laser performed below the 7% FEC limit at a received optical power of -7 dBm for b2b transmission, with the aid of channel equalisation. However, the PAM-4 optical transmission experiments were carried out with the SS-FP laser for the 72.5 mA FP laser bias and a 2 V_{pp} modulating signal amplitude which had been amplified with an RF amplifier. It was further demonstrated that the SS-FP laser for the 30 mA FP laser bias and directly modulated with the 0.5 V_{pp} 12.5 Gbaud/s PAM-4 signal could potentially produce better b2b transmission performance than the SS-FP laser when the 72.5 mA FP laser bias and the amplified 2 V_{pp} modulating signal is employed.

The development and investigation presented in this thesis has successfully demonstrated that simple DFB lasers, with appropriate optimisation, can be employed for optical signal transmission beyond the dispersion limited distances typically attained with DMLs, without any optical or electrical dispersion compensation. Furthermore, a self-seeded Fabry-Pérot (SS-FP) laser, has the potential to be utilised as a cost-effective directly modulated (DM) tunable laser source (TLS) for 12.5 Gbit/s NRZ-OOK and 25 Gbit/s PAM-4 optical signal transmission in NG-PON2 or future optical access networks employing WDM technology.

4.2 Future Work

The research in this thesis has shown the potential of simple directly modulated DFB lasers for long-reach PONs and the self-seeded Fabry-Pérot (SS-FP) laser as a cost-effective tunable laser source for subscriber ONUs in NG-PON2. Potential future work in need of further investigation is now described:

- As discussed in Chapter 2, the 2.7 dB extinction ratio, ER, of the signal transmitted from the MQW DFB laser (DML) modulated well above threshold, which achieved error-free transmission over 50 km of SSMF at a receiver sensitivity of -13.5 dBm without the use of optical or electronic dispersion compensation, would preclude the DML from NG-PON2, as a minimum ER of 6 dB is specified for NG-PON2 transmitters [1]. Future work would see the application of an optical filtering technique to increase the ER of the signal transmitted from the DML modulated well above threshold, while maintaining the adiabatic chirp properties of the signal, thus, enabling the enhanced transmission performance and extended transmission distance of the DML. A narrow optical filter could be used to selectively suppress the adiabatically chirped, or the red- or blue-shifted, “high” or “low” bit or symbol levels of the signal waveform, hence, increasing the intensity level separation. Alignment of the filter such that the linear region of the rising or falling edge of the filter is overlapped with the signal, results in the bit or symbol levels of the two- or multi-level constellation are attenuated, while the original relative level spacing is maintained [2]. The degree to which the ER of the optical signal transmitted from the DML is increased is the difference of the filter insertion-loss between the “high” and “low” symbols of the constellation, where the gain in the ER attained in the output signal is determined by the slope of the filter edge and the magnitude of the adiabatic chirp. In a previous study [3], the filter slope was aligned such that the attenuation introduced enhanced the ER of the signal by attenuating the “low” or “0” levels of the NRZ-OOK transmitted optical signal waveform. Thus, through optical filtering of the adiabatically chirped signal transmitted from the DML, the ER of the transmitted signal can be increased from 2.7 dB to >6 dB, while the dispersion tolerance and the extended transmission distance in the C-band is maintained.

An array of DFB lasers exhibiting similar device parameters (α, ϵ... etc.) and chirp properties, each with a narrowband optical filter, could be employed to demonstrate a directly modulated (DM) tunable chirped managed laser (CML) source. Moreover, the DFB lasers could be thermally tuned to realise a multichannel and wideband directly modulated (DM) tunable laser source (TLS). Both 12.5 Gbit/s NRZ-OOK and 25 Gbit/s PAM-4 formats could be employed with the DM tunable CML, which could produce aggregate line rates of 40 to 100 Gbit/s in the C-band, assuming 4x DFB lasers are utilised, and cover transmission distances of up to 50 km in SSMF. Regarding direct modulation of the chirp-managed DFB laser with the PAM-4 format, the optical filter could also be employed to counteract the eye diagram skewing resulting from direct modulation of the DFB laser, which would pre-compensate the transmitted signal, thus, mitigating the eye diagram skewing due to the effect of the CD in the optical fibre.

- In Chapter 3, a self-seeding Fabry-Pérot (SS-FP) laser has been developed and characterised and, furthermore, error-free 12.5 Gbit/s NRZ-OOK optical signal transmission over 25 km of SSMF has been demonstrated with the directly modulated (DM) SS-FP laser. Future work would see the use of a programmable tunable optical bandpass filter (TBPF) to evaluate the practical wavelength tunability of the directly modulated SS-FP laser. The switching time between wavelength channels and switch latency could be assessed, and the performance and wavelength drift of the SS-FP laser during burst mode operation could be investigated. Moreover, the length of the external cavity (EC) of the SS-FP laser, which, in its current form, is estimated to be ~10 m, could be reduced and the SSMF used in the EC could be replaced with polarisation maintaining (PM) fibre. Considering the inverse correlation between the FSR and the EC length, this would increase the separation, or FSR, between the external cavity modes and, moreover, would reduce the variation in the phase and optical power of the seed signal. It is envisioned that the combination of the reduction in the path length of the external cavity and the increased stability of the reinjected seed signal would reduce the beating of the longitudinal external cavity modes of the SS-FP laserand, consequently, reduce the low frequency (1/f) noise of the laser. This could be done initially using a custom built PM fibre planar optical waveguide assembly, exhibiting the shortest EC path length achieveable with optical fibre assemblies.

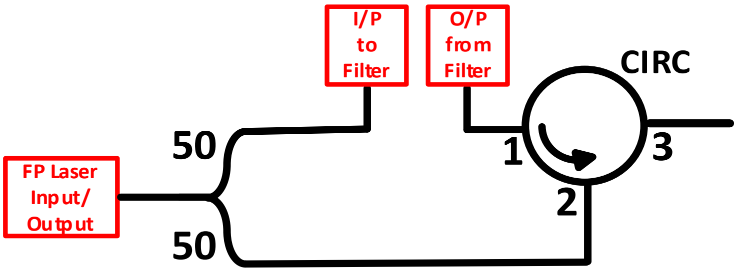

Figure 4.1: Schematic of custom built PM fibre planar optical waveguide assembly.

A schematic of the proposed optical waveguide assembly is shown in Figure 4.1. The logical next step is then the monolithic integration of the FP laser and the external cavity or optical waveguide, shown in Figure 4.1, in a single chip to be employed in next generation optical transmitters [4], [5]. The device could also include an electro-absorption modulator (EAM) and a semiconductor optical amplifier (SOA) to enable external modulation of the SS-FP laser, in order to increase the data rates and extend the transmission distances achieveable with the transmitter. Future design iterations of the SS-FP laser could also look to monolithically integrating the tunable filter on the same chip [6], [7].

References

[1] ITU-T Telecommunication Standardization Sector of ITU: 40-Gigabit-capable passive optical networks 2 (NG PON2): Physical media dependent (PMD) layer specification, Corrigendum 1. Recommendation ITU-T G.989.2 (08/2019) – Corrigendum 1.

[2] L.-S. Yan, Y. Wang, B. Zhang, C. Yu, J. McGeehan, L. Paraschis, and A. E. Willner, "Reach extension in 10-Gb/s directly modulated transmission systems using asymmetric and narrowband optical filtering," Opt. Express 13, 5106-5115 (2005).

[3] D. Mahgerefteh, Y. Matsui, X. Zheng and K. McCallion, "Chirp Managed Laser and Applications," in IEEE Journal of Selected Topics in Quantum Electronics, vol. 16, no. 5, pp. 1126-1139, Sept.-Oct. 2010, doi: 10.1109/JSTQE.2009.2037336.

[4] Y. Li, Y. Zhang, H. Chen, S. Yang and M. Chen, "Tunable Self-Injected Fabry–Perot Laser Diode Coupled to an External High-Q Si3N4 /SiO2 Microring Resonator," in Journal of Lightwave Technology, vol. 36, no. 16, pp. 3269-3274, 15 Aug.15, 2018, doi: 10.1109/JLT.2018.2838325.

[5] Z. Gao, X. Sun, and K. Zhang, "A wavelength tunable ONU transmitter based on multi-mode Fabry-Perot laser and micro-ring resonator for bandwidth symmetric TWDM-PON," Proc. SPIE 9772, Broadband Access Communication Technologies X, 97720S (12 February 2016).

[6] W. Zhang and J. Yao, "A silicon photonic integrated frequency-tunable microwave photonic bandpass filter," 2017 International Topical Meeting on Microwave Photonics (MWP), Beijing, China, 2017, pp. 1-4, doi: 10.1109/MWP.2017.8168635.

[7] Y. Liu, A. Choudhary, D. Marpaung, and B. J. Eggleton, "Integrated microwave photonic filters," Adv. Opt. Photon. 12, 485-555 (2020).

Appendix A

A.1 Single-mode Laser Rate Equations

Single-mode semiconductor laser dynamics and operating characteristics can be described with a set of coupled ordinary differential equations, or rate equations, which govern the recombination effects of the carriers, and the dynamics of the photons and carriers, within the laser cavity. The single-mode laser rate equations, describing the time evolution of, and the interaction between, the carrier density N, the photon density S, and the optical phase ϕ of the photons in the lasing mode, are given as [1]

$$\frac{dN(t)}{dt} = \frac{I(t)}{qV} - \frac{N(t)}{\tau_n} - g_0 \frac{N(t) - N_0}{1 + \epsilon S(t)} S(t) \tag{A.1}$$

$$\frac{dS(t)}{dt} = \Gamma g_0 \frac{N(t) - N_0}{1 + \epsilon S(t)} S(t) - \frac{S(t)}{\tau_p} + \Gamma\beta \frac{N(t)}{\tau_n} \tag{A.2}$$

$$\frac{d\phi(t)}{dt} = \frac{\alpha}{2}\left(\Gamma g_0 (N(t) - N_0) - \frac{1}{\tau_p}\right) \tag{A.3}$$

Equation A.1 is the carrier density rate equation, it describes the generation and depletion of carriers within the active layer volume, V, with respect to time. The rate of change of the carriers or electrons is equal to the difference between the total number of electrons injected into the active region and the number of electrons used for the generation of photons via stimulated and spontaneous emission. The effects of non-radiative carrier recombination processes are assumed to be small in comparison to the spontaneous emission. Equation A.2 is the photon density rate equation, which describes the change of the photon density in the active region with respect to time as a result of both spontaneous and stimulated emission processes. It also accounts for the depletion of photons within the active layer due to absorption and scattering losses, as well as facet coupling with external media. In addition to the stimulated emission, the spontaneous emission also contributes to the lasing mode. The term $g_0 \frac{N(t) - N_0}{1 + \epsilon S(t)}$ in the photon and carrier rate equations, represents the non-linear optical gain of the laser. Of particular importance is the term $1 + \epsilon S(t)$, which includes the gain compression, ϵ, and accounts for the non-linear behaviour of the optical gain of the laser above threshold due to the carrier and photon densities.

The third rate equation, equation A.3, is the optical phase rate equation and it describes the rate of change of the phase of the photons in the laser cavity with respect to time. The alpha parameter, α, or linewidth enhancement factor describes the amplitude-phase coupling effect and how fluctuations in the carrier density affects both the real and imaginary parts of the complex refractive index. Any carrier-induced variations in the refractive index of the active region of the laser results in variations in the phase of the photons.

The rate equations can be used to model the steady-state characteristics of a single-mode laser. By obtaining the steady state solution to the rate equations, an expression for the optical power output from the laser, P, can be determined and is given by

$$P(t) = \frac{V\eta h\upsilon}{2\Gamma\tau_p}S(t) \qquad \text{A.4}$$

where η is the differential quantum efficiency, h is Planck's constant, and υ is the optical frequency of the lasing mode. The rate equations may also be used to model the small and large signal modulation dynamics of single-mode lasers, as well as the noise performance of lasers.

References

[1] J. C. Cartledge and R. C. Srinivasan, "Extraction of DFB laser rate equation parameters for system simulation purposes," in Journal of Lightwave Technology, vol. 15, no. 5, pp. 852-860, May 1997, doi: 10.1109/50.580827.

Appendix B

B.1 MQW DFB Laser Numerical Model Parameters

Symbol	**Quantity**	**Value**	**Unit**
λ	Wavelength of laser emission	1550 x 10^{-9}	m
L	Length of the active region	300 x 10^{-6}	m
V	Volume of the active region	3.7 x 10^{-17}	m^3
Ar	Area of the active region	1.23 x 10^{-13}	m^2
Γ	Optical confinement factor	0.13	-
g_d	Differential gain coefficient	9.9 x 10^{-20}	m^2
N_o	Carrier density at transparency	1.7 x 10^{-24}	m^{-3}
A_{nr}	Non-radiative recombination coefficient	1 x 10^{8}	s^{-1}
B_r	Radiative recombination coefficient	4.6 x 10^{-16}	m^3/s
C_{nr}	Auger recombination coefficient	3 x 10^{-41}	m^6/s
τ_n	Carrier lifetime	1.03 x 10^{-9}	s
n_g	Group refractive index	3.2	-
v_g	Waveguide group velocity	9.3685 x 10^{7}	ms^{-1}
g_0	Linear gain coefficient	9.2748 x 10^{-12}	m^3/s
R_1	Facet 1 reflectivity	0.2744	-
R_2	Facet 2 reflectivity	0.2744	-
α_{int}	Internal cavity loss	550	m^{-1}
τ_n	Photon lifetime	2.1959 x 10^{-12}	s
β_{sp}	Spontaneous emission factor	2.5 x 10^{-6}	
α	Linewidth enhancement factor	TBD	-
ϵ	Gain compression factor	TBD	m^3

Table B.1: MQW DFB Laser Numerical Model Parameters.

Appendix C

C.1 IM/DD Numerical Model Description

A flow chart showing the different functional elements of the model of the IM/DD transmission link is shown in Figure C.1.

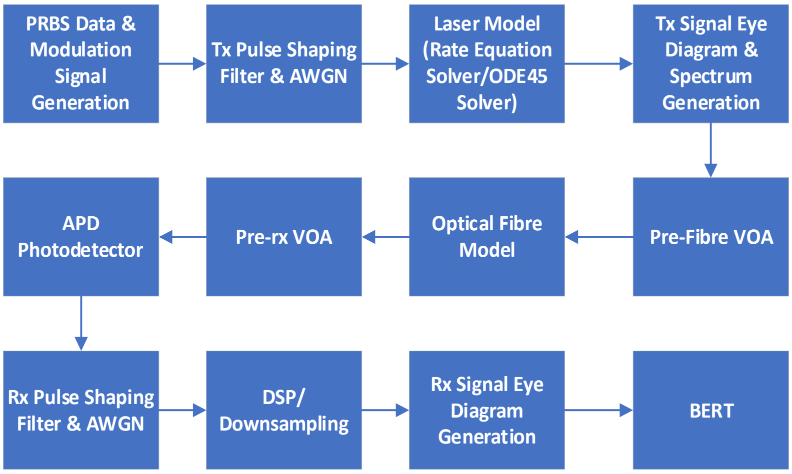

Figure C.1: DML and IM/DD system simulation flow chart.

The optical fibre model was developed based on a low power linear model, where the optical power of the signal input to the fibre was assumed to be well below 10 mW and only short-range and single channel transmission was considered. Thus, only the linear effects of the fibre, i.e. the optical loss and chromatic dispersion (CD), were accounted for in the fibre model and the power dependent non-linear Kerr effects (SPM, XPM, FWM) were not accounted for. The optical field of the signal output from the DML model is input to the optical fibre model having been attenuated by the pre-fibre VOA shown in Figure C.1. The fibre model firstly calculates the group velocity dispersion (GVD) parameter, β_2, using equation C.1. The GVD parameter β_2 describes the chromatic dispersion (CD), or the dispersion of the group velocity, and is responsible for optical pulse broadening [1].

$$D = \frac{d\beta_1}{d\lambda} = \frac{d}{d\omega}\left(\frac{1}{v_g}\right)\frac{d\omega}{d\lambda} = -\frac{2\pi c}{\lambda^2}\beta_2 = -\frac{\lambda}{c}\frac{d^2 n}{d\lambda^2} \qquad \mathrm{ps/(nm.km)} \qquad \text{C.1}$$

A typical value of 17 ps/nm.km was used for the SSMF dispersion parameter, D. The fibre model then determines the effects of the CD and attenuation on the complex amplitude of the input optical field for a given fibre length by utilising equation C.2 and the Fast Fourier Transform (FFT) and Inverse Fast Fourier Transform (IFFT) functions, which are built-in functions in MATLAB. Equation C.2 is the slowly varying envelope equation for linear optical pulse propagation in optical fiber, which can be derived from Maxwell’s equations [1], [2].

$$\frac{\partial A}{\partial z} = -\frac{\alpha_{att}}{2}A - \frac{j\beta_2}{2}\frac{\partial^2 A}{\partial T^2} \qquad \text{C.2}$$

The first term on the right hand side of equation C.2, which contains the fibre attenuation parameter, α_{att}, represents the linear attenuation of the optical pulse. The second term on the RHS of equation C.2, containing the second order mode propagation constant, or GVD parameter, β_2, corresponds to second order dispersion and is the most significant term in relation to PONs and optical access links. An outline of the method for simulating linear optical pulse propagation in optical fibre using Fourier methods is provided in [2]. The complex amplitude of the optical signal output from the fibre model, having been modified by the effects of the fibre CD and attenuation, is then sent to a pre-receiver VOA, which is used to control the optical power of the lightwave incident on the photodetector (PD). The modelled PD comprised a 10 GHz bandwidth APD with an integrated trans-impedance amplifier (TIA). The square law operation converts the optical field of the signal incident on the APD into optical power and, using appropriate values for the APD responsivity and the multiplication factor, M_{APD}, the model calculates the photocurrent, I_p, generated by the APD, using equation C.3.

$$I_p(t) = \left(\frac{\eta_d q}{hv}\right) M_{APD}.\,|E_s(t)|^2 \qquad \text{C.3}$$

The total noise current variance, σ^2, in the modelled photodector comprises the shot noise current variance, σ_S^2, and the thermal noise current variance, σ_T^2.

$$\sigma^2 = \sigma_T^2 + \sigma_S^2 \qquad \text{C.4}$$

Expressions for the APD shot and thermal noise current variances are given in equations C.5 and C.6, respectively.

$$\sigma_T^2 = \frac{4k_B T F_n \Delta f}{R_b} \qquad \text{C.5} \qquad \sigma_S^2 = 2qM_{APD}^2\left[k_A M_{APD} + (1-k_A)\left(2 - \frac{1}{M_{APD}}\right)\right] R_d P_{opt}\Delta f \qquad \text{C.6}$$

The shot and thermal noise currents are then added to the APD signal photocurrent, I_p, and, following current to voltage conversion, the signal is output from the PD model, where it is filtered by a 2nd order Butterworth low pass filter (LPF) with a 3-dB cut-off frequency of ~10 GHz. The filtered signal is then downsampled for subsequent bit-error ratio (BER) counting and used to generate the received signal eye diagram.

References

[1] G. P. Agrawal, “Nonlinear Fibre Optics,” Fifth edition, Academic Press, 2012.

[2] E. M. Wright, "Module 3 – Numerical Pulse Propagation in Fibers," Center for Integrated Access Networks, University of Arizona. http://data.cian-erc.org/supercourse/Graduatelevel/module_3/3_SC_GRAD_LEVEL_Module3_wright.pdf